Influence of Solvent and Scale-up Upon the Hydrogenation of 4-Phenyl-2-butanone

By

Nazita Sedaie Bonab

A thesis submitted to
The University of Birmingham
for the degree of
DOCTOR OF PHILOSOPHY

School of Chemical Engineering
College of Engineering and Physical Sciences
The University of Birmingham
August 2014

Abstract

The focus of this thesis is the role of the solvent and scale-up upon rate and selectivity in heterogeneous catalysed hydrogenations, which are ubiquitous in the production of fine chemicals and pharmaceuticals. A kinetic method has been developed based on rigorous statistical methods and sensitivity analysis for the catalytic hydrogenation of 4-phenyl-2-butanone in stirred tank reactors at two different scales using Pt/TiO_2 and Pt/SiO_2 catalysts. In this thesis, modelling carried out for a 100 mL scale reactor was validated against experimental data supplied by Queens University Belfast (QUB). Experimental measurements of rate and selectivity and model validation at a larger 3000 mL scale were both carried out as part of this study. The models were evaluated over a wide range of operational conditions at both scales for Pt/TiO_2 catalyst, and by using a systematic kinetic methodology it was possible to identify the dominant reaction route, derive physiochemically meaningful kinetic data and a reduced kinetic model that was applicable to the scale-up. Comprehensive kinetic analysis made it possible to gain some insight into the shift in reaction mechanism upon scale-up. Kinetic investigation of solvent effects was also carried out at the 100 mL scale for a range of solvents (protic, aprotic polar, apolar, ethers, and halogens) and both catalysts, again tested against experimental data supplied by QUB. The dominant effects of solvent on rate and selectivity of the chosen reaction system were identified as the degree of active site availability imposed by competitive adsorption of solvent on catalyst and the extent of which the solvents assist the product desorption from catalyst surface. The solvent effects upon scale-up give the remarkable result of a significant shift in the selectivity of the catalyst towards phenyl ring and ketone hydrogenation groups of 4-phenyl-2-butanone.

تقدیم به

خانواده عزیزم، پدر، مادر و خواهر نازنینم که همواره پشتیبان و مشوق

من در همه مراحل زندگی بوده اند.

Acknowledgements

First and foremost I would like to express my gratitude to my supervisor Prof. Mark Simmons for his continuous support and guidance during the course of my Ph.D study. I would like to thank him for his patience, and encouragements at all times and especially during writing of this thesis. Without him this thesis would have never been completed.

I would also like to thank my Co. supervisor Prof. Joe Wood for his continuous support and guidance.

I would also like to express my gratitude to Chemical Engineering staff for all the help and support during the course of my research and laboratory work, in particular Mrs. Lynn Draper.

I am greatly thankful to Iain Mc.Manus, Eihmear Connor, Dr. Helen Daly, Dr. Jillian Thompson, and Prof. Christopher Hardacre from Queen's University of Belfast for providing me with the experimental data and immense support throughout the course of this research.

I would like to thank my colleagues Dr. James Bennett, Dr. Martin Khzouz, Dr. Ju Zhu, Luke Dandy, and Dr. Marjan Rafiee for their constant support and friendship.

I am deeply indebted to my dearest friend Donya Jasteh for her continuous words of wisdom during the course of this thesis, "Don't watch the clock; do what it does. Keep going." -- Sam Levenson.

Most of all I would like to thank my father and mother for their constant support throughout every step of my life, and my beloved sister Aida, for always encouraging me towards every goal in my life.

Table of contents

List of Figures:

Figure 5.9: Fitted rate constants, k_{ket} (a) and k_{arom} (b), against selectivity after 2 hr. across the range of solvents tested for Pt/SiO2 catalyst in 100 mL scale: Alkanes (□), Primary alcohols (○), Secondary alcohols (▼), aromatics (×).

List of Tables:

Chapter 1: Introduction

1.1 Background and motivation

Mankind faces great challenges in developing benign processes for the chemical industry in the field of catalysis. In order to gain the full potential of catalysts, scientists must develop profound understanding of catalytic transformations in order to design process specific catalysts that can render products with molecular precision (Sá and Szlachetko, 2014). Understanding what is happening on the surface of the catalyst can help researchers monitor the catalyst performance across length scales from the molecular scale to the process plant. The work presented in this thesis was carried out as part of the EPSRC funded CASTech project, a joint research programme between academia and industry to investigate and optimise catalyst performance based upon such a multi-scale approach. The CASTech project aimed to combine advanced experimental probes and theoretical approaches to study the structure of liquids in catalytic systems at scales from the external (bulk) liquid phase to inside the porous catalysts[1]. Core competencies for the CASTech project included MR imaging techniques (University of Cambridge, UCam); computational fluid dynamics (UCam); spectroscopic methods (QUB); steady state isotopic transient kinetic analysis (SSITKA) (QUB); pilot-scale multiphase flow, reactions and kinetic modelling (University of Birmingham, UBir), and molecular simulations (University of Virginia). The industrial partners were Johnson Matthey Plc, Robinson Brothers Ltd, and Borregaard. The CASTech project consisted of five subtopics aiming towards different aspects of catalytic processes. The current study was part of the Subtopic#1:

---

[1] Taken from CASTech grant description:
http://www.researchperspectives.org/topicmaps/grant.php?id=F78D4EB1-66FA-457C-B57D-184FCAD572F7

- Understanding the properties and characteristics of multiphase interfaces - Advanced engineering through fundamental understanding of reactors and reactions.

The focus of the subtopic was the catalytic hydrogenation of unsaturated aldehydes and ketones (4-phenyl-2-butanone, citral, cinnamaldehyde, and ketoisopherone), as model reaction systems, with the focus on solvent and scale-up effects. The research presented in this thesis is focused on the investigation of the influences of different solvents and scale-up, using kinetic analysis.

Based on literature review presented in Chapter 2, selective hydrogenation of alpha-, and beta- unsaturated ketones and aldehydes is significant due to the production of unsaturated alcohols which are extensively used in the pharmaceuticals and fragrance industries. These compounds can contain multiple aldehyde, ring and unsaturated carbon bonds (C=C). The rate and selectivity of these compounds can be manipulated through the right choice of catalyst, solvent, reaction conditions and other operational conditions. Noble metal catalysts are commonly used for selective hydrogenation of aldehydes and ketones specifically platinum, palladium, and ruthenium supported on oxide supports (Mäki-Arvela et al., 2005). The most recent research on hydrogenation of these compounds using DFT and ATR-IR suggest that selectivity of these components are closely dependent upon the sterical conformation of the functional groups on catalyst surface and their adsorption strength (Chen et al., 2012), (Ide et al., 2012). Studies of selective hydrogenation of a similar compound, acetophenone on Pt/SiO_2 and Pt/Al_2O_3 are established to be due to specific sites available on supports (Manyar et al., 2013a), (Manyar et al., 2013b) that selectively hydrogenates the carbonyl group. The role of solvent on catalytic hydrogenations has gained wide attention during the past few years. Solvents account for the 80-90% mass utilization in a typical chemical/pharmaceutical batch operations and play a dominant role in the overall toxicity profile (Constable et al.,

2006). The works published so far on rate and selectivity when using different solvents are divided on the mechanism by which the solvents interact with substrate and catalyst. Solvents can affect the rate and selectivity of reactions through a variety of mechanisms: mass transfer and pore diffusion, the capacity to dissolve reactants, and interactions between different components of a reaction system. In order to investigate the solvents effects thoroughly a combination of experimental data, kinetic analysis and advanced characterization and simulation methods are needed (Akpa et al., 2012).

Another important problem in the field of catalytic reactions is the problems during the scale-up of batch processes. Stirred tank reactors are still widely used throughout the fine chemicals industry due to their flexibility and cost effectiveness. During scale-up of multiphase reactions, geometric, kinetic, bubble, and mixing lengths do not scale in proportion (Stitt, 2002). Problems usually arise from the presence of mass/heat transfer limitations and chemistry sensitivity issues. The nature of which these shifts affect the selectivity of a given reaction system when the reactants have a variety of functional groups is still not completely understood.

1.2 Scope of the Study

The aim of this study was to investigate the rate, selectivity, and kinetics of a model hydrogenation reaction system to compare the effects of solvents, mass transfer, and scale-up. 4-phenyl-2-butanone (PBN) was chosen as the model compound and Pt/TiO_2 and Pt/SiO_2 catalysts were chosen as Pt can hydrogenate both ketone and phenyl functional groups and shows varying degrees of activity in different solvents.

A kinetic modelling framework was developed to elucidate the mechanistic behavior of the different catalysts as a function of the solvent and scale of reaction using Athena Visual

Studio (Athena Visual Software Inc.). The models were developed on the basis of two sets of experimental data carried out at different scales. Data at a small 100 mL scale were provided by Queens University Belfast (QUB) as part of the CASTech project. Data at a larger 3000 mL scale was obtained by the author at the University of Birmingham.

- 100 mL reactor (QUB): A range of pressures (2-12 bar), temperatures (313-353 K), catalyst loadings (20-140 mg), initial concentrations (0.135-0.404 mol L^{-1}) stirring speeds (300-1400 rpm) and solvents were investigated to establish the kinetics of the reaction.

- 3000 mL reactor (Birmingham): A range of pressures (2-10 bar), temperatures (323-353 K), catalyst loadings (2-15 g), initial concentrations (0.135-0.404 mol L^{-1}), stirring speeds (400-980 rpm) and solvents were investigated to study the possible effects of mass transfer or other chemistry sensitive effects upon scale-up.

Kinetic modelling of heterogeneous reaction data often involves rate expressions which are over-parameterized. This complicates the convergence of parameter estimation and results in parameters which are physiochemically out of range and/or have high confidence intervals. The kinetic analysis methodology used in this thesis employs a sensitivity analysis to eliminate the insignificant parameters which pose the least impact on model response using norms of Jacobian Matrix, to produce physically realistic and robust reduced models. The elimination method involved pairing of the reaction pathways (ketone and ring hydrogenation routes) by equating the kinetic parameters (pre-exponential factors and activation energies). The relative significance of the key adsorption constants were also determined. The parameter eliminations were justified by using F-test, residuals, and parity plots, and condition numbers.

The kinetic models were developed in two stages. First the possibilities of different rate determining steps were investigated on temperature-varied data at the 100 mL scale to

determine the activation energies. Second, another set of models were suggested based on active site availability and competitive adsorption of substrate with H_2. These models were then fitted onto concentration-varied data. The models were then extended to the 3000 mL scale where significant shifts in rate and selectivity were observed. The results of this investigation are detailed in Chapter 4 and were carried out using Pt/TiO_2 as the catalyst and hexane as the solvent.

The model was then employed to elucidate mechanistic behavior of the reaction in various solvents observed by QUB at the 100 mL scale (the details of the solvents investigated can be found in § 5.2.1 and § 5.2.2) for both Pt/TiO_2 and Pt/SiO_2 catalysts. Experimental data for solvent effects at the 3000 mL scale are also presented. The results of this investigation are detailed in Chapter 5.

1.3 Thesis layout

Chapter 2 is a literature review which covers rate and selectivity profiles in hydrogenation of unsaturated ketones and aldehydes, solvent effects in hydrogenation reactions, kinetic models applied to hydrogenation of ketones and aldehydes, kinetic approaches to elucidate solvent effects, overview of the modelling software, and scale-up of stirred tank reactors. The apparatus and operational conditions for the experimental work carried out at Birmingham and QUB are presented in Chapter 3. Chapter 4 contains the results of the application of the kinetics methodology to the hydrogenation of PBN over Pt/TiO_2 in hexane at 100 mL and 3000 mL scale reactors. Full details of the rate and selectivity variations with operational conditions at both scales, and the kinetic models developed are documented in this chapter. Results of the kinetic modelling to elucidate solvent effects in the hydrogenation of PBN using Pt/TiO_2 and Pt/SiO_2 for various solvents at the 100 mL scale, and experimental results

at the 3000 mL scale, are reported in Chapter 5. Chapter 6 contains the conclusions from the study and recommendations for future work.

Publications arising from this Thesis

Journal

Wilkinson, S.K., McManus, I., Daly, H., Thompson, J.M., Manyar, H., Hardacre, C., Sedaie Bonab, N., ten Dam, J., Simmons, M.J.H., Stitt, E.H., D'Agostino, C., McGregor, J., Gladden, L.F., Solvent effects in the liquid-phase hydrogenation of 4-phenyl-2-butanone over Pt / TiO_2 Part 2: A kinetic analysis methodology to elucidate the roles of metal, support and solvent, J. Catal. (awaiting submission).

Conference Presentations

Sedaie Bonab, N., Wood, J., Simmons, M.J.H., Catalytic hydrogenation of phenyl-butan-2-one in a three-phase stirred reactor, International Symposium in Chemical Reaction Engineering, ISCRE 12, Maastricht, Netherlands, 2-5 Sept 2012 (Oral presentation).

Sedaie Bonab, N., Wood, J., Simmons, M.J.H., Solvent and mass transport effects in the catalytic hydrogenation of phenyl-butan-2-one in a three-phase stirred reactor, Catalysis in Multiphase Reactors CAMURE-8 International Symposium on Multifunctional Reactors ISMR-7, Naantali, Finland, 22-25 May 2011 (Oral presentation).

Chapter 2: Literature review

This Chapter contains a review of the literature concerning solvent effects and scale-up when carrying out heterogeneous hydrogenation reactions using noble metal catalysts. The aspects of catalytic hydrogenation reactions discussed include the rate and selectivity profiles for catalytic hydrogenation of alpha- and beta- unsaturated ketones and aldehydes, solvent effects, kinetic modelling approaches to elucidate solvent effects, and stirred tank reactors and scale-up.

2.1 Catalytic hydrogenation reactions: Fundamentals

Hydrogen is an important element used by the chemical industries. Approximately 4% of H_2 consumption is used for catalytic hydrogenation of organic compounds. Hydrogenation reactions can be carried out homogeneously using organometallic complexes or heterogeneously using metal supported catalysts. Though the activation of H_2 in soluble metal complexes has been widely studied using techniques such as Nuclear Magnetic Resonance (NMR), and Infrared Spectroscopy (IR), the actual mechanism of H_2 dissociation on metallic surfaces and its transfer to organic compounds still lacks detailed understanding at the molecular level (Chiusoli and Maitlis, 2006). Applications of catalytic hydrogenations are extensively reviewed in the book series *"Catalysis in Organic Reductions"* (Augustine, 1985), (Delannay, 1984), (Jennings, 1985), (Rylander et al., 1988). Some of the applications of catalytic hydrogenation include reduction of alkenes, alkynes, ketones and aldehydes, nitriles, nitro compounds, and aromatic rings.

During heterogeneous hydrogenation reactions, hydrogen gas is added to an organic molecule in the presence of a transition metal catalyst. The reaction begins by adsorption of the

hydrogen molecule and substrate on the catalyst metal surface. Heterogeneous reactions may be carried out using catalysts which are either:

- Supported (Slurry and fixed gel operations), or

- Unsupported (Primarily solution reactions).

The product distribution, nature of the functional group reduced, and the extent of reduction are direct functions of the type and the amount of catalyst used. The most commonly used heterogeneous catalysts are platinum (Pt), palladium (Pd), rhodium (Rh), and ruthenium (Ru) (these are all platinum group metals - PGMs) and nickel (Ni) (Smith, 2010). An extensive review of catalyst preparation methods can be found in (Schwarz et al., 1995). To summarize the general procedure involves transition of pure metals or metal salts onto supports via variety of techniques namely precipitation, complexion, gelation, crystallization, impregnation, etc. (Schwarz et al., 1995). No single catalyst mentioned above would reduce all functional groups and there are significant differences between them with regards to their chemo- and stereoselectivity. The rule of thumb is that 10% mol of catalyst is required per mole of compound, however the ratio would vary depending on catalyst type and substrate (Smith, 2010). Table 2.1 summarizes the most common catalysts and operational conditions for reduction of ketone and phenyl functional groups which are both the focus of this thesis.

Table 2.1: Recommended reaction conditions for catalytic hydrogenation of selected functional groups (Smith, 2010).

Functional group	Product	Catalyst	mol%	Temp. (ºC)	Press. (atm)
Ketones and aldehydes	Alcohol	A	3-5	25	1
		B	2-4	25	1-4
		C	30-100	25	1
Carboxylic acid aromatic	Hydroaromatic	B	4-7+AcOH or HCl/MeOH	25	1-4
		C	2	25	1
		D	20 + HCl/MeOH	65-200	130

A: 5% Pd/C; B: Pt/O$_2$; C: Raney Ni; D: 5% Rh(Al$_2$O$_3$)

In solid catalysts, supports are inert materials on which the metal catalyst adsorbs and is sited. Common supports are,

- Carbon: Platinum black and palladium are usually supported on.

- Oxide supports: Alumina, titania, silica, etc.

The role of the support is to effectively disperse the expensive transition metals to optimize available surface area for reaction (usually between 1-10 mol%), to control the rate and selectivity as well as making the catalyst more cost effective. Many factors tend to influence the reactivity of a certain catalyst. These factors are preparation method, addition of a promoting agent, reaction temperature, catalyst agglomeration, synergistic effects between multiple catalytic species, H$_2$ gas pressure and the ratio of H$_2$ to substrate, the age of the catalyst and finally the number of times it has been recycled. In many cases, if the catalyst is too active it may lead to the addition of compounds that bind to metal and lead to catalyst

poisoning. When the poison is bound to catalyst surface, H_2 and organic substrates cannot be adsorbed thus leading to loss of activity (Smith, 2010).

Heterogeneous catalysis is a surface phenomenon led by **active sites**. The nature of these active sites is determined by the metal particles coordination on the surface. (Maier, 1989) suggested three types of atomic arrangements: terrace-, step-, and kink- which are characterized by the number of nearest neighboring atoms. These atom types correspond to different transitional metal fragments as well as coordination states of that metal. Figure 2.1 represents metal coordination for active sites on flat surfaces and FCC type metals.
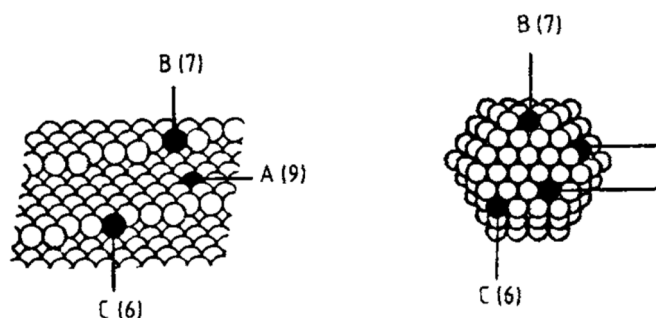
Figure 2.1: Metal partcile coordination types with respect to their neighboring atoms on flat surfaces and FCC metals. A = on (111) or (100) terraces, B = on steps or edges. C = on kinks or corners; taken from (Maier, 1989).

Since these coordination types correspond to different transition metals they exhibit varying selectivity towards different functional groups. There are several distinguishing characteristincs which set homogeneous and heterogeneous catalysts apart. Table 2.2 summrises the pros and cons for each catalyst type (Smith, 2010).

Table 2.2: Pros and cons of heterogeneous versus homogeneous catalysts.

Catalyst type	Pros	Cons
Heterogeneous	Easily recoverable Can be used in continous flow regimes	Insoluble and thus surface atoms accessible to hydrogenation Subjected to gas solubility in different solvents Susceptible to poisoning
Homogeneous	Soluble thus all molecules are accesible (less catalyst required) Requires use of non-polar solvents with higher H2 solubility	Ligands or solvents competing with active sites Less selective towards hetero-atom contatining functional groups Harder to recover

Since the focus of this thesis is on the hydrogenation of alpha- and beta- unsaturated ketones and aldehydes, the next section of this chapter will focus on the background and the research carried out so far in terms of catalyst types, solvent selection and kinetics of such reactions.

2.2 Overview of hydrogenation of alpha- and beta- aldehydes and ketones: Focus on aromatic compounds and supported platinum catalysts

The hydrogenation of unsaturated ketones and aldehydes to corresponding alcohols has extensive applications in the fragrance and drugs industries (Mäki-Arvela et al., 2005).

The chemoselective hydrogenation of carbonyl bonds in multi-unsaturated ketones and aldehydes is a demanding task (Singh and Vannice, 2001a), (Kluson and Cerveny, 1995). The theymodynamics favor C=C hydrogenation over C=O by ca. 35 kJ mol^{-1} (Mohr and

Claus, 2001). These compounds can be reduced using homogeneous catalysts but due to reasons stated in Table 2.2 the use of heterogeneous catalysts is more desirable. However, there are many factors affecting rate and selectivity of a catalyst. These factors are metal and support selection, metal precursor, catalyst preparation and activation methods, reaction conditions and operational mode (e.g. gas or liquid phase reactions). One of the key factors in catalyst design is relating the performance of the catalyst to its structure. In the case of hydrogenation reactions this task becomes further complicated due to the mechanisms involved (adsorption, reaction and desorption). Additionally, the reaction mechanism is further complicated by dissociative/non-dissociative and competitive/non-competitive adsorption of H_2 as well any possible solvent adsorption (Mäki-Arvela et al., 2005). In order to achieve high selectivity toward desirable intermediate products it is essential to gain in depth understanding of all these phenomena.

The π bond of a carbonyl compound can be reduced by heterogeneous catalysts to give alcohols. In the case of monometallic catalysts, the metals from group 10, e.g. Ni, Pt, and Pd are usually selected. From groups 8 and 9, Rh and Ru have also been used, respectively (Mäki-Arvela et al., 2005). Alumina, silica, and carbon are the most common supports used. The catalytic activity of metals is determined by their ability to activate C=C and C=O groups as well as H_2. Hydrogen adsorption mechanisms on the catalyst surface and reactivity is well documented by (Masel, 1996). They argue that the hydrogen is reactive on the surfaces of Co, Ni, Ru, Rh, Pd, Os, Ir, Pt as well as Sc, Ti, V, Y, Zr, Nb, Mo, La, Hf, Ta, W, Cr, Mn, Fe, Tc, and Re (Masel, 1996). On the other hand Cu has a slower uptake of hydrogen and Ag and Au are reported as inert (Masel, 1996). This is due to these metals having completely filled d orbitals, $5d^{10}$ and $4d^{10}$, which is believed to directly affect the adsorption. There are reports

correlating the width of d bands of metal catalysts with selectivity of alpha- and beta-unsaturated aldehydes (Ryndin et al., 2000).

An extensive review of the works published regarding hydrogenation of carbonyls using metal groups 8, 9, and 11 can be found within the work of (Mäki-Arvela et al., 2005). For the purpose of this thesis only the use of group 10 metals: Ni, Pd, and Pt and specifically Pt are going to be reviewed. Pt has been the most widely catalyst used for chemoselective hydrogenation of carbonyl compounds (Singh and Vannice, 2001a), (Singh and Albert Vannice, 2000b), (Malathi and Viswanath, 2001), (Recchia et al., 1999), (Singh and Vannice, 2000), (Singh and Vannice, 2001b), (Kijeński et al., 2002), (Hoang-Van and Zegaoui, 1997), (Consonni et al., 1999), (Torres et al., 1999), (Abid and Touroude, 2000), (Abid et al., 2001), (Ammari et al., 2004), (Liberková and Touroude, 2002), (Liberkova et al., 2002), (Englisch et al., 1997a), (Englisch et al., 1997b), (Dandekar and Vannice, 1999), (Kun et al., 2001), (Shirai et al., 2001), (Vergunst et al., 2001), (Huidobro et al., 2002), (Singh and Albert Vannice, 2000a), (Singh et al., 2000), (Vaidya and Mahajani, 2003), (Vannice and Poondi, 1997), (Silvestre-Albero et al., 2002), (Silvestre-Albero et al., 2003). Compared to Pt, Pd and Ni have been applied less for these types of hydrogenations (Mäki-Arvela et al., 2005).

The widely used compounds as model substrates for carbonyl hydrogenation are citral, cinnamaldehyde, crotonaldehyde, and acetophenone. These compounds either have isolated or conjugated C=C bonds. Thermodynamically isolated C=C bond should be easiest to hydrogenate followed by conjugated C=C and finally C=O bonds. Amongst these compounds cinnamaldehyde, acetophenone, p-isobutyl acetophenone, benzophenone, 3,4-dimethoxyacetophenone, and chalcone are aromatic ketones containing an unsaturated phenyl group. The selectivities towards main products, unsaturated alcohols or saturated ketones are reported in Table 2.3 and discussed below.

(Santori et al., 2004) studied hydrogenation of acetophenone, 3,4-dimethoxyacetophenone, benzophenone, and chalcone on Pt/SiO_2 and tin modified bimetallic and organometallic catalysts using 2-propanol as solvent under 10 bar of H_2 pressure and 353 K. For acetophenone, 1-phenylethanol (ketone hydrogenation) and cyclohexylmethylketone (ring hydrogenation) were produced with slightly more selectivity towards cyclohexylmethylketone. 3,4-dimethoxyacetophenone hydrogenation rendered 93% selectivity towards unsaturated alcohol product while no ring hydrogenation was observed due to –OCH3 groups electronically enriching the aromatic rings. Benzophenone hydrogenation resulted in 48% selectivity towards ring hydrogenated product cyclohexylphenylmethanol while ketone hydrogenation was 21%. This compound has two phenyl groups. 48% selectivity corresponds to hydrogenation of one of the ring groups. Chalcone also consists of two phenyl groups and a double C=C bond. Only 21% ketone hydrogenation was observed compared to 65% selectivity towards C=C bond and less than 15% towards other products containing ring hydrogenation. Higher selectivities were observed for all substrates when tin was added to Pt due to enhancing effects caused by ionic tin anchoring to the metallic surface, which favoured ketone hydrogenation.

(Liu et al., 2009) studied acetophenone hydrogenation using mesoporous Pt/Al_2O_3 catalyst. Methanol was used as solvent and reactions were carried out under 6 bar H_2 pressure and room temperature. High selectivity (> 97%) towards 1-phenylethanol was observed for all catalysts tested under different calcination temperatures. Catalyst activity however varied from 40%-89% conversions between low temperature (463 K) and high temperature (823 K) calcinations. No ring hydrogenation was reported using this catalyst at the applied conditions.

(Tundo et al., 2000) studied p-chloroacetophenone and acetophenone hydrogenation using Pt/C and Pd/C catalysts. A mixture of aqueous phase and Aliquant 336 (ammonium salt as

phase transfer catalyst) was used as solvent in order to assess the effect of basic and acidic media towards carbonyl and ring hydrogenation. Isooctane was used as the organic phase in some of the reactions and was well mixed with the aqueous phase. The reactions were carried out under atmospheric pressure and 323 K. This study was focused more on kinetic investigations and quantitative conversions and selectivity data were not reported. P-chloroacetophenone was dechlorinated and reduced to render 90% selectivity towards ethylcyclohexane. Small amounts of saturated ketone and unsaturated alcohol were detected. Hydrogenation of acetophenone in a neutral aqueous phase resulted in 40% selectivity towards the phenyl ring while the addition of acidic and basic phase shifted the selectivity towards ketone hydrogenation.

Catalytic hydrogenation of acetophenone over Pt/Al$_2$O$_3$ at 273 K and using h$_8$- and d$_8$-toluene as a solvent was studied by (Gao et al., 2006). In order to study the chemical issues associated with these solvents experimental design was carried out to incorporate FTR-IR and series of perturbations of substrate and intermediate products during reaction. The initial rate of reaction was reported as unusually high and there was a significant observable jump in concentrations of 1-phenylethanol and cyclohexylmethylketone corresponding to ketone and ring hydrogenation, respectively. Introducing 1-phenylethanol through series of perturbations resulted in an increase in the amount of substrate in liquid phase. This desorption was justified by adsorption of acetophenone over the support which was desorbed into the solvent upon introduction of 1-phenylethanol suggesting competitive adsorption of this compound with substrate over support. The competitive adsorptions of acetophenone and phenylethanol are further investigated in a recent study by (Chen et al., 2012).

(Chen et al., 2012) has recently reviewed hydrogenation of acetophenone using Pt/Al$_2$O$_3$ and n-hexane as solvent. The reaction pathway was monitored using Attenuated Total

Reflectance Infrared Spectroscopy (ATR-IR) coupled with modulation excitation spectroscopy (MES) and Phase Sensitive Detection (PSD). High selectivity towards ketone hydrogenation was observed which was corresponded to a $\eta^1(O)$ adsorption mode of substrate on catalyst active sites which corresponds to adsorption of oxygen atom on surface and parallel configuration of ring with catalyst surface. The adsorption modes of aromatic ketones are discussed in Chapter 4 in context with the results. Smaller portion of acetophenone was believed to have been interacted to catalyst through π-bonding of the aromatic ring leading to phenyl group hydrogenation. This work was a direct comparison to acetophenone hydrogenation works carried out in gas phase by (Chen et al., 2003) and (Reddy et al., 2009). These authors reported the selectivity towards ketone hydrogenation in gas phase to be driven by the decomposition/hydrogenolysis of the substrate which resulted in hydrocarbon fragments deactivating the active sites. Such behaviour was not observed in the liquid phase where selectivity towards ring and ketone is suggested to be the direct effect of adsorption modes and competitive desorption of intermediate products from catalyst surface.

(Shirai et al., 2001) studied cinnamaldehyde hydrogenation using Pt/SiO$_2$ catalyst and ethanol as solvent. Reactions were carried out under high H$_2$ pressure (120 bar) and 353 K. High selectivity towards unsaturated alcohol cinnamol alcohol was observed (90%). As stated before since this aldehyde compounds contain a conjugated double bond, hydrogenation of this functional group was dominant over the phenyl ring leading to the product hydrocinnamaldehyde. Similar results were reported by (Toebes et al., 2005) where hydrogenation of cinnamaldehyde over carbon-nanofibre supported platinum catalysts resulted in ketone and double bond hydrogenation with varying selectivities depending on nanofibre structure. High selectivity towards ketone hydrogenation of cinnamaldehyde was also reported by (Shi et al., 2013) where few layered reduced graphene (RGO) was used as

support for platinum. Reactions were carried out under mild condition and various solvents. More than 70% selectivity towards cinnamol alcohol was reported using alcohols as solvents. Pt/RGO catalyst exhibited higher performance over support free platinum nano-particles. The higher activity and selectivity over this catalyst was attributed to high dispersion of Pt over micro-pore free structure of RGO.

Hydrogenation of benzaldehyde was investigated in gas phase by (Vannice and Poondi, 1997) using Pt supported on TiO_2, SiO_2, and Al_2O_3. Reactions were done under atmospheric pressure and temperature was varied between 333 and 493 K. The effect of support, calcination temperature, and reaction temperature were investigated. Over Pt/TiO_2 high selectivity towards ketone hydrogenation was observed with 100% selectivity towards benzyl alcohol at high calcination temperatures. The extent of ketone hydrogenation was varied by calcination temperature as lower temperature resulted in 40% selectivity towards benzyl alcohol followed by formations of toluene and benzene through hydrogenolysis. These results are in line with previous gas phase reactions where hydrogenolysis was observed. No ring hydrogenation of benzaldehyde was reported. On the other hand, using SiO_2 and Al_2O_3 supports resulted in no ketone hydrogenation. The effect of calcination on ketone hydrogenation when using TiO_2 as support was attributed to formation of special sites at the platinum-titania interface which interact with oxygen end of carbonyl compound and polarize it towards hydrogenation. On the other hand ring and C=C functional groups were suggested to be independent of catalyst structure and more sensitive to Pt site availability.

(Toukoniitty et al., 2003b) studied asymmetric hydrogenation of 1-phenyl-1,2-propanedione over Pt/Al_2O_3 catalyst in the presence of cinchondine modifier. Ethyl acetate was used as solvent and reactions were carried out under 1.2-6.5 bar H_2 pressure and 288 K. 65% enantioselectivity was observed towards the main product of the reaction which was

hydrogenation of one of the two active pro-chiral carbonyl groups. Without the presence of modifier, < 5% ring hydrogenation was reported. It was concluded that phenyl ring hydrogenation is more favourable when there is more space on catalyst surface for ring adsorption. In the presence of modifiers which occupy the active sites no ring hydrogenation can be achieved. On a similar note, the first part of this study dealt with solvent effects in hydrogenation of this compound (Toukoniitty et al., 2003a). The results of this research are further discussed in solvent effects section of this Chapter.

Over the past few years novel characterization and qualitative/quantitative methods have been developed in order to study the interaction of substrate functional group with catalyst and adsorption geometries. (Chen et al., 2012) have successfully employed ATR-IR analysis in order to probe the adsorption/desorption dynamics of acetophenone and intermediate products over Pt/Al$_2$O$_3$ catalysts which has previously been reported by researchers. One of the methods that has gained wide spread popularity among researchers is molecular simulations based on Density Function Theory (DFT) calculations to examine the mechanism of H$_2$ dissociation as well as adsorption strength of substrates. This method has been successfully employed by (Ide et al., 2012) and (Manyar et al., 2013b). (Ide et al., 2012) have studied selective hydrogenation of unsaturated ketones (benzalacetone and methyl vinyl ketone) and unsaturated aldehydes (crotonaldehyde and cinnamaldehyde) over Pd/C, Pt/C, Ru/C, Au/C, Au/TiO$_2$, and Au/Fe$_2$O$_3$. Experiments were carried out using ethanol as solvent under 2 bar H$_2$ pressure and 333 K. The Pt and Ru catalysts were unable to produce unsaturated alcohols from ketone hydrogenation in contrast with the results published so far. DFT calculations were used to assess the activation barrier of C=O and C=C groups over model Pt (111) and Ru (0001) surfaces. It was found out that C=O groups have significantly higher activation barriers over Pt and Pd as opposed to Au where some ketone hydrogenation was observed.

The reason for the high activation barrier of C=O bonds was attributed to significantly lower steric hindrance of primary-secondary C=C versus the more sterically crowded C centre of C=O. Additionally, ease of hydrogenation of weaker Ru-CH$_2$R bonds over stronger Ru-OR bonds were reported. Relative desorption of unsaturated alcohols (UA) and saturated ketones (SK) were also reported. While SK can be easily desorbed from catalyst surface, UA is more strongly held to the surface. These results were in-line with previously reported acetophenone hydrogenation studies of (Gao et al., 2006) and (Chen et al., 2012) where strong adsorption of UA products were reported on Al$_2$O$_3$ supports. In the case of benzalacetone, binding energies of all functional groups were stronger on Ru than Pt as a result of favourable orientation of phenyl, carbonyl and C=C bonds as well as stronger bonds between oxygen and carbon with catalyst active sites. The primary products of benzalacetone hydrogenation are benzylacetone (SK) and an UA product. Desorption of benzylacetone was found to require much lower energy. Additionally, the presence of phenyl group was reported to increase the activation barrier of C=C bond which is agreement with the experimental results where presence of a ring functional group slows the C=C hydrogenation in compounds such as cinnamaldehyde.

(Manyar et al., 2013b) also used DFT calculations in order to investigate the adsorption mechanism of ketoisopherone and cinnamaldehyde using OMS-2 (octahedral molecular sieve) and Pt/OMS-2 catalysts. It was observed that for ketiosopherone hydrogenation, neither of these catalysts hydrogenated the ketone bond and high selectivity towards C=C bond hydrogenated product levodione was observed. On the other hand, cinnamaldehyde showed 80% selectivity towards cinnamol alcohols when 5% Pt was added to OMS-2. Using DFT calculations a significantly lower barrier for H$_2$ dissociation was found on Pt compared with OMS-2 which required water as solvent to facilitate H$_2$ dissociation. This H$_2$ dissociation

barrier was believed to be the reason behind favoured hydrogenation of C=C over C=O in OMS-2 which results in a more thermodynamically stable product to be favoured.

The previous part of this study dealt with using novel x-ray absorption spectroscopy coupled with high energy resolution fluorescence detection (XANES-HERFD) in order to investigate the influence of adsorbed products (Manyar et al., 2013a). The results of Pt/OMS-2 in hydrogenating C=C bond over carbonyl for ketoisopherone was in contrast with the expected behaviour of Pt. In comparison, reaction results in Pt/Al$_2$O$_3$ under the same reaction conditions as OMS-2 reactions, resulted in 91% selectivity towards ketone hydrogenated product 4-hydroxyisophorone. Consequently, a possibility of two types of sites for substrate adsorption was suggested to explain the differences in hydrogenation of ketone and ring functional groups. In situ XANES-HERFD measurements provide the shifts in FERMI energy levels (thermodynamic quantity: quantifying total chemical potential for electrons) which correspond to surface coverage of any molecule on catalyst/support surfaces. The spectra shows that Pt electrons, on average, are donated to the molecule adsorbed with higher energy shifts, i.e. a higher adsorption energy. Cinnamaldehyde adsorbs more strongly on both Pt (111 and 211) surfaces than OMS-2 reflected by the shift in DERMI energy level measured by XANES-HERFD, thus the C=O is preferentially hydrogenated. On the other hand ketoisopherone adsorbs on both Pt and OMS-2 surfaces. However, upon introduction of H$_2$, XANES-HERFD showed a slightly larger shift for Pt-H$_2$ than Pt-KIP, indicating that during hydrogenation H$_2$ competes with ketoisopherone and possibly displaces the substrate. Consequently, the reaction proceeds exclusively on support resulting in high C=C hydrogenation than C=O.

The combined results of DFT and XANES-HERFD provide a comprehensive explanation of substrate/catalyst interactions and adsorption states which are directly correlated to observed

rate and selectivity of a given reaction system and in this case aromatic ketones and aldehydes.

As it is shown in reviews above and Table 2.3 hydrogenation of alpha- and beta-unsaturated ketones and aldehydes can have vastly different rates and selectivities on platinum supported catalysts. The combination of state-of-the-art spectroscopy and theoretical calculations are powerful tools for investigation of the adsorption behaviour of reactants in catalytic liquid phase hydrogenations. Such information is crucial during the kinetic modelling and reactor design stages of chemical processes as will be demonstrated in Chapter 4 where a systematic kinetic modelling procedure was employed in order to build robust kinetic expressions.

It is essential to state that the works of (Ide et al., 2012), (Manyar et al., 2013a), and (Manyar et al., 2013b) on spectroscopy methods and DFT calculations reviewed above were carried out during the course of the CASTech project. Only the research published by (Ide et al., 2012) is a direct publication of CASTech project Subtopic#1 from the knowledge of the author of this thesis.

Table 2.3: Selectivities to ketone and ring hydrogenated products of unsaturated aromatic or non-aromatic ketones and aldehydes at a given conversion over monometallic platinum based catalysts.

Reactant	Product	Catalyst	Solvent	Conversion (%)	Selectivity (%)	Ref.
Acetophenone	1-phenylethanol[a]	Pt/SiO$_2$	2-propanol	100	31	(Santori et al., 2004)
	Cyclohexylmethylketone[b]				42	
3,4-dimethoxyacetophenone	Benzylalcohol[a]	Pt/SiO2	2-propanol	20	93	(Santori et al., 2004)
Benzophenone	Diphenylmethanol[a]	Pt/SiO2	2-propanol	100	14	(Santori et al., 2004)
	cyclohexylphenylmethanol[b]				48	
Chalcone	1,3-diphenylpropanol[a]	Pt/SiO$_2$	2-propanol	100	21	(Santori et al., 2004)
Acetopheone	1-phenylethanol[a]	Pt/Al$_2$O$_3$	Methanol	89	97.6	(Liu et al., 2009)

a: C=O hydrogenated product, b: Phenyl ring hydrogenated product, c: C=C hydrogenated product

Table 2.3: Continued.

Reactant	Product	Catalyst	Solvent	Conversion (%)	Selectivity (%)	Ref.
Acetophenone	Cyclohexylmethylketone[b]	Pt/C	Water	-	40	(Tundo et al., 2000)
Acetophenone	1-phenylethanol[a]	Pt/SiO$_2$	Gas phase	3.9	83	(Chen et al., 2003)
	Cyclohexylmethylketone[b]				1	
Acetophenone	1-phenylethanol[a]	Pt/Al$_2$O$_3$	n-hexane	61	71.6	(Chen et al., 2012)
	Cyclohexylmethylketone[b]				21.9	
Cinnamaldehyde	Cinnamol alcohol[a]	Pt/SiO$_2$	Ethanol	20	90	(Shirai et al., 2001)
	Hydrocinamaldehyde[c]				< 10	
Benzaldehyde	Benzylalcohol[a]	Pt/TiO$_2$	Gas phase	80	100	(Vannice and
		Pt/SiO$_2$			-	Poondi, 1997)
		Pt/Al$_2$O$_3$			-	

a: C=O hydrogenated product, b: Phenyl ring hydrogenated product, c: C=C hydrogenated product

Table 2.3: Continued.

Reactant	Product	Catalyst	Solvent	Conversion (%)	Selectivity (%)	Ref.
1-phenyl-1,2-propanedione	(R)-1-hydroxy-1-phenylpropanone[a] Cyclohexyl products (8)	Pt/Al$_2$O$_3$	Ethyl acetate	-	65 (ee)	(Toukoniitty et al., 2003b)
Cinnamaldehyde	Cinnamyl alcohol[a] Hydrocinamaldehyde[c]	Pt/CNF[1] Pt/CNF973[2]	2-propanol	60	37[1], 8[2] 32[1], 74[2]	(Toebes et al., 2005)
Cinnamaldehyde	Cinnamyl alcohol[a] Hydrocinamaldehyde[c]	Pt/RGO	Methanol	80.4	73.3 8.4	(Shi et al., 2013)
Cinnamaldehyde	Cannamol alcohol[a] Hydrocinamaldehyde[c]	Pt/OMS-2 OMS-2	Methanol/water	96 97	80[a] 86[a]	(Manyar et al., 2013b)

a: C=O hydrogenated product, b: Phenyl ring hydrogenated product, c: C=C hydrogenated product

2.3 Solvent effects during catalytic hydrogenations

Solvent use accounts for 80-90% of mass utilization in a typical fine chemical/pharmaceutical batch chemical operation (Constable et al., 2006). Within these processes, solvents play a critical role in the overall toxicity and environmental impact of the whole process. At their simplest, solvents are just a medium in which the reactions take place. As succinctly described by (Constable et al., 2006), the slow progress of the research carried out in the last few decades on solvent effects is due to focus of the researchers upon improved catalyst design towards better reactivity and selectivity rather than solvents. However, over the past few years more deliberate research has been made on solvent selection and optimization by e.g.(Kolář et al., 2002), (Elgue et al., 2004, Elgue et al., 2006), and (Gani, 2004, Gani et al., 2005).

Although the role of the solvent is often limited to the requirements of diluting and dissolving substrates, proper choice of solvent can greatly impact the reactivity and selectivity of catalytic reactions . For heterogeneous catalyzed reactions, the choice of solvent can cause changes in the following processes (and combinations thereof),

- Mass transfer rates

- Reaction mechanism

- Reaction kinetics

- Adsorption properties

Consequently in addition to solvent polarity, dielectric constant, acid/base properties of reaction medium, other factors such as solvation of substrates and products, gas solubility, mass transfer effects, improved heat transfer, and influence on catalyst deactivation need to be considered (Akpa et al., 2012). The focus of the work in this thesis on solvent effects is the

adsorption properties of substrate/products and reaction kinetics. Consequently, first half of this section of literature review deals with different solvent effects observed during catalytic hydrogenations, specifically on works that exhibited strong solvent/catalyst interactions towards limiting the site availability and the effect of solvent on product desorption from catalyst surface. The second half of this review summarizes the kinetic approaches taken so far in order to elucidate solvent effects for catalytic hydrogenations.

Solvent effects in heterogeneously catalyzed reactions have been reviewed by (Singh and Vannice, 2001a) and (Mäki-Arvela et al., 2005). The most important solvent effects in the hydrogenation of α,β-unsaturated ketones and aldehydes are stated as solvent polarity, hydrogen solubility, solvation of reactants, and interaction between catalyst and solvent. Over the past two decades, solvent effects in hydrogenation of the following α,β-unsaturated ketones and aldehydes have been widely investigated (See Table 2.4 for references)

- Cinnamaldehyde

- Citral

- Benzyl alcohol

- Acetophenone

- Crotonaldehyde

- Benzaldehyde

Some of the most recent trends found in literature regarding solvent effects are reviewed here. Varying results were reported in literature regarding the mechanism in which the solvents affect rate and selectivity during catalytic reactions. An overview of the significant works carried out on solvent effects in this field is summarized in Table 2.4 and discussed below. The majority of the work carried out so far on solvent effects has dealt with catalysts

containing noble metals from group 8 (Ru), group 9 (Rh, Ir), and group 10 (Ni, Pd, Pt) supported on oxide supports (Al_2O_3, SiO_2, TiO_2), carbon and novel supports like clay and graphene. The earliest results which support the initial rate following H_2 solubility and solvent dielectric constant usually comprise of works done using at most two or three solvents. This potentially leads to trends which are circumstantial or misleading and based upon the notion of choosing a limited pallete of commonly used solvents including ethanol, 2-propanol, and hexane. In case of solvent dielectric constant there is a clear discrepancy between the results published. Solvent polarity has increased the hydrogenation rates in works done by (von Arx et al., 1999), (Hájek et al., 2003), and (Shirai et al., 2001), (Mäki-Arvela et al., 2002), (Lafaye et al., 2004), and (Bennett et al., 2009) in hydrogenations of ketoisopherone (Pd/Al_2O_3 and Pt/Al_2O_3), cinnamaldehyde (Ru/Y, Ru/C, Ru/MCM-41, Pt/SiO_2), citral (Ni/Al_2O_3, $Rh-Ge/Al_2O_3$), and 2-pentyne (Pd/Al_2O_3). On the other hand, high reaction rates were also observed in hydrogenation of citral over Pd/SiO_2-AlPO_4 and acetophenone hydrogenation over Ni/Y catalysts with solvents having low dielectric constants (Aramendía et al., 1997), (Malyala et al., 2000). In works where solvent polarity decreased the rate of reaction, the results were justified by weak adsorption of substrate on catalyst surface, i.e. solvents prevent weakly adsorbed substrates to remain on active sites due to high solubility. This was apparent in the more recent results published by (Bertero et al., 2011), and (Shi et al., 2013) where a wider range of solvents were investigated (See Table 2.4). On a similar note, (Yadav and Mewada, 2012) has reported highest catalyst activity using methanol and 2-propanol in selective hydrogenation of acetophenone over Ag/OMS-2 catalyst compared with toluene and ethanol. Although ethanol is a polar solvent, the low catalyst activity was not fully explained. Low catalyst activity in polar solvents has also been reported in some works where the substrate was prone to acetal/diacetal formation (Aramendía et al.,

1997), (Zhang et al., 1998), (Rojas et al., 2007), (Shi et al., 2013). The acetal formation in alcohols was explained to be result of support acidity, using chlorine based salts during catalyst preparations and strong metal support interactions (SMSI) due to high reduction temperatures. Consequently, the effect of supports with regards to solvent effects is believed to be due to acetal formation originating from acidity of supports. This was reported by (Hájek et al., 2003) where the selectivity towards C=O hydrogenation of cinnamaldehyde decreased in 2-propanol when Ru/Y was used as catalyst instead of Ru/C.

In the case of hydrogen solubility there has also been discrepancy between the results published so far. (Bawane and Sawant, 2005) has reported higher rate of p-nitrophenol in methanol and 2-propanol compared to dimethylformamide over Raney Nickel catalyst. Same results have been reported by (Thakar et al., 2007b) for 4-isobutylacetophenone hydrogenation over Pd/SiO$_2$ using n-decane and cyclohexane. Citral hydrogenation was investigated by (Mäki-Arvela et al., 2002) over Ni/Al$_2$O$_3$ using alcohols (ethanol, 2-memthyl-2-propanol, 2-pentanol, and 2-propanol). Hydrogen solubilities were measured with a gas chromatograph coupled with a TC-detector. Highest solubility was obtained in 2-pentanol, whereas the highest reaction rate was observed in 2-propanol. Similar observations were found by (Toukoniitty et al., 2003b), (Bertero et al., 2011).

In order to explain the solvent effect on catalyst activity, various approaches have been taken. Among them are works are carried out by (Lo and Paulaitis, 1981), (Takagi et al., 1999), (Fajt et al., 2008), (Wan et al., 2014), (Ren et al., 2014), and (Wicaksono et al., 2014) within which the rate of reaction is correlated by hydrogen bond capabilities , i.e. hydrogen bond donating and accepting parameters. The early work carried out by (Lo and Paulaitis, 1981) deals with correlating rate constants with solvent activity coefficients predicted using UNIFAC method (Kontogeorgis and Gani, 2004). Based upon the assumption of thermodynamic equilibrium

between the transition state and the reactant, the reaction rate in any solvent i relative to a reference system $\emptyset$ (benzene) is given by,

$$relative\ rate = \frac{(k/k_0)_i}{(k/k_0)_\emptyset} = \frac{(\gamma_A^2/\gamma_M)_i}{(\gamma_A^2/\gamma_M)_\emptyset} \qquad (2.1)$$

where k_0 is the rate constant in an ideal reference system, γ_i is the activity coefficient for an individual species i. UNIFAC is applicable to a wide range of solution non-idealities and parameters are evaluated from extensive correlation of published vapor-liquid equilibrium data. Advantage of using UNIFAC in predicting activity coefficients is that the method relies on the number of functional groups in the transition state and not on the physical properties. (Lo and Paulaitis, 1981) were relatively successful in finding a correlation between observed and estimated rate data for hydrogenation of cyclohexene and acetone in presence of nickel catalysts in five solvents.

Other attempts based on the methods commonly used for description of solvent effects on kinetics of homogeneous reaction systems was explored by (Fajt et al., 2008) for hydrogenation of 6-ethyl-1,2,3,4-tetrahydro-anthracene-9,10-dione over Pd/Al_2O_3-SiO_2 using 20 solvents including alcohols, aromatics, alkanes, esther, ester, amine, and an alkylchloride. This technique uses multiple linear regressions derived on the basis of linear free energy relationships (LFER) to evaluate the solvent effects based on different physiochemical phenomena. The most widely used model is the Abraham-Kamlet-Taft (Kamlet et al., 1983) as shown in Equation 2.2,

$$XYZ = XYZ_0 + d.\delta + s.\pi^* + a.\alpha + b.\beta + h.\delta_H^2 \qquad (2.2)$$

where $d,\ s,\ a,\ b$, and h represent solvent independent parameters of the model and the rest of the parameters are independent variable characteristics of a given solvent: π^* represents

solvent polarity, α is hydrogen bond donor ability, β is the hydrogen acceptor ability, δ_H^2 is the Hilderband cohesion energy density, and is defined as the heat of evaporation of the solvent at 298 K per unit volume. The term $d.\delta$ is the correction term of polarizability.

The second important model is the Koppel-Palm model (Koppel and Palm, 1972) with modifications made by (Makitra et al., 1977) in the form shown in Equation 2.3.

$$XYZ = A_0 + A_1.f(n_D) + A_2.f(\varepsilon) + A_3.E_T + A_4.B + A_5.\delta_H^2 \tag{2.3}$$

In this model, A_1–A_5 are solvent independent parameters, A_0 is an intercept with the similar meaning to XYZ_0. The independent variables are the refractive index function $f(n_D)$, dielectric constant function $f(\varepsilon)$, electrophilic solvation ability E_T, nucleophilic solvation ability (B) of the solvent, and its Hildebrand cohesion energy density δ_H^2.

The highest reaction rates in the work of (Fajt et al., 2008) were reported in alcohols and triethylamine and the lowest corresponded to methylcyclohexane, chlorobenzene, 1,2-dichloroethane. None of the individual solvent parameters stated above were able to describe the reaction data individually and consequently AKT and KP models were used to explain the solvent effects. Both of these models were able to describe the experimental data, however each possessed certain limitations. The AKT model resulted in the closest correlation, however using the least-square method resulted in high degree of cross-correlation between certain parameters in each model. Consequently, the statistical significance of parameters were evaluated based on parameter p-value resulting in elimination of $\alpha, f(\varepsilon)$, and $f(n_D)$ from the models. As a result, the most significant parameters in each model were determined to be hydrogen bond acceptor capability in AKT model and nucleophilic solvation ability in KP. Another problem with this kind of approach apart from multicolliniearity is the degree of

uncertainty associated with experimental measurements of the Kamlet Taft parameters related to the dye and other factors (Wicaksono et al., 2014).

The most recent work carried out by (Wicaksono et al., 2014) in parallel with these models deals with the use of published tabulated data along with a combination of Tikhonov regularization and optimal design of experiments to overcome the uncertainty associated to experimental data and Kamlet Taft parameters. However, the amplified uncertainty in the data resulted in a lack-of-goodness in the solution of the model, distorting the rank of the candidate solvents. It was concluded that a combination of solvent data bank screening and solvent design based mixed-integer optimization is needed to optimize this approach. It should be noted that this was a generalized work of solvent screening for optimization of reaction rates for a wide range of applications and the case study involved solvolysis of tert-butyl chloride.

On a similar note, (Takagi et al., 1999) has defined a δ parameter defined as difference between hydrogen donor capability and hydrogen acceptor capability that was used to correlate with the catalyst activity in hydrogenation of benzyl alcohols over Ru/Al_2O_3 using a range of protic, aprotic polar and apolar solvents. However, 2-propanol and benzene were found to not follow into the trend observed with the values of δ. It was postulated that solvents with negative δ (hexane, methanol, ethanol, and acetic acid) are capable of accepting electrons and this negative value does not affect hydrogenation reactivity. Reaction in these solvents resulted in > 80% conversion. 2-propanol and hexane fell into the negative spectrum; however the catalyst activity was lowered due to competitive hydrogenation of benzene and substrate and suppression of hydrogenolysis by 2-propanol. Solvents with positive value (acetone, THF, dioxane, diethyl ether) are capable of transferring electrons and can bond to

the surface of the catalyst via an interaction between the pair of unshared electrons of their oxygen atoms, decreasing the hydrogenation rate as a result. (Wan et al., 2014) argues that when a wider range of solvents are investigated it becomes more apparent that rate and selectivity variations cannot be explained by using a single criterion based on dielectric constant, H_2 solubility, etc. Additionally, the use of AKT parameters in correlating rate constants with physiochemical solvent properties does not render satisfactory explanations across different catalytic systems as there is still a discrepancy between the parameters determined as significant by model versus the experimental works published. This discrepancy could be explained by examining the classes of solvents in which the AKT model could result in relatively satisfactory results. For example (Khodadi-Moghaddam and Sadeghzadeh Darabi, 2011) has recently found that in hydrogenation of cyclohexene over Pt/Al_2O_3, the reaction rate in various solvents (protic, aprotic polar, apolar) does not correlate with Kamlet taft parameters in polar aprotic and apolar solvents. However, in alcoholic solvents the rate increases with increasing hydrogen bond capability, polarazibility, normalized polarity parameter, relative static permittivity, dipole moment, acceptor number and decreases with increasing donor number and hydrogen bond acceptor basicity. This was explained to be due to increase in competitive adsorption of solvent on catalyst with the parameters stated above for alcoholic solvents.

The application of Kamlet Taft parameters has recently extended into correlating the solute-solvent interactions through Infrared Spectroscopy like the works of (Liu et al., 2003) (Liu et al., 2007), (Song et al., 2009). Based on these works the vibration frequency of solute (ν), such as C=O band of a compound can be correlated through linear solvation energy relationships (LSER) in the form of,

$$\nu = \nu_0 + (s.\pi^* + d.\delta) + a.\alpha + b.\beta \tag{2.4}$$

Excellent correlations between the C=O band vibrations in various solvents and LSER parameters were achieved along with physically meaningful explanations of solvent-induced stretching frequency shifts. However, it should be noted that these calculations were done without the presence of a catalyst. The perspective of using spectroscopy along with LSER parameters in the presence of catalyst can be an interesting area of research. It can be postulated that generalizing the correlation of rate constants with LSER/LFER parameters is too broad as rate constants are varied not only as a result of substrate/solvent interactions but also the solvent/catalyst interactions.

Solvent selection has also been reported to affect the selectivity of catalytic hydrogenations (Table 2.4). (Englisch et al., 1997b) has reported low selectivity towards C=O hydrogenation using cyclohexane and chloroform in hydrogenation of Crotonaldehyde over Pt/SiO$_2$ while the selectivity towards unsaturated alcohols was promoted with using 2-propanol and ethanol. The use of methanol however, resulted in 29% formation of by-products, thus separating it from other alcohols tested. On the other hand, (Červený et al., 1996) has reported solvent effect in the selectivity of C=C and C=O bonds of aldehyde compounds (cinnamaldehyde, and benzaldehyde over Ru/C catalyst), whereas the ketone substrate (acetophenone) did not show any selectivity variations towards C=O and ring in any solvents tested. On a similar note, (Takagi et al., 1999), has reported higher selectivity towards C=O hydrogenation in alcohols, and solvents containing sulfur and nitrogen in hydrogenation of acetophenone over Pt/Al$_2$O$_3$. Higher selectivity towards ring hydrogenation was observed over hexane and heptane. Similar results were reported by (Shi et al., 2013) for cinnamaldehyde hydrogenation over platinum supported on graphene. Solvent effect on selectivity of acetophenone hydrogenation over Ni/SiO$_2$ and Cu/SiO$_2$ was also studied by (Bertero et al., 2008, Bertero et al., 2011). Although high variations of initial rate were reported in varying solvents,

selectivity remained unchanged at 100% towards C=O. Citral hydrogenation has also been the subject of study by (Mukherjee and Vannice, 2006b) and (Rojas et al., 2007) over Pt/SiO$_2$ and Ir/TiO$_2$, respectively using comprehensive range of solvents. No selectivity effect towards C=O hydrogenation was observed with any of the solvents.

From the works reviewed above the following important conclusions can be drawn:

- There is no systematic method where the H$_2$ solubility and solvent polarity can be generalized for rates and conversions in catalytic hydrogenation of unsaturated ketones and aldehydes. The most important criterion governing the solvent polarity in different substrates and catalysts lies in the strength of adsorption of substrate on catalyst, i.e. if the substrate can strongly adsorb on catalyst surface then the polar solvents interaction with substrate can lower their activation barrier towards faster reaction. If the adsorption is weak the solvent will inhibit the substrate adsorption lowering the reaction rate. On the other hand for hydrogen solubility, solvent-catalyst interaction seems to be the missing link. In systems where there is no solvent adsorption on catalyst surface to inhibit site availability and product desorption from catalyst surface is not affected by the nature of the solvent, reaction rate is more likely to follow the H$_2$ solubility. Additionally, the nature of the solvent adsorption on catalyst is also of vital importance. For example in case of 2-propanol is has repeatedly been reported that dissociative adsorption of this solvent on catalyst results in higher H$_2$ spillage on active sites, thus increasing the rate of reaction.
- The same unsystematic behaviour can also be concluded for selectivity in hydrogenations of unsaturated aldehydes and ketones. However, a parallel can be drawn by focusing on solvent/catalyst interaction. The selectivity towards different functional groups is a significantly affected by the sterical conformation of the

substrate on catalyst surface and also by the ability of the solvent to remove successfully the intermediates and products as discussed on the reviews above. Solvents which possess lone oxygen pairs, nitrogen and sulfur can adsorb on the catalyst surface and alter the mode of adsorption towards hydrogenation of one functional group. This was apparent in certain works where hydrogenation of aromatic ring compound of acetophenone and benzaldehyde were suppressed by using protic and (primary and secondary alcohols) and chlorinated solvents. As is going to be demonstrated in the results chapters in this thesis, it is possible to gain mechanistic insights into the ability of the solvents in product desorption through systematic kinetic analysis.

As the role of solvent/substrate and solvent/catalyst interactions in manipulating the rate and selectivity of catalytic hydrogenation reactions is established, recent works based on novel characterization tools and molecular dynamic calculations has gained significance in exploring these interactions.

Two-dimensional nuclear magnetic resonance (NMR) relaxation time correlation measurements have been used by (Weber et al., 2009). From the ratio of NMR relaxation times, T_1/T_2, for the liquids confined in the pores, it was possible to determine the extent of relative strengths of the surface interaction for each liquid in hydrogenation of 2-butanone over Pd/Al_2O_3 and Ru/Al_2O_3 in water and 2-propanol. It was found that in Ru/Al_2O_3 water has a stronger interaction with catalyst surface than 2-propanol and 2-butanone. 2-propanol and 2-butanone had similar relative strengths of interaction. In Pd/Al_2O_3, the interaction of water was the strongest followed by 2-propanol; and finally 2-butanone was determined to be weakest. The fact that these solvents interact more strongly with Pd/Al_2O_3 suggests that 2-butanone would have limited access to active sites compared with Ru/Al_2O_3. This method

proved to be beneficial in providing information on behaviour of liquids inside porous catalysts and has also been employed during the course of CASTech project by University of Cambridge in investigation of the solvent effects in the hydrogenation of the chosen model reaction 4-phenyl-2-butanone. The results are in the process of being published along with the first part of this study carried out by Queens University Belfast (McManus et al., 2014a) (Reference is to be published).

Another important criteria discussed above is the ability of solvents in altering the activation barrier of functional groups. First principle density function calculations have recently gained attention in investigations of the reactivity trends of catalytic systems based on this observation. Among different studies, the work of (Ide et al., 2012) is a strong example of use of molecular simulations. The rate and selectivity of four different unsaturated ketone compounds were investigated over Pd, Pt, Fe, Ru, and Au catalysts supported on TiO_2, Fe_2O_3, and carbon. It was found that selectivity over these catalysts is most likely controlled by the significantly higher activation barriers to hydrogenate C=O bond compared with C=C bond. It was also possible to determine the strength of which the intermediate products were bound to the active sites.

Combination of these methods for solvent analysis is used in the work done by (Akpa et al., 2012). (Akpa et al., 2012) has studied the role of mixed water-alcoholic solvents in hydrogenation of 2-butanone over Ru/SiO_2 catalyst. A combination of measured rate data, pulsed field gradient (PFG) NMR measurements, THz Time domain Spectroscopy (THz-TDS), and DFT were used to gain more fundamental understanding of mixed solvent effects for catalytic hydrogenations. Though reviewing the mixed solvents systems is out of the scope of this thesis, this work is highlighted as an example of combined experimental and numerical investigations in the field of solvent effects. Results from DFT calculations showed that water

can significantly lower the activation energy for reaction as compared to the reactions done in 2-propanol, and can also alter the proposed reaction mechanisms through hydroxyl and alkoxy intermediates. In order to explain the sharp increase of the reaction rate in water/alcohol mixed solvents ($x_{H2O} \approx 0.8$ mole fraction) *ab initio* molecular dynamics were used which explained the role of water/alcohol composition on diffusivity variations of the charged reaction species through inter-connected hydrogen bonding network of water molecules.

From the works reviewed above it can be concluded that there is still a lot of ground to be covered in understanding solvent effects in catalytic hydrogenations. There is an essential need to investigate the roles of substrate/solvent and solvent/catalyst interactions systematically and across the length scales from surface of the catalyst to bulk liquid using variety of novel experimental and numerical methods. Using case studies like the work carried out here would be most beneficial towards further understanding of solvent effects. Using the solvent physiochemical properties to correlate the rate data in a given reaction system has been proven to be controversial as these parameters are only beneficial in describing the liquid side behaviour. Classification of solvent effects based on their descriptions of protic, aprotic polar, aplor also seems insufficient as various solvents within a same class can behave differently towards substrates and catalysts. From the reviews of the research so far it seems that there is a great need to approach the solvent classification towards their specific interactions rather than the conventional methods used to classify them to date.

Table 2.4: Summary of the significant works done so far on effect of solvent in catalytic hydrogenation reactions.

Reactant	Catalyst/solvents	Main conclusions	Ref.
Cyclohexene	Rh/Al_2O_3 Cyclohexane, n-heptane, ethyl acetate, methanol, benzene	• Initial rate follows H_2 solubility in all solvents except benzene. • Relatively no reaction in benzene.	(Boudart and Sajkowski, 1991)
Citral	Pd/SiO_2-$AlPO_4$ Methanol, cyclohexane, dioxane, tetrahidrofurane	• Initial rate does not follow solvent dielectric constant: higher rates of reduction in non-polar solvents (low dielectric constant). • Substrate/solvents interaction in alcohols: formation of acetals with citral C=O bond hindering site availability.	(Aramendía et al., 1997)
Crotonaldehyde	Pt/SiO_2 Ethanol, methanol, 2-propanol, cyclohexane, chloroform 10% v/v water with alcohols	• Selectivity to C=O bond dependent upon site availability. • Addition of > 5% v/v water to alcohols suppressed side reactions and promoted catalyst activity. • No effect of nature of alcohols on selectivity. • Low rate and selectivity towards C=O in cyclohexane and chloroform.	(Englisch et al., 1997b)

Table 2.4: Continued.

Reactant	Catalyst/solvents	Main conclusions	Ref.
Acetophenone	Raney nickel Cyclohexane, 2-propanol, 2-propanol-water (20% v/v)	• Rate in 2-propanol double than that of cyclohexane. • Addition of water increased rate by factor of 3 and resulted in high selectivity (99.5%) towards C=O hydrogenation. • Addition of water believed to inhibit the site availability towards ring adsorption.	(Masson et al., 1997)
Benzaldehyde Cinnamaldehyde Acetophenone	Ru/C Hexane, 2-propanol	• Hydrogenation of aldehydes was faster in 2-propanol. • Hydrogenation of acetophenone was faster in hexane. • No solvent effect on C=O and ring hydrogenations of acetophenone. • Solvent effect observed towards selectivity of C=C bond with cinnamaldehyde: highest in hexane. • Kinetic analysis concluded higher adsorption of aldehydes in 2-propanol, whereas acetophenone adsorbed more strongly in hexane.	(Červený et al., 1996)

Table 2.4: Continued.

Reactant	Catalyst/solvents	Main conclusions	Ref.
Cinnamaldehyde	Pd/C Toluene, decane, methylcyclohexane, decalin, ethanol, 1-propanol, 2-propanol, 1-butanol, 2-butanol	• Higher rate of reaction in polar solvents than non-polar. • Significant selectivity differences between non-polar solvents for C=C bond. • Formation of diacetals in polar solvents was observed.	(Zhang et al., 1998)
Benzyl alcohol	Ru/Al$_2$O$_3$ Pt/Al$_2$O$_3$ Methanol, ethanol, 1-propanol, 2-propanol, hexane, heptane, benzene, acetone, tetrahidrofuran, dioxane, diethyl ether, dimethyl sulfoxide, N,N-dimethyl-2-formamide, N-methyl-2-pyrrolidone	• Noble metal catalysts selectively adsorb solvents which contain oxygen, nitrogen, and sulfur. • Reaction conversions were explained by difference between solvent basicity (donor number) and acidity (acceptor number) • Low conversions in benzene and 2-propanol could not be explained by this criterion as benzene hydrogenates on Ru and 2-propanol and suppresses the hydrogenolysis. • Highest selectivity towards phenyl ring: hexane, and heptane followed by primary and secondary alcohols. • Highest selectivity towards C=O: sulfur and nitrogen containing solvents followed by diethyl ether and 2-propanol	(Takagi et al., 1999)

Table 2.4: Continued.

Reactant	Catalyst/solvents	Main conclusions	Ref.
Toluene	Ni/Al$_2$O$_3$ n-heptane, isooctane, cyclohexane	• At high temperature and pressures (20 bar and 423 K) hydrogenation rates were equal for n-heptane and isooctane but considerably lower in cyclohexane • At high temperatures rates followed the calculated H$_2$ solubility • No solvent-catalyst interaction was observed	(Rautanen et al., 2000)
Crotonaldehyde	Pt/K-10 (clay supported) 2-propanol, t-butyl alcohol, cyclohexanol, butyl ether, tetrahydrofuran, dichloromethane, chloroform, hexane	• Highest conversion observed in 2-propanol. • Highest selectivity towards C=O bond in t-butyl alcohol accompanied by a lower reaction rates. • All other solvents mostly selective towards C=C bond hydrogenation.	(Kun et al., 2001)
1-phenyl-1,2-propanedione	Pt/Al$_2$O$_3$ Ethylacetate, tetrahydrofuran, 1-octanol, 1-pentanol, cyclohexanol, 2-propanol, 1-propanol, acetone, ethanol	• Hydrogenation rate did not correlate with H$_2$ solubility. • Highest rate was observed in 2-propanol and was attributed to hydrogen donor capability. • Exceptionally low rates in THF and 1-pentanol were attributed to catalyst deactivation by solvent adsorption on active sites. • DFT calculations concluded no reactant conformation changes by solvents.	(Toukoniitty et al., 2003b)

Table 2.4: Continued.

Reactant	Catalyst/solvents	Main conclusions	Ref.
Citral	Pt/SiO$_2$ n-Amyl acetate, ethanol, ethyl acetate, cyclohexanol, cyclohexane, n-hexane, p-dioxane, THF	• Highest initial TOF observed in p-dioxane at all temperatures studied (298, 373, and 423 K). • Catalyst activity could not be correlated with dielectric constant and dipole moment. • Highest conversions observed in cyclohexanol (96%) and ethanol (94%). • No significant selectivity variations was observed across all solvents.	(Mukherjee and Vannice, 2006b)
Citral	Ir/TiO$_2$, Ir-Fe/TiO$_2$ n-heptane, 1-propanol, equimolar mixture of two	• Catalyst activity increased with dielectric constant. • Acetal formation upon high temperature reduction of catalyst due to increase acidity imposed by strong metal support interaction (SMSI) • 100% selectivity towards C=O hydrogenation to geraniol and nerol.	(Rojas et al., 2007)
Acetophenone	Cu/SiO$_2$ 2-propanol, cyclohexane, toluene, benzene	• 100% selectivity towards C=O hydrogenation to 1-phenylethanol. • Highest catalyst activity in 2-propanol attributed to dissociative adsorption of solvent on Cu forming extra atomic hydrogen that increases hydrogenation rate. • Lower catalyst activity in cyclohexane due to strong adsorption of aromatic solvents lowering site availability.	(Bertero et al., 2008)

Table 2.4: Continued.

Reactant	Catalyst/solvents	Main conclusions	Ref.
Acetophenone	Ni/SiO$_2$ 2-propanol, 1-propanol, ethanol, cyclohexane, toluene, tetrahydrofuran, γ-butyrolactone, methanol, benzene, acetonitrile	• No significant solvent effect on selectivity towards C=O hydrogenation to 1-phenylethanol • Due to significantly different nature of the solvents no universal satisfactory explanation could be obtained (H$_2$ solubility, dielectric constant, etc.) • Apolar solvents: Strong catalyst interaction limiting the site availability for hydrogenation. • Aprotic polar solvents: Strong adsorption on catalyst along with hindering acetophenone adsorption leading to lower rates than apolar solvents • Protic solvents: both carbon chain length and nature of solvent affecting the rate. H-bond formation of alcohols is explained to result in lower substrate adsorption. However, high activity of C$_2$-C$_3$ solvents was attributed to dissociate chemisorption of alcohols increasing the amount of chemisorbed hydrogen as well as C=O bond polarization through H-bond.	(Bertero et al., 2011)

Table 2.4: Continued.

Reactant	Catalyst/solvents	Main conclusions	Ref.
Cinnamaldehyde	Pt/RGO Cyclohexane, toluene, CHCl$_3$, ethyl acetate, dimethyl-formamide, dimethyl-sulfoxide, CH3CN, acetone	• Low catalyst activity in cyclohexane, toluene, dimethyl-formamide, and dimethyl-sulfoxide was attributed to poor reactant solubility. • Slightly higher conversions observed in CHCl$_3$, ethyl acetate and acetone, however selectivity towards C=O bond hydrogenation was low as large amounts of byproducts were formed. • High selectivity towards cinnamol alcohol was observed in alcohols with relatively no byproducts. • Traces of acetals were found when using methanol. • Conversion decreased with increasing solvent polarity. • Long chain alcohols improved C=O hydrogenation at lower conversions.	(Shi et al., 2013)
Ethyl-benzoylformate	Pt/Al$_2$O$_3$ (asymmetric hydrog.) Methyl cyclohexane, toluene, methyl acetate, tetrahydrofuran, 1-octanol, 2-propanol, 1-propanol, acetone, ethanol	• Initial hydrogenation rates correlate with solvent dielectric constant except some protic solvents and solvents that strongly adsorb on catalyst surface. • Highest reaction rates were observed in toluene and methyl cyclohexane while lowest was measured in tetrahydrofuran and ethyl acetate. • Advanced kinetic methodology employed to quantify enantioselectivity.	(Martin et al., 2013)

Table 2.4: Continued.

Reactant	Catalyst/solvents	Main conclusions	Ref.
2-butanone 2-pentanone phenol	Ru/C Water, methanol, ethanol, 2-propanol, 2-butanol, ɣ-butyrolacetone, acetonitrile, tetrahydrofuran, cyclohexane, n-heptane	• Highest catalyst activity observed in water followed by protic solvents. Much lower activity was observed in aprotic polar and apolar solvents. • Correlation between initial hydrogenation rate and hydrogen bond donation (HBD) capability of solvents was established with higher HBD corresponding to higher initial rate of hydrogenations. FTIR measurements confirmed C=O stretching in protic solvents lowering activation barrier. • High catalyst activity in aprotic apolar solvents were attributed to no catalyst/substrate and catalyst/solvent interaction. • Low catalyst activities in aprotic polar solvents were attributed to solvents occupying active sites through oxygen lone pairs, lowering site availability.	(Wan et al., 2014)

Table 2.4: Continued.

Reactant	Catalyst/solvents	Main conclusions	Ref.
2,4-dinitroethylbenzene	Ni/HY Ethanol, n-butyl alcohol, water, formamide, dimethyl formamide, tetrahydrofuran, ethyl acetate, benzene, toluene, hexane	• High reaction rates in protic solvents (ethanol, n-butyl alcohol, formamide and water), whereas poor catalyst activity was observed in aprotic polar and apolar solvents. • Best catalytic performance in protic solvents is concluded to not be due to their polarity and hydrogen bond accepting capability, but closely correlated with their hydrogen-bond donating capability. • The effect of hydrogen-bond donating capability to facilitate reaction rate is attributed to faster desorption of intermediates from catalyst surface. • In addition to this, formation of hydrogen bonds with the substrate adsorbed on catalyst surface can help polarize the N=O group lowering the activation barrier. • Dissociative nature of ethanol and water adsorption on catalyst surface was tested and found to not play a significant role in this reaction.	(Ren et al., 2014)

2.4 Kinetic modelling of catalytic reactions

2.4.1 Fundamentals of reaction kinetics

Kinetic equations are mathematical expressions used to describe the rate of chemical processes as a function of reaction conditions. The models can vary significantly in their mathematical form based upon the level of complexity of the reaction to reflect the chemical and physical meaning of the processes being examined. In their simplest form the rate of reaction for experimental data can follow the form of,

$$rate \propto f(t)(concentration)^n \tag{2.5}$$

which is called power-law model, with *n* as the reaction order (Berger et al., 2001). However, in heterogeneous catalytic reactions there are more than one processes occurring in series, which can be broken down into a number of identifiable steps with their known rate equations. Some or one of these rate equations can be combined to represent the overall rate of the reaction (Berger et al., 2001). These steps are,

1. Mass transfer of reactants to the catalyst sites

2. Adsorption of reactants onto the catalyst

3. Chemical reaction

4. Desorption of products from catalyst

5. Mass transfer of products to bulk liquid

The most commonly used rate expressions that takes these surface processes into account are based upon Langmuir-Hinshelwood (LH) type or Hougen-Watson (HW) type models (Hougen, 1962). LH and HW type rate expressions are derived by invoking one of the processes above as rate determining step (RDS) on an ideal catalyst surface with monolayer

59

adsorption of molecules. The LH model assumes that one process (sorption or reaction) on the surface is the RDS, thus all the adsorption/desorption steps are quasi-equilibrated and Langmuir isotherm can be used to relate surface concentrations to bulk concentrations or partial pressures (Vannice, 2005b). This yields a kinetic expression of the form,

$$rate \propto \frac{(kinetic\ factor)(driving\ force)}{(adsorption\ term)^n} \qquad (2.6)$$

The numerator represents the reaction term, while denominator accounts for the effect of sorption processes. For a reaction of A + B $\rightarrow$ C (not equilibrium limited), the rate of C based on LHHW type expression is given by,

$$r = \frac{k_r K_{A,Ads} P_A K_{B,Ads} P_B}{1 + K_{A,Ads} P_A + K_{B,Ads} P_B + K_{C,Ads} P_C} \qquad (2.7)$$

where k_r is the rate constant for the surface reaction, and $K_{i,Ads}$ correspond to the adsorption coefficients of reactants and products (Berger et al., 2001). The LHHW-type expressions have been found to fit a wide range of reactions. There is evidence that suggests that the assumption of a single rate determining step for catalytic reactions is not feasible as the rate-controlling steps can vary with temperature, pressure, or conversion (Belohlav and Zamostny, 2000). However, exploring the fundamentals of rate determining steps was outside of the scope of the current study. LHHW models can be expanded to incorporate the effect of gas solubility and dissociative/associative and competitive/non-competitive modes of H_2 adsorption on catalyst surface based on proposed reaction mechanisms (Table 2.5).

2.4.2 Kinetic modelling of alpha- and beta- unsaturated aldehydes and ketones

The review of the literature on hydrogenation of alpha- and beta- unsaturated ketones and aldehydes revealed that most of the studies focus on selectivity issues and limited quantitative kinetic data are reported. An overview of the kinetics models most widely employed for hydrogenation of aldehydes and ketones is presented in Table 2.5. Most of the works reviewed here deal with kinetics of hydrogenations of acetophenone, benzaldehyde, cinnamaldehyde, 4-isobutylacetophenone, p-chloroacetophenone, and p-isobutyl acetophenone over noble metal catalysts supported on oxide supports (See Table 2.5 for references). The majority of these studies assume the surface reaction to be the rate determining step. Single and two-site models based on dissociative/associative and competitive/con-competitive modes of hydrogen adsorption have also been investigated. From the literature, models based on either of the sorption processes as rate determining steps were ruled out of the kinetic analysis based on lack of goodness-of-fit, making the surface reaction as the most probable rate determining step for catalytic hydrogenation of unsaturated aldehydes and ketones. As will be demonstrated in Chapter 4, during kinetic modelling of catalytic reactions the over-parameterized LHHW rate expressions impose complications towards finding physiochemically meaningful reaction parameters within acceptable confidence intervals. In order to overcome this issue, a combination of sound initial considerations and systematic statistical analysis is employed to reduce the number of parameters and build robust kinetic models that can shed more insight into solvent and scale-up effect for hydrogenation reactions. A comprehensive discussion on issues of over-parameterization and the approaches taken by researchers to tackle this complication are discussed within the results of the Chapter 4.

Table 2.5: Kinetic models previously applied to modelling hydrogenation of aromatic aldehydes and ketones.

Rate model	Mechanistic details	References
General LHHW form: $$r = \frac{k_b K_a [R]}{(1 + K_a [R] + \sum K_I [I])^n} \times \theta_H$$ Non-competitive, associative: $$\theta_H = \frac{K_H C_H}{1 + K_H C_H}$$ Non-competitive, dissociative: $$\theta_H = \frac{\sqrt{K_H C_H}}{1 + \sqrt{K_H C_H}}$$ Competitive, associative: $$r = \frac{k_b K_a [R] \, K_H C_H}{(1 + K_a [R] + \sum K_I [I] + K_H C_H)^n}$$ Competitive, dissociative: $$r = \frac{k_b K_a [R] \, \sqrt{K_H C_H}}{\left(1 + K_a [R] + \sum K_d [I] + \sqrt{K_H C_H}\right)^n}$$	Surface reaction is rate determining step (RDS) θ_H: competitive, non-competitive, dissociative, and associative modes of H_2 applied in different studies Other types of RDS assumptions were not able to describe the reaction data in any of these studies.	(Červený et al., 1996) (Neri et al., 1997) (Bergault et al., 1998) (Rajashekharam et al., 1999) (Mathew et al., 1999) (Tundo et al., 2000) (Belohlav and Zamostny, 2000) (Hájek et al., 2004) (Toebes et al., 2005) (Gao et al., 2006) (Thakar et al., 2007a) (Marchi et al., 2007) (Bertero et al., 2008) (Divakar et al., 2008) (Virtanen et al., 2009)

2.4.3 Kinetic modelling to elucidate solvent effects

To understand better the solvent effects in hydrogenation reactions, various approaches has been undertaken to drive the intrinsic kinetics of reactions in various solvents. Table 2.6 summarises the overview of these kinetic approaches. All rate models discussed in this section are listed in this table.

(Zhang et al., 1998) and (Yadav and Mewada, 2012) have used rate models based on power-law to establish the solvent effects on kinetic rate constants of cinnamaldehyde and acetophenone over Pd/C and Ag/OMS-2 catalysts, respectively. (Zhang et al., 1998) has established a difference between calculated activation energies in 2-propanol and toluene. Consequently, the lower activation barrier of cinnamaldehyde in 2-propanol compared with toluene was stated to be the reason behind the low observed reaction rate. On the other hand, (Yadav and Mewada, 2012) has concluded that the weak adsorption of acetophenone on catalyst surface using LHHW kinetic models has led the rate expressions to be simplified to power-law model. LHHW models were used in kinetic modelling of cinnamaldehyde, acetophenone, and benzaldehyde over Ru/C catalyst using hexane and 2-propanol to evaluate the values of measured adsorption coefficients with respect to these two solvents (Červený et al., 1996). The adsorption constants of substrates with respect to benzaldehyde in hexane were evaluated. Adsorptivity of substrates hydrogenated in both solvents increased in the sequence of benzaldehyde>cinnamaldehyde>acetophenone concluding that aldehydes were more strongly adsorbed on the catalyst when 2-propanol was used as solvent.

Table 2.6: Rate models previously applied to modelling heterogeneous hydrogenation of parallel-consecutive reactions in order to elucidate solvent effects

Rate model	Mechanistic details	References
$r = k_b[R]^n[H_2]^m$	- Power law model. - Pseudo first-order: n=m=1.	(Zhang et al., 1998) (Yadav and Mewada, 2012)
$r = \dfrac{k_b K_a[R]}{(1 + K_a[R] + \sum K_d[I])^n} \times \theta_H$	- Surface reaction is RDS - Competitive adsorption of organics. - Different modes of H_2 adsorption (θ_H) –refer to Table 2.5.	(Červený et al., 1996) (Wood et al., 2009)
$r = \dfrac{K_{a,b,c}[R]}{\left(1 + K_{a,c}[R]\right)}$	- Michaelis-Menton approach. - Lumped process constants in numerator and denominator.	(Gamez et al., 1998)

Table 2.6: Continued.

Rate model	Mechanistic details	References
$r = \dfrac{k_b' K_a[R]}{(1 + K_a[R] + \sum K_d[I])^n} \times \theta_H$ $k_b' = k_b e^{\alpha_1/\varepsilon}$	• Surface reaction is RDS. • Solvent effects included using transition state theory-Kirkwood treatment. • Inclusion of solvent dielectric constant into rate constant.	(Toukoniitty et al., 2003a) (Martin et al., 2013)
$r = \dfrac{k_b K_a[R]}{\left(1 + K_a[R] + \dfrac{[P]}{K_c}\right)^n}$	• Surface reaction is RDS • Product desorption term included which showed solvent type dependency.	(Mounzer et al., 2010)

Table 2.6: Continued.

Rate model	Mechanistic details	References
$r = \dfrac{k_b K_a [R]}{(1 + K_a[R] + \sum K_d[I])^n} \times \theta_{HS}$ $\theta_{HS} = \dfrac{\alpha\sqrt{K_H C_H}}{1 + \alpha\sqrt{K_H C_H}}$ $\alpha = exp\left(\dfrac{\mu^0_{H_2} \parallel no.\,solv - \mu^0_{H_2} \parallel solv}{2RT}\right)$	• Surface reaction is RDS. • Solvent effect on adsorption equilibrium constant of H_2.	(Singh and Vannice, 1999)
$r = \dfrac{k_b K_a [R]}{(1 + K_a[R] + K_s[S])^n} \times \theta_H$	• Surface reaction is RDS. • Assumes solvent adsorbs on catalyst surface and competes with organics.	(Kishida and Teranishi, 1968) (Lemcoff, 1977) (Chang et al., 2000) (Mikkola et al., 2001) (Mukherjee and Vannice, 2006a) (Bertero et al., 2008)

(Gamez et al., 1998) has investigated the kinetics of ethyl pyruvate hydrogenation in presence of Pt/Al$_2$O$_3$ in toluene, ethanol, and propylene carbonate (Table 2.6). The rate law based on Michaelis-Menten was proposed to evaluate the solvent effect on lumped adsorption kinetic in the denominator (Berg et al., 2002).

$$r = \frac{K_{a,b,c}[R]}{(1+K_{a,c}[R])} \tag{2.8}$$

It was found that in toluene the rate data approached zero order kinetics over early parts of the reaction due to high value of adsorption term $K_{a,c}$, despite the low values of ethyl pyruvate concentration used. In cases of ethanol and propylene carbonate, the values of $K_{a,c}$ were five and eight times lower than toluene, resulting in a positive apparent rate order over the range of concentrations studied. The difference between the adsorption terms in solvents were explained based on their solvating abilities for polar solute molecules.

Kinetics of solvent effects for enantioselective hydrogenations has also been the subject of various studies (Toukoniitty et al., 2003a) and (Martin et al., 2013). In order to elucidate the solvent effects through kinetic investigation, Kirkwood treatment and transition state theory were used (Laidler, 1987). This method constitutes the incorporation of dielectric constant and dipole moment into rate constants. The work of (Toukoniitty et al., 2003b) involved hydrogenation of 1-phenyl-1,2-propanedione over modified Pt/Al$_2$O$_3$ catalyst. No correlation of reaction rate with H$_2$ solubility and dielectric constant was established, however, the enantioselectivity was able to be modelled as a function of dielectric constant. On a similar note, (Martin et al., 2013) discovered that the initial hydrogenation rate of ethyl benzoylformate over modified Pt/Al$_2$O$_3$ correlates with dielectric constant in most solvents except for some proric solvents and solvents which exhibited strong interactions with catalyst surface. Again, no correlation with H$_2$ solubility was established in this work.

Another widely credited mechanism for elucidating the solvent effects is based on the work of (Singh and Vannice, 1999). The approach taken in this work for hydrogenation of benzene over Pd/η-Al$_2$O$_3$ was based on the hypothesis that fractional coverage of the hydrogen on catalyst active sites is influenced by the nature of the solvent. The solvent effect is incorporated into the surface coverage of the H$_2$ by correcting the value using chemical potential of the dilute gas ($\mu_{H_2}^O$) in different solvents as described by the following equations.

$$\theta_{HS} = \frac{\alpha\sqrt{K_H C_H}}{1+\alpha\sqrt{K_H C_H}} \tag{2.9}$$

$$\alpha = exp\left(\frac{\mu_{H_2}^O \| no.solv - \mu_{H_2}^O \| solv}{2RT}\right) \tag{2.10}$$

α denotes the equilibrium constant for the sums of the elementary steps that describe the dissociative adsorption of hydrogen on catalyst surface. It was shown that fractional coverage of hydrogen can increase with increasing hydrogen solubility through partial pressure of the gas and the use of liquid H$_2$ concentrations were recommended instead of partial pressures.

As documented in Table 2.6, the majority of the research carried out on the kinetics of solvent effects involves addition of a solvent adsorption constant into rate expression denominator. However, the solvent concentration was calculated using the linear relationship between the reactant and solvent. Doing this creates a mathematically high value over $K_{solv}C_{solv}$ in denominator thus creating a bias towards the K_{solv} value. A lumped adsorption value was suggested by (Mukherjee and Vannice, 2006a), constrained over a narrow range in order to fit the rest of the parameters. This resulted in satisfactory fits however narrowing the adsorption constants over a range was not statistically justified.

In order to account for the role of solvent in facilitating product desorption (Mounzer et al., 2010) has incorporated a product desorption term into the rate expressions. The findings of

this work are discussed in context with the kinetic investigations of solvent effects used in the current work in Chapter 5.

From the reviews above it is clear that majority of the kinetic work carried out so far in elucidating solvent effects cannot render mechanistic insights which can be categorized as systematic over wide range of solvents with varying physiochemical properties. Additionally, none of these works offer any universal explanation of chemo-selectivity in different solvents.

2.4.4 Overview of the modelling software

The modelling process was carried out using the kinetic package Athena Visual Studio V14.2 (W.E. Stewart), (W. E. Stewart, 2008). Athena offers an integrated environment for modelling, parameter estimation, model discrimination, and experimental design. The package has its own built-in DDAPLUS and GREPLUS solvers; hence no code for numerical integration needs to be written. The concentrations of compounds are considered as response values which are dependent on multiple reactions in our study resulting in a set of differential equations to be solved implicitly:

$$\frac{dy}{dt} = f(y, \beta) \tag{2.11}$$

Where y denotes model responses (organic concentration), β denotes to kinetic parameters and t denotes time.

The model parameters can be estimated by minimization of weighted sum of squares of residuals,

$$SS_{RES} = \sum_i^m \sum_j^n w_{i,j} (C_{i,j,obs} - C_{i,j,cal})^2 \tag{2.12}$$

or by using the Bayesian framework in which the probability of model M_k is calculated, which describes the observed data Y within the error space Σ, (W. E. Stewart, 2008), (Hsu et al., 2009),

$$p(M_k|Y,\Sigma) = \frac{L(Y,\Sigma|M_k).p(M_k)}{C} \tag{2.13}$$

where $p(M_k|Y,\Sigma)$ is the likelihood function which assesses the probability of the model response y generated by the model M_k (containing parameter vector β) and C denotes to normalization constant. The term $p(M_k)$ is prior distribution which accounts for prior knowledge of experimenter on boundary values of model parameters (e.g. a prior knowledge of activation energy being between 5-100 kJ mol^{-1} can be defined for the parameter) (W. E. Stewart, 2008), (Kopyscinski et al., 2012), (Box and Draper, 1965).

For multi-response parameter estimation, Athena uses a built-in GREPLUS solver to minimize the objective function $f(\beta)$ and calculate the maximum posterior probability of the parameter β and posterior distribution of the assumed model.

$$f(\beta) = (n_b + m_b + 1).ln|v(\beta)| \tag{2.14}$$

Where n is the number of responses, m is the number of events per response and $|v(\beta)|$ denotes to the determinant of the covariance matrix of responses (W. E. Stewart, 2008). Each element in covariance matrix is defined as

$$v_{ij}(\beta) = \sum_{u=1}^{n}[Y_{iu} - f_{iu}(\xi_u,\beta)].[Y_{ju} - f_{ju}(\xi_u,\beta)] \tag{2.15}$$

Where $f_{iu}(\xi_u,\beta)$ is the predicted value for response i and event u (Box and Draper, 1965). Simply each element of the matrix is sum of the product of the deviation of observed and predicted responses i and j. In a single response model the objective function leads to residual

sum of squares (RSS) and a system with four responses like this study results in the following matrix,

$$v(\beta) = \begin{bmatrix} v_{11} & v_{12} & v_{13} & v_{14} \\ v_{21} & v_{22} & v_{23} & v_{24} \\ v_{31} & v_{32} & v_{33} & v_{34} \\ v_{41} & v_{42} & v_{43} & v_{44} \end{bmatrix}$$

Where the index values i and j = 1, 2, 3, 4 represents PBN, PBL, CBN, CBL, respectively.

The GREPLUS solver based on Bayesian estimation approach is different from the DDAPLUS solver which is based on Newtonian algorithm to solve ODEs. The minimization of the objective function is achieved by quadratic programming starting from user's initial guess for parameters. In each iteration the objective function is approximated locally as a quadratic expansion, constructed from experimental data and models defined by user. This approximated function is consecutively minimized and when necessary the resulting step is shortened to ensure descent of the true function. These steps are repeated until a convergence criterion is met or maximum number of iterations is reached (W. E. Stewart, 2008), (Caracotsios, 2013).

To estimate parameter sensitivity the solver uses a direct coupled method,

$$B(t) = \frac{\delta y(t)}{\delta \beta} \tag{2.16}$$

$$\frac{\delta}{\delta \beta}\left(\frac{dy_i}{dt}\right) = \frac{d}{dt}B(t) = \frac{df}{dy_i} \cdot B(t) + \frac{df}{d\beta} \tag{2.17}$$

Where $B(t)$ denotes sensitivity function for each model response defined as a function of time which allows it to be solved alongside the main system ODEs, improving solver efficiency and robustness (Caracotsios and Stewart, 1985).

For repeated experiments the weighing factor can be calculated from the following equation,

$$w_{i,j} = \frac{1}{S_{i,j}^2} \qquad (2.18)$$

where $S_{i,j}^2$ is the error variance for repeated experiments under the same reaction conditions (j_{th}) of component i and can be calculated using the following expression,

$$S_{i,j}^2 = \frac{\sum_k^{n_{e,j}}(C_{i,j,k} - \bar{C}_{i,j})^2}{n_{e,j} - 1} \qquad (2.19)$$

with $C_{i,j,k}$ being molar concentration of component i for the j_{th} experimental condition (mol l⁻¹), $\bar{C}_{i,j}$ being average molar concentration of component i for the j_{th} experimental condition, and $n_{e,j}$ is the number of repeated experiments for the j_{th} experimental condition.

If no repeated experiments are performed for an experimental condition the weighting factor can be calculated by,

$$w_{i,j} = \frac{1}{C_i} \times 100 \qquad (2.20)$$

If no weighting factors are specified the software assumes it as one for all experimental points. Though it has previously been reported that Bayesian framework is more applicable to modelling the multi-response data (Hsu et al., 2009) both solvers were tested for our system and the convergence was proved to be the same for both. Consequently, nonlinear least square method (NLS) was chosen to carry out the rest of the modelling process. NLS also provides the user with a complete set of statistical parameters which were beneficial in model optimization.

2.5 Stirred tank reactors

2.5.1 Reactor design and scale-up

Stirred tank reactors (STRs) are commonly used in in industry for production of chemicals over a range of scales. They are used in processes requiring uniform profiles of component concentrations, temperature and physical properties (Paul et al., 2004). The most common reactor geometry is a round tank, with a dished bottom and top, which is somewhat taller than its diameter. This is to allow for a liquid height of approximately equal to the vessel diameter and allow for enough headspace for gas, inert gas, evolved gas, sparged gas, or foam in multiphase reactions (Patterson, 2005). A typical schematic of a stirred tank with important geometric parameters is given in Figure 2.2. The standard nomenclature for vessel dimensions is given below and they were used in design of experiments as discussed in Chapter 3 (Houson, 2011).

A comprehensive overview of the design parameters including the feeding position to enhance the gas to liquid mass transfer in fed-batch reactions, baffle design to enhance mixing efficiency, and impeller types can be found in the *Handbook of Industrial Mixing* (Paul et al., 2004).

- Power, P (W)
- Rotation rate, N (rev s^{-1})
- Volume, V (m^3)
- Fluid dynamic viscosity, μ_L (Pa.s)
- Fluid density, ρ_L (kgm^{-3})
- Impeller diameter, D, (m)
- Tank diameter, T, (m)
- Impeller width, W, (m)
- Fill height, H (m)
- Impeller clearance, C (m)
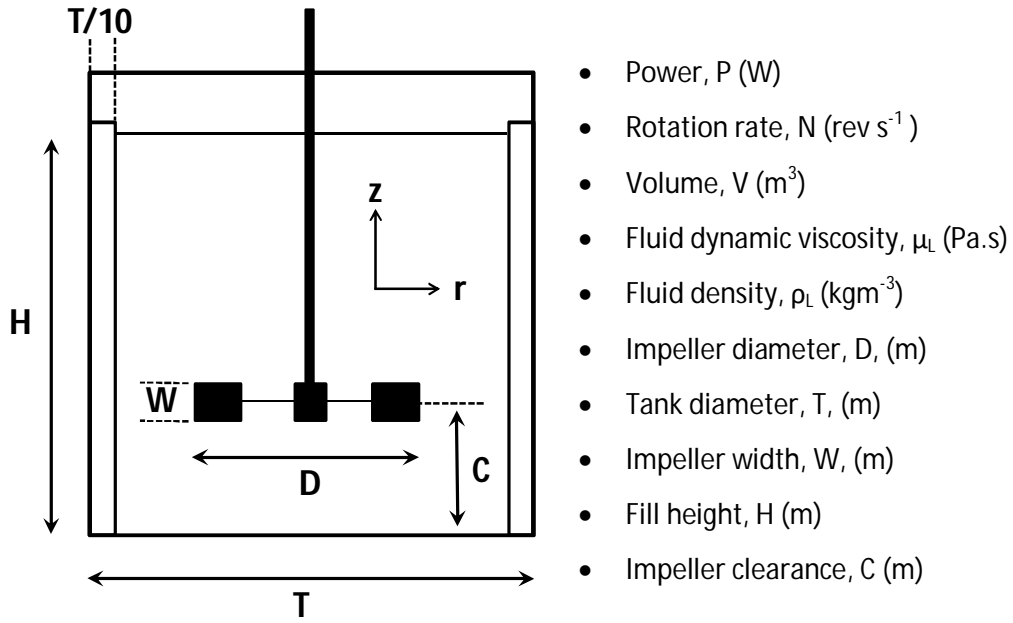
Figure 2.2: Schematic and characteristic dimensions of a cylindrical stirred tank; Taken from (Stitt and Simmons, 2011).

1. Impeller diameter/tank diameter: D/T ~ 0.3 – 0.5

2. Fill height / tank diameter: H/T ~ 1 for single impeller systems

3. Baffle width / tank diameter: ~ 0.1

4. Impeller clearance / tank diameter C/T ~ 0.2 – 0.25

The choice of impeller type is dependent on the type of process. Different impellers (radial and axial) are applicable in gas-liquid and gas-liquid-solid operations. The stirring power has been measured for a range of impeller locations, size relative to tank size, and baffle number and size in details by (Oldshue, 1983) and (Tatterson, 1991). The impeller power number, N_P, is given as follows:

$$N_P = P/\rho_L N^3 D^5 \tag{2.21}$$

Power number depends on the flow regime as defined by the dimensionless Reynolds number *Re*:

$$Re = \rho_L N D^2 / \mu_L \qquad (2.22)$$

For Re < 10 the flow regime is laminar and for Re > 2×10^4 the flow is turbulent. The values in between correspond to transitional flow regimes. For turbulent flows the power number is independent of Re and values for different impeller types are documented in (Paul et al., 2004). The total volumetric energy dissipation of impeller is then defined as:

$$\bar{\varepsilon}_T = P / \rho_L V \qquad (2.23)$$

The time required to achieve homogeneity by convective turbulence within STRs is defined as the mixing time. Evaluation of mixing times and its change in patterns during scale-up is of vital importance. The following correlations exist for STRs with H=T,

$$\theta_{m=}5.3\frac{N_P^{-1/3}}{N}\left(\frac{D}{T}\right) \qquad \text{(Nienow, 1997)} \qquad (2.24)$$

$$\theta_{m=}5.9T^{2/3}(\bar{\varepsilon}_T)^{-1/3}\left(\frac{D}{T}\right)^{-1/3} \qquad \text{(Ruszkowski)} \qquad (2.25)$$

For geometrically similar vessels (constant D/T), the following are applicable with regard to mixing time (Stitt and Simmons, 2011):

- $\theta_m N$ is constant for all impellers with same power numbers regardless of the impeller shape. This keeps the mixing time constant for scale-up routines which require constant N.

- At the same total power input per unit mass ($\bar{\varepsilon}_T$)
    - For a given tank size (T), all impellers result in the same mixing time.

- As a result upon scale-up at constant $\bar{\varepsilon}_T$ mixing time increases with tank size in $\theta_m = T^{2/3}$.

The choice of scale-up criterion can have drastic effects on mixing performance. The usual protocol involves the following criterion for scale-up procedures,

- Constant mixing time (constant N): $\frac{P_2}{P_1} = \left(\frac{V_2}{V_1}\right)^{5/3}$

- Constant turbulent mixing behaviour ($\bar{\varepsilon}_T$): $\frac{P_2}{P_1} = \left(\frac{D_2}{D_1}\right)^{3} = \left(\frac{V_2}{V_1}\right)$

- At constant heat transfer rate: $h_P \propto \bar{\varepsilon}_T^{2} T^{-1/9} \left(\frac{D}{T}\right)^{2/9}$

- Constant solid suspension: $N_{JS} \propto D^{-0.85}$, N_{JS} is the minimum impeller speed required on the onset of particle suspension from bottom of the tank calculated using Zwietering correlation (Zwietering, 1958).

Use of above criteria for scale-up of reactors from lab scale to plant is shown in Figure 2.3. This plots the ratio of $(\bar{\varepsilon}_T)_{(Plant)}/(\bar{\varepsilon}_T)_{(Lab)}$ versus V_{Plant}/V_{Lab}. Scaling up at constant mixing time would require 100 fold increase in power input for every 1000 times increase in in reactor volume rendering this criterion unfeasible unless the scale-up is very small. Scaling up at constant solid suspension, shear, and heat transfer rate causes decrease in $\bar{\varepsilon}_T$ on scale-up. In general, scale-up at constant $\bar{\varepsilon}_T$ is the better choice to ensure consistent flow regimes (Stitt and Simmons, 2011).
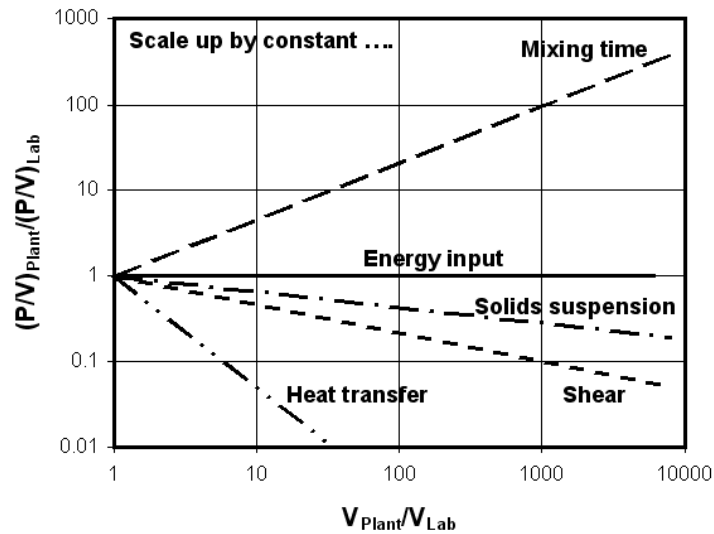
Figure 2.3: Scale-up diagram. Taken from (Stitt and Simmons, 2011).

However, different chemical systems would require different approaches to scale-up. Homogeneous systems usually pose no complications during scale-up since the rate-determining step is the reaction step and changing the scale does not alter this. On the other hand, when the overall rate of the reaction is not solely controlled by kinetics, multivariable problems could arise during scale-up that would require more detailed analysis. A general overview of the rate and selectivity issues for gas-liquid-solid systems is discussed here. One of the main challenges in multiphase systems is achieving good dispersion of gas when scaling up. During scale-up this becomes more difficult resulting in decline in volumetric gas-liquid mass transfer coefficient. This would directly affect the rate of reaction as limited gaseous reactant is available for reaction. As a result, deterioration in the rate of mass transfer needs to be fully considered during scale-up. The solid phase or catalysts can affect the rate and selectivity based on two key variables (Stitt and Simmons, 2011):

- Catalyst loading: Variations in catalyst loading can limit the exotherm generation rate and enable better temperature control on scale-up. in some cases, catalyst loading can also alter the selectivity of a reaction (Stitt and Simmons, 2011).

- Catalyst particle size: Particle size can significantly affect the reaction rate and selectivity. Three phase reactions are usually limited by intra-particle diffusion. Increasing the particle size alters the rate of reaction by lowering the "effectiveness factor" and can change the selectivity by changes in surface concentrations of reactants (Stitt and Simmons, 2011).

Scale-up of multiphase reactions can also be affected by sensitivity of a given chemistry to scale-up variables. This requires the use of robust kinetic models that can determine the dominant reaction routes in a given chemistry. Determination of robust kinetic models is essential in order to resolve the problems that can rise in reactions that run successfully in lab scale but require certain plant design requirement during scale-up. To the best knowledge of the author, this issue has never been addressed in literature.

As demonstrated in Chapter 4, the dominant reaction route of hydrogenation of the model reaction system chosen (4-phenyl-2-butanone) shifts when scaling the reactor from 100 mL to 3000 mL. With use of a systematic kinetic analysis it possible to determine the dominant reaction routes and monitor this shift during scale-up using limited kinetic data. As specified by (Patterson, 2005), scale-up of complex reaction systems continues to be based on combination of both experimental and simulation results. When chemical reaction rate constants are available, simulations would render more reliable results. As a result, the shifts in dominant reaction routes during scale-up that impact the rate and adsorption constants need to be determined for a successful simulation. The findings of Chapter 4 address this gap in the literature.

2.5.2 External and internal mass transfer limitations

In gas-liquid-solid reaction systems, where the catalyst is solid particle/pellets and reactants are in gas and liquid phase, the gaseous reactant needs to first diffuse from the gas phase to the liquid and then to the catalyst surface and ultimately through the catalyst pores to adsorb and participate on surface reactions. The gas to liquid and solid to liquid mass transfer can be schematically described as presented in Figure 2.4.
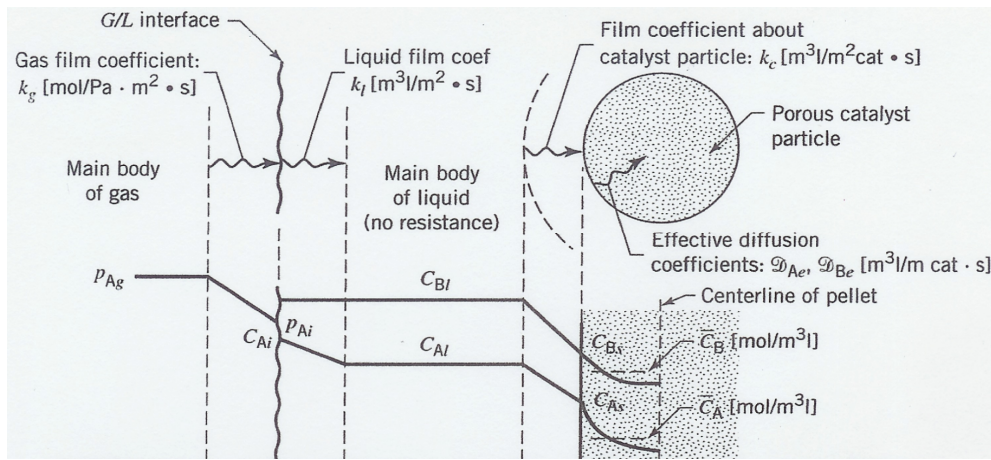
Figure 2.4: Gas concentration profile under mass transfer resistances (Levenspiel, 2006).

For solid-liquid mass transfer the overall transfer rate is defined by the volumetric gas-liquid mass transfer coefficient, K_{LA} (Stitt and Simmons, 2011).

$$R = K_L a (C^* - C) \qquad (2.26)$$

whre C^* is the concentration in the gas phase and C is the concentration in bulk liquid, and a is the interfacial area of gas per unit volume ($m^2\ m^{-3}$) defined as

$$a = \frac{6\varphi}{d_{32}} \qquad (2.27)$$

Experimental evaluations of $K_L a$ can be done by using a physical adsorption method, as described by (Dietrich et al., 1992). In the current study the 100 mL reactor used by Queen's University Belfast (details in Chapter 3) is of gas-inducing type (GIR). In GIRs, holes are machined on hollow shaft of the reactor and are located in gas and liquid phase. Angular velocity of the impeller then induces a pressure drop between the top and the bottom of the shaft, introducing the gas into the liquid phase. The 3000 mL reactor used for scale-up experiments by University of Birmingham is a surface aeration reactor (SAR), where the impeller provides the mixing and gas adsorption into the liquid phase. The hydrodynamics and mass transfer parameters are usually different with these two systems. Almost all the literature correlations available for prediction of $K_L a$ in agitated reactors are dependent on the system and/or operational conditions. (Lemoine et al., 2003) (Lemoine and Morsi, 2005) has done extensive research in gathering these correlations to develop empirical and back-propagation neural network (BPNN) correlations to predict the $K_L a$ for any given reactor system. For our purpose of the study however, relevant correlations for $K_L a$ values of H_2 in hexane (Chapter 4) were determined for SAR and GIR reactor as follows,

$$Sh = 3 \times 10^{-4} Re^{1.45} Sc^{0.5} We^{0.5} \quad \text{(GIR) (Dietrich et al., 1992)} \tag{2.28}$$

- H=T
- Correlations suggested by (Chang et al., 1991), (Chang and Morsi, 1991), and (Chang and Morsi, 1991) were also investigated for GIR reactor. All correlations rendered gas-liquid effectiveness factor (η_{G-L}) values of > 0.99.

$$Sh = 51.7 \times 10^9 Re^{-1.12} Fr^{2.20} (1 - W_s)^{4.31} \quad \text{(SAR) (Mizan, 1992)} \tag{2.29}$$

- 0.992<Fr<2.073
- 67,100<Re<1,643,000

- $0 < W_s < 30$

The rate of solid-liquid mass transfer (R) can be characterized using solid-liquid mass transfer coefficient, K_{SL},

$$R = K_{SL} a_P (C_s - C) \tag{2.30}$$

where C_s is the concentration at solid surface, and C is the concentration in the bulk liquid, and a_p is the interfacial area of solid per unit volume ($m^2 \ m^{-3}$) defined as

$$a_P = \frac{6\varphi}{d_P} \tag{2.31}$$

where φ is the solid volume fraction in reactor (Stitt and Simmons, 2011). Solid-liquid mass transfer can be predicted using a modified *Froessling equation* for $N = N_{JS}$ (Chapman et al., 1983).

$$Sh = 2 + 0.72 Re_P^{1/2} Sc^{1/3} \tag{2.32}$$

The absence/presence of mass transfer limitations for this work were determined by use of dimensionless Carberry number (Ca) details of which are discussed in context with the results in Chapter 4.

Chapter 3: Materials and methods

Introduction

This chapter summarises the materials and methods used for experiments done by QUB and the author of this thesis. The catalysts used were described along with preparation method, and characterization for gathering physical properties of each catalyst. An overview of the reactor set-up used for both 100 mL and 3000 mL scale experiments is presented. Additionally, full lists of experiments done by author of this thesis in 3000 mL reactor are listed. The breakdown of experiments done provided by QUB can be found in Appendix A (Table A.1 and Table A.2).

3.1 Materials

This section introduces the materials used throughout this work including catalysts, substrate, and solvents.

3.1.1 Catalysts

Two catalysts were used in this study.

- A bespoke P25 4% platinum on titania (Pt/TiO$_2$) manufactured in Johnson Matthey Technology Centre by *Dr. H. Daly* from Queens University of Belfast (QUB).
- An industry standard 5% platinum on silica (Pt/SiO$_2$) supplied by Johnson Matthey (Product Nu # 11000.SPR1-5).

The catalyst preparation procedure of the bespoke catalyst and the characterisation of both are described below. The P25 4% Pt/TiO$_2$ was chosen because preliminary reaction results by

QUB showed unusual solvent effects and further experiments were done using standard Pt/SiO$_2$ catalyst for comparisons of support effect.

3.1.2 P25 4% Pt/TiO2 catalyst preparation

P25 4% Pt/TiO$_2$ catalyst was prepared using incipient wetness impregnation technique using platinum nitrate solution (assay 16.07%, Johnson-Matthey, UK), as platinum precursor. 1.24 mL platinum nitrate solution (0.2 g platinum) was diluted with enough demineralized water to give the 4 wt% platinum loading and a solution of equal volume corresponding to the total pore volume of the support. After impregnation, the catalyst was dried at 393 K for 12 hours followed by calcination in air at 773 K for 4 hours. Before use, the catalyst was sieved into size fraction of < 100 µm.

3.1.2.1 Catalyst characterisation

Physical properties of the Pt/TiO$_2$ and Pt/SiO$_2$ catalysts are listed in Table 3.1. Some of the properties measurements were carried out by Iain McManus and Eihmear Connor at QUB (marked in the table) as well as the data obtained by the author. The density of the particles was determined using Helium Pycnometer (Micrometrics AccuPyc II 1340); porosity by Mercury Porosimetry (Micrometrics AutoPore IV); particle size distributions by Mastersizer (Malvern 2000); and Nitrogen Physisorption Analyzer was used (Micrometrics ASAP 2010) to acquire BET surface areas using N$_2$ as adsorbent at 77 K. The physical information of catalysts was used for mass transfer calculations in Chapter 4.

Table 3.1: Physical properties of catalysts.

Properties	P25 4 wt% Pt/TiO$_2$	5 wt% Pt/SiO$_2$
Particle density (kg m^{-3})	3570	2320
BET surface area (m^2 g^{-1})	QUB: 51.20 UBir: 45.98	QUB:294* UBir: 245
Support BET surface area* (m^2 g^{-1})	57.74	310
Porosity %	80.05	1
Pt metal dispersion* %	2.91	3.82
Average pore diameter (nm)	59.4	55.8
d$_{32}$ for $\leq 60\,\mu m$, 3000 ml (μm)	3.256	23.62
d$_{32}$ for $\leq 45\mu m$, 100 ml* (μm)	3.636	21.44

*Provided by QUB.

3.1.3 Reagent and Solvents

All chemicals and solvents used in the current study for 100 mL and 3000 mL scale experiments are presented in Table 3.2 and Table 3.3, respectively. For the purpose of the current study solvents of more than 99% purity were used to minimize the effect of impurities.

Table 3.2: Chemicals and solvents used in 100 mL scale reactions.

Material	Supplier	Specification (grade)
Benzylacetone	Sigma Aldrich	HPLC
Hexane	Sigma Aldrich	HPLC
Heptane	Sigma Aldrich	HPLC
Deacene	Sigma Aldrich	HPLC
Octane	Sigma Aldrich	HPLC
Cyclohexane	Sigma Aldrich	HPLC
Dichloroethane	Riedel De Haën	99%
1-propanol	Sigma Aldrich	HPLC
Methanol	Sigma Aldrich	HPLC
Ethanol	Sigma Aldrich	HPLC
1-pentanol	Sigma Aldrich	HPLC
1-octanol	Sigma Aldrich	HPLC
1-butanol	Sigma Aldrich	HPLC
2-propanol	Fluka	$\leq 99.9\%$
2-butanol	Sigma Aldrich	HPLC
2-octanol	Sigma Aldrich	HPLC
2-pentanol	Sigma Aldrich	HPLC
Trifluoroethanol	Fluorochem	99%
Hexanol	Sigma Aldrich	HPLC

Table 3.2: Continued.

Material	Supplier	Specification (grade)
Tert-butyl alcohol	Sigma Aldrich	HPLC
Toluene	Sigma Aldrich	HPLC
p-Xylene	Fluka	≥98%
m-Xylene	Sigma Aldrich	HPLC
t-butyl toluene	Sigma Aldrich	HPLC
Diethyl ether	Sigma Aldrich	HPLC
Dibutyl ether	Sigma Aldrich	HPLC
1,4-dioxane	Sigma Aldrich	HPLC
Ethyl acetate	Sigma Aldrich	HPLC

Table 3.3: Chemicals and solvents used in 3000 mL scale experiments.

Material	Supplier	Specification (grade)
Benzylacetone	Sigma Aldrich, UK	98+% purity (ACS)
Hexane	Sigma Aldrich, Ge	99+% purity (ACS)
Heptane	Sigma Aldrich, UK	99+% purity (ACS)
Ethanol	VWR, UK	99+% purity
1-propanol	Sigma Aldrich, UK	99+% purity (ACS)
2-pentanol	Alfa Aeser, UK	99+% purity
Cyclohexanol	Alfa Aeser, UK	99+% purity
Tert-butyl alcohol	Alfa Aeser, UK	99+% purity
t-butyl toluene	Sigma Aldrich, UK	99+% purity (ACS)
Diethyl ether	Sigma Aldrich, UK	99+% purity (ACS)
1,4-dioxane	Alfa Aeser, UK	99+% purity
Ethyl acetate	Alfa Aeser, UK	99+% purity

3.2 Experimental Apparatus

All lab scale experiments were carried out in Queen's University of Belfast (QUB) by *Iain McManus* and *Eihmear Connor*. The author of this thesis is thankful to QUB for kindly providing us with the data for comparison and modelling. All the descriptions regarding catalyst synthesis and reaction procedures at 100 mL scale are reported as was provided by QUB.

3.2.1 100 mL scale reactor set-up

Experiments done by QUB were carried out in a 50-100 ml (T = 40 mm) stainless steel autoclave manufactured by H.E.L. Group. The schematic diagram of the reactor is presented in Figure 3.1. The reactor is equipped with a heating/cooling coil, thermocouple, and a sampling line located in impeller region. The mixing is achieved by a 24 mm (D/T = 0.6) 6-blade gas inducing radial impeller placed 10 mm (C/T = 0.25) from the bottom of the reactor. The gas is introduced to the liquid from head space through a single inlet on the hollow shaft located 71 mm from top of the impeller outlets. The autoclave is also equipped with a baffle cage with length and width of 80 mm and 3 mm, respectively. During experiments gas uptake, temperature and pressure are monitored and logged by relevant PC software. The reactor was operated in a semi-batch mode. For all experimental reactions the reactor was filled with 50 mL of solvent resulting in fill height (H) of 110.5 mm.
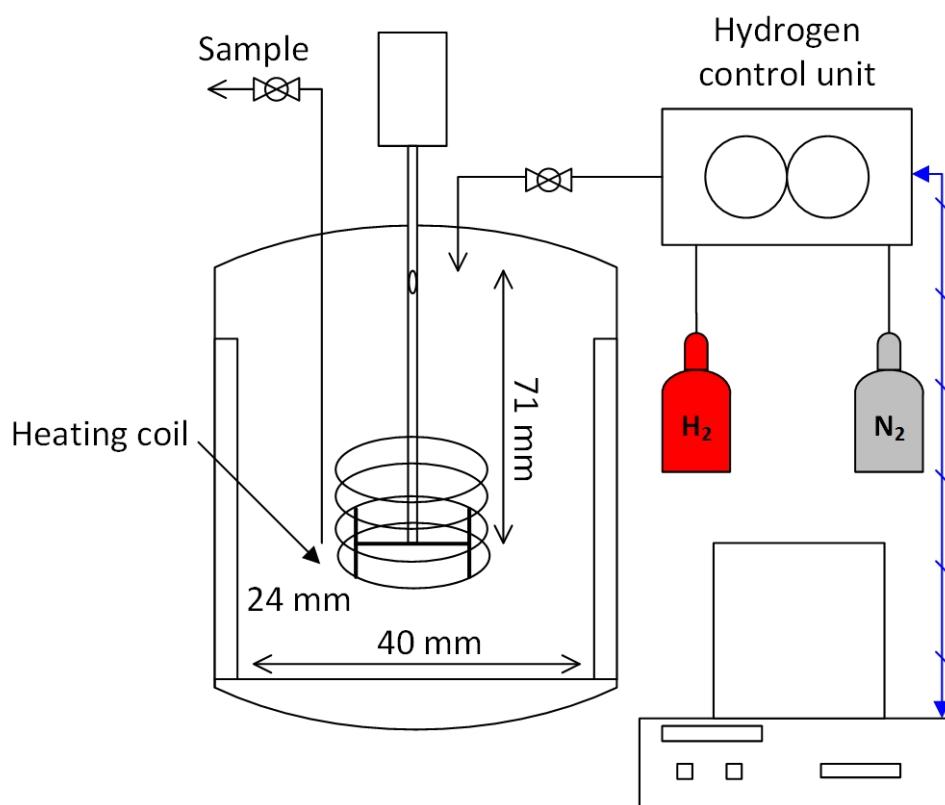
Figure 3.1: Schematic diagram of the 100 mL reactor.

3.2.2 3000 mL reactor set-up

Experiments done by the author of this thesis were carried out in a 3000 mL (T = 150 mm) stainless steel "dead-end" reactor as shown in Figure 3.2 and 3.3. The reactor was equipped with a heating jacket, thermocouple, and pressure transducer. The mixing was achieved by a 6-blade Rushton Turbine (D/T = 0.5) operating in surface aeration mode which was placed at third of the height of the reactor (C/H = 1/3). The design of experiments were done to establish fill height of equal to reactor diameter (H=T) resulting in the total gas hold-up of 11.6 %.

The energy input for reactions in base conditions was adjusted based on an industrially acceptable value. This will be thoroughly discussed in further sections (§3.3). Gas was introduced from the bottom of the reactor to maintain the desired head pressure and samples

were taken through the same line using a two way valve used to switch between gas input and reactor discharge. This reactor was equipped with stroboscope for in-situ bubble size measurements using online video-microscope system. Preliminary experiments were done to determine of bubble size measurement along the catalytic reactions in different solvents. However, due to size of catalysts used (< 100 μm) the images taken were too opaque for image analysis.
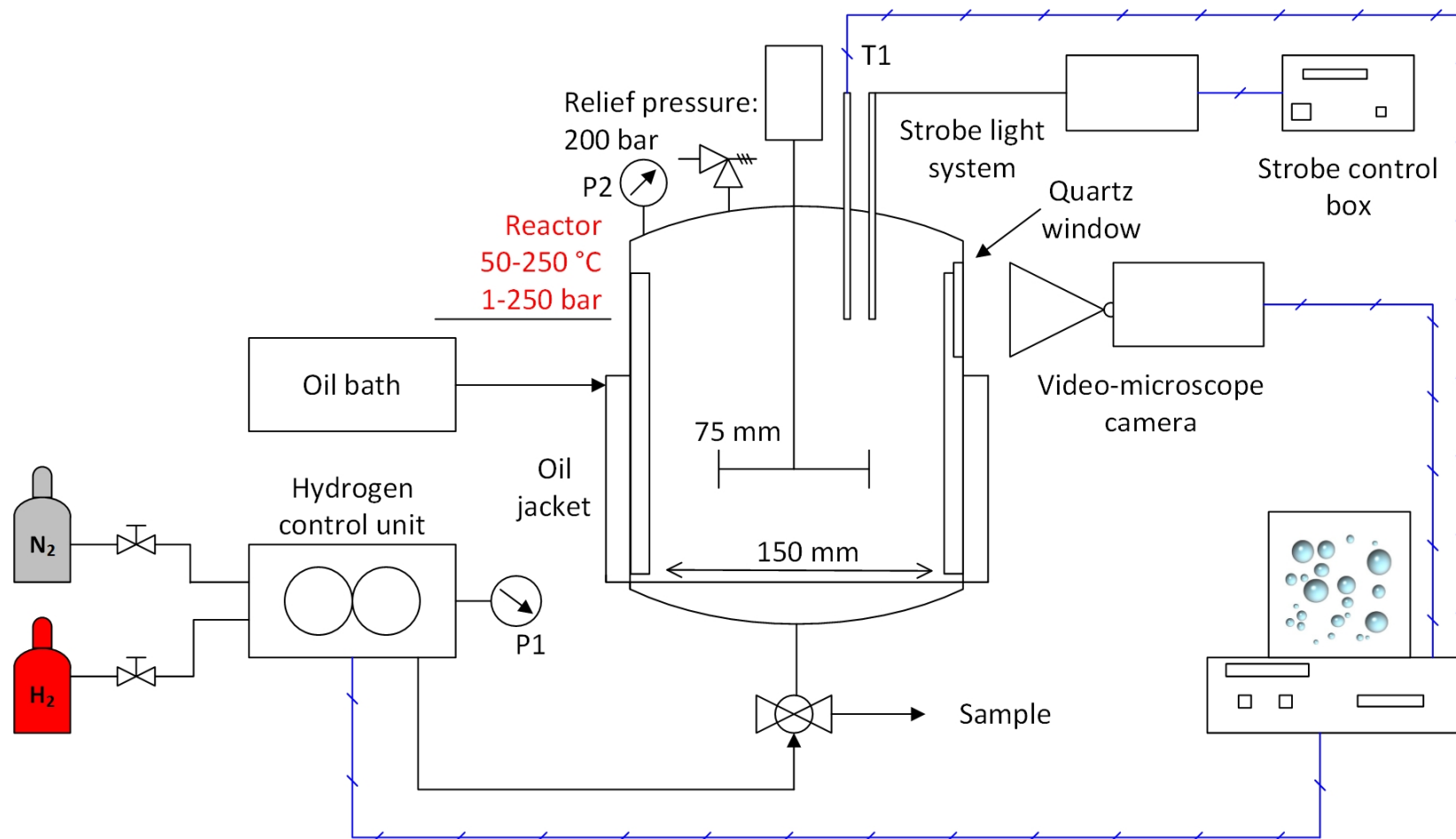
Figure 3.2: Schematic diagram of the 3000 mL reactor.

T1	P1, P2	Mass flow controller
Thermocouple (1/8")	Pressure gauge, digital transducer	Supplied by Hydrogen Control Unit (HCU)
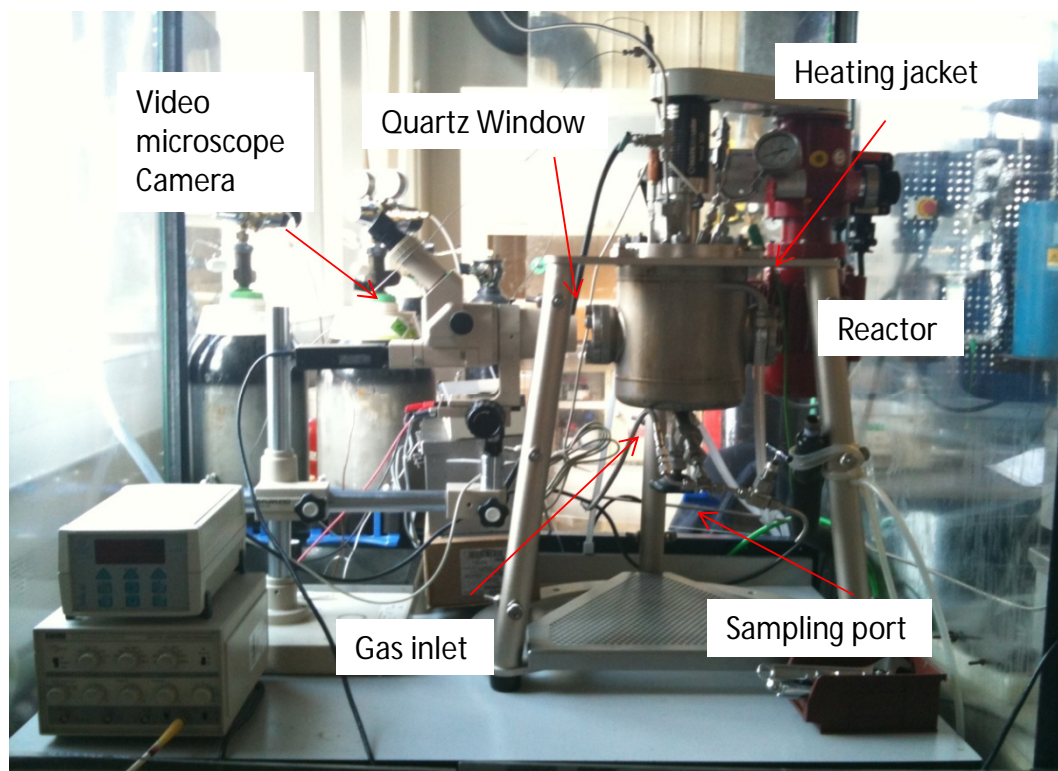
Figure 3.3: 3000 mL reactor used for UOB experiments.

3.3 Choice of energy input for base condition

In order to investigate the gas dispersion in reactors at different energy inputs and determine critical aeration speed, a visual investigation was carried out in replica glass reactors made with the same dimensions as reactors used for hydrogenation experiments. As stated before, 100 mL reactor was equipped with a gas-inducing radial/turbine impeller and 3000 mL reactor was equipped with a Rushton turbine impeller operating at surface aeration mode. The reactors were filled with the same amount of hexane used in catalytic reactions (100 mL reactor: 50 mL solvent; 3000 mL reactor: 2550 mL solvent). The same impeller used for 100 mL scale experiments was provided by QUB for this experiment and similar impeller speeds as reaction conditions were tested (Figure 3.4). A hollow shaft and a solid shaft were used to compare the on-set of gas induction between surface aeration and impeller gas induction for

100 mL reactor. It was observed that for impeller speeds less than 1100 rpm, no gas dispersion was observed and at higher energy inputs it is hard to distinguish between surface aeration and gas induction. It should be noted that these observations were done under atmospheric conditions (Figure 3.4).

For 3000 mL reactor, the agitation speed was increased slowly to make an estimation of the critical aeration speed (N_{CRE}) by using the visual method suggested by (Patwardhan and Joshi, 1998). Critical impeller speed or onset of surface aeration is the speed at which gas bubbles start to get entrapped at the surface (Patwardhan and Joshi, 1998). Figure 3.5 demonstrates the visual assessment of N_{CRE}. N_{CRE} was established to be approximately 320 rpm. The speed was then increased up to 1100 rpm and the images taken are shown in Figure 3.6. As it is illustrated below the reactor was fully dispersed from energy input of 3.5 W kg^{-1} onward. Consequently, it was initially chosen as the base energy input for scale-up experiments to ensure the presence of mass transfer limitations for scale-up studies. However, as going to be discussed in Chapter 4 (§4.3.1, §4.3.2), for reaction of PBN over Pt/TiO$_2$ catalyst and hexane as solvent, the selectivity profiles are independent of energy input and H$_2$ partial pressure. Additionally, the mass transfer assessment concluded no presence of external/internal mass transfer limitations for H$_2$ and PBN (§4.5.1). The hydrodynamic performance of gas-inducing and surface-aerating impellers is reviewed in Chapter 2 (§2.5.2)
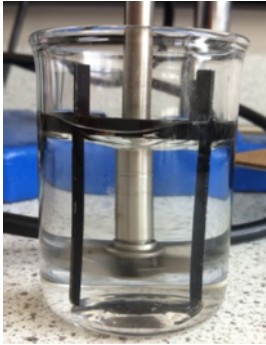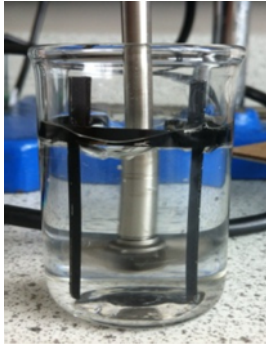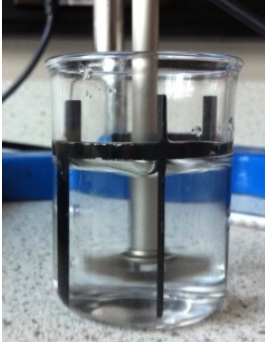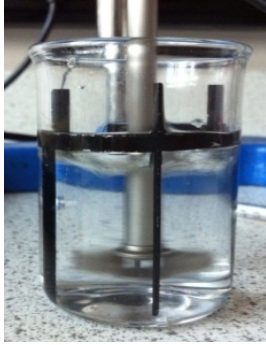
Gas induction through hollow shaft			
Gas induction through surface aeration			
500 rpm $\bar{\varepsilon}_T \sim 0.5$ W kg^{-1}	800 rpm $\bar{\varepsilon}_T \sim 2.0$ W kg^{-1}	1100 rpm $\bar{\varepsilon}_T \sim 5.0$ W kg^{-1}	1400 rpm $\bar{\varepsilon}_T \sim 10.0$ W kg^{-1}

Figure 3.4: Mixing behaviour of 100 mL reactors with increasing power input using hollow and solid shafts.
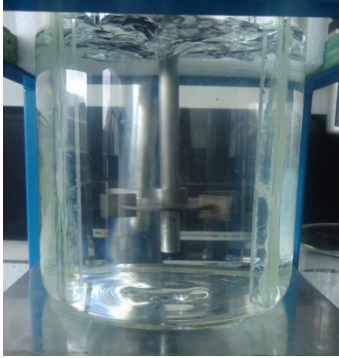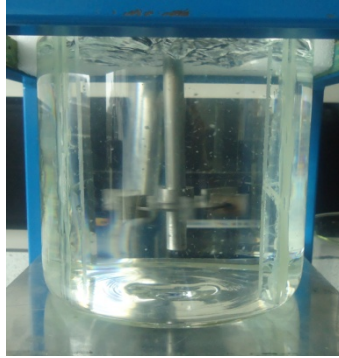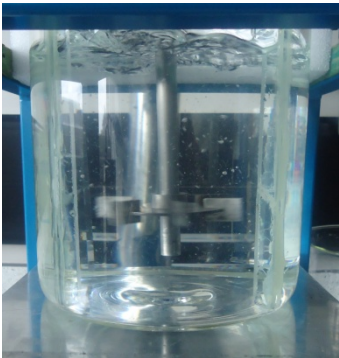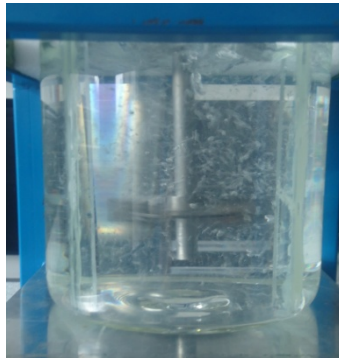
N < 260 rpm	N ~ 270	N ~ 280
$\bar{\varepsilon}_T$ < 0.36 W kg^{-1}	$\bar{\varepsilon}_T$ ~ 0.41 W kg^{-1}	$\bar{\varepsilon}_T$ ~ 0.46 W kg^{-1}
None: No bubble formation.	Negligible: Less than five bubbles and in clusters.	Very low: several bubbles form in clusters and specific regions.
N ~ 300	N_{CRE} ~ 320	N > N_{CRE}
$\bar{\varepsilon}_T$ ~ 0.56 W kg^{-1}	$\bar{\varepsilon}_T$ ~ 0.68 W kg^{-1}	$\bar{\varepsilon}_T$ < 1.0 W kg^{-1}
Low: bubbles break away from clusters but still at low density.	Onset: increased density of bubbles throught the tank.	High: very high density of bubbles, violent movement of liquid surface, noise, and splashing.

Figure 3.5: Estimation of the critical aeration speed through surface aeration for 3000 mL scale reactor.

| 550 rpm | 700 rpm | 980 rpm | 1100 rpm |
| $\bar{\varepsilon}_T \sim 3.5$ W kg^{-1} | $\bar{\varepsilon}_T \sim 7.0$ W kg^{-1} | $\bar{\varepsilon}_T \sim 15.0$ W kg^{-1} | $\bar{\varepsilon}_T \sim 20.0$ W kg^{-1} |
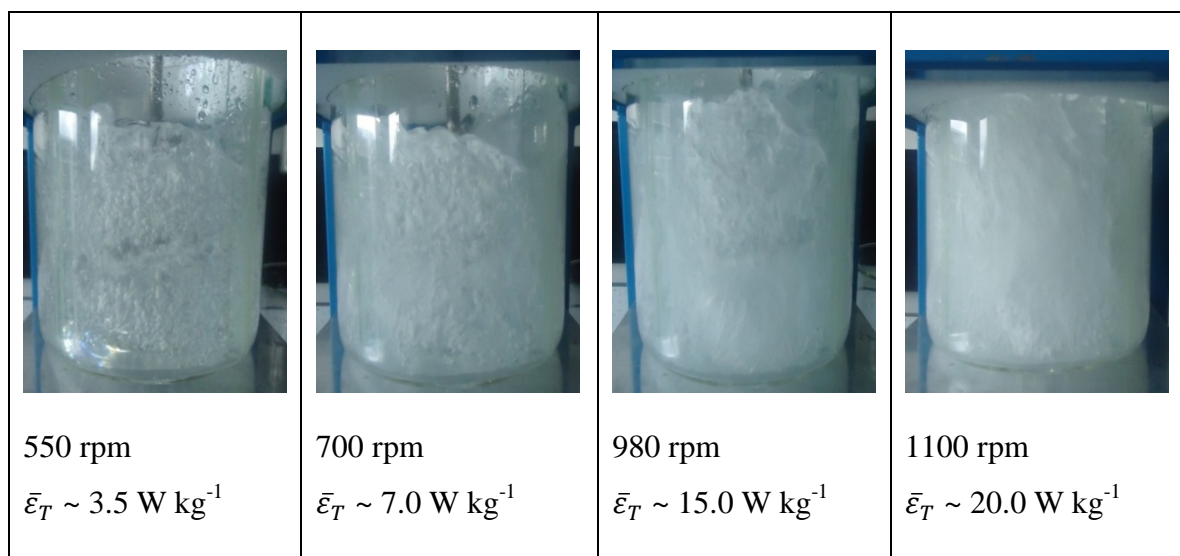
Figure 3.6: Visual assessment of flow intensity for impeller speeds used in catalytic hydrogenation of PBN.

3.4 Hydrogenation reaction procedures

3.4.1 Catalytic hydrogenations in 100 mL reactor (base conditions)

3.4.1.1 Catalyst reduction

For the reactions using Pt/TiO$_2$ catalyst, the reactor was charged with catalyst (0.1 g) along with 30 mL of solvent and was sealed and purged in discrete intervals of three to five times with high pressure H$_2$. The mixture was then heated to 333 K while stirring at 800 rpm (2 W kg^{-1}). Once the required temperature had been reached, the reactor was held at this temperature allowing the catalyst to reduce for 1 hr. under 1 bar of H$_2$ and 1000 rpm (4.7 W kg^{-1}). The choice of reduction temperature was made based on Temperature Program Reduction (TPR) measurements done by QUB. The Figure 3.7 represents the TPR profile provided by QUB. Methodology involved heating catalyst at 5 K min^{-1} from 268-1073 K under 5% H$_2$ in argon. Hydrogen uptake was monitored by a Thermal Conductivity Detector

96

(TCD). Based on the TPR profile, two peaks at 258 K and 313 K were observed. The reduction if catalyst was done at 333 K to ensure Pt reduction only and avoid strong metal support interactions (SMSI) which are the result of support reduction at temperatures higher than 573 K.
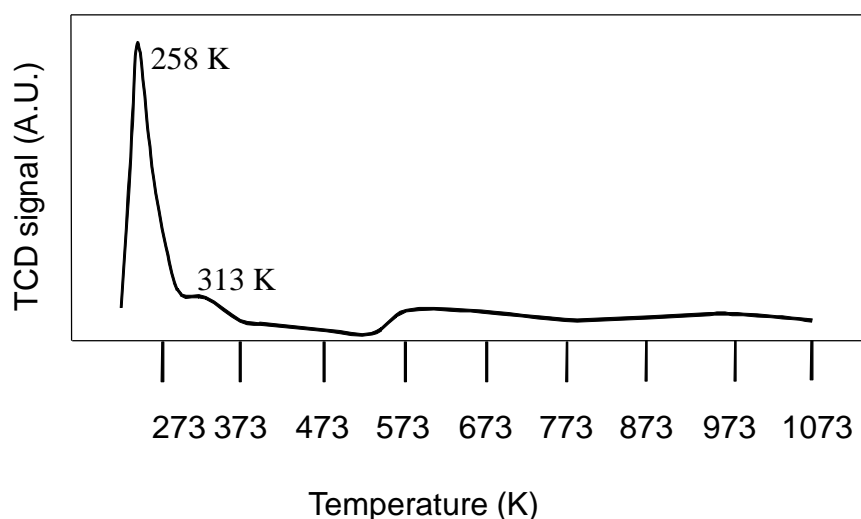
Figure 3.7: TPR profile of fresh Pt/TiO2 catalyst; provided by QUB.

For the reactions with Pt/SiO_2, the reduction step made no difference to the overall rate of reaction rate and selectivity as stated by QUB. Consequently, experiments were started without any catalyst pre-reduction.

3.4.1.2 Reaction procedures (Base condition)

After reduction, the reactor was left to cool down; then 4-phenyl-2-butanone (2 g) and an additional 20 ml of solvent were added to the reactor. The reactor was resealed and purged with H_2 again. The reaction mixture was stirred at 800 rpm (2 W kg^{-1}) while heating to 343 K. Once the desired temperature was obtained, the reactor was pressurised to 5 bar H_2 and quickly the impeller speed was set to 1400 rpm (10.0 W kg^{-1}). The first sample was taken as

soon as the impeller speed was set. The samples of approximately 2 mL were taken from the reactor and experimental runs were monitored for 2 hr. Sampled taken were then loaded to an off-line Gas Chromatogram for analysis. After each experiment reactor was washed with acetone at high temperature.

3.4.2 Catalytic hydrogenations in 3000 mL reactor

3.4.2.1 Catalyst reduction

For the reactions using Pt/TiO_2, the reactor was charged with catalyst (5 g) along with 2550 mL of solvent. The reactor was then sealed and purged continuously with N_2 for one minute which was recommended by reactor manufacturer to be sufficient for purging every litre of headspace. The mixture was heated to 333 K while stirring at 250 rpm (0.34 W kg^{-1}). Once the required temperature had been reached, the reactor was held at this temperature allowing the catalyst to reduce for 1 hr. under 1 bar of H_2 and 1000 rpm (21.5 W kg^{-1}).

For the reactions with Pt/SiO_2, experiments were started without any catalyst pre-reduction. However, experiments in 2-propanol, hexane, and ethanol were repeated with catalyst reduction at 333 K and 1 bar H_2 for comparisons.

3.4.2.2 Reaction procedures (Base condition)

After catalyst reduction the reactor was left to cool down; then 100 g of PBN was added to the reactor and it was resealed and purged with N_2. The scale-up experiments were conducted keeping the same PBN initial concentration and reagent/catalyst ratio as the 100 mL scale experiments. The reaction mixture was stirred at 250 rpm (0.53 W kg^{-1}) while heating to 343 K. Once the desired temperature was attained, the reactor was pressurised to 5 bar H_2 and

quickly the impeller speed was set to 550 rpm (3.5 W kg^{-1}). The first sample was taken as soon as the impeller speed was set. The samples of approximately 2-3 mL were taken from the reactor while monitoring each run for five to six hr. and loaded to an off-line Gas Chromatogram for analysis (§3.6.1). After each experiment the reactor was washed with 4% v/v Decon-water at 343 K for 1 hr. and left to dry overnight. Preliminary experiments using ex-situ catalyst reduction, and different washing agents (acetone and 2-propanol at 343 K) showed no rate and selectivity effects in base conditions. The possibility of catalyst deactivation was ruled out by monitoring the mass balances. No traces of hydrocarbon fragments (CO, benzene, toluene, and methane) were observed in GC analysis of reactions.

3.5 Reaction conditions

This section summarises the operational conditions for experiments carried out at 3000 mL scales. For 100 mL scale, the details of reaction conditions are disclosed in Appendix A.

3.5.1 Reactions using 4% P25 Pt/TiO$_2$

The Pt/TiO$_2$ catalyst was used to investigate the effect of scale-up upon rate and selectivity of PBN hydrogenation in hexane. Hexane was chosen for initial scale-up comparisons due to high rate of reaction observed in 100 mL scale experiments (§5.2.1). The parameters investigated were agitation speed, H$_2$ partial pressure, temperature, catalyst loading, and initial substrate concentration.

Further reactions in 100 mL scale were done in a range of solvents comprising of protic, aprotic polar, apolar, ethers, aromatics and halogenated solvents. In order to investigate the effect of solvents upon scaling-up to 3000 mL, four solvents from 100 mL scale were chosen

from each class which showed the highest reaction rates (2-propanol, 1-propanol, diethyl ether, hexane, and t-butyl toluene).

3.5.2 Reactions using 5% Pt/SiO$_2$

The Pt/SiO$_2$ catalyst was chosen to compare the rate and selectivity of PBN in different solvents with respect to the support. The 100 mL scale data covered a range of solvents comprising of alkanes, alcohols, and aromatics. The 3000 mL scale experiments were done in six of the same solvents used in 100 mL scale experiments and five others with increasing alcohol chain length. Table 3.4 and Table 3.5 represent range of conditions and solvents used in 3000 mL scale experiments.

Table 3.4: Experimental conditions of PBN hydrogenation over Pt/TiO$_2$ in 3000 mL reactor.

Run	Initial Conc. (mol)	Catalyst mass (g)	Press. (bar)	Energy input (W kg^{-1})	Temp. (K)	Solvent
Varying catalyst mass m$_{cat}$ (g)						
1	0.270	0	5	3.5	343	Hexane
2	0.270	2	5	3.5	343	Hexane
3	0.270	5	5	3.5	343	Hexane
4	0.270	7	5	3.5	343	Hexane
5	0.270	15	5	3.5	343	Hexane
Varying pressure P$_T$ (bar)						
6	0.270	0.10	2	3.5	343	Hexane
3	0.270	0.10	5	3.5	70	Hexane
7	0.270	0.10	10	3.5	70	Hexane
Varying energy input $\bar{\varepsilon}_T$ (W kg^{-1})						
8	0.270	0.10	5	1.5	343	Hexane
3	0.270	0.10	5	3.5	343	Hexane
9	0.270	0.10	5	7.0	343	Hexane
10	0.270	0.10	5	20	70	Hexane
Varying Temperature T (K)						
11	0.270	0.10	5	10	313	Hexane
12	0.270	0.10	5	10	323	Hexane
13	0.270	0.10	5	10	333	Hexane
3	0.270	0.10	5	10	343	Hexane
14	0.270	0.10	5	10	353	Hexane
Varying initial PBN concentration C$_i$ (mol L^{-1})						
15	0.132	0.10	5	10	343	Hexane
3	0.270	0.10	5	10	343	Hexane
16	0.397	0.10	5	10	343	Hexane
Varying Solvents						
3	0.270	0.10	5	3.5	343	Hexane
17*	0.270	0.10	5	3.5	343	Hexane
18	0.270	0.10	5	3.5	343	2-propanol
19*	0.270	0.10	5	3.5	343	2-propanol
20	0.270	0.10	5	3.5	343	1-propanol
21	0.270	0.10	5	3.5	343	t-butyl toluene
22	0.270	0.10	5	3.5	343	Diethyl ether

*catalyst was not reduced prior to reactions.

Table 3.5: Experimental conditions of PBN hydrogenation over Pt/SiO$_2$ in 3000 mL reactor.

Run	Initial Conc. (M)	Catalyst mass (g)	Press. (bar)	Energy input (W kg^{-1})	Temp. (K)	Solvent
				Varying Solvents		
1	0.270	0.10	5	3.5	343	Hexane
2*	0.270	0.10	5	3.5	343	Hexane
3	0.270	0.10	5	3.5	343	Heptane
4	0.270	0.10	5	3.5	343	2-propanol
5*	0.270	0.10	5	3.5	343	2-propanol
6*	0.270	0.10	5	3.5	343	2-propanol
7	0.270	0.10	5	3.5	343	1-propanol
8	0.270	0.10	5	3.5	343	Ethanol
9	0.270	0.10	5	3.5	343	2-pentanol
10	0.270	0.10	5	3.5	343	2-m-2-propanol
11	0.270	0.10	5	3.5	343	Cyclohexanol
12	0.270	0.10	5	3.5	343	Ethyl-acetate
13	0.270	0.10	5	3.5	343	t-butyl toluene
14	0.270	0.10	5	3.5	343	Diethyl ether

*Catalyst was reduced prior to reactions.

3.6 Analytical Methods

3.6.1 Gas chromatograph

All the 100 mL scale experimental data were provided as calculated concentrations or with calibration curves.

A Varian CP-3380 GC equipped with FID detector was used to examine the liquid products from reactions in 3000 mL scale. Two different columns were used as the first one was contaminated and replaced:

1) SUPELCO γ-DEX™ 225 column (L × I.D. =30 m × 0.25 mm, d$_f$ = 0.25 μm).

2) RESTEK RTX-1702 column (L × I.D. =30 m × 0.25 mm, d$_f$ = 0.25 μm).

Table 3.6: GC conditions for analysis of PBN hydrogenation products.

	Parameters	Column#1	Column#2
Gas and flow rate	Carrier gas	Helium	Helium
	Split flow rate	100 ml min^{-1}	150 ml min^{-1}
	Head pressure	18 psig	35 psig
Injector	Temperature	473 K	513 K
	Injection volume	5 µl	3 µl
Detector	Temperature	473 K	473 K
	Range	10	10

Figure 3.8 shows analysis method used to separate the peaks. The same method was applied to both columns. The oven temperature was set to 323 K at start, followed by a raise from 323 K to 353 K at 15 K min^{-1}. Final ramp was done from 353 K to 393 K at 2 K min^{-1}. An example of a typical chromatogram and calibration curves are documented in Appendix A. Propagation of error arising from reaction reproducibility (five repeats at base conditions), GC auto-sampler injection reproducibility, and calibration sample preparation reproducibility are included in results as error bars.
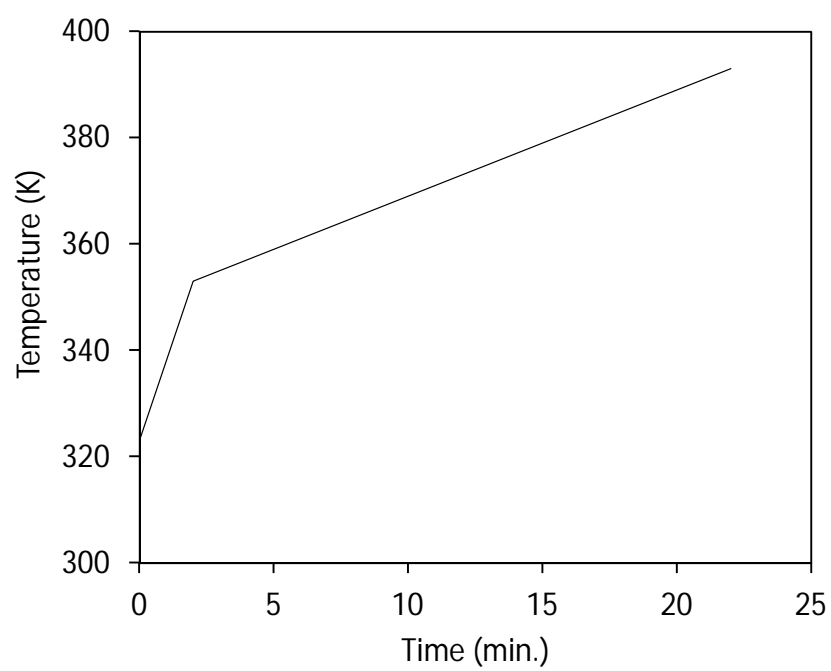
Figure 3.8: GC method for quantitative analysis of PBN hydrogenation.

Chapter 4: Hydrogenation of 4-phenyl-2-butanone in hexane: Effect of scale upon mass transfer, reaction kinetics and selectivity

4.1 Introduction

Catalysis plays an important role in chemical, energy and environmental sector by manipulating the selectivity of heterogeneous reaction systems towards the desired product, thus reducing the energy consumption and minimizing waste products. While the catalyst design represents one side of the reaction engineering process, the other important side is an efficient and intelligent reactor design methodology to optimise each catalyst specifically developed for a given reaction system. With the pressure the chemical industry has been facing in recent years for more sustainable and environmentally friendly processes, it is necessary to gain improved understanding of the complex multiphase reactions and multicomponent interactions across length scales to be able to address the long established design and scale-up difficulties associated with multiphase reactions.

The traditional approach to reactor design has been sequential, from lab scale catalyst development, through pilot plant studies to a full-scale manufacturing process, often with disconnect between the research carried out at each step. A more sustainable design method requires an integrated approach which focuses on maintaining a link over the whole range of length scales from what is happening on the surface of the catalyst (micro-scale) to what is happening inside the reactor (macro-scale) and the final process (industrial-scale) (Nehlsen et al., 2007). The implementation of this approach requires the optimization of catalyst nano-scale structure alongside the macro-scale reactor design which still has not been adopted across industry to the required extent (Kiwi-Minsker and Crespo-Quesada, 2011). A major limitation is the cost and design complications associated with building integrated systems

encompassing the best catalyst testing equipment and in-situ characterisation techniques, the latter of which possess their own restrictions. In addition, knowledge of key parameters influencing the reaction system at each length scale is incomplete. These shortcomings in existing studies form the core foundations of the current research.

As previously discussed in Chapter 1, the aim of this research, in collaboration with, Queen's University of Belfast, Cambridge University, University of Virginia, and Johnson Matthey Plc, was to breakdown the key parameters influencing the rate and selectivity of a model multiphase reaction which exhibits shifts in rate and product distribution with a set of reactor design variables namely catalyst, solvent, operational conditions, and scale-up at each length scale. The aim is to study the effect of these key variables by developing novel in-situ and ex-situ characterisation methods. Within this multiscale investigation, the aim of this section of the study was to investigate the effect of scale-up and mass transfer limitations on rate and selectivity of this model multiphase reaction when scaling from a small scale reactor (100 mL scale) to a larger scale reactor (3000 mL reactor).

The scale-up of many multiphase reaction systems is subjected to a number of variations in performance (rate and selectivity) as a function of operating scale due to a several key factors (Stitt and Simmons, 2011):

a) Shifts in heat transfer rate as a result of reduced surface area/volume ratio which would directly influence heat-up, cool-down, temperature maintenance, and gas diffusion across phase interfaces.

b) Reactant feed time and/or removal of product in semi-batch.

c) Sensitivity to mixing as a result of variations in circulation time, shear, mass transfer between phases and etc.

To gain process understanding and explore the effect of design variables on sensitivity of a given system the usual protocol emphasised by (Stitt and Simmons, 2011) is an intelligent and adequate form of experimental design to investigate the reaction response to the typical scale-up variables. The primary focus of this process is to identify and eliminate the possible design effects on transport properties in a chemical reactor which would inadvertently result in shifts in rate and product distribution. Consequently, most of the focus in research community so far has been based on the assumption that the most important criteria causing the reactor maloperation (specifically in heterogeneous reactions as scale increases) arises from hydrodynamic effects on mixing (residence time distribution, marco-and micro-mixing etc) and heat and mass transfer across interfaces. This assumption is justified by the level of effort is spent at the laboratory scale to eliminate the transport effects to elucidate the true kinetics of reactions; it is very difficult to completely eliminate them as the scale increases since geometric, mixing, bubble, and kinetic lengths do not scale in proportion (Stitt, 2002).

However, this assumption limits the role of chemical engineer's investigation, be it experimental or simulations to the point of diffusion of chemicals to the catalyst pores across length scales e.g. (Patterson, 2005) leaving the solution of the rest of the problem to chemists e.g. (Ide et al., 2012) to tackle the selectivity issues through catalyst design in nano- and micro-scale where the following processes occur:

a) Adsorption of molecules to catalyst surface

b) Catalytic reaction

c) Desorption of products from catalyst surface

But what if the effect of design variables on product distribution of a range of heterogeneous systems during scale-up goes beyond the boundary of diffusion? Hence the question arises of

what part of the above processes might be affected by design variables and what can be done to elucidate these effects? The aim is to tackle them through experimental and simulation efforts by combining the works of chemists and chemical engineers across length scales.

In this chapter, an example of such a heterogeneous reaction system is presented where the product distribution profiles in a 100 mL scale reactor and a 3000 mL scale reactor are independent of hydrodynamics at each scale but still there is a prominent shift in selectivity profiles between two scales that cannot be explained through transport effects.

An attempt has been made by suggesting a step-by-step and rigorous kinetic investigation between both scales to identify the micro-scale process causing this selectivity shift between two scales. As this chapter will confirm, modelling the kinetics of reactions in both scales is of vital importance in such cases to investigate the scale effect on chemistry sensitive systems.

The model reaction chosen for the current study is the selective hydrogenation of 4-phenyl-2-butanone (PBN). In the first part of this chapter the changes in product selectivity of the PBN hydrogenation using a particulate catalyst comprised of 4 wt% Pt supported on P25 TiO_2 are presented and discussed. Two scales are considered: a 100 mL scale using a HEL reactor[2] and a larger 3000 mL scale reactor[3] in the Reaction Engineering Laboratory at Birmingham. The experiments at both scales were carried out in a range of coincident operational conditions the details of which were given in Chapter 3. Experiments at 100 mL scale were run for 2 hours and in 3000 mL for 5 hours using Hexane as the solvent. The experimental data in the 100 mL scale reactor at varying temperature and initial PBN concentrations were used to develop

---

[2] This work was carried out by James Mc Manus at Queens University Belfast and the dataset was supplied to the author as part of the EPSRC CASTech project.
[3] This work was carried out by the author.

the kinetic models best describing the selectivity at this scale and the dominant kinetic constants were identified. A rigorous kinetic investigation based on sound initial considerations and model refinement procedure was employed at this stage of the investigation. The same kinetic procedure was then used to model the experimental data at 3000 mL scale in order to investigate the applicability of the best model at the 100 mL scale to the 3000 mL scale data, identify the micro-scale process affected by scale-up and subsequently explain the shift in product distribution observed. The results of these kinetic investigations were used further to elucidate solvent effects at both scales which are discussed in Chapter 5.

4.2 Reaction System

PBN contains both phenyl and carbonyl functional groups, thus the molecule can undergo both aromatic ring and ketone hydrogenation. 4-phenyl-2-butanol (PBL) and 4-cyclohexyl-2-butanone (CBN) are primary products formed by hydrogenation of the carbonyl and aromatic ring sites of PBN molecule, respectively. Both primary products can further hydrogenate into 4-cyclohexyl-2-butanol (CBL). Figure 4.1 shows the reaction schematic and a typical reaction profile for PBN hydrogenation carried out in hexane. Phenyl ring hydrogenation of PBN results in production of CBN and carbonyl group hydrogenation produces unsaturated alcohol PBL.

(a)
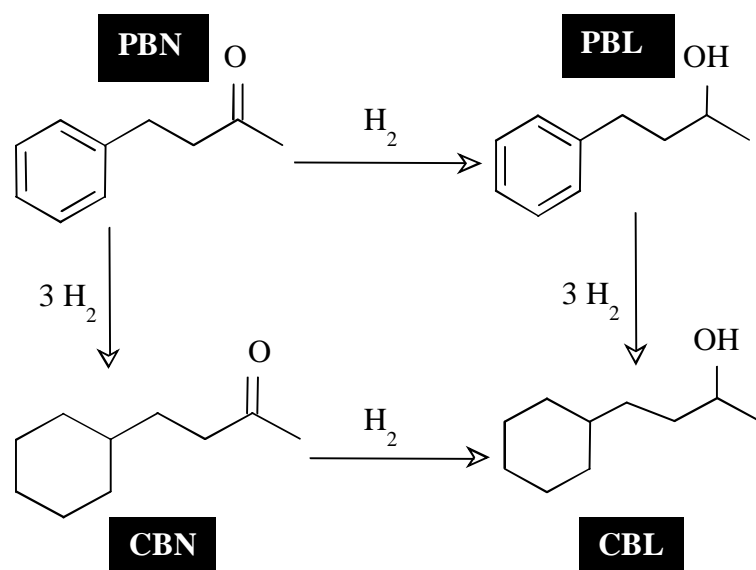
(b)
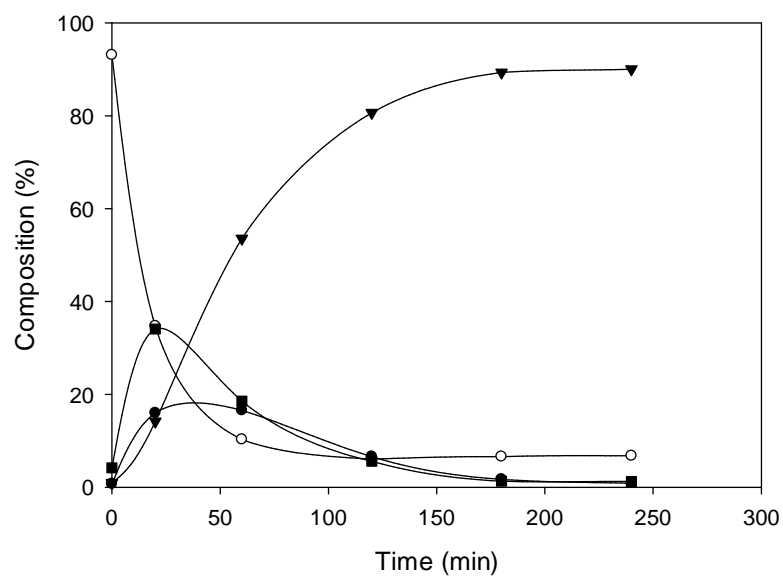
Figure 4.1: (a) reaction schematics and (b) reaction profile for hydrogenation of PBN: PBN
(○), PBL (■), CBN (●), CBL (▼). [3000 mL scale, T = 343 K, P_T = 5 bar, C_{PBNi} = 0.270 mol
L^{-1}, m_{CAT}/m_{PBN} = 0.15, and $\bar{\varepsilon}_T$ = 10 W kg^{-1}]

4.3 Effect of hydrodynamics on selectivity – Comparison of two scales

4.3.1 Effect of energy input and hydrogen partial pressure: 343 K, m_{CAT}/m_{PBN} = 0.05, CPBNi = 0.270 mol L^{-1}

The effect of hydrodynamic parameters on the rate and selectivity at both scales were investigated by varying energy input and hydrogen partial pressure. Comparison of initial rates and Turnover frequency (TOF) are discussed further in §4.4.1 and §4.5.1. Figure 4.2 shows the changes in selectivity versus conversion with increasing energy input from 0.5-10 W kg^{-1} at the 100 mL scale and 1.5-20 W kg^{-1} at the 3000 mL scale. Figure 4.3 shows the selectivity versus conversion with increasing hydrogen total pressures from 2-12 bar in 100 mL scale and 2-10 bar in 3000 mL scale. The total energy dissipations for each scale are calculated from their respective power number values for radial impellers (Equation No. 2.23). In order to present the information clearly, the selectivity of CBL is plotted on separate axes to prevent overlaying of the data. At the 100 mL scale, there is minimal effect of changing energy input upon the selectivity of any of the products (Figures 4.2a1-a2), thus the selectivity profile is independent of the energy input. The selectivity towards PBL is about 40% at the start of the reaction and decreases continuously with conversion to less than 20% as more CBN is produced and also as it further hydrogenates to form CBL. Thus, PBL is the dominant product at the start of the reaction until 10% conversion is reached and a crossover is observed with the CBN selectivity profile as it becomes the main product of the reaction, with more than 70% selectivity at higher conversions. For conversions greater than 40%, CBN selectivity remains relatively constant which is accounted to be due to preference of the catalyst to hydrogenate the ring group of PBL to produce CBL making the ring hydrogenation the prominent reaction pathway in 100 mL scale. This postulation is later confirmed in §4.2.2.

CBL selectivity is more than 30% at the start of the reaction where there is more PBL present in the system and decreases as more CBN is formed which does not convert to CBL as fast as PBL.
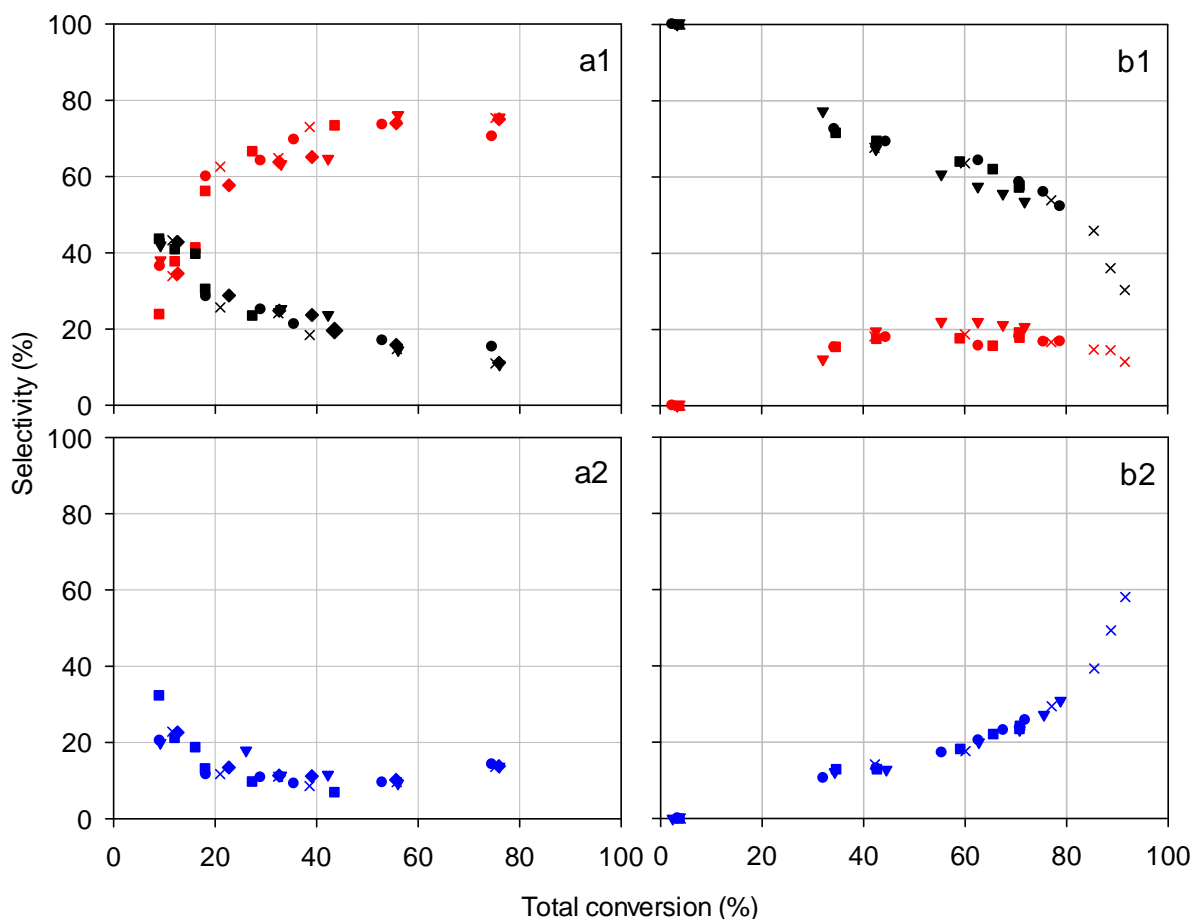
(a) 100 mL: 0.1 W kg^{-1} ($\square$), 0.5 W kg^{-1} ($\circ$), 2.0 W kg^{-1} (∇), 5.0 W kg^{-1} ($\times$), 10.0 W kg^{-1} ($\lozenge$)

(b) 3000 mL: 1.5 W kg^{-1} ($\square$), 3.5 W kg^{-1} ($\circ$), 7 W kg^{-1} (∇), 20.0 W kg^{-1} ($\times$)

Figure 4.2: Selectivity towards PBN hydrogenation products with fill colour of legend symbols as shown in bracketed text (**PBL**), (**CBN**), and (**CBL**) with increasing energy input at both scales. [T = 343 K, P_T = 5 bar, C_{PBNi} = 0.270 mol L^{-1}, m_{CAT}/m_{PBN} = 0.05]

The selectivity at the 3000 mL scale possesses a radically different profile to the 100 mL scale (Figure 4.2b1-b2). The selectivity profiles are again independent of energy input; increasing the impeller speed does however affect the product distribution within the reaction screening time (5 hrs) where at a very high energy input of 20 W kg^{-1} at conversions > 80 % CBN selectivity starts to drop continuously as it hydrogenates to CBL along with PBL. At the start the reaction is 100% selective towards PBL and as the reaction proceeds PBL selectivity decreases as it hydrogenates to CBL and as CBN is formed. Selectivity towards CBN never exceeds 20% as the conversion increases compared with more than 70% selectivity achieved at the 100 mL scale. At the start of the reaction no CBL was formed but its selectivity continuously increases to 60% at 90% conversion when increasing the energy input to 20.0 W kg^{-1}, making it the main reaction product at these conditions.

The dramatically different selectivity profiles observed at both scales indicates there must be some form of scale effect on either reaction route responsible for PBN hydrogenation to intermediates or active sites availability in 3000 mL scale. Since the selectivity profiles are independent of energy input at both scales this shift in selectivity cannot be due to presence/absence of mass transfer limitations. This statement is further confirmed via kinetic analysis at both scales.

Figure 4.3 represents the selectivity versus conversion plots for PBL, CBN, and CBL with varying H$_2$ total pressure at both scales.
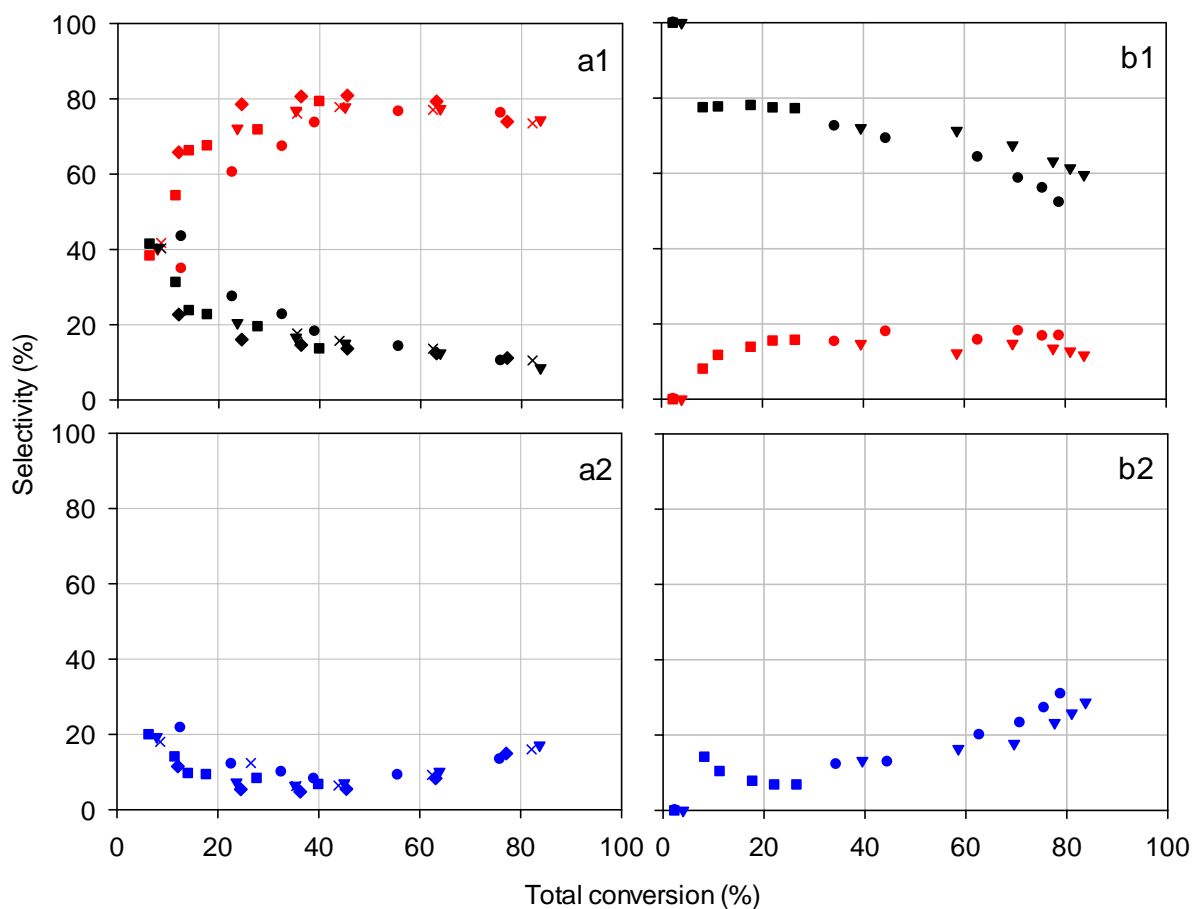
(a) 100 mL: 2 bar (□), 5 bar (○), 8 bar (▽), 10 bar (×), 12 bar (◊)

(b) 3000 mL: 2 bar (□), 5 bar (○), 10 bar (▽)

Figure 4.3: Selectivity towards PBN hydrogenation products (**PBL**), (**CBN**), and (**CBL**) with increasing H_2 total pressure at both scales. [T = 343 K, C_{PBNi} = 0.270 mol L^{-1}, m_{CAT}/m_{PBN} = 0.05, 100 mL: $\bar{\varepsilon}_T$ = 10 W kg^{-1}, 3000 mL: $\bar{\varepsilon}_T$ = 3.5 W kg^{-1}]

At the 100 mL scale, the H_2 pressure has a more prominent effect upon selectivity than energy input for conversions less than 50%, with the PBL selectivity decreasing slightly with pressure. At conversion higher than 50% however the effect of pressure on selectivity is dampened. The overall trend of the selectivity profiles however still remain similar to what

114

was observed with increasing energy input across all pressures. At the start of reaction equal amounts of PBL and CBN are formed and as the reaction proceeds PBL selectivity decreases continuously while CBN selectivity reaches the maximum of 80% at around 40% conversion and then starts to slightly drop as it hydrogenates further to CBL (at pressures > 8 bar). The crossover between PBL and CBN selectivity happens at around 10% conversion. CBL selectivity however never exceeds 20% across all conversions. At 3000 mL scale (Figure 4.3b1-b2), the selectivity appears to be less affected by H_2 pressure, the general trend is the reaction being 100% selective towards PBL at the start of the reaction followed by a continuous drop of PBL selectivity as the conversion increases. The selectivity towards CBN never exceeds 20% and only starts to drop from 60% conversion onwards at higher pressure (12 bar). CBL selectivity shows a continuous increase to more than 30% at conversions more than 80% at which point both PBL and CBN are both being further hydrogenated.

4.3.2 Effect of temperature and catalyst mass: $P_T = 5$ bar, $C_{PBNi} = 0.270$ mol L^{-1}, and 100 mL: $\bar{\varepsilon}_T = 10$ W kg^{-1}, 3000 mL: $\bar{\varepsilon}_T = 3.5$ W kg^{-1}

Figure 4.4 shows selectivity versus conversion as a function of temperature. At 100 mL scale (Figures 4.4a1-a2), a similar evolution of selectivity with conversion is observed as before, however with a shift in crossover between PBL and CBN selectivity happening at 20% conversion. Up to 20% conversion for all temperatures, PBL is the main product with more than 40% selectivity. After the cross over, CBN formation increases to more than 70% before dropping to produce CBL at 60% conversion. CBL selectivity is 30% at the start of the reaction and goes through a minimum whilst more CBN is being formed and starts to peak up to 20% at higher conversions as both PBL and CBN (in lesser extent and at $T_r > 353$ K) are further hydrogenated.

Examining the effect of temperature more closely at 100 mL scale (Figures 4.5a1-a2) at reaction times of 10 and 120 minutes, as the temperature increases from 313 K to 353 K the selectivity towards PBL decreases and selectivity towards CBN increases as the reaction proceeds. At a reaction time of 10 minutes the PBL and CBN selectivities cross over at 333 K while at 120 minutes (higher conversions) CBN is the main product at all temperatures. This behaviour can be attributed to difference between activation energies of hydrogenating carbonyl versus phenyl functional groups. As will be further demonstrated in the modelling section, saturating the aromatic ring requires higher activation energy compared with carbonyl bond. Since the rate constants abide the Arrhenius rule increasing temperature would result in increase in formation of CBN.

$$k_i = k_{bi} \, e^{-\frac{E_a}{R.T}} \tag{4.1}$$

At 3000 mL scale (Figures 4.4b1-b2), at fixed reaction times of 30 and 120 minutes (Figures 4.5b1-b2) we observe that instead of the continuous trend observed in 100 mL scale, PBL selectivity goes through a slight minimum at 333 K while CBN selectivity goes through a maximum at this point at both 30 and 120 minutes.
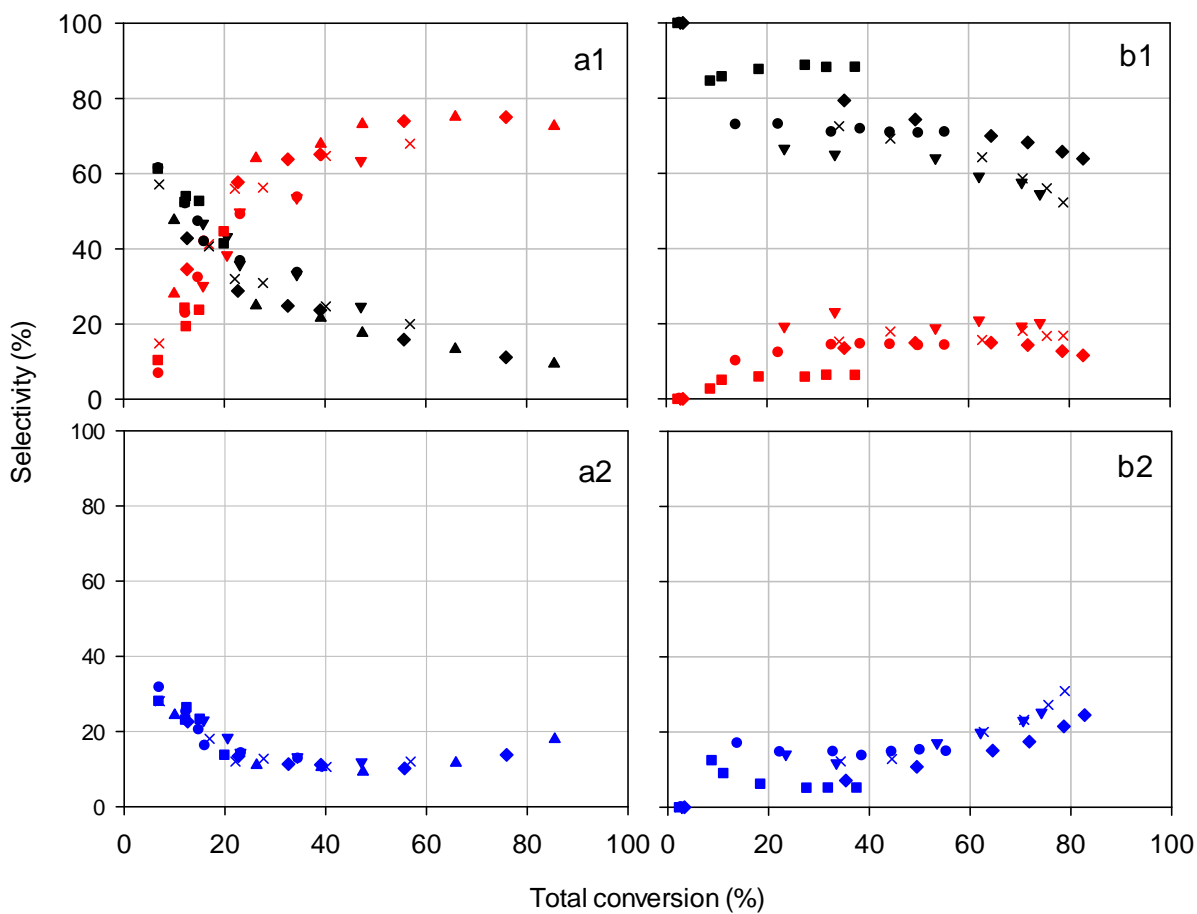
(a) 100 mL: 303 K (□), 313 K (○), 323 K (▽), 333 K (×), 343 K (◊), 353 K (△)

(b) 3000 mL: 313 K (□), 323 K (○), 333 K (▽), 343 K (×), 353 K (◊)

Figure 4.4: Selectivity towards PBN hydrogenation products (**PBL**), (**CBN**), and (**CBL**) with increasing temperature at both scales. [P_T = 5 bar, C_{PBNi} = 0.270 mol L^{-1}, m_{CAT}/m_{PBN} = 0.05, 100 mL: $\bar{\varepsilon}_T$ = 10 W kg^{-1}, 3000 mL: $\bar{\varepsilon}_T$ = 3.5 W kg^{-1}]
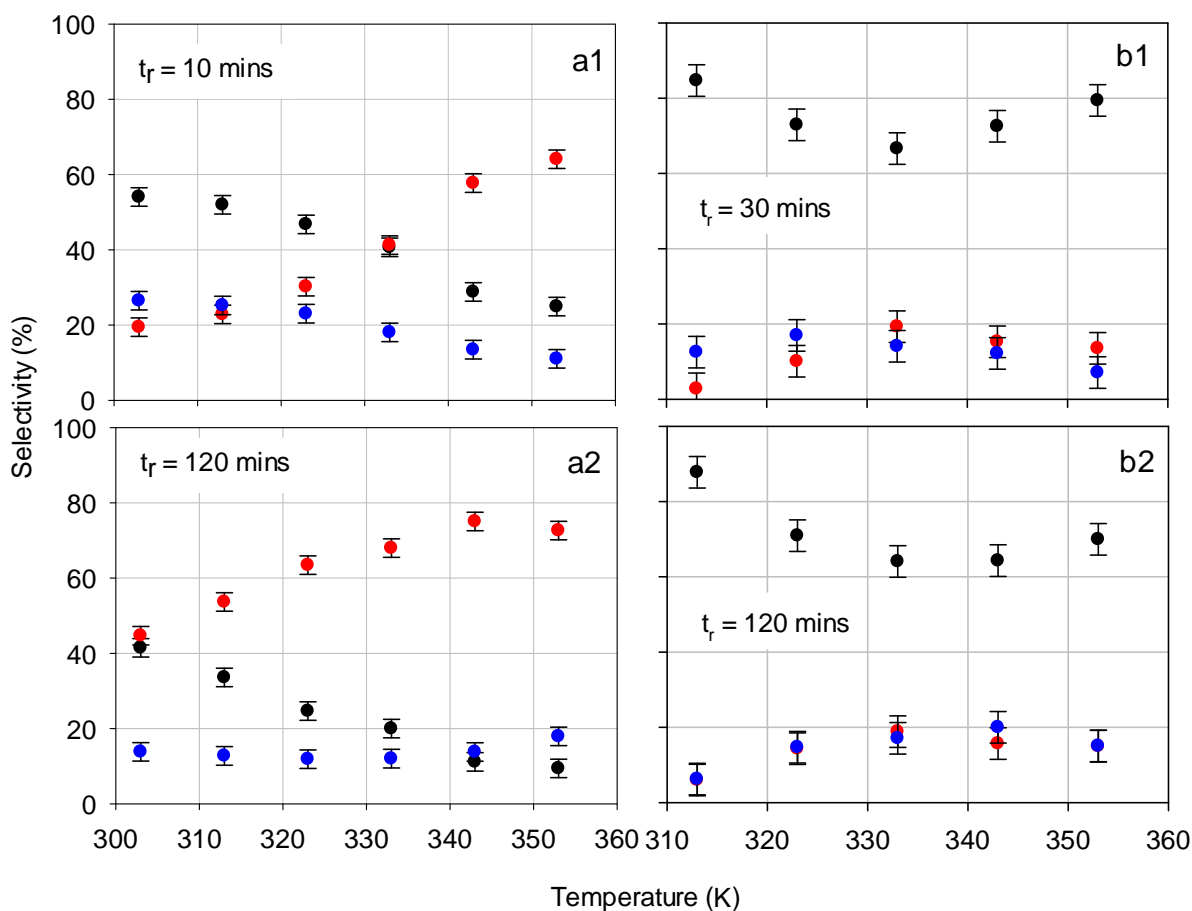
Figure 4.5: Selectivity towards PBN hydrogenation products (**PBL**), (**CBN**) and (**CBL**) with increasing temperature at 10 and 120 mins in 100 mL scale (a), and 30 and 120 mins in 3000 mL scale (b). [P_T = 5 bar, C_{PBNi} = 0.270 mol L^{-1}, m_{CAT}/m_{PBN} = 0.05, 100 mL: $\bar{\varepsilon}_T$ = 10 W kg^{-1}, 3000 mL: $\bar{\varepsilon}_T$ = 3.5 W kg^{-1}]

Figure 4.6 presents the selectivity versus conversion plots with increasing catalyst loading in 100 mL scale (Figure 4.6a1-a2) and 3000 mL scale (Figure 4.6b1-b2). At 100 mL scale, the selectivity trend remains similar as it was observed before across all catalyst loadings as the reaction proceeds and the crossover between PBL and CBN selectivity is observed at around 10% conversion. Subtle effects are detected with increasing catalyst loading for conversions less than 50% with PBL selectivity decreasing while more CBN is formed at higher catalyst

118

to reagent ratios. Looking at the effect of m_{CAT}/m_{PBN} more closely at 10 and 120 minutes (Figure 4.7a1-a2) it becomes more apparent that at lower conversions PBL selectivity continuously decreases as more CBN is produced with the crossover at $m_{CAT}/m_{PBN} = 0.02$, while at higher conversions, CBN selectivity is independent of catalyst loading while PBL is being continuously hydrogenated to CBL. This observation establishes that ring hydrogenation is the dominant reaction route in 100 mL scale and while it becomes independent of the amount of active sites available for PBN at a certain point, the PBL hydrogenation to CBL is still highly dependent on active site availability.
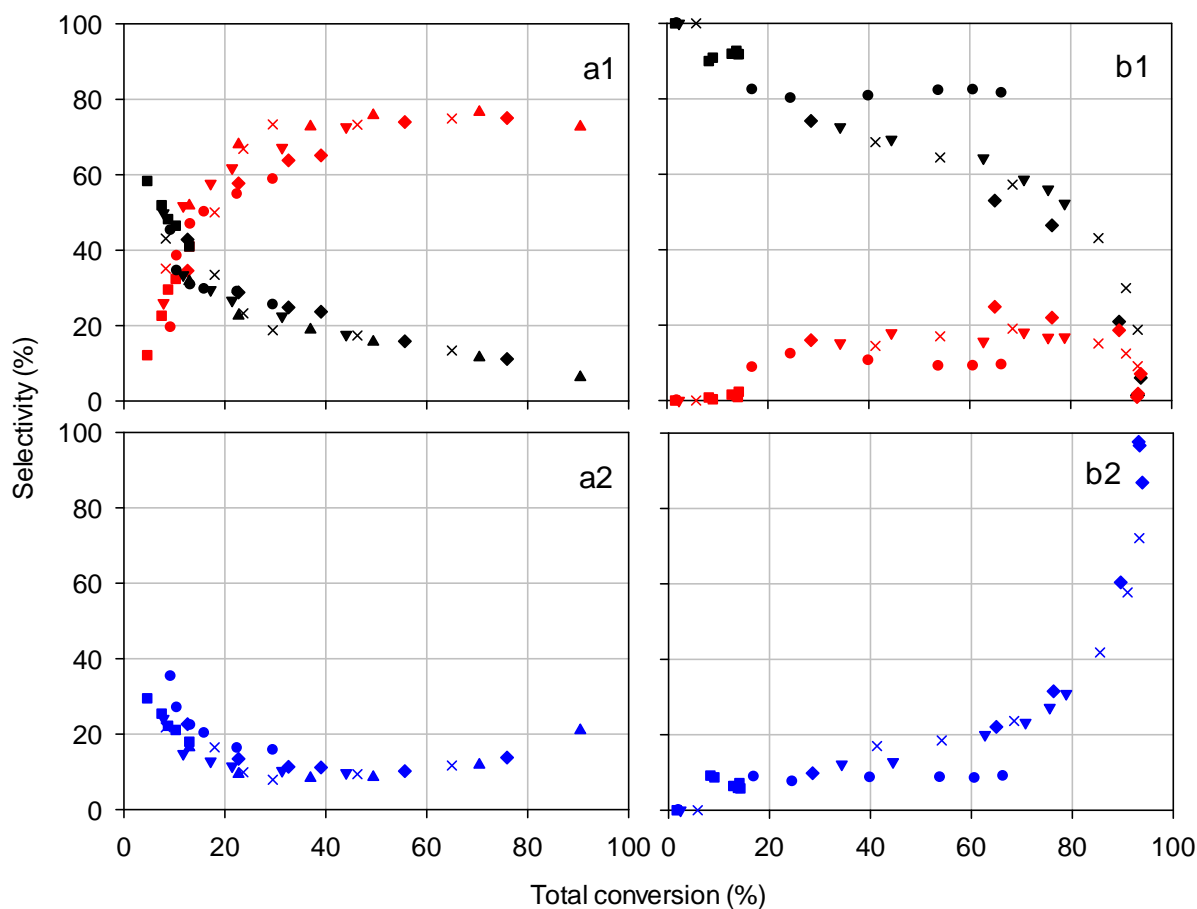
(a) 100 mL: 0.01 (□), 0.02 (○), 0.03 (▽), 0.04 (×), 0.05 (◊), 0.07 (△)

(b) 3000 mL: 0 (□), 0.02 (○), 0.05 (▽), 0.07 (×), 0.15 (◊)

Figure 4.6: Selectivity towards PBN hydrogenation products (**PBL**), (**CBN**), and (**CBL**) with increasing catalyst loading, m_{CAT}/m_{PBN} (-) at both scales; [T = 343 K, C_{PBNi} = 0.270 mol L^{-1}, 100 mL: $\bar{\varepsilon}_T$ = 10 W kg^{-1}, 3000 mL: $\bar{\varepsilon}_T$ = 3.5 W kg^{-1}]

At 3000 mL scale (Figure 4.6b1-b2), the range of m_{CAT}/m_{PBN} investigated is higher than for the 100 mL scale with an experiment conducted at m_{CAT}/m_{PBN} = 0.15. The same selectivity profile observed with increasing energy input, pressure and temperature is again observed across all reagent to catalyst ratios. Furthermore, at higher catalyst loadings (m_{CAT}/m_{PBN} =

0.07 and 0.15) the reaction goes to completion and at conversions > 90% both PBL and CBN are completely hydrogenated to CBL resulting in 100% selectivity towards the final product at the end of the reaction screening time (5 hr.). Compared to results at 100 mL scale, at $m_{CAT}/m_{PBN} = 0.07$, the reaction is still more than 70% selective towards CBN and far from completion to the final product even at 90% conversion reached at this high catalyst to reagent ratio.

Looking at the effect of increasing catalyst mass more closely at the 3000 mL scale at reaction times of 30 and 120 minutes (Figure 4.7b1-b2), it becomes more apparent that PBL selectivity continues to decrease as more CBN and CBL are being formed with increasing active site availability. Consequently, the increase in amount of available active sites triggers ring hydrogenation of PBL more than carbonyl bond on CBN resulting in a continuous decrease of PBL selectivity towards formation of CBL. Only at conversions > 90% CBN starts to rapidly hydrogenate to PBL.

In 100 mL scale, where there is an abundance of CBN in the system, selectivity profiles demonstrate a very slow conversion of CBN compared with PBL for conversions > 50%. Furthermore, the higher selectivity of CBL in 100 mL scale at conversions < 15% where selectivity of PBL is also higher than CBN confirms that when it comes to intermediates, ring hydrogenation prevails carbonyl regardless of the scale. It is postulated that the adsorption/desorption of PBL and CBN plays an important role driving this process in both scales. As in 100 mL scale there is an abundance of CBN in the system as the reaction proceeds so a lower CBL selectivity would be expected since carbonyl hydrogenation is a slow process for both PBN and CBN at this scale. On the other hand, in 3000 mL scale where PBL is the abundant product in system up to halfway through the reaction, the high selectivity

to CBL would be expected when more active sites are available as the ring hydrogenation of PBL always dominates carbonyl hydrogenation of CBN. It was also postulated that the competitive modes of adsorption of ring versus carbonyl bonds of PBN on active sites may play an important role in the selectivity difference. All these assumptions are investigated thoroughly in kinetics sections §4.4 and §4.5.

The available academic literature reports that platinum is able to hydrogenate both carbonyl and phenyl functional groups to the same extent (Chen et al., 2003), (Santori et al., 2004), (Toebes et al., 2005), (Gao et al., 2006), (Reddy et al., 2009), (Liu et al., 2009), (Tundo et al., 2000). Most of these previous studies are carried out on similar molecules to this study such as acetophenone, benzaldehyde, and cinnamaldehyde using platinum supported on TiO_2, SiO_2, Al_2O_3, activated carbon, and carbon nanofibers. These studies show either similar rates of hydrogenation of both aromatic and phenyl groups or high selectivity between 70-99% towards unsaturated alcohols depending on the support type. This makes this catalyst a good choice to study parallel-consecutive reactions by altering parameters such as solvent type, scale and mass transfer rates. A detailed review of the previous literature on hydrogenation of alpha- and beta-unsaturated aromatic aldehydes and ketones can be found in Chapter 2.
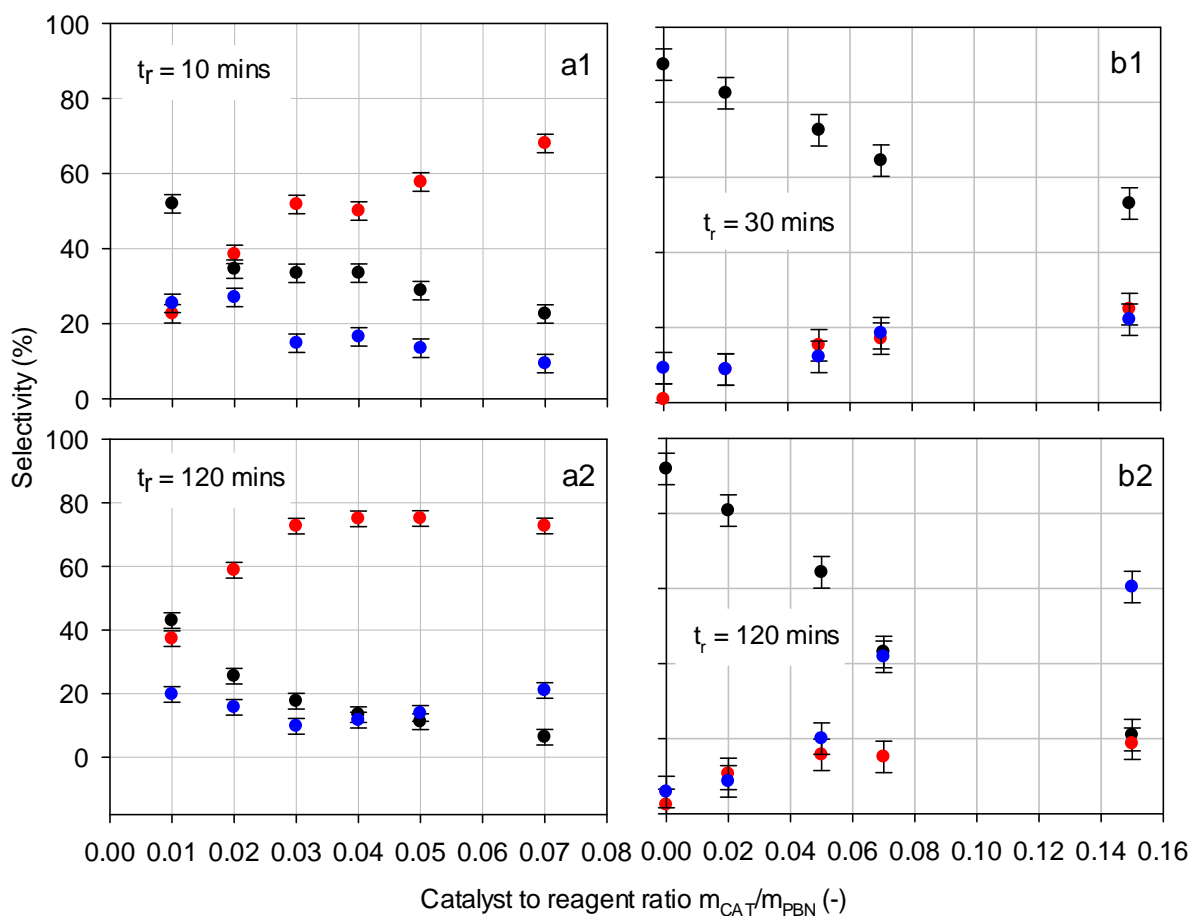
Figure 4.7: Selectivity towards PBN hydrogenation products (**PBL**), (**CBN**) and (**CBL**) with increasing catalyst loading, m_{CAT}/m_{PBN} (-) at 10 and 120 mins in 100 mL scale (a1-2), and 30 and 120 mins in 3000 mL scale (b1-2). [P_T = 5 bar, T = 343 K, C_{PBNi} = 0.270 mol L^{-1}, 100 mL: $\bar{\varepsilon}_T$ = 10 W kg^{-1}, 3000 mL: $\bar{\varepsilon}_T$ = 3.5 W kg^{-1}]

4.4 Detailed kinetic modelling of 100 mL scale data

Reaction kinetic expressions enable our understanding of the chemical process taking place inside a reactor to be translated into mathematical models that can be used in catalyst and reactor design. There is a considerable academic literature on the kinetic modelling of the heterogeneous hydrogenation reactions, as discussed in Chapter 2. With such reactions, there

is more than one rate process occurring in series. These processes can be broken down into a number of steps, all with their own relevant rate equations, which can be combined to obtain the overall rate of reaction. These processes can be summarized as follows (Berger et al., 2001):

1. Mass transfer of reactants to the catalyst surface

2. Adsorption of molecules to catalyst surface

3. Catalytic reaction

4. Desorption of products from catalyst surface

5. Mass transfer of products away from catalyst surface

One of the key issues is the complexity of kinetic models especially in steps 2-4 where surface processes themselves are comprised of number of discrete steps which in their simplest form would be adsorption-reaction-desorption as stated above. The more complex the kinetic model is, a more complex design of experiments is required to build and validate the models. Such an approach is not convenient from industrial point of view which requires justification of the need to build complex models and with it, the range of experiments and physiochemical investigations to be carried out (Berger et al., 2001). Additionally, the complexity of models makes it more difficult to estimate the kinetic parameters within acceptable physiochemical ranges which can describe the experimental observations accurately in lab-scale and further during process optimisation.

There are a number of approaches that can be taken to simplify the model to a certain point which requires a combination of sound initial considerations, reparameterization of the key kinetic parameters, and model refinement through rigorous statistical analysis. This approach

was used in the current study to build robust kinetic models for both scales in order to explain the selectivity shift observed as the reactor scale was increased.

Chemical processes occurring on the surface of the catalyst are best described via the Langmuir-Hinshelwood (LH) model, and the associated Langmuir-Hinshelwwod-Hougen-Watson (LHHW). The LHHW type expressions are derived based on the assumption that the adsorption of all components can be described by the Langmuir-Hinshelwood model and that one surface process (adsorption, reaction, or desorption) is rate determining.

From theoretical considerations and previous studies one can determine the most probable rate-determining step and initial estimates of kinetic parameters for the fitting procedure. In its simplest form, LHHW assumes that all reactants adsorb on the surface of the catalyst yielding an expression in the form of

$$rate \propto \frac{(kinetic\ factor)(driving\ force)}{(adsorption\ term)^n} \tag{4.2}$$

The numerator is the reaction term, while denominator accounts for the effects of sorption processes. The model can include either competitive or non-competitive adsorption of reaction species as well as dissociative or associative adsorption of gaseous reactant.

As discussed in Chapter 2, kinetics of hydrogenation of α,β-unsaturated ketones has been extensively studied with the primary focus being on catalyst design rather than addressing issues with model optimization. In the current study a rigorous kinetic modeling procedure coupled with statistical analysis was used to first derive the best model to describe the behavior of PBN hydrogenation in 100 mL scale and then apply the derived model to reactions carried out in 3000 mL scale to investigate the scale-up effects observed. These

models are used subsequently to model reactions in different organic solvents in both scales in Chapter 5.

4.4.1 Kinetic modelling of heterogeneous hydrogenation reactions in literature

Kinetics of liquid-phase hydrogenation reactions have been widely studied. Though PBN has never been used as a sample molecule, other forms of α,β-unsaturated aromatic ketones and aldehydes like acetophenone, 4-isobutylacetophenone, benzaldehyde, and cinnamaldehyde have been widely used in studying catalyst, solvent, and reactor design etc. Table 4.1 provides a summary of rate models that have previously been employed to such reactions. All these studies rely on the traditional approach of starting from simplest form of LHHW and further expanding it to include the competitive/non-competitive and associative/dissociative modes of hydrogen based on R^2 value to demonstrate the goodness of fit. In majority of these studies, the models assuming the surface reaction as the rate determining step were the most successful in describing the intrinsic kinetics.

Table 4.1: Rate models previously applied to modelling hydrogenation of aromatic aldehydes and ketones.

Rate model	Mechanistic details	References
General LHHW form: $$r = \frac{k_b K_a [R]}{(1 + K_a[R] + \sum K_I[I])^n} \times \theta_H$$	Surface reaction is rate determining step (RDS)	(Červený et al., 1996) (Neri et al., 1997) (Bergault et al., 1998)
Non-competitive, associative: $$\theta_H = \frac{K_H C_H}{1 + K_H C_H}$$	θ_H: competitive, non-competitive, dissociative, and associative modes of H_2 applied in different studies	(Rajashekharam et al., 1999) (Mathew et al., 1999) (Tundo et al., 2000)
Non-competitive, dissociative: $$\theta_H = \frac{\sqrt{K_H C_H}}{1 + \sqrt{K_H C_H}}$$		(Belohlav and Zamostny, 2000)
Competitive, associative: $$r = \frac{k_b K_a[R] K_H C_H}{(1 + K_a[R] + \sum K_I[I] + K_H C_H)^n}$$	Other types of RDS assumptions were not able to describe the reaction data in any of these studies	(Hájek et al., 2004) (Toebes et al., 2005) (Gao et al., 2006) (Thakar et al., 2007a) (Marchi et al., 2007)
Competitive, dissociative: $$r = \frac{k_b K_a[R]\sqrt{K_H C_H}}{\left(1 + K_a[R] + \sum K_d[I] + \sqrt{K_H C_H}\right)^n}$$		(Bertero et al., 2008) (Divakar et al., 2008) (Virtanen et al., 2009)

4.4.2 Analysis of chemical regime

In order to determine the intrinsic kinetics of reaction, and gain more insight into mechanistic behavior of PBN, it was necessary to establish the absence of the internal and external mass transfer resistances in the range of experimental conditions investigated. For this purpose, gas-liquid, liquid-solid, and internal diffusion limitations were examined separately.

When gas-liquid mass transfer is limiting, the hydrogen consumption becomes independent of catalyst loading resulting in the hydrogen flux through gas-liquid interface, φ_{G-L} to take the form of

$$\varphi_{G-L} = K_L a \ (C_{H_2}^* - C_{H_{2-g}})V_L \tag{4.3}$$

where $K_L a$ is volumetric gas-liquid mass transfer coefficient, $C_{H_2}^*$ is the concentration of hydrogen in liquid phase and $C_{H_{2-g}}$ is the concentration of hydrogen in gas-liquid interface. In order to determine if gas-liquid mass transfer was limiting, the influence of the energy input and mass of catalyst on the initial hydrogenation rate was examined and the initial Turnover frequency was calculated using the following equation from % value of metal dispersion provided by QUB using CO chemisorption (metal loading = 2.91 %):

$$\text{TOF}_i \ (\text{s}^{-1}) = \frac{\text{moles of PBN hydrogenated (mol s}^{-1})}{\text{total moles of catalyst active site in reacton}} \tag{4.4}$$
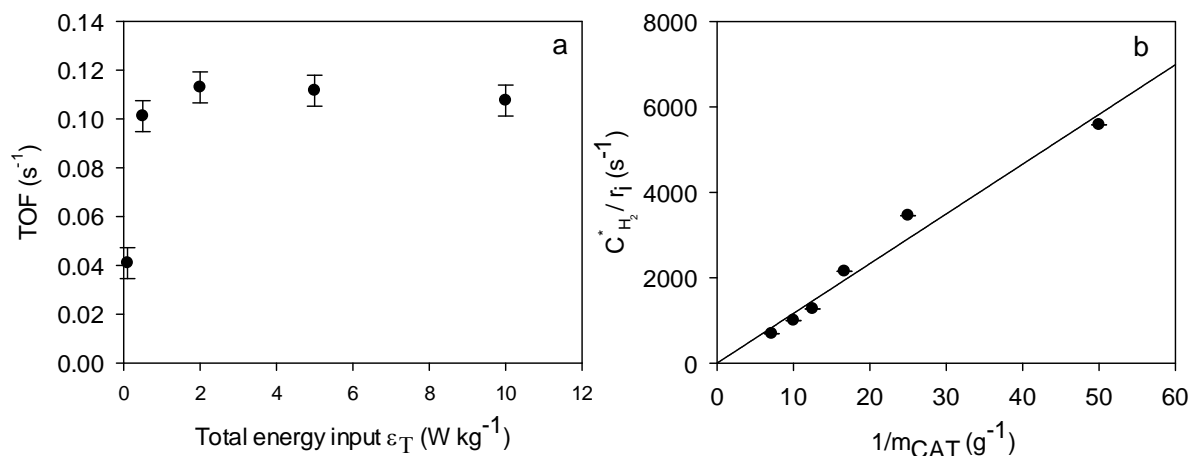
Figure 4.8: Effect of energy input (a) and catalyst loading (b) on PBN initial TOF/ hydrogenation rate. [T = 343 K, C_{PBNi} = 0.27 mol L^{-1}, P_T = 5 bar, $\bar{\varepsilon}_T$ = 10 W kg^{-1}]

The results plotted in Figure 4.8 show that initial rate is independent of impeller speed above 2 W kg^{-1} thus the chosen energy input of 10 W kg^{-1} for the base conditions (Figure 4.8a) lies in the independent range. Figure 4.8b shows a linear dependency of the normalized activity with catalyst weight passing through the origin, proving that the gas-liquid mass transfer is non-existent for the range of operational conditions chosen.

Another criterion, based on observed rate data have been applied to test the absence of mass transfer limitations. The experiments would be within the kinetic regime if the reaction rate does not deviate more than 5% from the ideal situation, i.e. (Crezee et al., 2003)

$$\frac{\text{rate}_{\text{observed}}}{\text{rate}_{\text{ideal}}} = 1 \pm 0.05 \tag{4.5}$$

In this analysis (Table 4.3), initial reaction rates corresponding to different temperatures and initial PBN concentrations have been used to evaluate the worst case scenarios.

For gas-liquid and solid-liquid mass transfer limitations, the Carberry number can be calculated (Ca_{G-L}), which is the ratio between observed volumetric reaction rate to the maximum transfer rate. To calculate the maximum transfer rate, the gas-liquid volumetric mass transfer coefficient of hydrogen in hexane was determined by using a correlation based on dimensionless numbers proposed by (Dietrich et al., 1992) for lab-scale gas inducing stirred reactors with an aspect ratio of unity ($H_L/D_T = 1$). The choice of correlation was previously discussed in Chapter 2. All the dimensionless numbers in correlations are defined in Table 4.2 and definition of parameters can be found in Nomenclature.

$$Sh = 3 \times 10^{-4} Re^{1.45} Sc^{0.5} We^{0.5} \tag{4.6}$$

For a first order reaction the external gas-liquid effectiveness factor (η_{G-L}) can be expressed as:

$$\eta_{G-L} = 1 - Ca_{G-L} \tag{4.7}$$

where Ca_{G-L} is Carberry number with respect to gas-liquid mass transfer. From Table 4.3 it can be concluded that the effectiveness factor (η_{G-L}) for all cases is larger than 0.95 indicating the gas-liquid transport limitations can be neglected.

Determination of solid-liquid mass transfer effects is more difficult and can approximately be determined by means of the Carberry number (Ca_{L-S}) comprising liquid-solid mass transfer coefficient (K_{LS}). K_{LS} was determined using a correlation based on the dimensionless Sherwood number (Sh) proposed by (Sano et al., 1974):

$$Sh = 2 + 0.4\, Re_P^{3/4} Sc^{1/3} \tag{4.8}$$

The values of hydrogen diffusivity (D) are calculated using Wilke-Chang correlation (Wilke and Chang, 1955).

Table 4.4 confirms that the values of effectiveness factor η_{L-S} exceed 0.95 for all experimental conditions indicating the absence of external transport effects.

The internal mass transfer through catalyst pores is strongly dependent on catalyst particle size. For the purpose of this study the P25 4% Pt/TiO$_2$ catalyst was sieved to particle sizes less than 40 µm. The particle size distributions were obtained using a Malvern Mastersizer 2000 Chapter 3. The arithmetic mean particle size is in the order of $d_{10} = 10$ µm and the Sauter mean diameter is in the order of $d_{32} = 1$ µm. The density, porosity, and tortuosity were also measured by means of Mercury Porosimetry (see §3.1.1). The values were used to calculate the effective diffusivity (D_{eff}) which was further applied to Wagner-Weisz-Wheeler modulus (M_w) to evaluate the absence of internal diffusion limitations (Table 4.2). All the calculated values are much lower than 0.15 (Table 4.4) meeting the Weisz-Prater criterion for a diffusion free regime (Levenspiel, 1999).

The same approach can be used to verify that PBN mass transfer limitations could also be excluded by using the following correlation to calculate the diffusivity of PBN in dilute solutions (< 10 mol%) of any solvent (except water) (King et al., 1965):

$$D_{ij}^0 = 4.4 \times 10^{-15} \frac{T}{\eta_2} \left(\frac{v_2}{v_1}\right)^{1/6} \left(\frac{L_2^{vap}}{L_1^{vap}}\right)^{1/2} \tag{4.9}$$

Molar volume (v_i) and enthalpy of vaporization (L_i^{vap}) at normal boiling point for hexane were taken from Chemical Properties Handbook (Yaws, 1999). For PBN the value of L_i^{vap} was taken from online chemical database (www.chemspider.com) and the value of v_i was

calculated using the correlation suggested by (Schotte, 1992) for organic compounds by utilizing group contribution method,

$$v_i = 0.32 \, (L - 1) + \sum A_j G_j \tag{4.10}$$

where L is the compound chain length, A_j is the number of groups j in the compound, and G_j is the group contribution for group j as provided in the paper.

Based on these observations, these results demonstrate that at the energy input of 10 W kg^{-1}, total pressure of 5 bar H$_2$, temperatures, and PBN concentrations chosen the system was operating under the kinetic regime. An example of mass transfer calculations are documented in Appendix B.

Table 4.2: Parameters and correlations used in verification of mass transfer effects.

External mass transport (G-L)	External mass transport (L-S)	Internal mass transport
$Ca_{G-L} = \dfrac{r_v^{obs}}{K_L a C^*}$	$Ca_{L-S} = \dfrac{r_v^{obs}}{K_{LS} a C_b}$	$M_w = L^2 \dfrac{(-r_v^{obs}/C_i)}{D_{eff}}$
$Re = \dfrac{d_i^2 \rho_L N}{\mu_L}$	$Sh = 2 + 0.4 Re^{3/4} Sc^{1/3}$	$D_{eff} = D \dfrac{\varepsilon_P}{\tau_P}$
$We = \dfrac{d_i^3 \rho_L N^2}{\sigma_L}$	$Re_P = \left(\dfrac{N_P d_i^5 N_I^3 d_P^4 \rho_L^3}{\mu_L^3 V_L} \right)^{1/3}$	Spheres: $L = \dfrac{R}{3}$
$Sh = \dfrac{K_L a d_i}{D}$	$Sc = \dfrac{\mu_L}{\rho_L D}$	(Levenspiel, 1999)
$\eta_{G-L} = 1 - Ca_{G-L}$	$D = \dfrac{1.173 \times 10^{-16} (\emptyset M)^{1/2} T}{\mu_L V_m^{0.6}}$	
(Meille et al., 2004)	$\eta_{L-S} = 1 - Ca_{L-S}$	
	(Crezee et al., 2003)	

Table 4.3: Overview of criteria chosen to evaluate the absence/presence of external and internal mass transfer of H_2 and PBN within the experimental range at 100 mL scale.

Run	T (K)	P_T (bar)	m_{CAT} (g)	C_{PBNi} (mol l^{-1})	η_{G-L} (H_2)	η_{L-S} (H_2)	M_w (H_2)	η_{L-S} (PBN)	M_w (PBN)
1	303	5	0.1	0.270	0.99	0.99	0.0004	0.99	0.0001
2	313	5	0.1	0.270	0.99	0.99	0.0005	0.99	0.0001
3	323	5	0.1	0.270	0.99	0.99	0.0009	0.99	0.0003
4	333	5	0.1	0.270	0.99	0.99	0.0009	0.99	0.0003
5	343	5	0.1	0.135	0.99	0.99	0.0015	0.99	0.0009
6	343	5	0.1	0.202	0.99	0.99	0.0012	0.99	0.0005
7	343	5	0.1	0.270	0.99	0.99	0.0011	0.99	0.0003
8	343	5	0.1	0.337	0.99	0.99	0.0011	0.99	0.0003
9	343	5	0.1	0.404	0.99	0.99	0.0012	0.99	0.0003
10	353	5	0.1	0.270	0.99	0.99	0.0015	0.99	0.0005

4.4.3 Analysis of apparent rate order

In order to gain a quick insight into the mechanistic details of the kinetics governing hydrogenation of PBN and choosing the best model to describe the experimental results, the dependency of initial TOF calculated using Equation (4.4) for different initial PBN concentrations and H_2 partial pressures were investigated. The results are plotted in Figure 4.9.

The effect of hydrogen pressure on PBN hydrogenation over 4% Pt/TiO_2 was investigated in hexane at 343 K and C_{PBNi} = 0.270 mol L^{-1}. The catalytic tests were conducted at total pressures, 2, 5, 8, 10, and 12 bar, corresponding to partial pressures of 0.93, 3.93, 6.93, 8.93, and 10.93 bar, respectively. The values were obtained by considering that at 343 K, hexane vapor pressure is 1.067 bar (Antoine equation), and vapor pressure of PBN and products are negligible. The effect of PBN initial concentration on catalytic activity was studied at 343 K and P_T = 5 bar. PBN concentration was varied between 0.135-0.404 mol L^{-1}.

The initial reaction rates were calculated by differentiation of the curves at zero time using the linear and nonlinear curve fitting software Table Curve® 2D v.5 (SYSTAT Software Inc.) for best kinetic or polynomial fits ($R^2 \sim 0.995$-0.999).

The apparent reaction rate orders were calculated by applying linear and nonlinear regressions, considering a power low dependency for both hydrogen partial pressure and PBN concentration:

$$r_{PBNi} = k(P_{H_2})^n (C_{PBNi})^m \tag{4.11}$$

The results show that the initial rate increases linearly with pressure (Figure 4.9a) by a first order dependency on H_2 partial pressure. The results in Figure 4.9b illustrate that at lower initial PBN concentrations (< 0.270 mol L^{-1}) the catalytic activity decreases by increasing PBN concentration. The negative reaction order with respect to PBN at lower concentrations indicates that at this range the interaction of PBN with surface active sites is very strong. At PBN concentrations higher that 0.270 mol L^{-1} the reaction rate tends toward a near zero order with respect to PBN concentration indicating that the catalyst surface becomes saturated at these concentrations.

The negative apparent order with respect to initial reagent concentration has previously been reported for hydrogenation of aromatic ketone and aldehydes acetophenone, p-chlorobenzophenone, 4-isobutylacetophenone, and cinnamaldehyde over ruthenium, platinum, palladium, and copper catalysts (group 8, 10 and 11 metals) (Bertero et al., 2008), (Gao et al., 2006), (Bawane and Sawant, 2004), (Thakar et al., 2007a), (Mathew et al., 1999), (Virtanen et al., 2009).
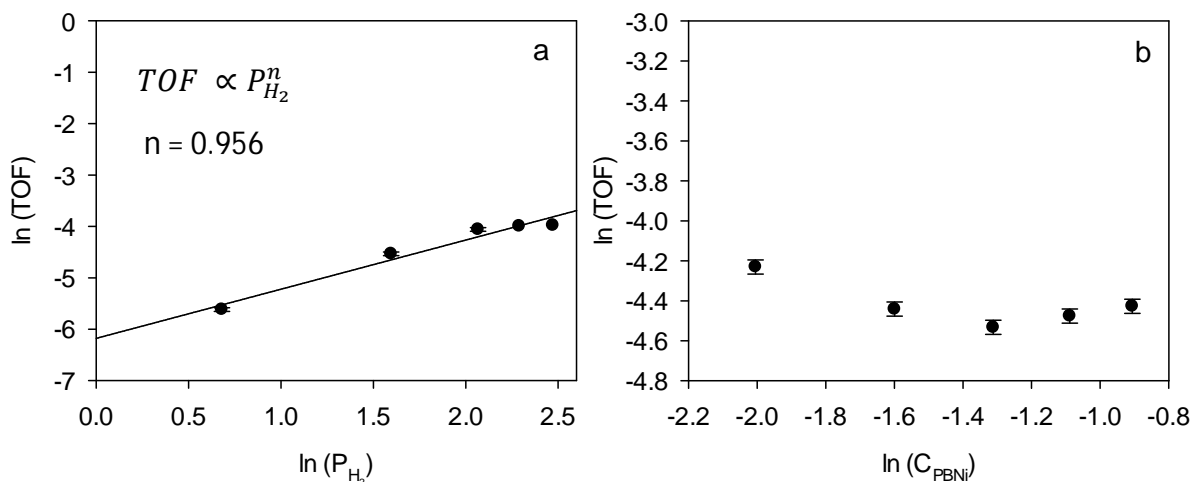
Figure 4.9: Plot of initial TOF (s^{-1}) versus hydrogen partial pressure (bar) (a) and initial PBN concentration (mol L^{-1}) (b); [T = 343 K, m_{CAT}/m_{PBN} = 0.05, $\bar{\varepsilon}_T$ = 10 W kg^{-1}]

The nonlinear regression for Equation (4.11) results in the values of 1.02 for hydrogen pressure and -0.05 for PBN initial concentrations (R^2=0.964)

Furthermore, the analysis of initial TOF for formation of PBL, CBN, and CBL (Figure 4.10) indicates that rates of formation of PBL, CBN, and CBL are also tending towards negative order behavior with increasing initial PBN concentration. PBL formation rate however shows a slight increase for initial PBN concentrations higher than 0.270 mol L^{-1}.
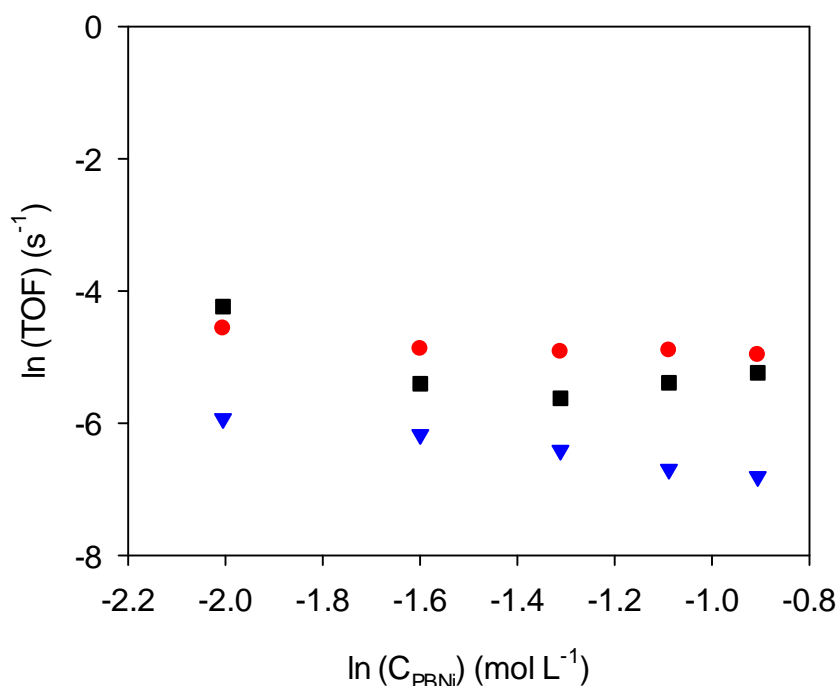
Figure 4.10: Plot of initial TOF (s^{-1}) for formation of PBN hydrogenated products, PBL formation (□), CBN formation (○), CBL formation (▽), against different initial PBN concentrations; [P$_T$ = 5 bar, T=343 K, m$_{CAT}$ = 100 mg, $\bar{\varepsilon}_T$ = 10 W kg^{-1}]

The influence of temperature on catalyst activity was investigated for temperatures ranging from 303-353 K. The results given in Figure 4.11 show that the catalyst activity increases with temperature and the lumped apparent activation energy was determined by numerical linear regression using an Arrhenius type function Equation (4.1). A value of E$_a$ = 35.6 W kg^{-1} was obtained which is approximately equal to the average value of individual activation energy values obtained further for ring and carbonyl groups in kinetic section §4.4.7.
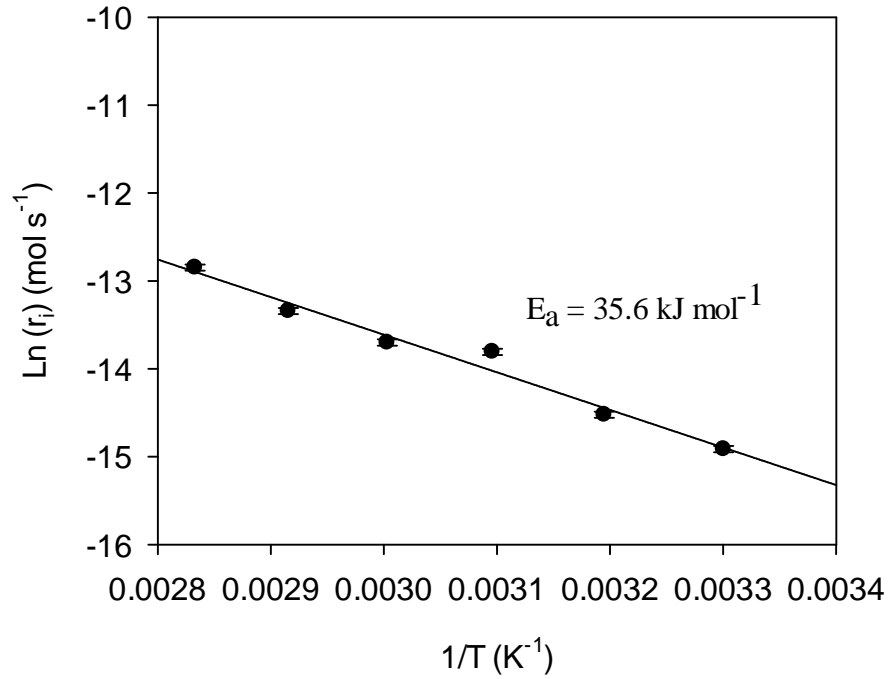
Figure 4.11: Effect of temperature on catalyst activity; [P_T = 5 bar, C_{PBNi} = 0.270 mol L^{-1}, m_{CAT}/m_{PBN} = 0.05, $\bar{\varepsilon}_T$ = 10 W kg^{-1}]

Since in the previous section (§4.4.2) the mass transfer limitations were excluded the observed activation energy is the true lumped activation energy of PBN. Low activation energy is yet another indication of system being under the influence of mass transfer and a high activation energy observed here is another indication that in this system kinetic regime dominates within the operational conditions investigated and kinetics are temperature sensitive (Fogler, 2001) (Bertero et al., 2008).

Figure 4.12a shows the evolution of PBN concentration with time at different temperatures with the rate of hydrogenation of PBN clearly increasing with increasing temperature.
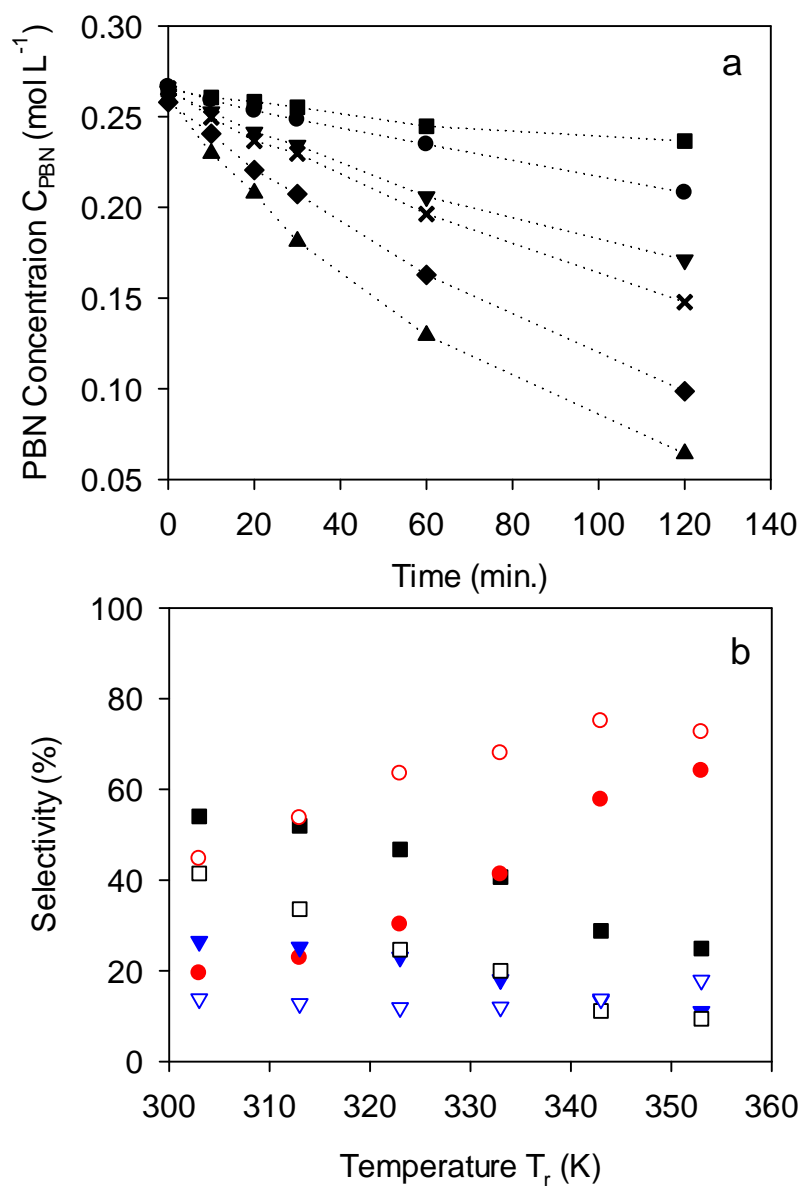
(a): 303 K (□), 313 K (○), 323 K (▽), 333 K (×), 343 K (◊), 353 K (△)

(b): PBL selectivity (□), CBN selectivity (○), CBL selectivity (▽); Closed symbols: 10 mins, open symbols: 120 mins.

Figure 4.12: Evolution of PBN hydrogenation with reaction time for different reaction temperatures (a), and plot of initial TOF (s^{-1}) against temperature. [P_T = 5 bar, C_{PBNi} = 0.270 mol L^{-1}, m_{CAT}/m_{PBN} = 0.05, $\bar{\varepsilon}_T$ = 10 W kg^{-1}]

At lowest temperature (303 K) only 10% conversion is achieved after 2 hr. vs 80% achieved at 353 K. As a reminder of temperature effect on selectivity at 10 and 120 mins of reaction time (Figure 4.12b), increasing temperature results in more CBN formation specifically at higher conversions. The selectivity towards PBL continuously decreases as it hydrogenates to CBL and more CBN is formed. CBL selectivity decreases with increasing temperature at 10 mins (lower conversions) and peaks up with temperature after 120 mins (higher conversions) as more PBL is hydrogenated.

An observation was made to look further into the complexity of the PBN hydrogenation using the following equation (Wilkinson et al., 2014):

$$r_{PBN \to products} = \frac{dC_{PBN}}{dt} = \frac{[PBN]_{t(n+1)} - [PBN]_{t(n)}}{t_{n+1} - t_n} = k[PBN]_{t(n)}^n \qquad (4.12)$$

Where t_{n+1} is the time of concentration measurement, t_n is the time previous concentration and n is the apparent reaction order. By plotting $\ln(r_{PBN \to products})$ against $\ln([PBN]_{t(n)})$ values on n were determined for different temperatures (Table 4.4).

Table 4.4: Apparent reaction order dependency with increasing temperature.

Reaction Temperature (K)	n (-)	R^2
303	12.6	0.72
313	3.8	0.76
323	2.7	0.79
333	2.1	0.48
343	1.2	0.77
353	1.5	0.90

As shown in Table 4.4, values of n decrease with increasing temperature. Evolution of n with temperature is a simple indicator that species adsorption are required in kinetic rate model expressions (Wilkinson et al., 2014). These observations were considered when developing models to describe the kinetics of PBN hydrogenation at 100 mL scale.

4.4.4 Model derivation

Based on the previous observations and conclusions the following mechanism can be established at first for PBN hydrogenation on platinum,

$$PBN + * \; \underset{K_{a-1}}{\overset{K_a}{\rightleftharpoons}} \; PBN^* \tag{4.13a}$$

$$PBN^* \; \underset{k_{b-1}}{\overset{k_b}{\rightleftharpoons}} \; PBL^* \tag{4.13b}$$

$$PBN^* \; \underset{k_{b-1}}{\overset{k_b}{\rightleftharpoons}} \; CBN^* \tag{4.13c}$$

$$PBL^* \; \underset{k_{b-1}}{\overset{k_b}{\rightleftharpoons}} \; CBL^* \tag{4.13d}$$

$$CBN^* \; \underset{k_{b-1}}{\overset{k_b}{\rightleftharpoons}} \; CBL^* \tag{4.13e}$$

$$PBL^* \; \underset{K_{c-1}}{\overset{K_c}{\rightleftharpoons}} \; PBL + * \tag{4.13f}$$

$$CBN^* \; \underset{K_{c-1}}{\overset{K_c}{\rightleftharpoons}} \; CBN + * \tag{4.13g}$$

$$CBL^* \; \underset{K_{c-1}}{\overset{K_c}{\rightleftharpoons}} \; CBL + * \tag{4.13h}$$
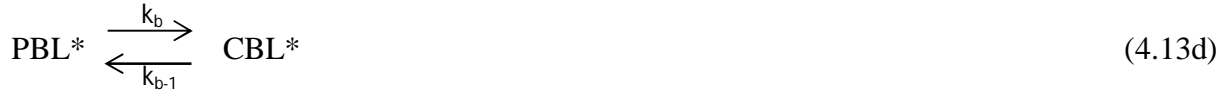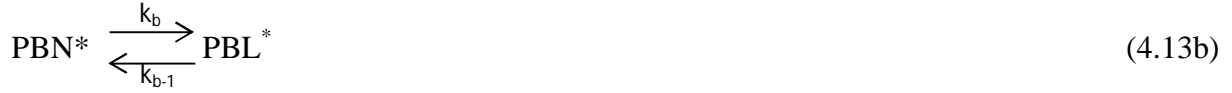
Where * denotes to active sites. In conjugation with this the following assumptions were also made to develop the LHHW models:

- For initial model description, it was assumed that the surface reaction is rate limiting for hydrogenation steps and all organic reactants and products (PBN, PBL, CBN, and CBL) competitively adsorb on active sites. To make a more thorough examination of kinetics of this system, models based on reactant adsorption and final product desorption as the rate determining steps were also examined. The possibility of two or more sites was not ruled out and was investigated in later stages of the modelling process. Furthermore, based on previous selectivity observations which demonstrated the importance of intermediate

141

product desorption on selectivity, kinetic models including product desorption terms were also developed. This approach has previously been employed by (Mounzer et al., 2010) in order to account for solvent effect on intermediate product removal from catalyst surface in oxidation reactions.

- Species adsorption/desorption steps were considered as reversible and quasi-equilibrium steps. Equilibrium description for adsorption was originally tested using Van Hoff-type expression and was fitted to data at different temperatures. However, the enthalpies of adsorption (ΔH_{ads}) were always found to be statistically insignificant and indeterminate and were excluded from the modelling process. Furthermore based on previous literature on kinetic modelling of hydrogenation reactions, over a narrow range of temperatures, the temperature dependency of adsorption terms is usually quite negligible (Mathew et al., 1999), (Chang et al., 2000), (Patil et al., 2006), (Bertero et al., 2008). Consequently, the $K_{ads/des}$ terms were modelled as constants.

- The hydrogen partial pressure was kept constant during the hydrogenation reactions. Though hydrogen solubility has long been established to be temperature and solvent dependent, it was assumed as a constant during model refinement process due to efficient mixing. Both associative and dissociative modes of H_2 adsorption were first assumed as dihydrogen adsorption is dissociative on Pt and other noble metals (Vannice, 2005a), however the fitted parameter K_{H_2}, equilibrium adsorption constant, was always found to be indeterminate during the parameter estimation process and consequently was omitted during the parameter estimation process. Also within the pressure range tested here (2-12 bar) the reaction is first order with respect to hydrogen; therefore the K_{H_2} in denominator could be neglected. This was further justified by fitting the models to experiments at higher pressure that did not show negative deviation from original data. However, this does not

142

exclude the importance of this parameter but acknowledges that a wider range of experiments are needed to explore it.

- In the simplest model a single type of active site was assumed to be available to both organics and H_2. The competition of H_2 for active sites with organics was also considered given the negative apparent rate order with respect to PBN, and was investigated at further stages of model refinement process specifically when modelling the concentration data.

As a result, four models based on LHHW were developed to merit all these considerations. The summary of these models is presented in Table 4.5.

The modelling process for 100 mL data was divided into two stages. At the initial stage the models in Table 4.5 were fitted to the data at different temperatures and an intensive model optimization process was carried out to assess these models in terms of parameter estimation and robustness. Modelling the multi-temperature data (Table 4.6: series A) at first will both remove the insignificant parameters from rate expression as well as identify the most robust model from initial candidates. The activation energies were also determined during this stage. At the second stage, six further models were developed based on the observations made during fitting the temperature varied data and previous selectivity analysis to investigate the mechanism of the active sites, competitive adsorption of the organics with each other, and different denominator terms to account for the negative apparent reaction order observed. These models were fitted to experiments with varied PBN starting concentrations (Table 4.6: series B). This will discriminate models further and single out the best model which will finally be tested against the experiments carried out in 3000 mL scale and also experiments in a range of solvents in both scales (Chapter 5). Table 4.6 summarizes the two stage approach taken for this modelling process.

Table 4.5: Candidate rate expressions for modelling temperature varied data.

Equation No.	Rate expression	Mechanistic details
4.14a	$r = \dfrac{k_b \, K_a \, [R]}{(1 + K_a[R] + \sum K_d[I])}$	a) Surface reaction between reactant and H_2 is RDS b) Competitive organics adsorption on active sites
4.14b	$r = \dfrac{k_b \, K_a \, [R]}{(1 + K_a[R] + \dfrac{P}{K_c} + \sum K_d[I])}$	a) Surface reaction between reactant and H_2 is RDS b) Product desorption term is included in denominator
4.14c	$r = \dfrac{k_a[R]}{(1 + \dfrac{P}{K_{b,c}} + \sum K_d[I])}$	a) Adsorption of organic reactant to active sites is RDS b) Competitive adsorption of organics on active sites
4.14d	$r = \dfrac{k_b \, K_{a,b} \, [R]}{(1 + K_{a,b}[R] + \sum K_d[I])}$	a) Desorption of final product from catalyst surface is RDS b) Competitive adsorption of organics on active sites

*a,b, and c denote to adsorption, reaction, and desorption, respectively on their own.

*a,b denotes to lumped modes of adsorption and reaction.

*b,c denotes to lumped modes of reaction and desorption.

144

Table 4.6: Modelling stages taken for PBN hydrogenation in 100 mL scale.

Modelling stage	Variable parameters	Constant parameters
A	Multi-temperature data: • 303-353 K	• P_T = 5 bar • C_{PBNi} = 0.270 mol L^{-1} • Solvent: hexane • m_{CAT}/m_{PBN} = 0.05 • $\bar{\varepsilon}_T$ = 10 W kg^{-1}
B	Multi-concentration data: • 0.135-0.404 mol l^{-1}	• T = 343 K • Rest is same as above

4.4.5 Kinetic modelling procedure

The modelling process was carried out using the kinetic package Athena Visual Studio V14.2 (W.E. Stewart), (W. E. Stewart, 2008). The kinetic models tested here are comprised of a set of linear and non-linear (e.g. activation energies in Arrhenius equation) parameters. As previously discussed in Chapter 2, the Levenberg-Marquardt procedure, an indirect method for constrained optimization of parameters is most applicable for this model refinement procedure (Marquardt, 1963). More detailed review of Athena interface and solvers can be found in Chapter 2. All response variables in this current system are dependent upon multiple reactions as shown at the start of this section resulting in a set of differential equations to be solved implicitly:

$$\frac{dy_i}{dt} = f(y_i, \beta)$$ (4.15)

Where y_i denotes model response for organic i, β denotes kinetic parameters and t denotes time.

The kinetic parameters were estimated by minimization of weighted sum of squares of residuals (chosen Athena solver),

$$SS_{RES} = \sum_i^m \sum_j^n w_{i,j}(C_{i,j,obs} - C_{i,j,cal})^2 \tag{4.16}$$

To estimate parametric sensitivity the solver uses a direct coupled method,

$$B(t) = \frac{\delta y(t)}{\delta \beta} \tag{4.17}$$

$$\frac{\delta}{\delta \beta}\left(\frac{dy_i}{dt}\right) = \frac{d}{dt}B(t) = \frac{df}{dy_i}.B(t) + \frac{df}{d\beta} \tag{4.18}$$

Where $B(t)$ denotes sensitivity function for each model response defined as a function of time which allows it to be solved alongside the main system ODEs, improving solver efficiency and robustness (Caracotsios and Stewart, 1985).

To minimize the cross-correlation between activation energy, Enthalpy of adsorption and pre-exponential factors the Arrhenius and Vant Hoff equations can be re-parameterized as followed,

$$k_i = A_{i,T_{base}}.exp\left(\left(\frac{E_a}{T_{base}.R}\right).\left(\left(1 - \frac{T_{base}}{T}\right)\right)\right) \tag{4.19a}$$

$$K_i = B_{i,T_{base}}.exp\left(\left(\frac{\Delta H_i}{T_{base}.R}\right).\left(\left(1 - \frac{T_{base}}{T}\right)\right)\right) \tag{4.19b}$$

where the base temperature, T_{base}, was chosen as 373 K, thus $A_{i,T_{base}}$ is the value of rate constant k_i at 373 K. Usually in the kinetic studies involving the use of re-parameterised Arrhenius equation either the average temperature of the range investigated (T_{avr}) or the reference temperature chosen in the experimental range ($T_{ref.}$) are used as T_{base} (Smeds et al., 1995), (Salmi et al., 2007), (Thakar et al., 2007a), (Usman et al., 2011). (Schwaab et al., 2008) argues that an optimum reference temperature can be defined for re-parameterization of the Arrhenius equation through minimisation of the norm of the parameter correlation matrix by manipulating the reference temperatures in order to overcome the convergence difficulties. However, such an approach is beyond the scope of the current study and also subsequent analysis of T_{base} showed a slight improvement on residuals if T_{base} was chosen as 373 K rather than the values of T_{avr} (328 K) or T_{ref} (243 K).

When needed the k_i and K_{ADS} values were lumped within models to avoid cross-correlation and the remaining parameters where then calculated by backing out the estimations.

An example of the source code written in Athena for the current study is documented in Appendix C. The code written by the user is converted to an executable file by software.

4.4.6 Model refinement: modelling process and parameter elimination example[4]

Parameter Reduction steps

The starting models in Table 4.5 all comprised of twelve parameters at the beginning of modelling process (4 pre-exponential terms, 4 activation energies, and 4 adsorption/desorption constants). The procedure taken for parameter estimation and model discrimination was based on the work of (Quiney and Schuurman, 2007) on gas phase reactions which used the Jacobian Matrix to carry out sensitivity analysis in order to systematically eliminate non-influential parameters on model responses from rate expressions:

- Each model was fitted at first with 12 parameters. For all the models tested the 12 parameter expressions initially resulted in more than four parameters being estimated as either indeterminate or with non-acceptable confidence intervals.

- The first step of this procedure consisted of analyzing each parameter estimated based on their initial results and noting those which are indeterminate, out of range (negative values of activation energies and adsorption constants) and statistical significance by comparing t-values to critical t-value for 95% confidence interval.

- The second step of this procedure was examination of each parameter estimated for their impact on the model response by calculating the norm of Jacobian Matrix from the derivatives vector for each parameter, defined as,

---

[4] The author would like to acknowledge the assistance of S.K. Wilkinson (School of Chemical Engineering, University of Birmingham) with Athena Visual Studio and the procedure used for model estimation and discrimination was developed by both the author and S.K Wilkinson.

$$norm(J_k)_m = \sqrt{\Sigma_i \left(\beta_j \frac{\delta y_i}{\delta \beta_j} \right)^2} \qquad (4.20)$$

The Jacobian Matrix for each experiment is a matrix of all first order partial derivatives of a vector or scalar function with respect to another vector (Caracotsios and Stewart, 1985):

$$J_k = \begin{bmatrix} \dfrac{dy_1}{d\beta_1} & \cdots & \cdots & \dfrac{dy_1}{d\beta_l} \\ \vdots & \ddots & \cdot & \vdots \\ \vdots & \cdot & \ddots & \vdots \\ \dfrac{dy_k}{d\beta_1} & \cdots & \cdots & \dfrac{dy_k}{d\beta_l} \end{bmatrix} \qquad (4.21)$$

Where k and l denote to the number of model responses and parameters, respectively. j_k is generated for m experiments which would be 30 in this study consisting of 6 temperature runs with 5 reaction time measurements.

The value of $norm(J_k)$ provides information about relative influence of one parameter compared to others on model response by quantifying the significance of all 12 parameters through the sensitivity function, *B(t)*. Comparing the 'lumped' sensitivities, the lowest value means that the parameter is either indeterminate or has large 95% confidence interval and very little influence on the model response hence can be removed systematically from the model.

- From the Jacobian Matrix it is possible to study the cross-correlation of parameters as a further measure on over-parameterization in a model. The cross-correlation coefficients can be calculated for all parameter interactions using the following expression (Marquardt, 1963):

$$(CC)_{j1,j2} = \frac{(J_k^T J_k)^{-1}_{j1,j2}}{\left[(J_k^T J_k)^{-1}_{j1,j1} \cdot (J_k^T J_k)^{-1}_{j2,j2} \right]} \qquad (4.22)$$

Where CC denotes to cross-correlation coefficient ranging from $-1<CC<+1$, subscript T denotes to matrix transpose and j_1 and j_2 are the two parameters considered respectively. CC values close to -1 or $+1$ suggest a strong cross-correlation between the two parameters.

The cross-correlation of rate and adsorption constants was specifically taken into consideration where a high value indicated not both parameters are needed in rate expression.

- At this point of the analysis one the following decisions can be made in order to improve the kinetic model:

a) Full or partial removal of a parameter from one or more rate expressions by setting the values of K_{ADS} or E_a terms to zero for some or all rate models. This approach is needs to be carried out carefully using full analysis of statistical impact of the eliminated parameter on model responses.

b) Equate two or more parameters, for example two reaction pathways with the same mechanism (ketone or ring) may share the same E_a and k_i values. Such approach has previously been successfully employed in transient kinetic analysis of selective oxidation of n-butane in order to increase the model robustness by reducing the number of parameters in kinetic models which would consequently result in release of degree of freedoms (Wilkinson et al., 2013). This approach requires careful considerations specifically based on the selectivity profiles to assess the dominant reaction routes and might be limited to the experimental range investigated.

c) Fix the value of a parameter like activation energies or heats of adsorption based on previous literature studies (Dumesic and Trevino, 1989).

- Removing each parameter will generate a new set of fitting parameters, sensitivities, cross-correlation coefficients, and residuals. The quality of fit after each elimination was accessed by using a statistical "additional sum of squares" F-test to analyze if the change in Sum of Square of Residuals by removing one parameter is statistically significant (Norman R. Draper, 1998):

$$F = \frac{\left(\frac{RSS_1 - RSS_2}{P_2 - P_1}\right)}{\left(\frac{RSS_2}{n - P_2}\right)} \qquad (4.23)$$

Where RSS_1 and RSS_2 are residual sum of squares in the nested and original model respectively, P_1 and P_2 are number of parameters and n is the total number of observations. In the current study P_2-P_1 is always one as parameters are removed individually. The F statistic is compared with the critical value, F_{crit} for 95% confidence interval ($p = 0.05$). If F is smaller than F_{crit}, the removal, equating, or fixing the parameter is statistically acceptable.

- By removing each parameter the condition number of the Jacobian Matrix will be consequently reduce as the number of linear dependent columns are similarly reduced. The condition number is defined as,

$$C(J_k) = \|J_k\| \cdot \|J_k^{-1}\| \qquad (4.24)$$

- The resulting "best" model from temperature varied data was chosen as a basis to develop further models to fit concentration varied data. These models were developed in terms of competing active sites. The same procedure as above was carried out again to refine and discriminate the models if necessary.

- After all the analysis above were carried out the site models were discriminated based on their resulting goodness of fit, evolution of F-value during parameter elimination,

residuals, parity plots, and a series of advanced statistical criteria generated by the Athena software via Lack-of-Fit analysis.

- At the final stage hydrogen concentration was included as a first order basis into the "best" resulting model from concentration varied data to investigate the applicability of the model developed in 100 mL scale on 3000 mL scale via introduction of appropriate mass transfer effects.

Parameter reduction example

In this section an example of the analysis carried out for parameter estimation based on steps above is presented. The model chosen as an example is the surface reaction RDS with product desorption term (Model 4.14b). A breakdown of the model is:

$$r_1 = r_{PBN \to PBL} = \frac{k_1 K_{PBN}[PBN]}{\left(1 + K_{PBN}[PBN] + \frac{[PBL]}{K_{PBL}} + K_{CBN}[CBN] + K_{CBL}[CBL]\right)}$$

$$(4.25)$$

$$r_2 = r_{PBN \to CBN} = \frac{k_2 K_{PBN}[PBN]}{\left(1 + K_{PBN}[PBN] + \frac{[CBN]}{K_{CBN}} + K_{PBL}[PBL] + K_{CBL}[CBL]\right)}$$

$$(4.26)$$

$$r_3 = r_{PBL \to CBL} = \frac{k_3 K_{PBL}[PBL]}{\left(1 + K_{PBL}[PBL] + \frac{[CBL]}{K_{CBL}} + K_{PBN}[PBN] + K_{CBN}[CBN]\right)}$$

$$(4.27)$$

$$r_4 = r_{CBN \to CBL} = \frac{k_4 K_{CBN}[CBN]}{\left(1 + K_{CBN}[CBN] + \frac{[CBL]}{K_{CBL}} + K_{PBN}[PBN] + K_{PBL}[PBL]\right)}$$

$$(4.28)$$

Model 4.14b has 12 parameters at the beginning; Pre-exponential factors ($A_{1\text{-}373}$-$A_{2\text{-}373}$) and lumped activation energies (E_{a1}-E_{a4}) within rate constants (k_1-k_4), and four adsorption constants. The estimated 12 parameters for the initial run of this model on temperature varied data are presented in Table 4.7.

Table 4.7: Estimated parameters, confidence intervals, and t-values for Model 4.14b with 12 parameters.

Parameter	Unit	Status	Fitted value	95% confidence interval	t-value
$A_{1,373}$	mol L^{-1} min^{-1}	Estimated	0.0159	± 0.013	2.39
$A_{2,373}$	mol L^{-1} min^{-1}	Estimated	0.102	± 0.019	10.3
$A_{3,373}$	mol L^{-1} min^{-1}	Estimated	0.216	± 0.326	1.31
$A_{4,373}$	mol L^{-1} min^{-1}	Estimated	0.0079	± 0.0066	2.40
Ea_1	kJ mol^{-1}	Estimated	30.9	± 7.11	8.62
Ea_2	kJ mol^{-1}	Estimated	47.3	± 2.00	46.8
Ea_3	kJ mol^{-1}	Estimated	85.1	± 83.5	2.02
Ea_4	kJ mol^{-1}	Indeterminate	7.18	-	-
K_{PBN}	L mol^{-1}	Estimated	8.17	± 3.11	5.21
K_{PBL}	L mol^{-1}	Estimated	0.0044	± 0.009	0.92
K_{CBN}	L mol^{-1}	Indeterminate	0.0671	-	-
K_{CBL}	L mol^{-1}	Estimated	0.0139	± 0.013	2.14

The value of R^2 for this model was 0.9993 but assessing the parameters listed in Table 4.7 clearly demonstrates that the model is over-parameterized:

- The parameters K_{CBN} and Ea_4 are indeterminate and the estimated Ea_4 value is not physiochemically acceptable.

- Apart from $A_{2,373}$, Ea_1, and Ea_2 none of the other parameters are estimated with acceptable confidence intervals (at least an order of the magnitude lower).

- The t-values for $A_{3,373}$ and K_{PBL} is well below the critical value t_{crit} which is $\pm$ 1.98 for degree of freedom of 108 (120 experimental observations minus 12 parameters) and 95 % confidence interval ($p = 0.05$) indicating that presence of this parameter in model is statistically insignificant.

- Indeterminate status and small t-values might as well be due to the over-parameterisation of this model. Consequently, some of these parameters might still be significant at later stages of the modelling process.

The second stage of the model refinement entitled looking into the norms of the Jacobian Matrix to determine the least influential parameters on model response. Figure 4.13 shows the Jacobian norms for all parameters over all four model responses.

- Initially the relative significance of each parameter on all model responses were investigated (Figure 4.13a) specifically for the lowest model responses PBL and CBL.

- K_{PBL} and K_{CBN} show the lowest impact on CBL response function and $A_{4,373}$ and Ea_4 are the least influential parameters on PBL response.

- Assessing the normalised norms of Jacobian Matrix across parameters indicates that Ea_4 has the least relative impact on all model responses.

Following the analysis of Jacobian Matrix involved looking into cross-correlation factor between all parameters. Table 4.8 summarizes the cross-correlation coefficients for all 12 parameters during the first model run.

- Ea_4 and K_{PBL} have zero values as both were indeterminate.

- $A_{3,373}$ and $A_{4,373}$ show the highest cross-correlation with Ea_3.

- $A_{1,373}$, $A_{2,373}$, and $A_{4,373}$ show a strong cross-correlation with K_{PBL} indicating that the presence of this parameter in conjugation with rate constant might not be necessary specially in rate expressions r_1, r_2, and r_4.

- Among K_{ADS}, K_{PBN} shows a strong cross-correlation with K_{PBL}.
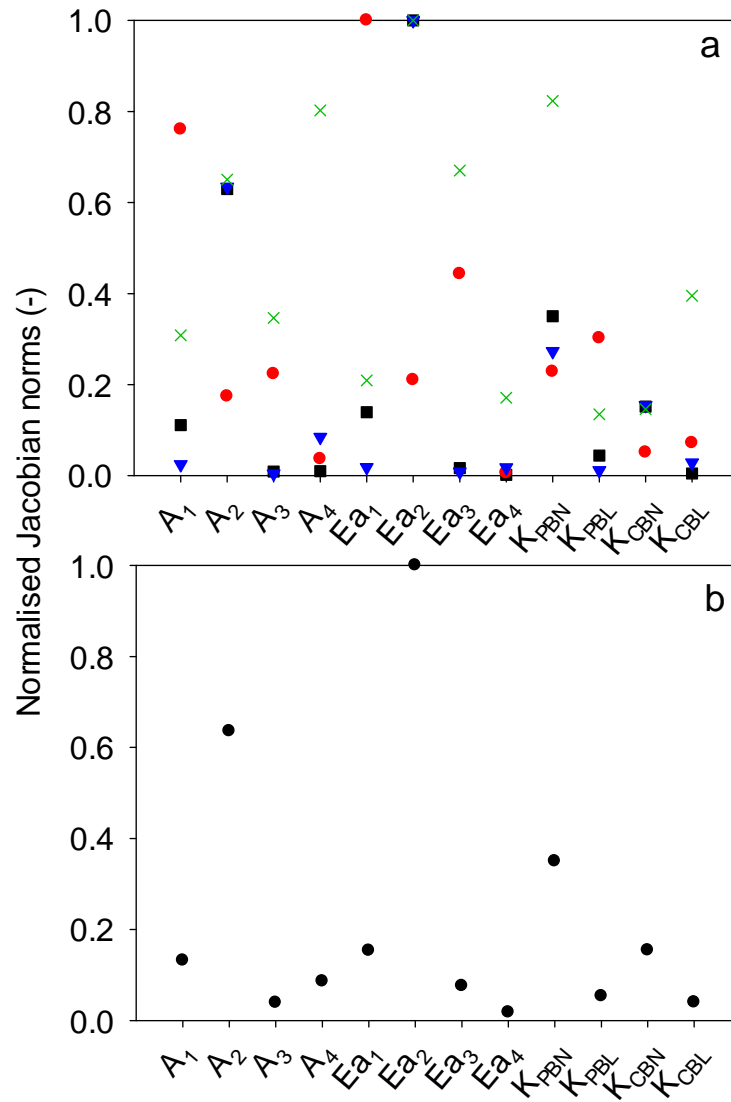
Figure 4.13: Normalised norms of Jacobian Matrix with respect to individual model responses

(a): PBN (□), PBL (○), CBN (▽), CBL (×); and with respect to model parameters (b)

Table 4.8: Cross-correlation coefficients for Model 4.14b comprising 12 parameters.

	$A_{1,373}$	$A_{2,373}$	$A_{3,373}$	$A_{4,373}$	E_{a1}	E_{a2}	E_{a3}	E_{a4}	K_{PBN}	K_{PBL}	K_{CBN}	K_{CBL}
$A_{1,373}$	1											
$A_{2,373}$	0.666	1										
$A_{3,373}$	0.338	0.339	1									
$A_{4,373}$	0.621	0.852	0.618	1								
E_{a1}	0.47	-0.19	0.133	-0.081	1							
E_{a2}	-0.623	-0.485	-0.48	-0.624	-0.305	1						
E_{a3}	0.494	0.633	0.897	0.824	0.003	-0.547	1					
E_{a4}	0	0	0	0	0	0	0	0				
K_{PBN}	0.745	0.951	0.365	0.825	-0.044	-0.689	0.605	0	1			
K_{PBL}	-0.903	-0.852	-0.421	-0.823	-0.109	0.598	-0.673	0	-0.851	1		
K_{CBN}	0	0	0	0	0	0	0	0	0	0	0	
K_{CBL}	-0.327	-0.329	-0.701	-0.697	-0.134	0.46	-0.605	0	-0.362	0.383	0	1

From the observations above Ea_4 appears to be a weak parameter by being indeterminate, showing the lowest sensitivity value with respect to other parameters, and having low t-value. Setting this parameter to zero would mean that the PBN $\rightarrow$ PBL reaction route is a fast process with no temperature sensitivity which contradicts previous selectivity observations with increasing temperature. Furthermore, breaking the C=O bond definitely has an energy barrier which could constitute as a rate determining step itself (Chang et al., 2000). Consequently, the value of Ea_4 was equated with Ea_1 which represents the activation energy for both ketone hydrogenation routes. This approach was subsequently used for further parameter reduction.

After each removal the F-value for each parameter from individual residuals, the overall model F-value, and condition numbers were calculated to assess the statistical impact of elimination in order to avoid over-simplification of the model. Figure 4.14 demonstrates the parameter reduction process from 12 parameters down to 4 parameters for the entire model.

The parameter reduction consisted of equating the reaction pathways for ketone and ring hydrogenation paths in terms of both pre-exponentials and activation energies and complete removal of some K_{ADS} terms from rate models. The overall F-value of the whole system did not breach the critical F-value (F_{crit}) for the first 7 parameters removed (Figure 4.14a), demonstrating that eliminating these parameters did not have a significant statistical impact on entire system response.

Only the elimination of 8th parameter results in a large F-value at which point the model becomes Pseudo First Order concluding yet again that the species adsorption is significant for the current system. Looking at the individual responses (Figure 4.14b), CBL response is most affected by parameter elimination, and being the lowest model response compared to others make it significant to assess the statistical impact of elimination on it. The elimination of 6th parameter exceeds F-value for CBL however the residual is corrected by the subsequent elimination. Further removal of parameters which reduces model to total of 4 parameters shows the highest impact on PBN and CBL responses.

A brief overview of order of parameters removed is presented in Table 4.9.

At the end of the of the model refinement process the temperature dependency of K_{CBN} was tested to assess the validity of the previous assumption made to model this value as constant by incorporating Vant Hoff relationship into the source code (Equation 4.19b). The value of ΔH_i came out as positive with poor confidence interval and lowest J_{norm} value and setting it to zero had no statistical impact upon model response in terms of F-test thus validating the previous assumption.

The model robustness was tested by varying the initial guess for all 5 parameters between 10^{-3}-10^{1}. The model always converged to the final results presented in the next section (Table 4.10).
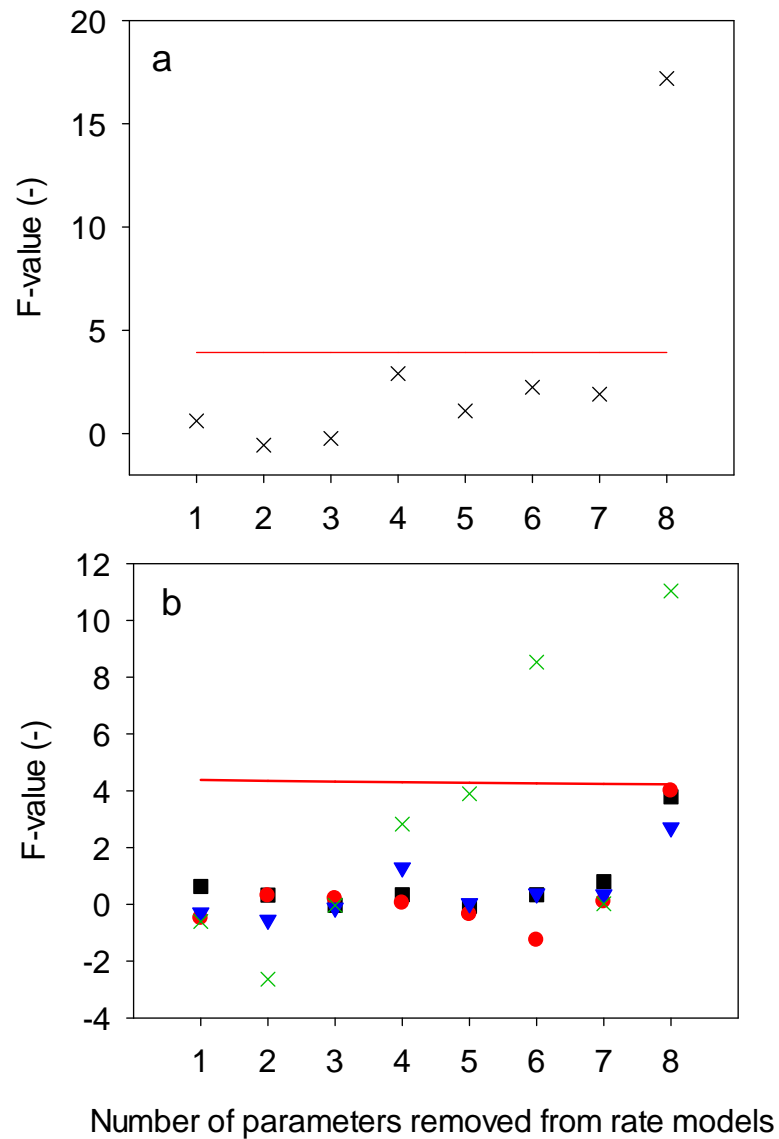
Figure 4.14: Evolution of model F-value after each successive parameter removal for up to 8 eliminations with respect to rate model (a) and individual model responses PBN ($\square$), PBL ($\circ$), CBN (∇), CBL ($\times$), (b).

Table 4.9: Order of parameters removed from Model 4.14b

Total No. of parameters in model	Parameter removed	RSS ($\times 10^4$)	Removal justification[a]
12	-	6.85	-
11	Ea_4	6.89	• Indeterminate • Equated to Ea_1: ketone hydrogenation route
10	$A_{4,373}$	6.86	• Equated to $A_{1,373}$: ketone hydrogenation route
9	K_{CBL}	6.84	• Poor confidence interval
8	K_{PBL}	7.02	• Un-feasible value • Poor confidence interval
7	Ea_3	7.09	• Equated to Ea_2: ring hydrogenation route
6	K_{PBN}	7.23	• Negative value
5	$A_{3,373}$	7.35	• Equated to $A_{2,373}$: ring hydrogenation route
4	K_{CBN}	8.44	• Statistically significant • Remained in model

a: in addition to the lowest Jacobian norm

The only adsorption constant significant to all model responses was concluded to be K_{CBN}. This parameter was remained in the model reducing the whole model to the following:

$$r_1 = r_{PBN \rightarrow PBL} = \frac{k_1[PBN]}{(1 + K_{CBN}[CBN])}$$

$$\text{(4.29)}$$

$$r_2 = r_{PBN \rightarrow CBN} = \frac{k_2[PBN]}{\left(1 + \dfrac{[CBN]}{K_{CBN}}\right)}$$

$$\text{(4.30)}$$

$$r_3 = r_{PBL \rightarrow CBL} = \frac{k_3}{(1 + K_{CBN}[CBN])}$$

$$\text{(4.31)}$$

$$r_4 = r_{CBN \rightarrow CBL} = \frac{k_4 K_{CBN}[CBN]}{(1 + K_{CBN}[CBN])}$$

$$\text{(4.32)}$$

The fitting results for all models in Table 4.6 are presented and discussed in the next section.

4.4.7 Modelling results of the temperature varied data

Once all the models in Table 4.5 undergone the same elimination approach to optimize them the resulting fits were compared in terms of F-values, parity plots, confidence intervals, residuals and critically analysed for further development of kinetic models for fitting concentration varied data. Just like the example in section above (§4.4.6) for all the rate models in Table 4.5 the model optimization contained a number of steps involving pairing of reaction pathways with the same mechanism: ketone hydrogenation (k_1 with k_4 to k_{ket}) and ring hydrogenation (k_2 and k_3 to k_{arom}); and complete removal of some of the K_{ADS} terms. Adsorption parameters K_{PBN}, K_{PBL} and K_{CBL} were knocked out at various stages of the process leaving K_{CBN} behind, adsorption constant of the selective product CBN.

The F-statistics for all models after each successive parameter removal is presented in Figure 4.15. F-value for surface reaction RDS and reactant adsorption RDS models exceeded the F_{crit}

once (4th parameter) and twice (2nd and 5th parameter) during the estimation process, respectively however the residuals were corrected at the 7th parameter removal. F-value for product desorption RDS model exceeded F-value once at 6th parameter removal but was subsequently corrected when 7th parameter was eliminated.
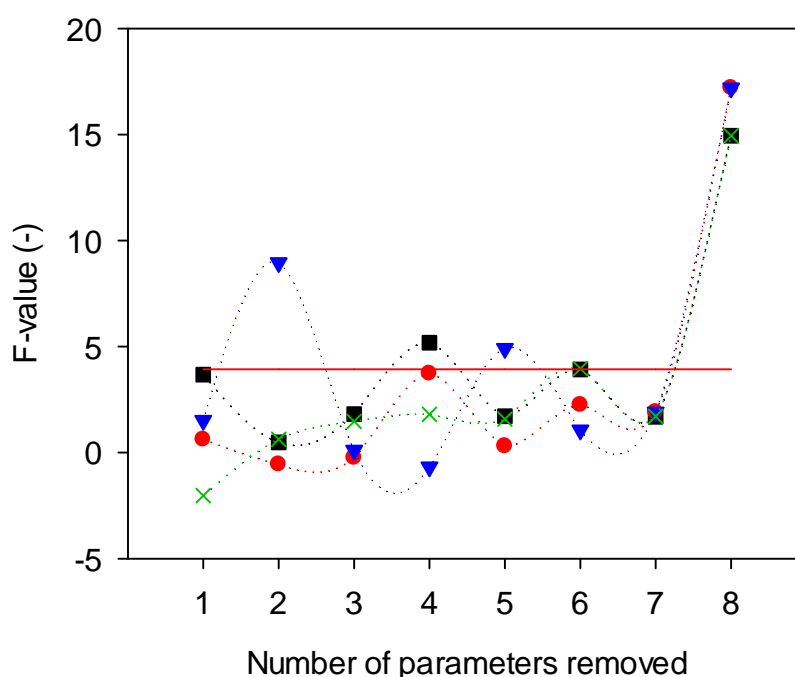
Figure 4.15: Calculated F-value for successive parameter removal across the entire model responses for 4 models investigated: Surface reaction RDS (□); Model 4.14b: surface reaction RDS with product desorption (○); Model 4.14c: reactant adsorption RDS (▽); Model 4.14d: final product desorption RDS (×).

Surface reaction RDS model with product desorption term was the only model in which F-value did not exceed F_{crit} until the removal of 8th parameter. This implies the significance of the product desorption term for the selective product CBN and suggests that this parameter should be considered when constructing the models for the next stage of the process.

Looking at the dropped-out K_{ADS} terms more closely, specifically in case of surface reaction RDS models (Model 4.14a-**simplest form of LHHW**), after the 6th parameter removal the J_{norm}s values for both K_{PBN} and K_{CBN} (Figure 4.16) are relatively high. However K_{CBN} removal would be statistically significant in terms of F-value of the overall system response and the fitted value of K_{PBN} would be negative suggesting that the model cannot properly estimate this value whilst it's still a significant parameter. From this observation it was concluded that most probably there are two distinct sites on platinum for ring and ketone hydrogenation routes and fitting it as one constant for all rate equations would result in an indeterminate parameter that cannot be estimated.

This theory was initially put into test when developing the model assuming desorption of final product is RDS (Model 4.14d). Initially this model constituted of 11 parameters and an extra adsorption constant for PBN was assumed to look into different modes of adsorption. However, one K_{PBN1} was eliminated early on during parameter reduction process and after 6 parameters were removed the remaining K_{PBN2} and K_{CBN} were still the two significant K_{ADS} terms. This implies that fitting the K_{PBN} term as a single site basis is unsuccessful and models based on 2-site basis might be the way to tackle this problem.
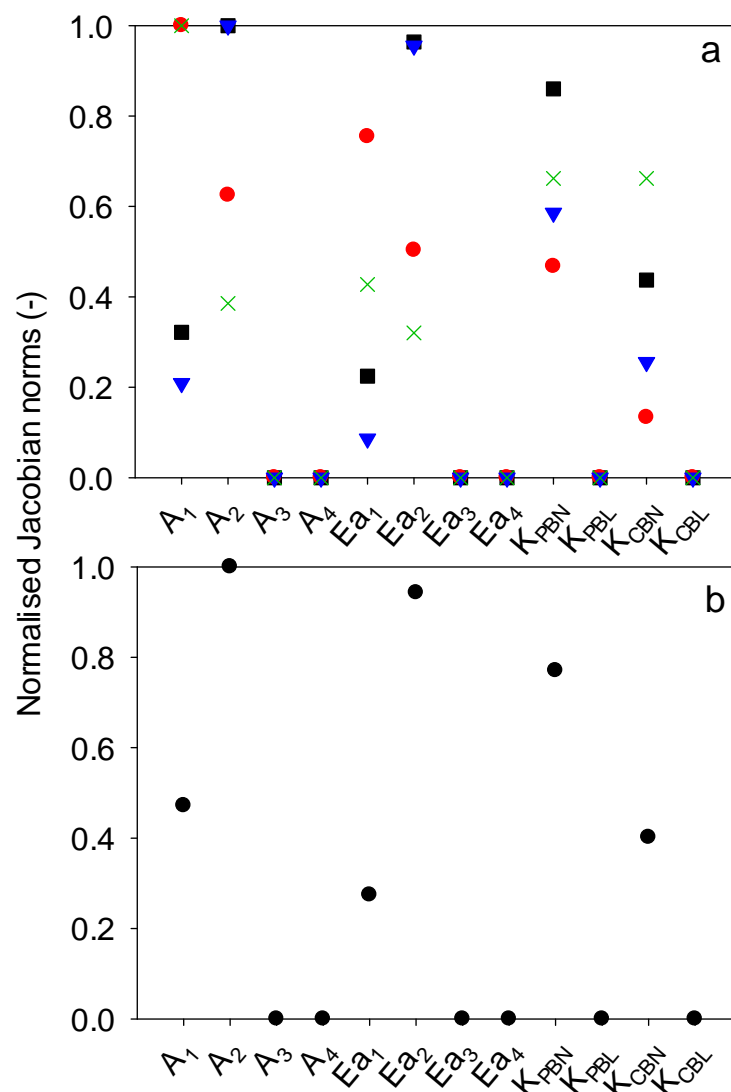
Figure 4.16: Normalised Jacobian norms with respect to all model responses (a): PBN ($\square$), PBL ($\circ$), CBN (∇), CBL ($\times$), and individual parameters (b) after eliminating 6 parameters.

These observations are in line with previous works of (Toukoniitty et al., 2003b) on kinetic analysis of 1-phenyl-1,2-propanedione (containing both ring and ketone functional groups) hydrogenation over modified Pt/Al$_2$O$_3$. They took into account both multisite adsorption and

also changes in adsorption modes when varying the modifier concentration to drive the best kinetic model. The fitting values of all parameters for each model are presented in Table 4.10.

Table 4.10: Fitting parameters from kinetic modelling of multi-temperature data.

		Parameters					
		$A_{ket,373}$	$A_{arom,373}$	$E_{a,ket}$	$E_{a,arom}$	K_{CBN}	SSR
Estimate	Model 4.14a	0.0034	0.0325	27.7	48.3	1.26	7.27×10^{-4}
95% Conf. Int.		$\pm 10^{-4}$	$\pm 10^{-3}$	$\pm 10^{0}$	$\pm 10^{0}$	$\pm 10^{-1}$	
Estimate	Model 4.14b	0.0034	0.0312	27.9	47.8	1.27	7.38×10^{-4}
95% Conf. Int.		$\pm 10^{-4}$	$\pm 10^{-3}$	$\pm 10^{0}$	$\pm 10^{0}$	$\pm 10^{-1}$	
Estimate	Model 4.14c	0.0036	0.0333	28.7	48.7	0.57	5.35×10^{-4}
95% Conf. Int.		$\pm 10^{-4}$	$\pm 10^{-3}$	$\pm 10^{0}$	$\pm 10^{0}$	$\pm 10^{-1}$	
Estimate	Model 4.14d	0.0034	0.0324	27.8	48.3	1.26	7.27×10^{-4}
95% Conf. Int.		$\pm 10^{-4}$	$\pm 10^{-3}$	$\pm 10^{0}$	$\pm 10^{0}$	$\pm 10^{-1}$	

* Units: Refer to Table 4.7.

Examining the values in Table 4.10, it can be seen that final estimates for all models are very similar to each other in value and confidence intervals. E_a value for ring hydrogenation step is higher than ketone which is in agreement with the previous experimental observations (§4.4.3). Similarly, the value of $A_{arom,373}$ is an order of magnitude higher than $A_{ket,373}$ which reflects the selectivity difference between two hydrogenation routes. The estimated values of E_a in a similar system, p-isobutyl acetophenone hydrogenation were 42 and 47 kJ mol^{-1} for ketone and ring hydrogenation, respectively, whilst the heat of adsorption of reactant was -5 kJ mol^{-1} (Mathew et al., 1999). Similarly, in a kinetic study of ketone hydrogenation over Raney nickel catalyst, heat of adsorption parameters were estimated in the range of -5 to -15

kJ mol^{-1} (Chang et al., 2000). On the other hand (Virtanen et al., 2009) estimated a value of 26 kJ mol^{-1} for ketone hydrogenation of cinnamaldehyde molecule on supported ionic liquid catalysts. Furthermore, values in the range of 42-50 kJ mol^{-1} were reported by (Neri et al., 1997) for activation energies of ketone and double bound hydrogenation of cinnamaldehyde over alumina supported ruthenium catalyst.

The presence of K_{CBN} in final models is very similar to findings of (Mounzer et al., 2010) which suggested that desorption of the selective intermediate product using n-hexane as the solvent is a critical component of reaction kinetics and selectivity.

It should be noted that model Model 4.14a and Model 4.14d are similar in their mathematical form at 5 parameters. Model 4.14b and Model 4.14c are also mathematically similar at 5 parameters with the key difference of Model 4.14b having K_{ADS} terms in rate expression numerators and physical meaning of kinetic constants as lumped adsorption/reaction or reaction/desorption terms in subsequent models.

All the models were also examined for cross-correlation of parameters via condition number, $C(J_k)$, Equation (4.24). As parameters are removed from model descriptions, the number of linear dependent columns is reduced within the Jacobian matrix. Higher values of condition number reflect a greater degree of cross-correlation between parameters in the system. Figure 4.17 shows the condition number for all models investigated after each parameter elimination.
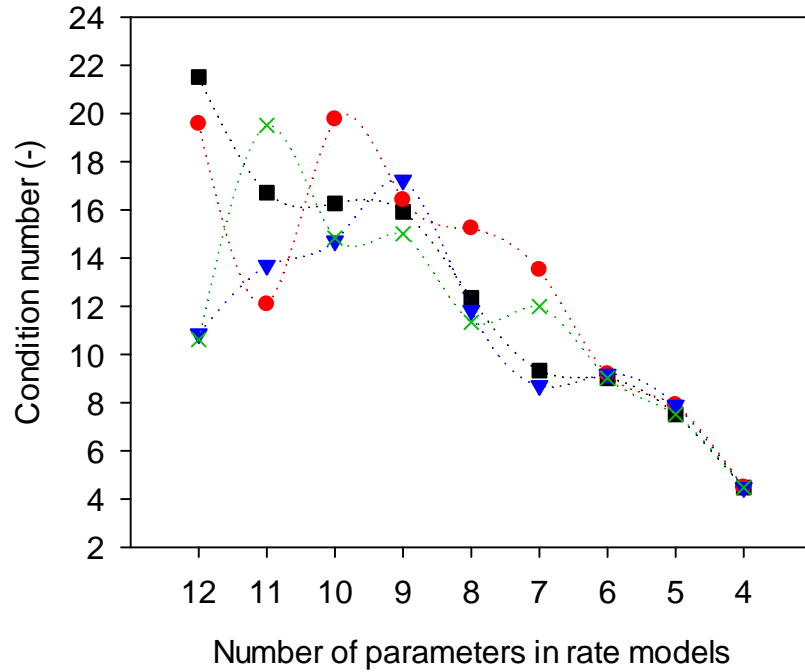
Figure 4.17: Changes in condition number with the number of parameters present in rate models: Model 4.12a: surface reaction RDS (□); Model 4.12b: surface reaction RDS with product desorption (○); Model 4.12c: reactant adsorption RDS (∇); Model 4.12d: final product desorption RDS (×).

The value of $C(J_k)$ is very similar for all models at 5 parameter thus it is better to discriminate them by looking at the profiles as a whole when the number of parameters in models are reduced. For surface reaction RDS model the value decreases continuously with removal; same in the surface reaction RDS with product desorption term apart from a sudden decline when removing the first parameter. For the reactant adsorption RDS model $C(J_k)$ shows a little oscillation for the first 3 parameters removed due to indeterminate parameters that become estimated after each removal and afterwards starts to decline continuously as elimination progresses. Final product desorption RDS model shows an increase in $C(J_k)$ for

the first 3 parameters removed due to more than 3 indeterminate parameters which were estimated after subsequent removals, increasing the number of linear dependent columns in Jacobian Matrix and then following the same decline as the other models.

To examine the quality of fit for the temperature varied data the parity plots for all model responses were plotted for the surface reaction RDS with product desorption term. To assess the fit the values are compared in terms of their deviation by more than 20% against the ideal estimate. The parity plot for PBN is presented in Figure 4.18.
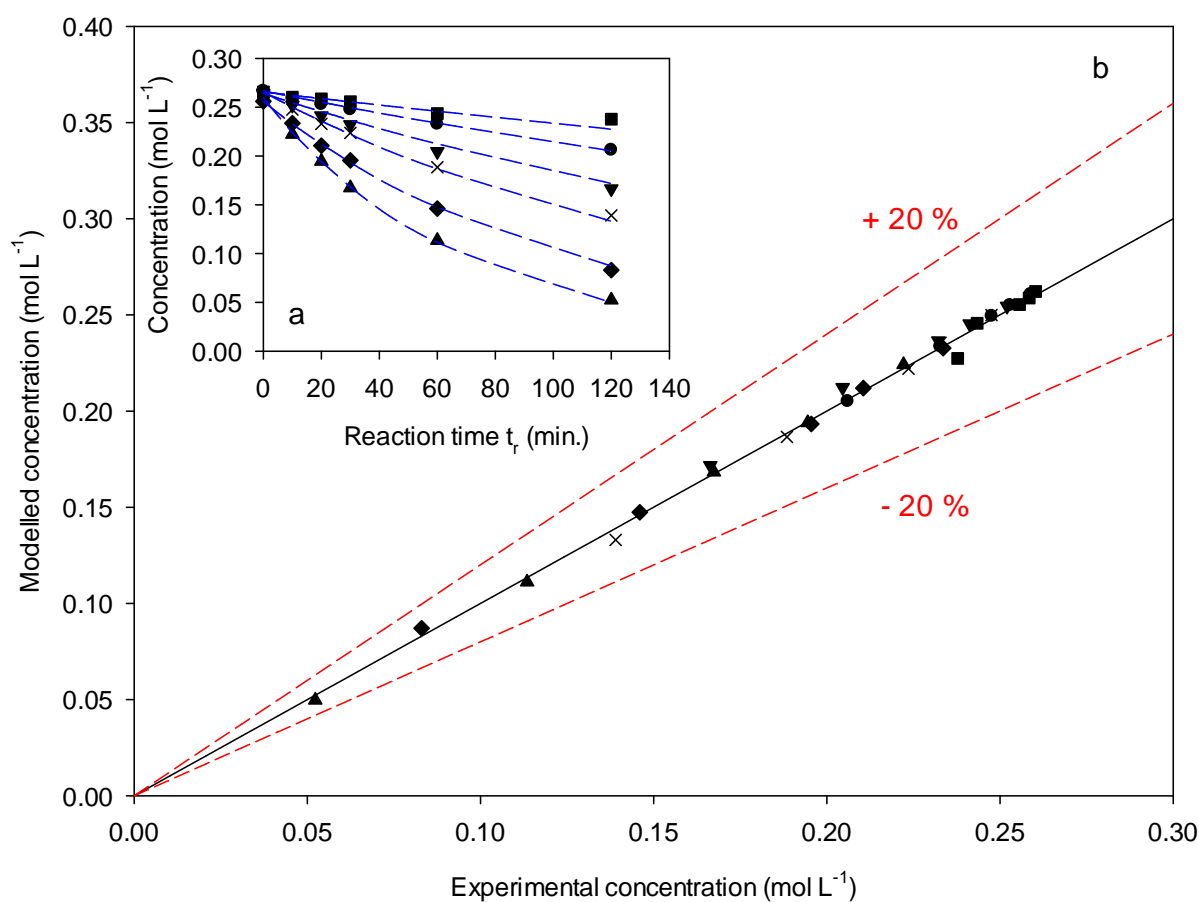
Figure 4.18: Modelled concentration data for PBN (a) and parity plot (b) for all temperatures investigated: 303 K (□), 313 K (○), 323 K (▽), 333 K (×), 343 K (◇), 353 K (△).

From Figure 4.18 it is apparent that the model estimates the PBN data closely with the estimated concentrations showing very small deviations from ideal estimate.

The parity plot for PBL is shown in Figure 4.19. In terms of PBL 6 data points are estimated with more than 20% deviation from ideal estimate. Most of the deviation occurs at lowest and highest temperatures at higher conversions (Figure 4.19b). Among all model responses PBL has always accounted for the highest residuals for all models considered.
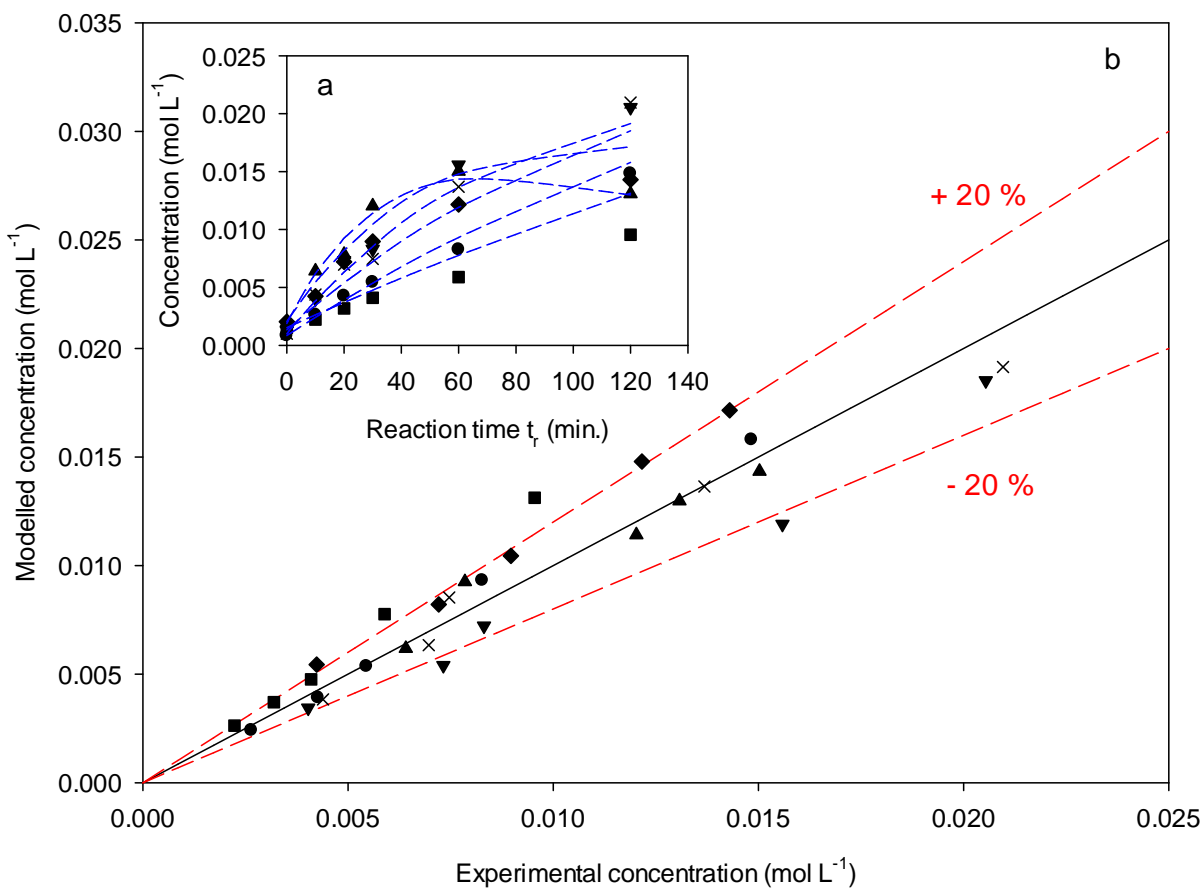
Figure 4.19: Modelled concentration data for PBL (a) and parity plot (b) for all temperatures investigated 303 K (□), 313 K (○), 323 K (▽), 333 K (×), 343 K (◊), 353 K (△).

CBN parity plot is presented in Figure 4.20. The fit for CBN is quite satisfactory with only two data points showing more than 20% deviation.
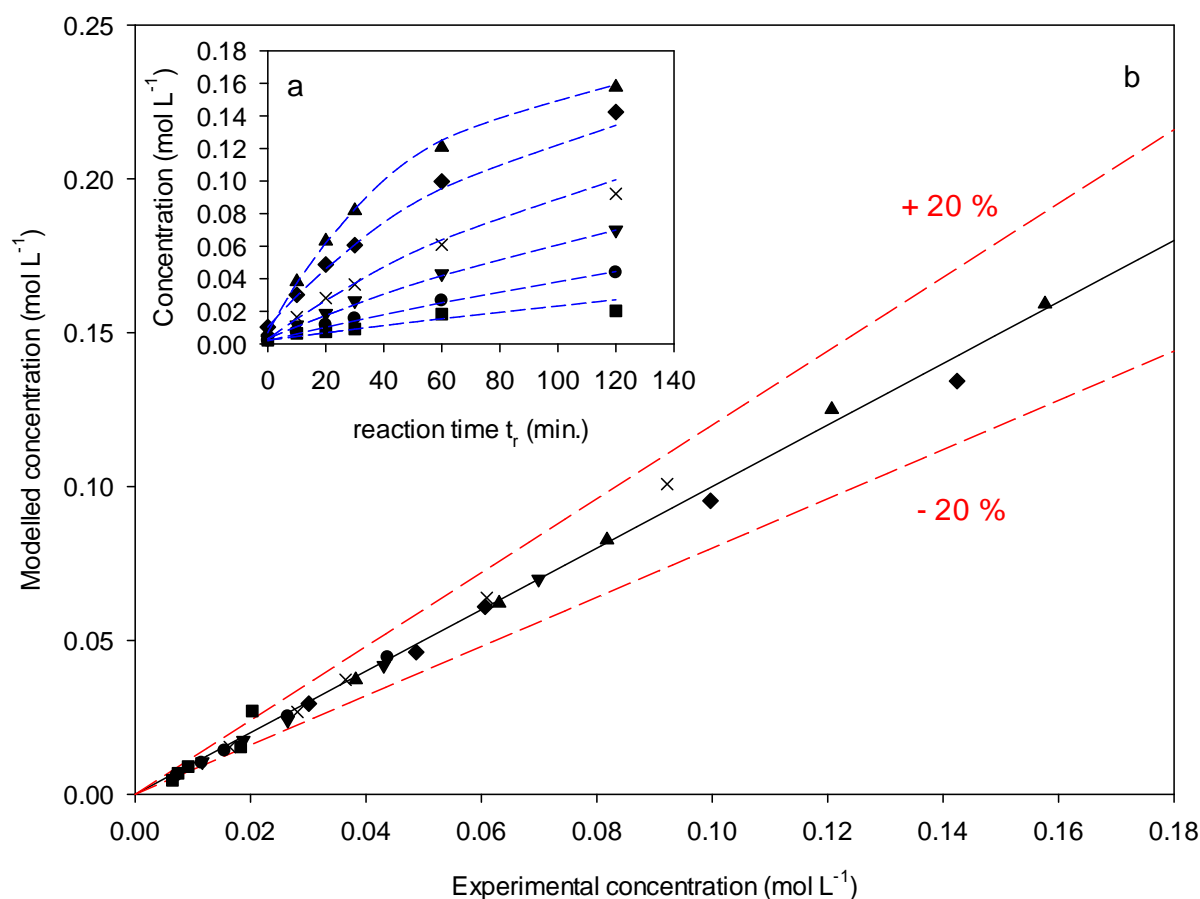
Figure 4.20: Modelled concentration data for CBN (a) and parity plot (b) for all temperatures investigated: 303 K (□), 313 K (○), 323 K (▽), 333 K (×), 343 K (◊), 353 K (△).

Parity plots for CBL shows more than 20% deviation for 17 data points accounting for the lowest concentrations at 303 and 313 K and the starting concentrations for higher temperatures (Figure 4.21a-b). However, the overall fit is still very acceptable (Figure 4.21c).
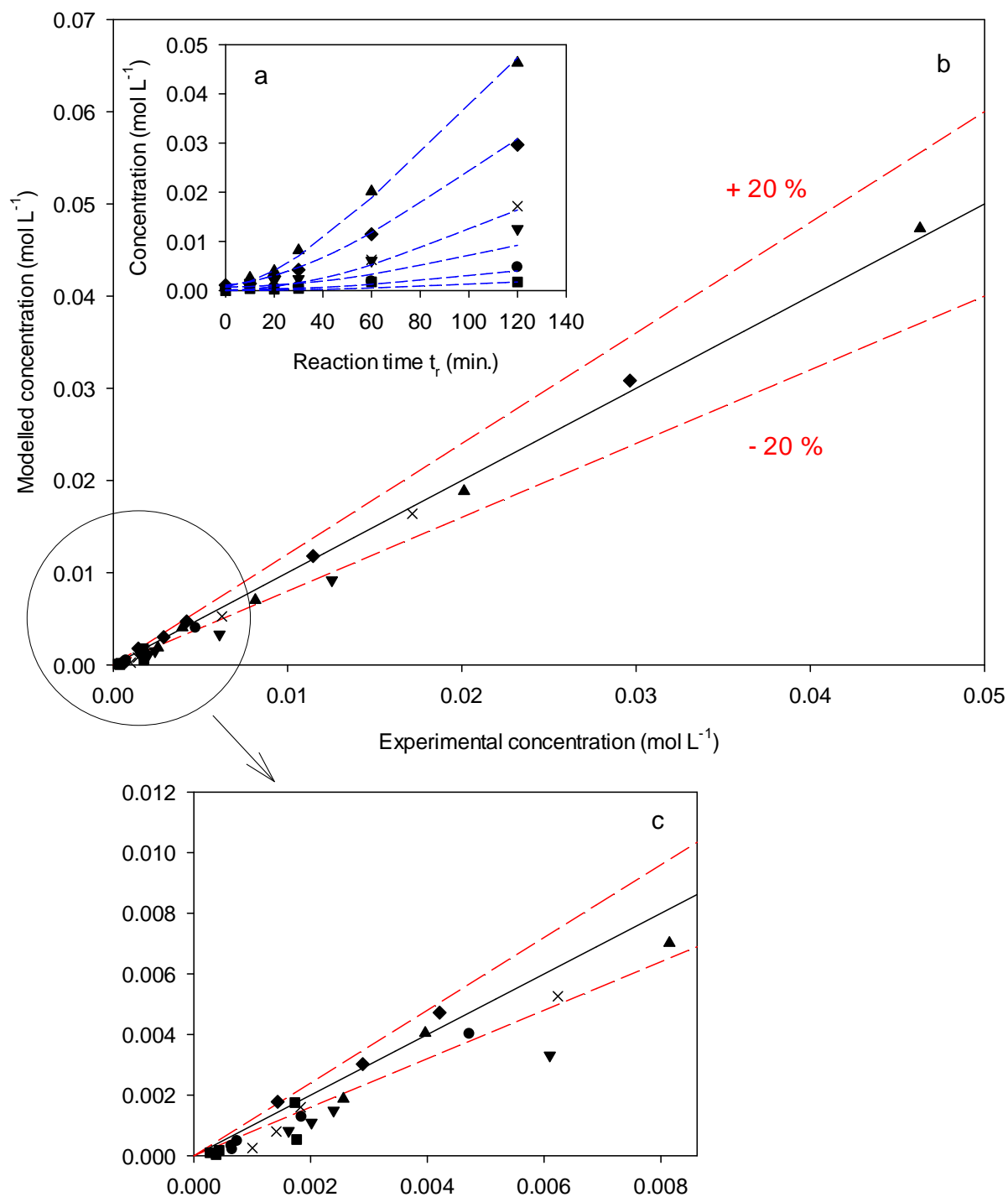
Figure 4.21: Modelled concentration data for CBL (a) and parity plot (b,c) for all temperature investigated: 303 K (□), 313 K (○), 323 K (▽), 333 K (×), 343 K (◇), 353 K (△).

Based on these observations and previous studies of (McManus et al., 2014b) and (Chen et al., 2012) it was postulated that two types of active sites are available for PBN hydrogenation, a Pt site which is largely selective towards aromatic ring hydrogenation and a site at the interface between Pt and oxide support, possibly an oxygen vacancy site in the TiO_2 structure, resulting in ketone hydrogenation. The presence of this site was thoroughly discussed in Chapter 2.

Looking into the previous studies on hydrogenation of similar molecules like acetophenone (AP) it has been suggested that enhancement of hydrogenation of phenyl group may depend on the electron effect of promoter and on the rate of carbonyl hydrogenation (Chen et al., 2003).

The adsorption geometries of AP on Pt/SiO_2 were assumed to be the controlling factor in molecular decomposition and hydrogenation of functional groups and were investigated using Infrared Spectra (IR). It was found out that in gas phase AP adsorbs in two modes of $\eta^1(O)$ and $\eta^2(C,O)$ on the surface of the platinum as shown in Scheme 4.1. $\eta^1(O)$ mode is where AP coordinates to Pt through the oxygen atom of carbonyl group resulting in a parallel aromatic ring arrangement. In $\eta^2(C,O)$ mode the carbonyl group coordinates by means of π-electrons of C=O resulting in a tilted ring group arrangement relative to surface. The $\eta^2(C,O)$ configuration of AP is proposed to be the intermediate for reagent decomposition into hydrocarbon fragments. On the basis of these observations it was concluded that the selectivity of AP hydrogenation is strongly dependent on the formation of hydrocarbon fragments (CO, benzene, toluene, and methane) originating from AP decomposition/hydrogenolysis and strong adsorption of aromatic ring containing product (1-

phenylethanol (PE)) on the Pt surface. These fragments subsequently inhibit the bonding between phenyl group and Pt suppressing AP ring hydrogenation.
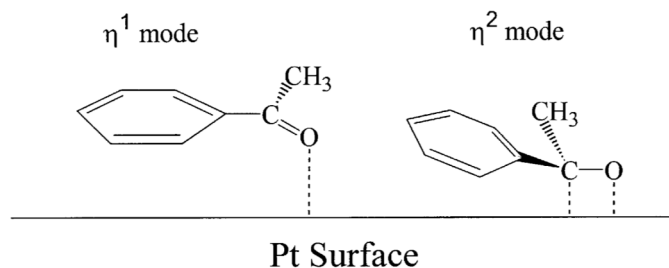
Scheme 4.1: Adsorption modes of AP on platinum surface

On the other hand a more recent study carried out by (Chen et al., 2012) in liquid phase using hexane as solvent and Pt/Al_2O_3 as catalyst in a batch reactor coupled with in-situ Attenuated Total Reflectance Infrared Spectroscopy (ATR-IR) coupled with modulation excitation spectroscopy (MES) and phase sensitive detection (PSD) studies has found out that AP adsorbs not only on platinum but also on Lewis acid sites of the oxide support through one of the oxygen lone pairs. Consequently, it was concluded that AP was most likely adsorbed on Pt surface in the $\eta1(O)$ configuration and high selectivity to PE (selectivity > 80%) observed in separate catalytic tests in autoclave reactor (298 K, 1 bar H_2) as results of the favored hydrogenation of the carbonyl group was attributed to this mode of adsorption. On the other hand X-sensitive benzene mode of adsorption was also observed with the band intensity increasing as the hydrogenation progressed along with ν (C=O) band on Al_2O_3. Much lower ring hydrogenated product (cyclohexylmethylketone, CMK) was produced and was attributed to π-bonded surface aromatic complex (selectivity < 20%). The decomposition of AP to hydrocarbon fragments was strongly suppressed in liquid-phase as $\eta^2(C,O)$ mode was not observed. The ATR-IR investigation of reaction pathway during hydrogenation demonstrated

that PE strongly adsorbs on the alumina support and competes with AP. AP desorbed from support either returns to bulk or adsorbs on the on Pt in η1(O) mode. The competitive adsorption studies of AP and Ethylbenzene (EB-containing only ring functional group) showed only minor effects of presence of EB on adsorption behavior of AP. The competitive adsorption of AP and CMK was not carried out.

Along similar lines, during the course of the CASTech project Density Function Calculations (DFT) of PBN on clean platinum (Pt (111)) were carried out using toluene as solvent[5]. Toluene showed the highest selectivity towards PBL of around 60% thus it was postulated that there might be a possible toluene adsorption on Pt blocking ring hydrogenation (selectivity differences with solvent to be discussed further in Chapter 5).

The following adsorption geometries (Scheme 4.2) were reported for low toluene coverage with heats of adsorption for ring and carbonyl of -0.55 and -0.18 eV, respectively thus concluding a more stable adsorption of ring on Pt compared with carbonyl. The activation barrier of hydrogenation of carbonyl was calculated to be lower than ring and subsequently the high selectivity towards CBN in hexane was attributed to the stability of ring adsorption on Pt.
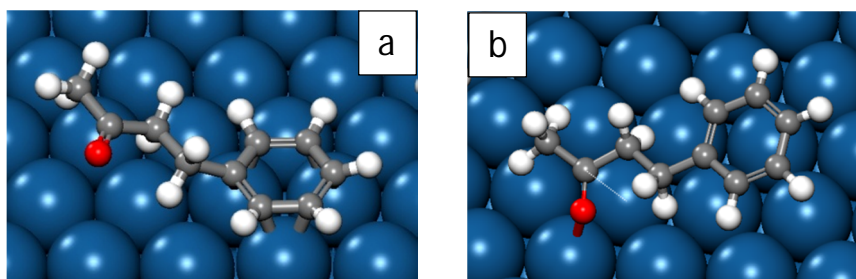
Scheme 4.2: PBN adsorption on Pt(111) from DFT calculations[1]: Ring adsorption (a); Carbonyl adsorption (b)

These observations were also considered when developing rate equations for kinetic modelling of concentration varied data.

4.4.8 Modelling of the concentration varied data

The modelling results from temperature varied data have afforded an initial mechanistic understanding to the kinetics governing this system. The next step is to develop models to explain the experiments where initial PBN concentration is varied to examine the active site basis in terms of selective sites towards ring and carbonyl, product desorption terms and competitive adsorption of organics and H_2 molecules.

The previous observations in section §4.4.3 showed initial reaction rates with increasing PBN initial concentration tending towards an apparent rate order of -0.05. This negative order behavior is consistent with reaction mechanism that features competition between organics and hydrogen (denominator power $\geq$ 2) as well as an influence of product desorption which was demonstrated in section §4.4.7. It was also demonstrated in the previous section that K_{PBN} though indeterminate in single site models is still an important parameter to investigate and the possibility of two distinct sites each selective towards hydrogenating ring or carbonyl was suggested.

Based on these observations 6 models based on different active site assumptions were developed as shown in Table 4.11.

Table 4.11: Candidate active site models for PBN hydrogenation reactions with varying initial concentration.

Equation No.	Kinetic model
4.33a-b	$$\theta_{v,arom} = \theta_{v,ket} = \dfrac{1}{\left(1 + K_{a,arom}\cdot[R] + K_{a,ket}\cdot[R] + \dfrac{[P]}{K_{c,arom}} + \dfrac{[P]}{K_{c,ket}}\right)^{n}}$$ • Both ketone and ring hydrogenations occur on the same sites
4.34a-b	$$\theta_{v,arom} = \dfrac{1}{\left(1 + K_{a,arom}\cdot[R] + \dfrac{[P]}{K_{c,arom}}\right)^{n}}$$ $$\theta_{v,ket} = \dfrac{1}{\left(1 + K_{a,ket}\cdot[R] + \dfrac{[P]}{K_{c,ket}}\right)^{n}}$$ • Ketone and ring hydrogenations occur on different sites
4.35a-b	$$\theta_{v,arom} = \dfrac{1}{\left(1 + K_{a,arom}\cdot[R] + \dfrac{[P]}{K_{c,ket}}\right)^{n}}$$ $$\theta_{v,ket} = \dfrac{1}{\left(1 + K_{a,ket}\cdot[R] + \dfrac{[P]}{K_{c,arom}}\right)^{n}}$$ • Ketone and ring hydrogenations occur on different sites • PBL blocks ring hydrogenation site and CBN competes with PBN for carbonyl hydrogenation site. **n = 2 (b) if organics compete with H_2, n = 1 (a) if not.**

Models 4.33a-b assume a single site model for hydrogenation of both ring and carbonyl groups. Models 4.34a-b assume that ring and carbonyl hydrogenation occur on different reactive sites and their corresponding intermediate products desorption is an inhibiting factor in their rates. Models 4.35a-b are also 2-site models with the difference that desorption of the corresponding intermediate product of each reactive site is inhibiting the reaction of the other, thus, PBL competes with PBN for ring hydrogenation sites and CBN competes with PBN for carbonyl hydrogenation sites.

All rate models in Table 4.11 are initially comprised of 6 parameters (2 rate constants and 4 adsorption/desorption constants). Fitting the concentration data to the models with n = 1 resulted in only three or four parameters being estimated in either case and model optimization did not render any improvement in case of residuals and indeterminate parameters.

The models featuring competitive adsorption of compounds with H_2 (n = 2) were much more successful in describing the kinetics as a function of reagent concentration. The two site models were the only ones that could estimate all 6 parameters and within acceptable confidence intervals.

The RSS values for the single site and two site model featuring n = 2 were in order of 10^{-4}, which is an order of magnitude improvement on models comprising n = 1. Furthermore, all models were compared using Athena's discrimination and lack-of-fit option and the results are reported in Table 4.12. Athena's discrimination process entitles the use of RSS, Mean Absolute Error (*MAE*), Akaike Information Criterion (*AIC*), and Akaike probability share (Π_{AIC}).

The MAE is a quantity used to measure the error of model predictions against experimental outcomes.

$$MAE = \frac{1}{n}\sum_{i=i}^{n}|f_i - y_i| = \frac{1}{n}\sum_{i=1}^{n}|e_i| \tag{4.36}$$

AIC is defined as,

$$AIC = m\frac{2}{n} + ln\left\{\frac{1}{n}RSS\right\} \tag{4.37}$$

with the assumption of normally distributed errors. *m* is the number of estimated parameters and *n* is the number of observations . The model with the lowest *AIC* number is preferred. Different models can also be compared by calculating Akaike Probability Share (π_{AIC}) which is given by

$$\pi_{AIC} = \frac{L_k}{\sum_{i=1}^{k}L_k} \tag{4.38}$$

Where L_k is the likelihood of model *k* that is defined as (Kopyscinski et al., 2013)

$$L_k = exp\left\{\frac{AIC_{min}-AIC_k}{2}\right\} \tag{4.39}$$

Based on Table 4.12, the discrimination process identifies the two site model (4.35b) as the best model describing the kinetics with lowest MAE and AIC values of 11.08% and -11.79, respectively and highest relative likelihood and probability share, Π_{AIC}. Meaning, this model has a likelihood (L_K) of 100%, whereas the models featuring single site (4.33b) and two site (4.34b) models featuring n =2 have likelihoods of 85% and 89%, respectively. The non-competitive models (n = 1) only show likelihood of <50% meaning that their probability is nearly ½ compared to competitive models. The distribution of residuals for all model responses was evaluated as well and it was observed that the single site models and con-

178

competitive models show a distribution of residuals which are strongly dependent on initial concentration and 2-site models and competitive models show a normal distribution of residuals independent of C_{PBNi} (Appendix D).

The apparent success of Model (4.35b) in modelling the kinetics of concentration varied data is interesting when taking into consideration the selectivity results observed in 3000 mL scale. This is further discussed in subsequent sections where theories on reasons behind the shift in selectivity profile when scaling to 3000 mL are listed and explained. The schematic representation of Model 4.35b is presented in Scheme 4.3.

Table 4.12: Model discrimination and lack-of-fit results for all models in Table 4.11.

Model No.	N_P total	N_P estimated	RSS	R^2	L_k	MAE (%)	AIC	Π_{AIC}	Rank
4.34a	6	4	2.92×10^{-3}	0.9961	0.482	25.08	-10.33	0.115	Worst
4.33a*	5	3	2.98×10^{-3}	0.9961	0.484	25.54	-10.34	0.115	
4.35a	6	4	2.86×10^{-3}	0.9962	0.489	17.21	-10.33	0.117	
4.33b*	5	4	9.46×10^{-4}	0.9987	0.848	20.39	-11.46	0.202	
4.34b	6	6	8.19×10^{-4}	0.9989	0.891	18.26	-11.56	0.213	
4.35b	6	6	6.53×10^{-4}	0.9991	1	11.08	-11.79	0.238	Best

*Only models undergone model refinement with K_{PBL} being eliminated: Indeterminate and statistically insignificant

** N_P refers to number of parameters in rate models
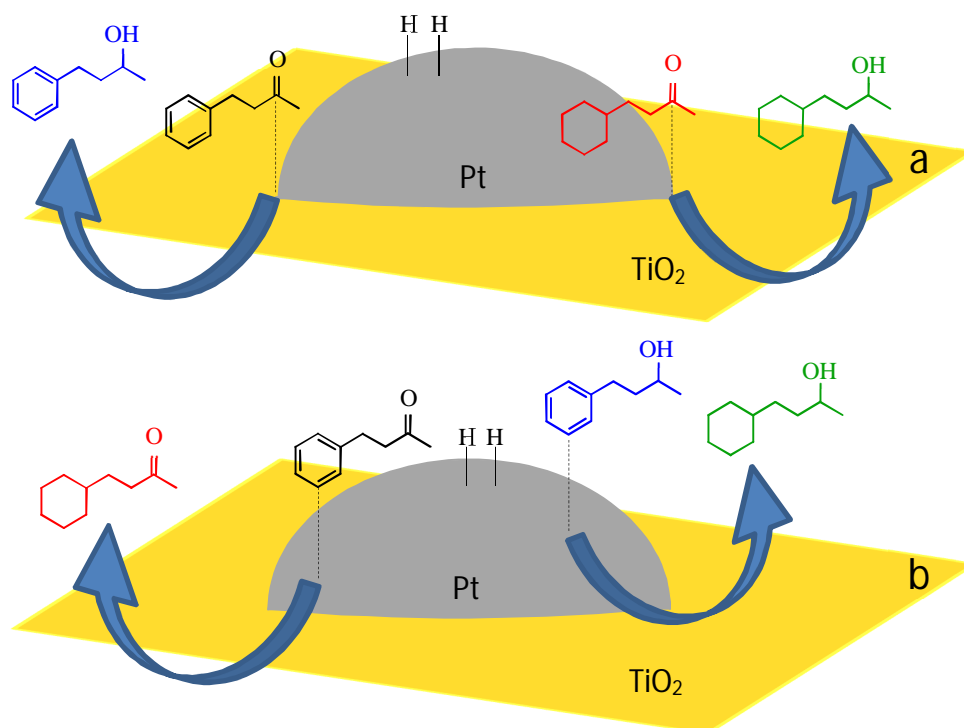
Scheme 4.3: Schematic representation of Model 4.35b: Ketone adsorption site (a), ring adsorption site (b).

Table 4.13 shows the fitting results for all active site models featuring competitive adsorption. The success of two site model in predicting all parameters and ranking as the best model based on lack-of-fit analysis validates the previous assumption of selective active sites. All models have higher $K_{a,arom}$ values reflecting the dominance of this mode of adsorption when using hexane as solvent. It was not clear from previous section (§4.4.7) whether or not ketone hydrogenation occurs on Pt sites as well or only on oxygen vacancy sites between Pt and support or both. If so, this might explain the relative success of the single site competitive

model in explaining kinetics as well. k_{ket} is significantly higher in single site model compared with two site which is likely due to cross-correlation of this term with $K_{a,arom}$ in former model. Fitting multiple adsorption modes on a single site basis as different adsorption constants had been rarely successful as parameter cross-correlation is often induced. Previous modelling results of temperature varied data confirms this where K_{PBN} was always found to be highly cross-correlated with pre-exponential factors for ketone hydrogenation routes.

Table 4.13: Parameter estimates and confidence intervals for models featuring competition between organics and H_2.

Parameter	Model No. 4.33b	Model No. 4.34b	Model No. 4.35b
k_{ket}	0.019 ± 0.004	0.0057 ± 0.002	0.0106 ± 0.004
k_{arom}	0.101 ± 0.021	0.1278 ± 0.033	0.0753 ± 0.012
$K_{a,ket}$	-	2.510 ± 0.894	5.755 ± 1.437
$K_{a,arom}$	8.540 ± 1.130	10.200 ± 1.64	6.441 ± 0.682
$K_{c,PBL}$	Eliminated	0.023 ± 0.012	0.012 ± 0.002
$K_{c,CBN}$	0.067 ± 0.012	0.058 ± 0.012	0.115 ± 0.058

* Units: Refer to Table 4.7.

The K_{PBL} for the single site model was found to be indeterminate and statistically insignificant and was consequently eliminated. The K_{PBL} in in two site model was found to be statistically significant and removal of this parameter would result in a drastic drop in *RSS* and *MAE* values.

Figures 4.22-25 represent the modelled concentrations for all reaction responses for all initial PBN concentrations as well as the parity plots for Model (4.35b). The model estimates PBN rate closely (Figure 4.22a-b).
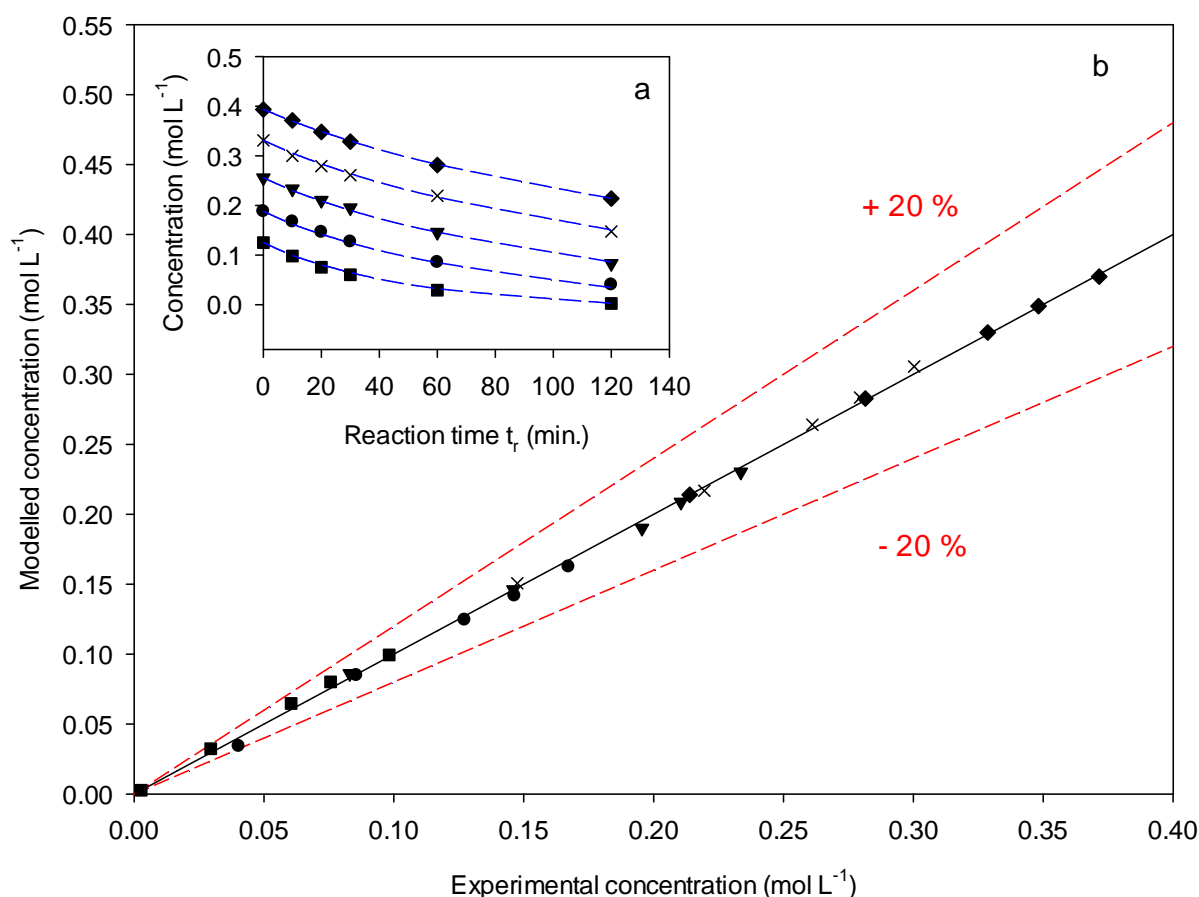
Figure 4.22: Modelled concentration data for PBN (a) and parity plot (b): 0.135 mol L^{-1} ($\square$), 0.202 mol L^{-1} ($\circ$), 0.269 mol L^{-1} (∇), 0.337 mol L^{-1} ($\times$), 0.404 mol L^{-1} ($\diamond$).

The fitting results for PBL are presented in Figure 4.23. The model descriptions of PBL data are satisfactory. PBL shows the highest deviation across all data and probably accounts to the highest error to *MAE* with 6 data points deviating slightly more than 20% from ideal fit.
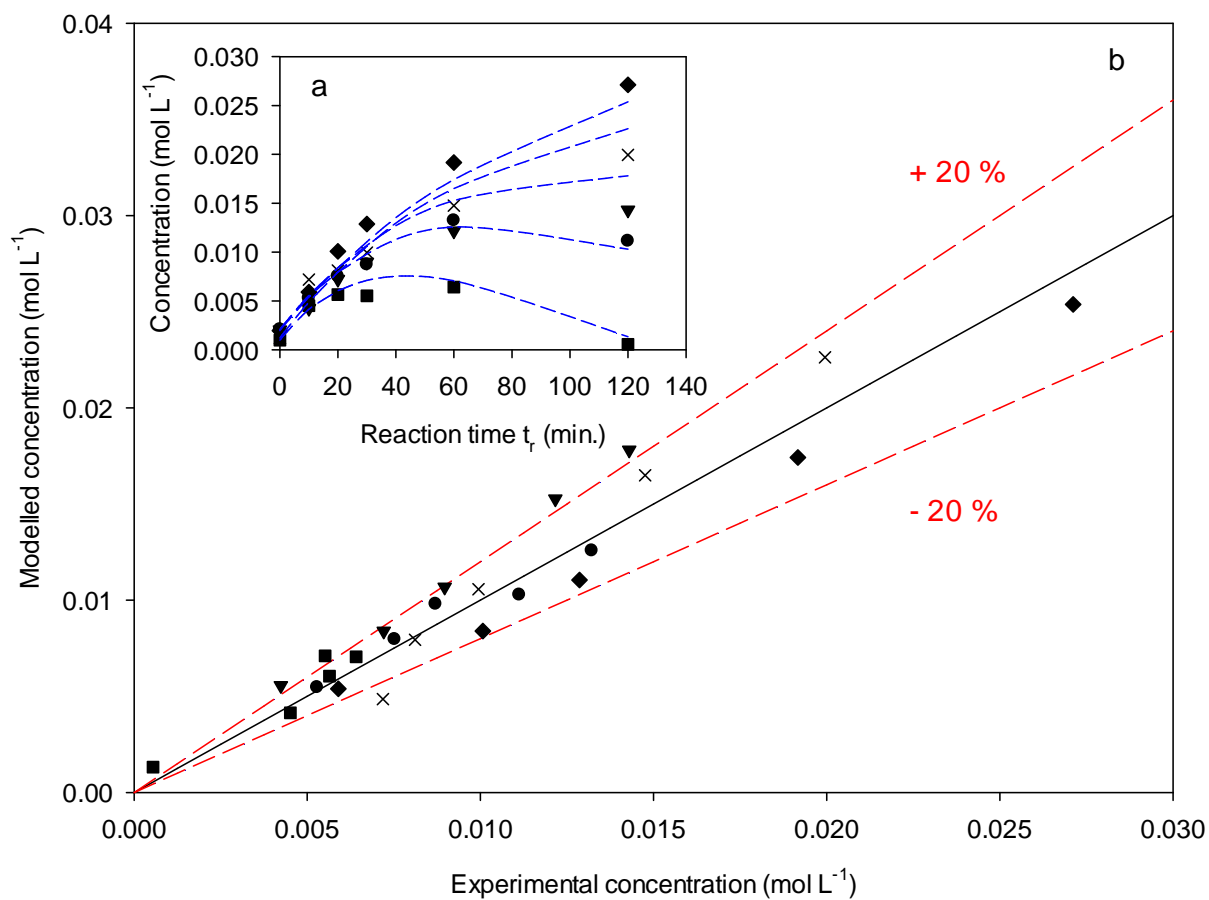
Figure 4.23: Modelled concentration data for PBL (a) and parity plot (b): 0.135 mol L^{-1} ($\square$), 0.202 mol L^{-1} ($\circ$), 0.269 mol L^{-1} ($\triangledown$), 0.337 mol L^{-1} ($\times$), 0.404 mol L^{-1} ($\lozenge$).

Figure 4.24 shows the fitting results for CBN. The model fits CBN data closely with deviations less than ±20%.
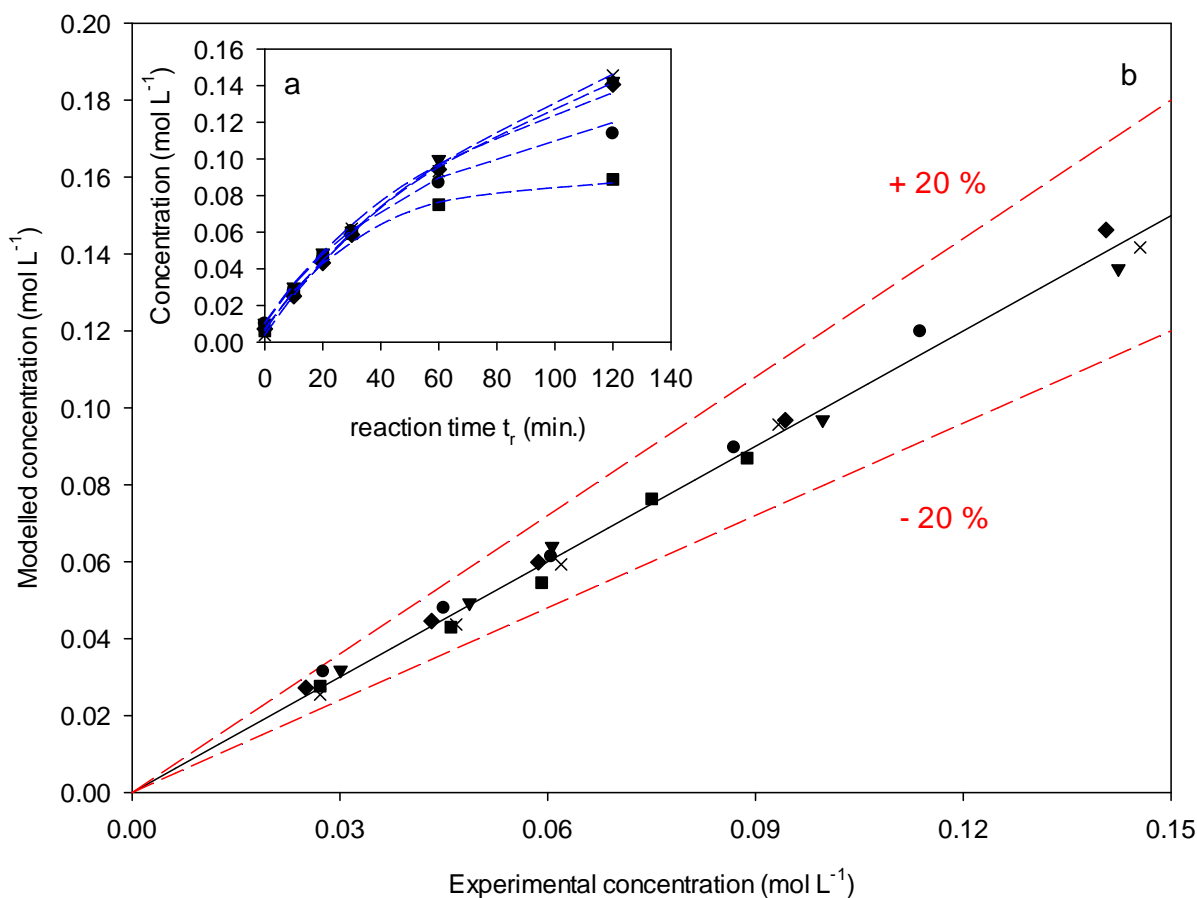
Figure 4.24: Modelled concentration data for CBN (a) and parity plot (b): 0.135 mol L^{-1} (□),

0.202 mol L^{-1} (○), 0.269 mol L^{-1} (▽), 0.337 mol L^{-1} (×), 0.404 mol L^{-1} (◊).

Figure 4.25 represents the model fit and parity plots for CBL response. CBL shows 8 data points deviating slightly from 20% specifically at the lowest conversions. This might be due to very low concentration of CBL compared with intermediate products at low conversions which would make them difficult to estimate more closely.
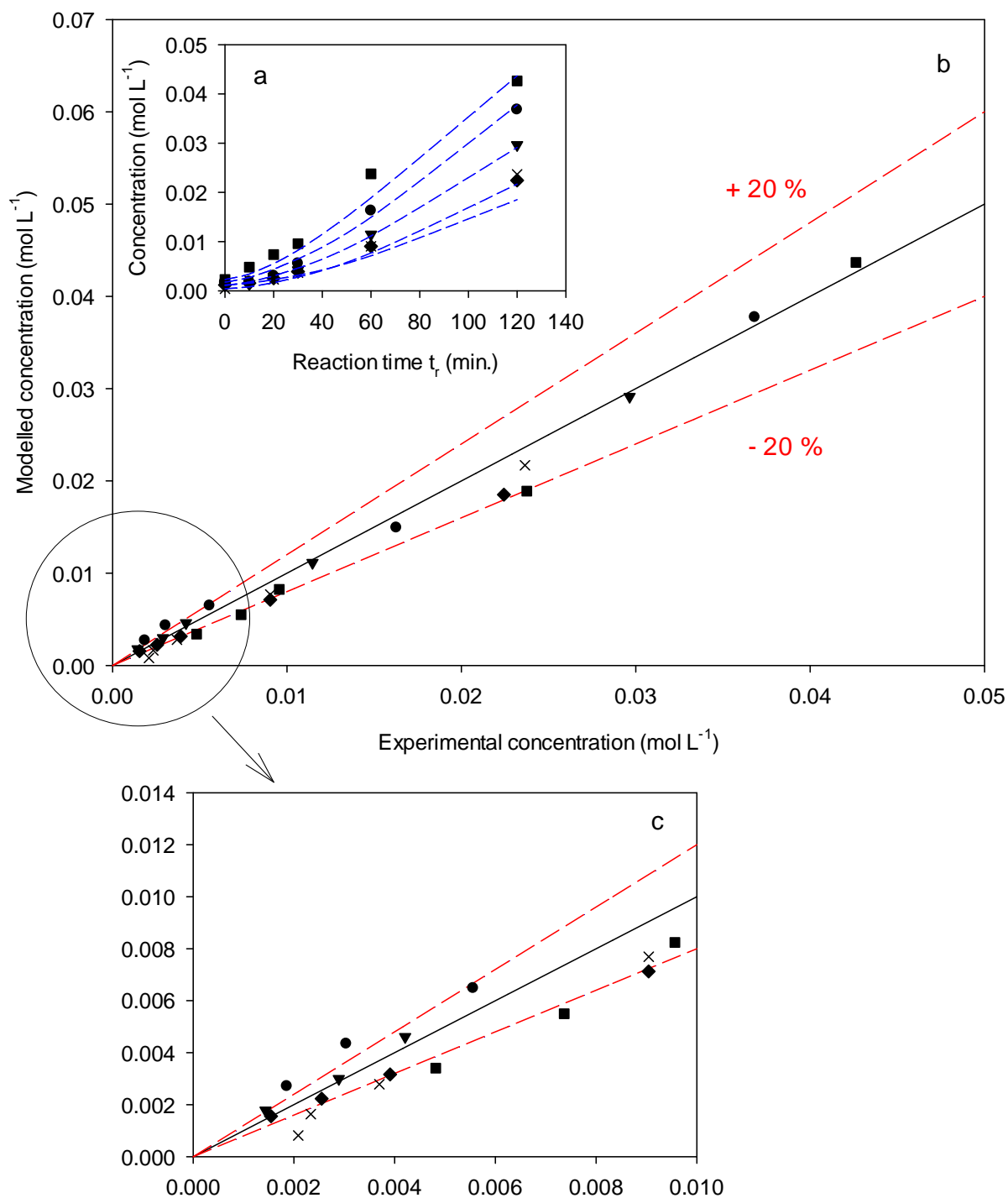
Figure 4.25: Modelled concentration data for CBL (a) and parity plot (b,c): 0.135 mol L^{-1} (□),

0.202 mol L^{-1} (○), 0.269 mol L^{-1} (▽), 0.337 mol L^{-1} (×), 0.0404 mol L^{-1} (◊).

The significance of the approach taken here to optimize the rate models lies in the final fitting results from chemical engineering point of view. Most of the studies dealing with multiphase reactions where species adsorptions are important, struggle with proper estimation of the K_{ADS} terms. In more than a few occasions the parameter estimation led to negative values or poor confidence intervals for the resulting fit thus forcing the researchers towards various methods to cut the parameters without proper analysis.

The following procedures are commonly used by researchers during kinetic modelling without proper statistical assessment:

- Cutting the adsorption terms of products with lowest model response or lumping the adsorption constants of same type molecules together (alcohols, ketones, etc) as an initial consideration before parameter estimation to free degree of freedoms (Marchi et al., 2007), (Crespo-Quesada et al., 2011), (Rebrov et al., 2009), (Patil et al., 2006), (Gao et al., 2006).

- Cutting or fixing the adsorption terms from rate models if the estimated parameter value is physiochemically unacceptable without analyzing the statistical impact of the elimination (Bertero et al., 2008), (Chang et al., 2000), (Toppinen et al., 1997), (Salmi et al., 2007).

- Combining the rate constants with adsorption terms and fixing the value over a narrow range to force the other kinetic constants towards meaningful values (Mukherjee and Vannice, 2006a).

- Applying constraints over the range of parameters or multiplying the adsorption terms by a constant factor to optimize the adsorption constant ratios based on apparent rate order to force the other parameters towards positive estimates and higher R^2 values (Bertero et al., 2008), (Bergault et al., 1998).

- Cutting a reaction route based on physiochemically unacceptable values of rate and adsorption constants (Marchi et al., 2007).

- Rejecting models based on physiochemically unacceptable parameters at the initial run (Marchi et al., 2007), (Chang et al., 2000), (Mathew et al., 1999), (Bawane and Sawant, 2005), (Usman et al., 2011).

- Solving the rate models algebraically to independent isothermal data sets and search for straight line Arrhenius-van't Hoff plots although it has long been established by (Pritchard and Bacon, 1975) that this approach leads to rejection of models due to physiochemically unacceptable parameter estimates (Rode et al., 2001), (Chang et al., 2000), (Patil et al., 2006), (Sitthisa et al., 2011), (Serna et al., 2009), (Mathew et al., 1999), (Neri et al., 1997), (Bawane and Sawant, 2004), (Bawane and Sawant, 2005).

- Only considering one or two criteria from the following to discriminate the remaining models: average relative error (%RR), R^2, residual distribution, parity plots, etc (Marchi et al., 2007), (Mathew et al., 1999), (Patil et al., 2006), (Bertero et al., 2008), (Serna et al., 2009), (Gao et al., 2006).

- Overlooking the inability of a certain model which generates unreliable adsorption terms (Toukoniitty et al., 2003b), (Hoffer et al., 2004).

- Not reporting the confidence intervals on estimated parameters (Mathew et al., 1999), (Patil et al., 2006), (Mukherjee and Vannice, 2006a), (Rode et al., 2001), (Neri et al., 1997).

- Not re-parameterizing Arrhenius-van't Hoff which always results in high cross-correlation between pre-exponentials and activation energies leading to highly nonlinear problems (Chang et al., 2000), (Virtanen et al., 2009), (Mathew et al., 1999).

- Not disclosing the reasoning behind rejected kinetic models (Virtanen et al., 2009).

The problem with these approaches is that the apparent rate order is not a reliable term to base the models on to accurately describe the kinetic behaviour. Furthermore constructing kinetic models in such a manner could limit the kinetic models to narrow operating conditions which would be problematic for further process optimization. The negative parameter estimates or large confidence intervals encountered at the beginning of the parameter estimation process might as well be due to over-parameterization of the model as was seen here as well and sensitivity analysis is required to determine if the said parameters are still significant and might be able to be estimated when insignificant parameters are eliminated systematically. The following procedures are recommended to researchers for parameter estimation:

- Do not solve the kinetic models algebraically on individual isothermal data sets. Make use of the parameter estimation softwares with built in ODE solvers like Athena, Modest etc. If not available, ODE solver function in Matlab is the next best thing.

- Always make use of re-parameterization before parameter estimation.

- Do not cut the adsorption terms based on negative values and use sensitivity analysis, cross-correlation matrix, statistical F-test and t-values to assess the impact of elimination systematically.

- Since nonlinear Levenberg-Marquardt method is sensitive to initial guess for parameters an initial observation can be made by changing the order of parameters over a meaningful range to assess the bios towards certain parameters (Hsu et al., 2009).

- Make use of multi-temperature data in order to investigate the dominant reaction routes and adsorption terms and develop models in accordance to get a better estimate of these values using multi-concentration isothermal data.

- Although out of scope of this work, fixing the values of hydrogen adsorption constant by using literature reported values of entropy and enthalpy of adsorption on a specific catalyst are commonly used. Statistical assessment of this approach is recommended (Thakar et al., 2007a).

- Do not discriminate the models before a complete model refinement is applied.

- Make use of available statistical tools and combine them with observed RSS, confidence intervals, parity plots, and residual plots to discriminate the models.

- Though not available here at each data point, replicated experiments are highly useful during lack-of-fit analysis and model discrimination.

- Double check the model robustness and convergence at the end of the procedure by varying the scale of initial guess of parameters.

Limiting the kinetic models over a narrow range of operating conditions might also arise from over-simplification of kinetics as was reported for over-parameterized models (Berger et al., 2001). Consequently, one needs to look critically at the reaction behavior specifically the evolution of selectivity with operating conditions and develop the models based on the observed dominant pathways. As with our case previous observations concluded that the ring hydrogenation is the dominant pathway in this system and CBN adsorption plays an important role in kinetics of it. These observations perfectly reflect the final model developed from fitting multi-temperature data. The final estimates are also need to be compared with initial observations to assess their physiochemical meaning.

Additionally, the most accurate way of estimating the K_{ADS} terms is to physically measure them in a series of batch adsorption experiments for every intermediate and inhibitor like the works of (Mounzer, 2009); doing so becomes extra complicated and time consuming as the

reactions become more complex and not all the compounds are industrially available. Consequently, using the sensitivity analysis based on derivatives gives the engineer the right tools to elucidate the significant parameters in rate models to be able to construct robust kinetic models and avoid over-simplification. Still, it is highly recommended as additional work in future to fully assess the limitations of the proposed approach over varied operational conditions.

4.5 Detailed kinetic modelling of 3000 mL scale data

This section deals with detailed kinetic analysis of the PBN hydrogenation in 3000 mL scale. First a detailed analysis of initial rates was carried out to investigate and quantify if external and internal mass transfer resistances were limiting the reaction under the chosen operational conditions.

The best models and parameter estimates from previous section were fitted to the experimental observations in 3000 mL at base conditions. Proper mass transfer effects (negligible) were applied to the hydrogen concentration in order to investigate if this model would be able to estimate the rate and selectivity profiles observed in 3000 mL scale.

4.5.1 Analysis of initial rates and mass transfer evaluations

To assess the chemical regime governing the PBN hydrogenation when scaling up to a 3000 mL reactor the reactions were carried out in varying energy input, H_2 pressure, temperature and catalyst loading. The results of changes in initial TOF with energy input and pressure are presented in Figure 4.26a-b. The results demonstrate linear increase with energy input and H_2 pressure initially indicating that some form of transfer limitation might exist. The measurement of different resistances r_{GL}, r_{LS}, and r_{reac} which correspond to gas-liquid, solid

liquid, and internal reaction resistances can be determined approximately by plotting the inverse of reaction rate versus inverse of catalyst loading (Figure 4.26c).
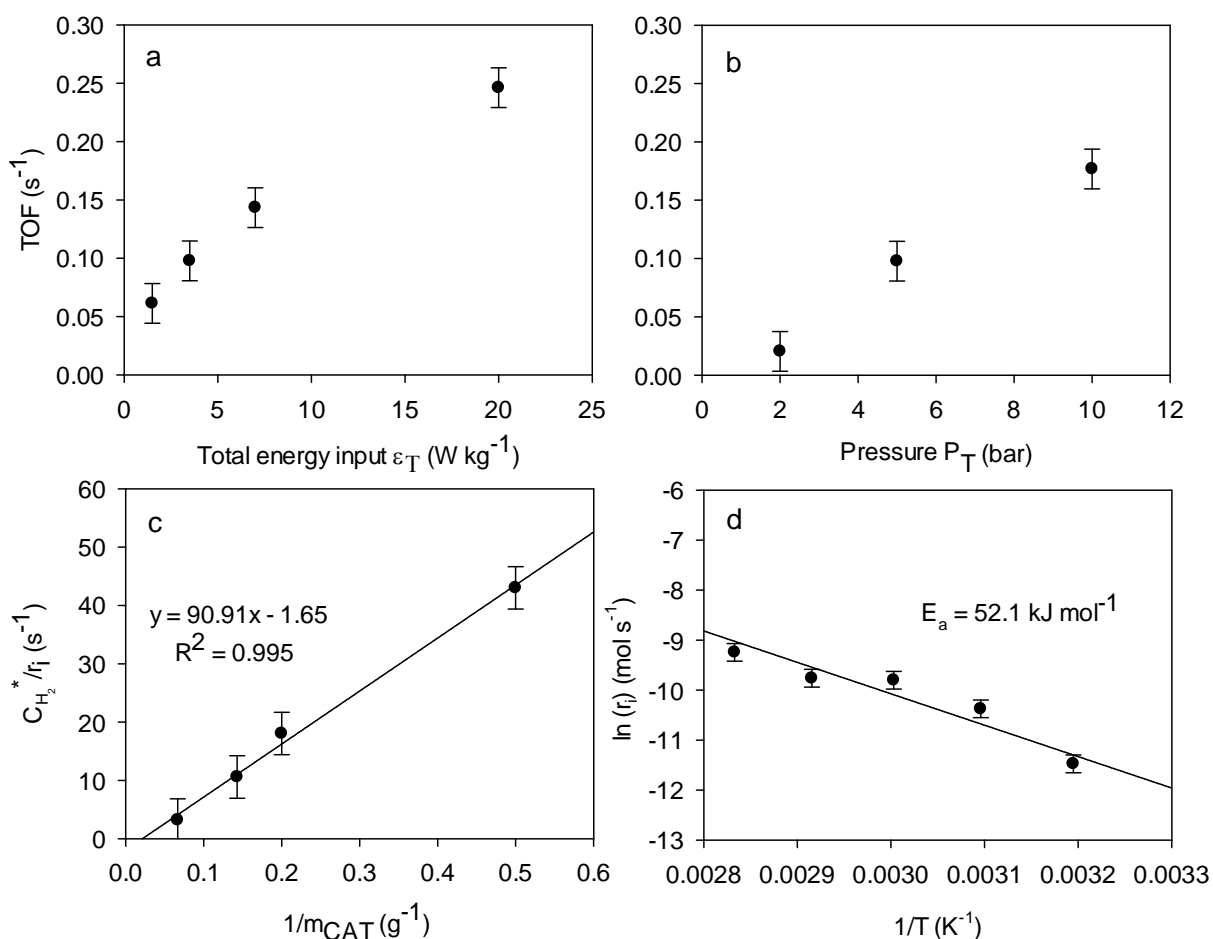
Figure 4.26: Analysis of initial rates for PBN hydrogenation in 3000 mL scale:

(**a,b**): Initial TOF with increasing total energy input and total pressure; [hexane, 343 K, C_{PBNi} = 0.27 mol L^{-1}, m_{PBN}/m_{CAT} = 0.02 , **a**: P_T = 5 bar, **b**: $\bar{\varepsilon}_T$ = 3.5 W kg^{-1}]

(**c**): Mass transfer plot; [hexane, 343 K, C_{PBNi} = 0.27 mol L^{-1}, P_T = 5 bar, $\bar{\varepsilon}_T$ = 3.5 W kg^{-1}]

(**d**): Arrhenius plot; [hexane, m_{PBN}/m_{CAT} = 0.02, C_{PBNi} = 0.27 mol L^{-1}, P_T = 5 bar, $\bar{\varepsilon}_T$ = 3.5 W kg^{-1}]

The following resistances can be deduced from the intercept and slope of the plot.

$$Intercept = r_{GL} = \frac{1}{k_{GL}a_b} \approx 00$$

$$Slope = r_{LS} + r_{reac} = \frac{1}{K_{SL}a_p} + \frac{1}{\eta k} = 90.01 \ g \ s$$

The results show a linear dependence of the normalized activity with catalyst weight passing below the origin, indicating that the gas-liquid mass transfer is non-existent for the range of operational conditions chosen. To further prove this observation and determine the solid-liquid and internal mass transfers the same approach as Section §4.4.1 was used for experiments carried out at varying temperatures and concentrations. The gas-liquid volumetric mass transfer coefficients were calculated using the correlation developed by (Mizan, 1992) for the H_2 in hexane and the range of Reynolds and solid concentrations proposed.

$$Sh = 51.7 \times 10^9 Re^{-1.12} Fr^{2.20}(1 - W_s)^{4.31} \tag{4.40}$$

Using this correlation gas to liquid mass transfer coefficients ($k_L a$) were calculated to be between 0.072 and 0.084 s^{-1} over the range of temperatures and PBN initial concentrations investigated. These values correspond to Carberry numbers between 0.002 and 0.012. These calculations confirm the previous experimental observations of normalized catalyst activity (Figure 2.26c) concluding that gas-liquid mass transfer is non-existent within the experimental range investigated.

The liquid to solid mass transfer coefficients (k_{LS}) were calculated to be between 0.8 and 1.3 s^{-1} corresponding to Carberry numbers in order of magnitude 10^{-4} resulting in > 0.99 values of external catalyst effectiveness factor indicating that the reaction is not limited by liquid to solid mass transfer with respect to hydrogen. The Weisz-wheeler modulus (M_w) for all

conditions is less than 0.15 which is the Wesiz-Prater criterion for a diffusion free regime (Levenspiel, 1999).

The same approach was taken to exclude the liquid-solid and internal transport limitations for PBN. According to external catalyst effectiveness and Weisz-wheeler modulus factors for PBN reported in Table 4.14 it is safe to exclude external and internal transport limitations with respect to reactant as well.

Based on these observations it is concluded that possibly the reaction happens throughout the catalyst surface. From the Figure 2.26c and mass transfer calculations the r_{LS} is calculated to be 0.8 g s and r_{reac} is calculated to be 90.029 g s hence indicating that the resistance to reaction is limiting within the chosen operational conditions and it can be overcome by increasing temperature and the amount of catalyst (Figure 2.26c-d).

Based on mass transfer investigations in this section it is apparent that the selectivity difference observed between 100 mL and 3000 mL reactions cannot be due to the transport limitations of H_2 and PBN on reaction rate.

Table 4.14: Overview of criteria chosen to evaluate the absence/presence of external and internal mass transfer diffusions for H_2 and PBN in 3000 mL scale.

Run	T (K)	P (bar)	m_{CAT} (g)	C_{PBNi} (mol l^{-1})	η_{G-L} (H_2)	η_{L-S} (H_2)	M_w (H_2)	η_{L-S} (PBN)	M_w (PBN)
2	313	5	5	0.270	0.998	0.99	0.0002	0.99	5×10^{-5}
3	323	5	5	0.270	0.995	0.99	0.0006	0.99	0.0002
4	333	5	5	0.270	0.991	0.99	0.0009	0.99	0.0002
5	343	5	5	0.135	0.988	0.99	0.0012	0.99	0.0006
7*	343	5	5	0.270	0.990	0.99	0.001	0.99	0.0003
9	343	5	5	0.404	0.994	0.99	0.0005	0.99	0.0001
10	353	5	5	0.270	0.987	0.99	0.0012	0.99	0.0003

* Base conditions**.**

4.5.2 Kinetic analysis of 3000 mL data

In order to determine if the best kinetic model derived from 100 mL scale would be able to determine the rate and selectivity of 3000 mL scale data as well, the process modelling with ODE solver option of Athena was used to incorporate the estimated kinetic constants and calculated mass transfer effects (although extremely negligible) on the hydrogen concentration. This Athena solver option computes the ODE models defined in the source code (Model 4.35b in this case) against the initial conditions given by the user (initial concentrations of PBN, PBL, CBN, and CBL at 3000 mL base conditions; Table 4.15B) and results are numerical solutions of the defined model. An example of the source code written for this solver is documented in Appendix C.

The results from the simulation above against the experimental values for base conditions in 3000 mL are presented in Figure 4.27. Interestingly, using this model resulted in a relatively satisfactory estimation of rate of PBN however selectivity of none of the products could be estimated as the modelled values deviated considerably from experimental measurements.
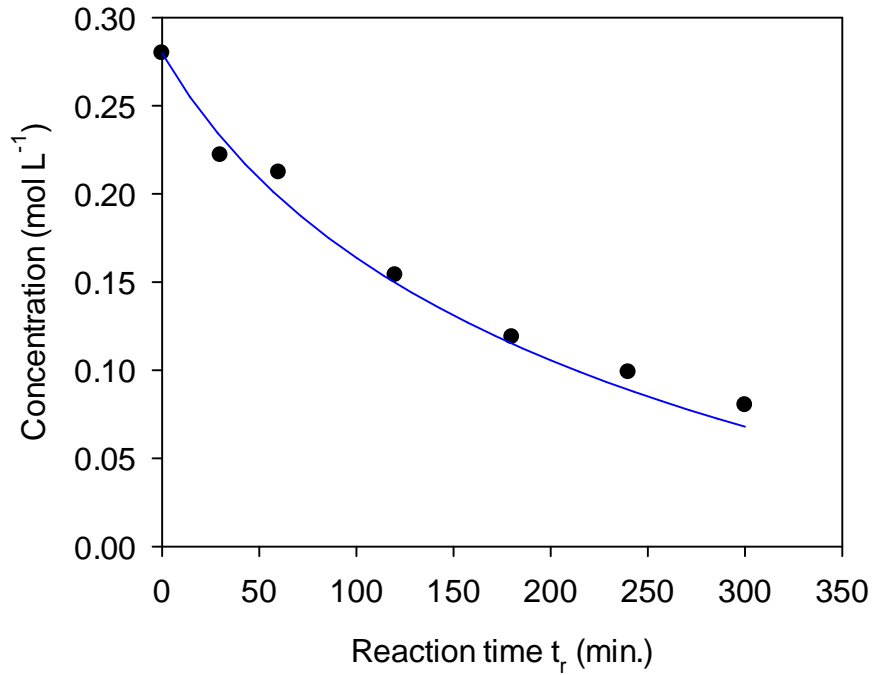
Figure 4.27: Numerical estimation of PBN rate from Model 4.35b versus the 3000 mL scale experimental data at base conditions. [Hexane, 373 K, $P_T = 5$ bar, $C_{PBNi} = 0.270$ mol L^{-1}, $m_{CAT}/m_{PBN} = 0.05$, $\bar{\varepsilon}_T = 3.5$ W kg^{-1}]

This concludes that the kinetic parameters estimated using 100 mL scale experiments are not able to describe the selectivity profiles observed in 3000 mL scale and there is probably a major shift in values of rate and adsorption constants when scaling-up. Consequently, the same approach used for 100 mL experiments was applied to carry out the parameter estimation for 3000 mL data in order to investigate this possible shift.

Table 4.15: Modelling stages taken for PBN hydrogenation in 3000 mL.

Modelling stage	Variable parameters	Constant parameters
A	Multi-temperature data: • 313-343 K	• P_T = 5 bar • C_{PBNi} = 0.270 mol L^{-1} • m_{CAT}/m_{PBN} = 0.05 • $\bar{\varepsilon}_T$ = 3.5 W kg^{-1} • Solvent: hexane
B	Multi-concentration data: • 0.135**, 0.270*, 0.404** mol L^{-1}	• Same as above

* Base condition

** Not used during parameter estimation process due to observed high experimental uncertainty.

4.5.3 Modelling of the temperature varied data

Once all the models in Table 4.5 undergone the same elimination approach described previously to optimize them for the temperature varied data in 3000 mL scale (Table 4.14A), the following conclusions were drawn:

• After model optimization for all models the adsorption/desorption constant of PBL remained in the models and its removal was statistically significant unlike in 100 mL where CBN always remained as the significant sorption constant.

• The model with surface reaction RDS with product desorption terms (Model 4.14b) was the most robust model where F-value did not breach the F_{crit} during the parameter elimination (Figure 4.28). This model was also the best in explaining kinetics of multi-

temperature data in 100 mL scale. The F-statistics for all models after each successive parameter removal is presented in Figure 4.28. F-value for surface reaction RDS and final product desorption models started to exceed the critical value from removal of 3rd parameter onwards and for both model the residuals were not corrected until 8 parameter was removed (models become pseudo-first order).

F-value for reactant adsorption model exceeded the critical value a number of times and residuals did not correct at 7th and 8th removal. Robustness of surface reaction RDS with product desorption term model in terms of F-value suggests that the intermediate product desorption is a significant factor in 3000 mL scale as well and should be considered when constructing models for the next stage of the modelling process.
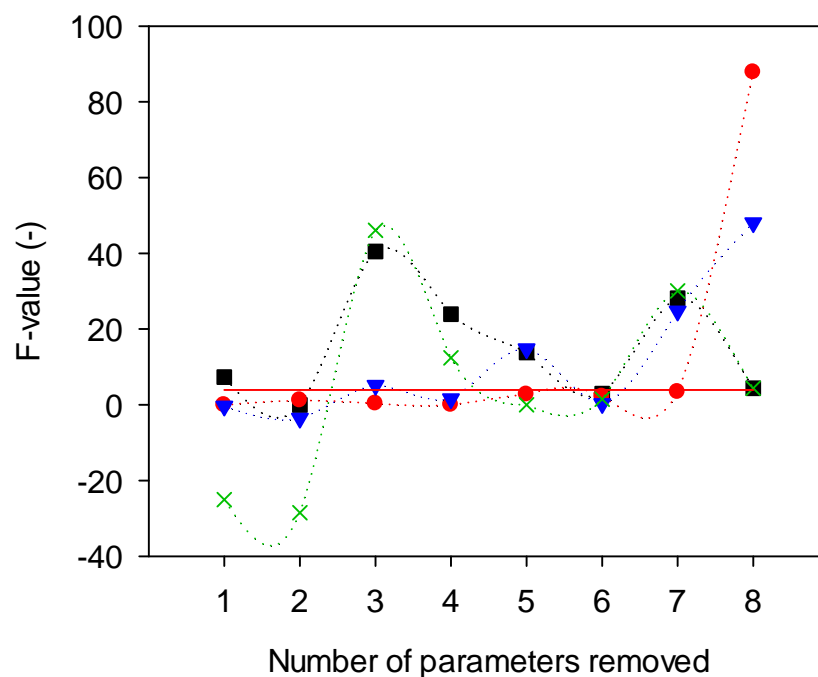
Figure 4.28: Calculated F-value for successive parameter removal across the entire model response for suggested kinetic models in Table 4.5: Model 4.14a: surface reaction RDS (□); Model 4.14b: surface reaction RDS with product desorption (○); Model 4.14c: reactant adsorption RDS (∇); Model 4.14d: final product desorption RDS (×).

- During the parameter elimination process the pre-exponential factors were equated for ketone and ring hydrogenation routes however it was further observed that for all models during the process the $A_{i,373}$ values for series reaction routes (k_{r1} and k_{r2}- Scheme 4.4) were in similar order of magnitude rather than for the hydrogenation of similar functional groups (observed in 100 mL scale). As it was previously discussed in section §4.3.2 at 3000 mL scale with increasing temperature CBN hardly hydrogenates to CBL in comparison with PBL. Consequently, it deemed safe to also assume that for temperatures lower than 353 K no CBN is being hydrogenated to CBL. All these possibilities were investigated during

model optimization (Scheme 4.4) using the statistical approach suggested previously. The fitting values of all parameters for each model and RSS values for individual responses considering these three reaction routes for surface reaction RDS model with product desorption term (Model 4.14b) are presented in Table 4.16-17.

- The fitting results for all model responses for the three reaction routes investigated are presented in Figure 4.29-32. Comparing the investigated dominant routes A, B, and C in terms of rate constants suggests that equating the k_{ket} and k_{arom} (A) rather than pathways $r1$ and $r2$ (B) results on the best fit for selective product PBL (Figure 4.30) which is also confirmed when comparing RSS values (Table 4.16) for individual responses where route A results in an RSS value an order of the magnitude lower. However route B showed significant improvement in modelling CBN (Figure 4.31) with an order of magnitude improvement in RSS values specifically for temperatures higher than 333 K. For temperatures lower than 333 K route C resulted in better CBN fits. In case of CBL route B results in a slightly better fit specifically at higher temperatures (Figure 4.32).

- Examining the estimated kinetic values in Table 4.15; the final parameter estimates show an improvement in confidence interval for routes B and C over A. The values of $A_{ket,373}$ are either twice as high or an order of magnitude higher than $A_{arom,373}$, depending on the route chosen which reflects the higher TOF for PBN ketone hydrogenation rather than ring hydrogenation when scaling-up. The presence of K_{PBL} in final models rather than K_{CBN} suggests that desorption of this selective product in 3000 mL is significant. The failure of route A in describing the kinetics of 3000 mL scale data as opposed to 100 mL scale data especially with respect to CBN and CBL implies that this simplification is not applicable to the kinetics at this scale. This conclusion was expected since it was previously established in section §4.3.2 that ketone and ring hydrogenation routes in 3000 mL scale are not in

199

proportion like 100 mL scale. At this scale for PBN the carbonyl group hydrogenation is preferred while between PBL and CBN ring hydrogenation to CBL dominates over carbonyl hydrogenation of CBN. This justifies the failure of route A in describing the kinetics of CBN and CBL as equating the two ring hydrogenation routes in this scale is clearly systematically incorrect while assuming route B and C with higher rate of reactions for kr1 (PBN→PBL→CBL) compared to kr2 (PBN→CBN→CBL) results in better estimation of CBN and CBL.
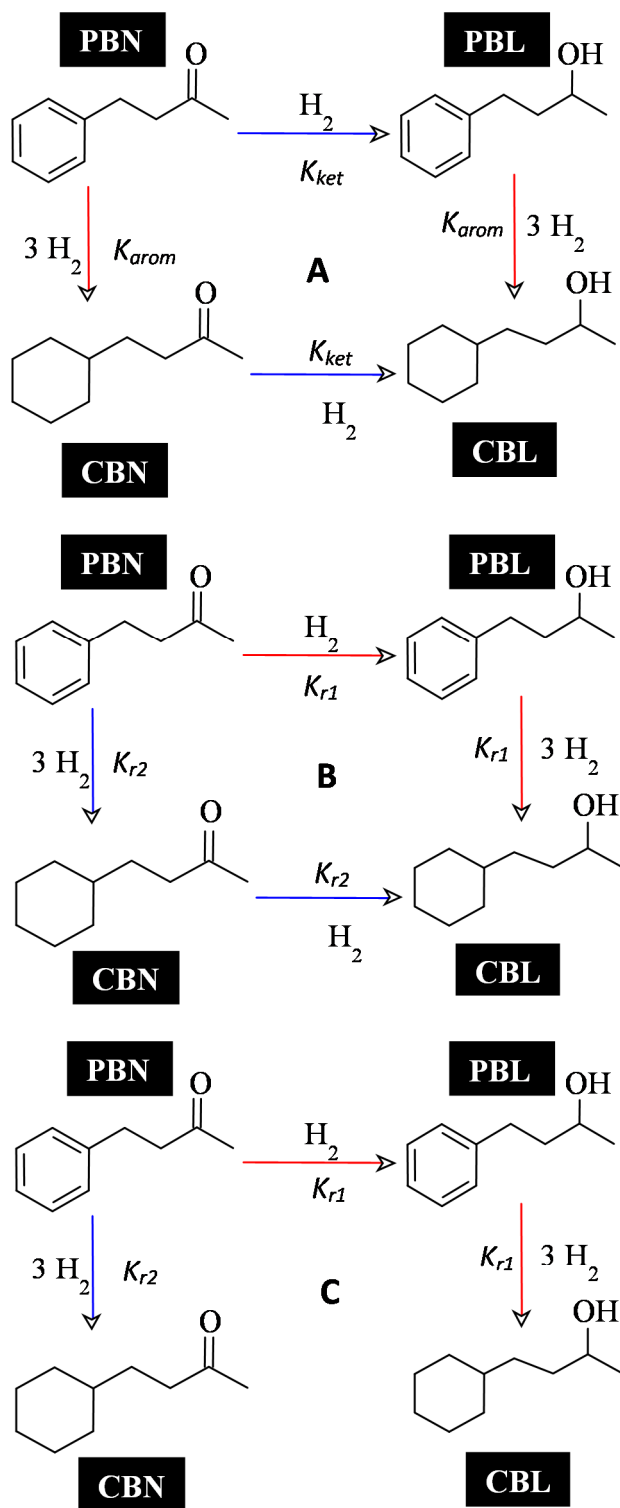
Scheme 4.4: Schematics for hydrogenation of PBN with additional investigated reaction routes (A, B and C) considered during model optimisation.

Table 4.16: Fitting parameters of kinetic modelling of multi-temperature data in 3000 mL scale for the Model 4.14b.

		Parameters					
		$A_1{}^*$	$A_2{}^*$	$E_{a,ket}$	$E_{a,arom}$	K_{PBL}	RSS
Estimate	**Route A**	0.029^a	0.009^a	50.1	55.9	0.16	7.05×10^{-3}
95% Conf. Int.		$\pm 10^{-3}$	$\pm 10^{-3}$	$\pm 10^0$	$\pm 10^0$	$\pm 10^{-1}$	
Estimate	**Route B**	0.024^b	0.012^b	50.5	56.6	9.08	6.75×10^{-3}
95% Conf. Int.		$\pm 10^{-3}$	$\pm 10^{-3}$	$\pm 10^0$	$\pm 10^0$	$\pm 10^0$	
Estimate	**Route C**	0.027^b	0.012^b	48.4	72.4	0.27	7.28×10^{-3}
95% Conf. Int.		$\pm 10^{-3}$	$\pm 10^{-3}$	$\pm 10^0$	$\pm 10^0$	$\pm 10^{-1}$	

* ***a**: $A_1 = A_{ket,373}$, $A_2 = A_{arom,373}$*; **b**: $A_1 = A_{r1,373}$, $A_2 = A_{r2,373}$

Table 4.17: RSS values for all model responses for kinetic modelling of multi-temperature data in 3000 mL for the Model 4.14b.

		Model response			
		PBN	**PBL**	**CBN**	**CBL**
RSS	**A**	3.19×10^{-3}	7.92×10^{-4}	1.48×10^{-3}	1.59×10^{-3}
RSS	**B**	3.59×10^{-3}	1.46×10^{-3}	7.39×10^{-4}	9.67×10^{-4}
RSS	**C**	3.41×10^{-3}	1.55×10^{-3}	8.61×10^{-4}	1.45×10^{-3}
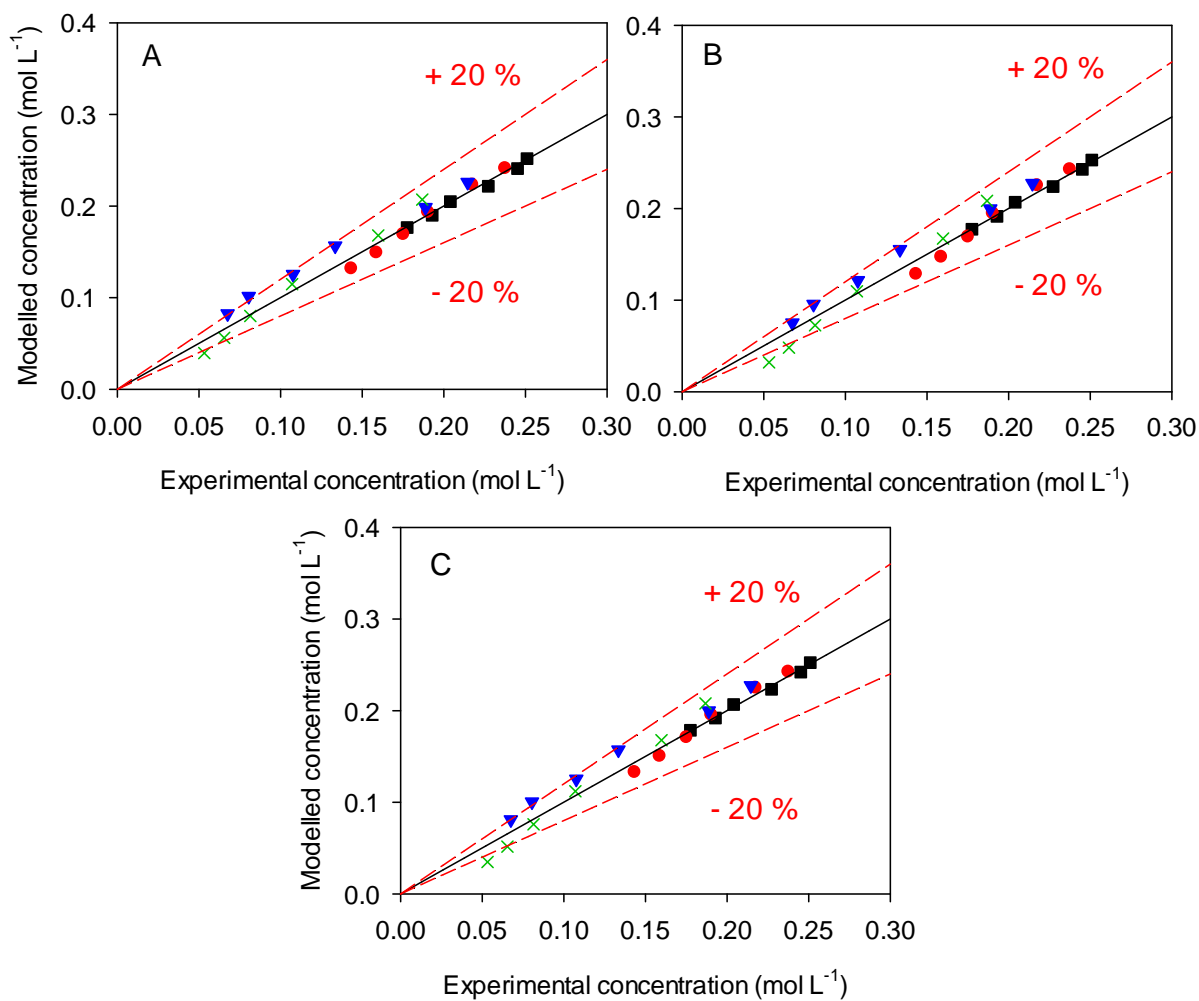
Figure 4.29: Modelled concentration data for PBN from Model 4.14b for reaction routes A, B, and C investigated for all temperatures: 313 K ($\square$), 323 K ($\circ$), 333 K (∇), 343 K ($\times$). [hexane, P_T = 5 bar, C_{PBNi} = 0.270 mol L^{-1}, m_{CAT}/m_{PBN} = 0.05, $\bar{\varepsilon}_T$ = 3.5 W kg^{-1}]
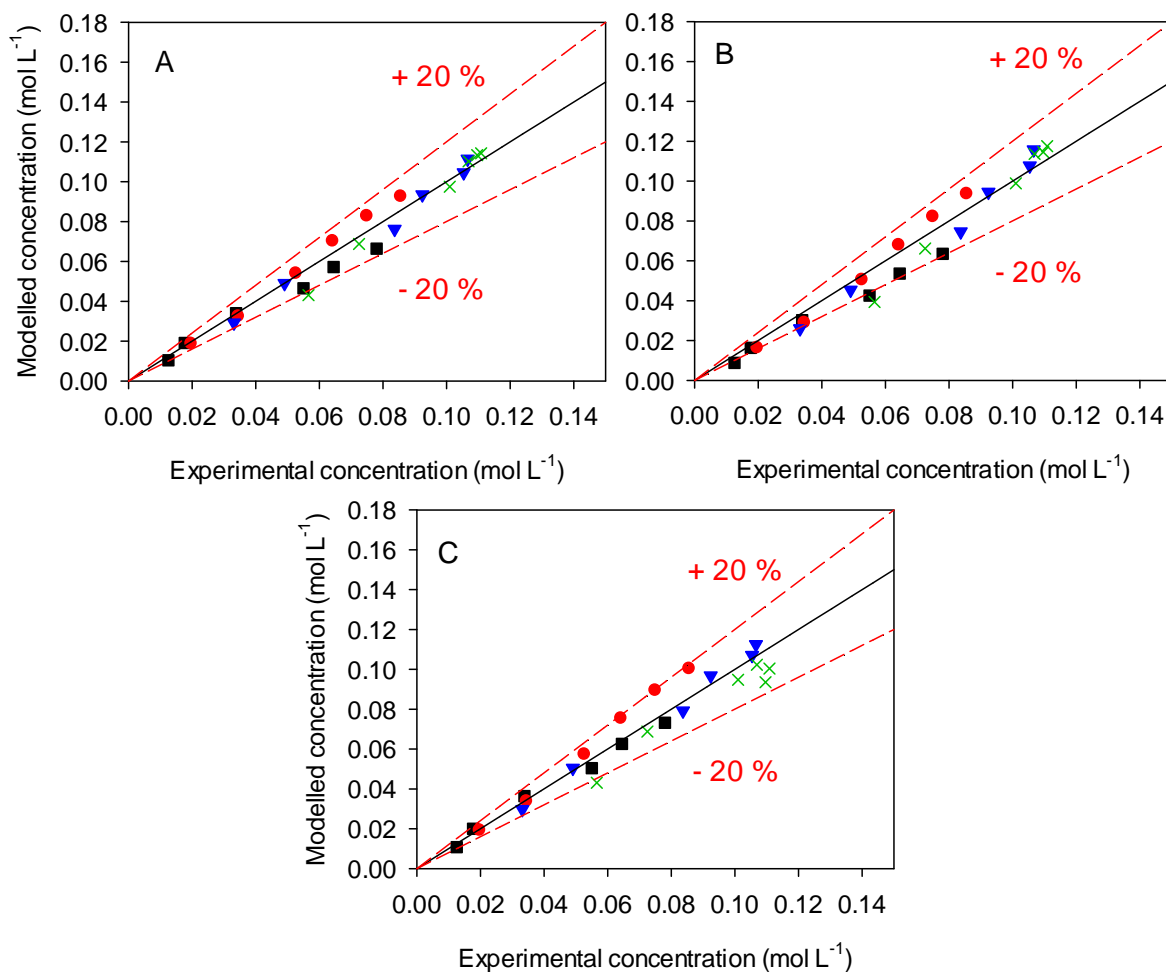
Figure 4.30: Modelled concentration data for PBL from Model 4.14b for reaction routes A, B, and C investigated for all temperatures investigated: 313 K (□), 323 K (○), 333 K (▽), 343 K (×); [hexane, P_T = 5 bar, C_{PBNi} = 0.270 mol L^{-1}, m_{CAT}/m_{PBN} = 0.05, $\bar{\varepsilon}_T$ = 3.5 W kg^{-1}]
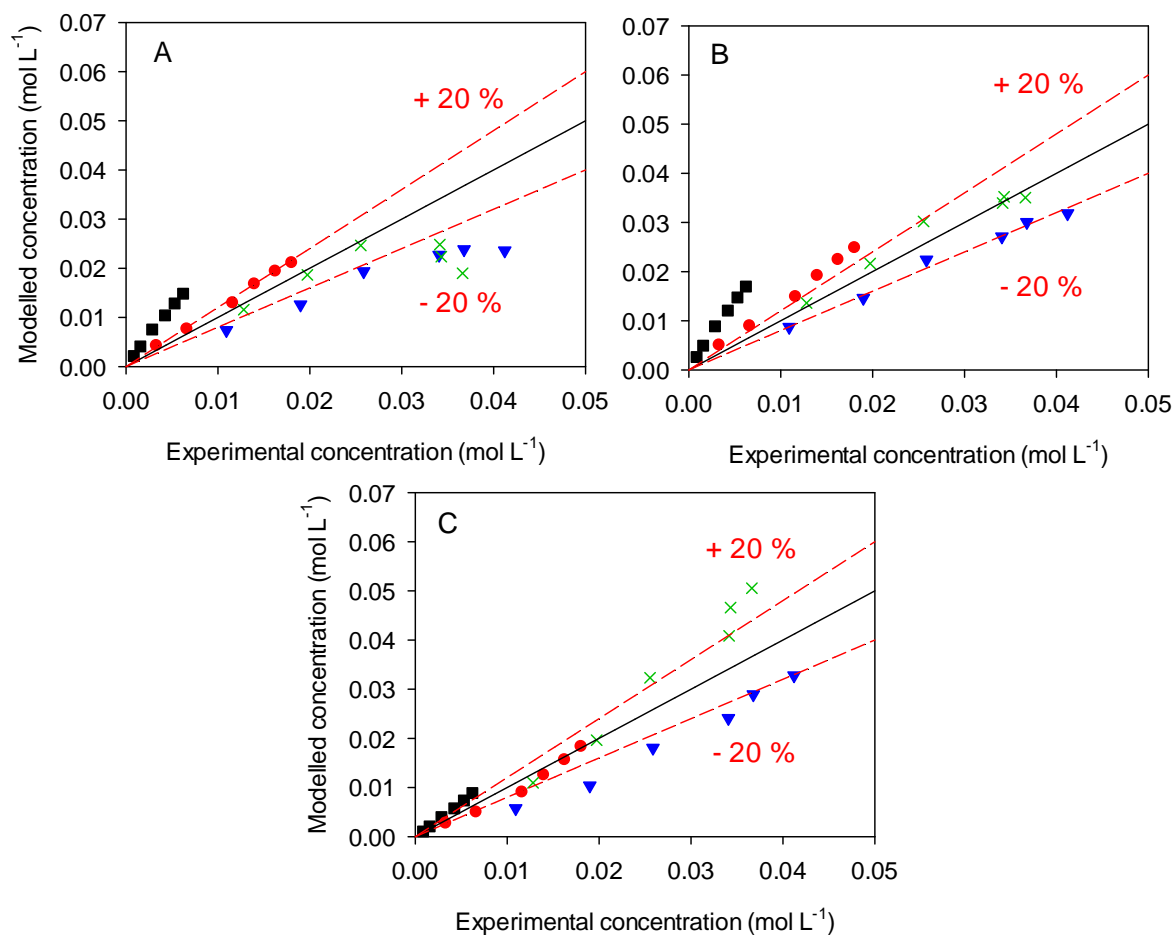
Figure 4.31: Modelled concentration data for CBN from Model 4.14b for reaction routes A, B, and C investigated: 313 K (□), 323 K (○), 333 K (∇), 343 K (×); [hexane, P_T = 5 bar, C_{PBNi} = 0.270 mol L^{-1}, m_{CAT}/m_{PBN} = 0.05, $\bar{\varepsilon}_T$ = 3.5 W kg^{-1}]
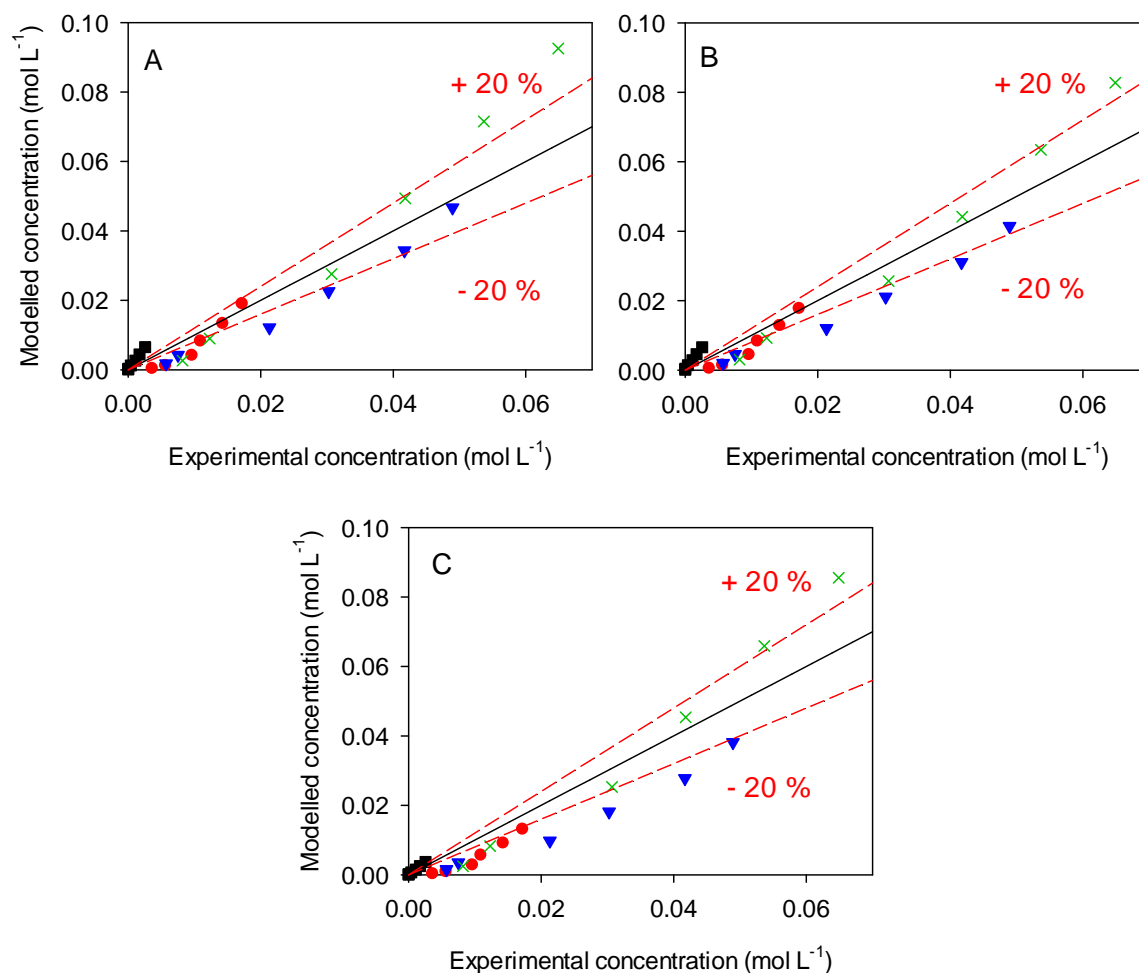
Figure 4.32: Modelled concentration data for CBN from Model 4.14b for reaction routes A, B, and C investigated for all temperatures investigated: 313 K (□), 323 K (○), 333 K (▽), 343 K (×); [hexane, P_T = 5 bar, C_{PBNi} = 0.270 mol L^{-1}, m_{CAT}/m_{PBN} = 0.05, $\bar{\varepsilon}_T$ = 3.5 W kg^{-1}]

4.5.4 Fitting the active site models to experimental data at base conditions

The modelling results from temperature varied data have resulted in mechanistic insights into the kinetics of PBN hydrogenation in 3000 mL scale. Based on the investigations above the following conclusions were drawn,

- The surface reaction RDS model with product desorption term is the most robust model in terms of statistical impact of parameter elimination during model refinement process. This observation is in line with previous kinetic analysis of 100 mL scale data.

- Desorption of PBL is significant in 3000 mL data compared with that of CBN in 100 mL scale.

- The relative success of route B and C in describing the formation of CBN and CBL suggests a shift in dominant reaction routes when scaling up to 3000 mL scale.

The next step involved fitting the active site models developed previously (Table 4.11) on concentration data in order to examine the models in terms of reactant adsorption and product desorption modes at the 3000 mL scale. Previous kinetic analysis concluded the competitive adsorption of H_2 and organics on Pt/TiO$_2$ surface thus only the models featuring competitive adsorption mode (n = 2) were considered for this part of the study. Due to limited amount of catalyst allocated to each research group within CASTech it was not possible to carry out more experiments with varying concentrations at this scale. Consequently, only the experimental observations in the base conditions (Table 4.14) were used to fit the kinetics of this section due to uncertainty of other two other initial PBN experiments observed during initial TOF analysis. This might not be feasible due to low number of experimental observations in comparison with parameters resulting in loss of degree of freedom however it was still possible to draw some mechanistic insights with regards to active site basis.

All competitive models in Table 4.11 used in this section initially comprised of 6 parameters (2 rate constants and 4 adsorption/desorption constants). Fitting the models to experimental data at base conditions failed to estimate the K_{PBN} terms both in single and two site models resulting in negative or indeterminate estimations. Consequently, parameter elimination was

applied to determine the statistical significance of K_{PBN} terms and it was observed that eliminating K_{PBN} did not have any impact on model outcome in terms of RSS and F-value. Despite this outcome after K_{PBN} elimination from rate equation desorption of intermediate products could be estimated with good confidence intervals specifically in two site Model 4.33-35b. On the same notes, the PBN adsorption constants for carbonyl and ring sites were fixed at values estimated from 100 mL scale and it was observed that assuming a higher K_{PBN} for carbonyl hydrogenation route throws off the model completely while keeping the values the same as 100 mL scale results in the model convergence with proper estimation of intermediate desorption constants. This concludes that the effect of scale on sorption processes is not due to stronger adsorption of PBN on active sites and the adsorption strength of PBN on either site is independent of scale.

For all models the mechanisms A, B, and C were tested and the following conclusions were drawn:

- The single site model resulted in the worst fit and was unable to estimate desorption constants for intermediate products.

- Both two site models (4.34d and 4.35b) resulted in good fits with a slightly better fit for Model 4.35b in terms of RSS. This concludes that the same kinetic model is applicable to both scales and consequently the differences should lie in the dominant reaction routes and values of kinetic constants between both scales.

- For both two site models stated above mechanism C was the most successful in describing the kinetics (Figure 4.33) with lowest RSS and MEA values suggesting that at the $m_{CAT}/m_{PBN} = 0.05$ CBN does not hydrogenate to CBL within the reaction screening time. This signifies the importance of catalyst site availability in order to hydrogenate carbonyl

bond of CBN as it was previously stated that based on selectivity profile versus catalyst loading only at conversions > 90% at high catalyst loadings (m_{CAT}/m_{PBN} = 0.15) CBN hydrogenates to CBL where there is no PBN in system to compete for carbonyl hydrogenation. If more experiments with varying initial PBN concentrations were available it would have been interesting to investigate the shift in reaction mechanism as well as the changes in K_{PBN} with scale.

Table 4.18 shows the fitting parameters for all three mechanisms investigated for Model 4.35b. k_{ket} values were found to be an order of magnitude higher than k_{arom}, reflecting the higher TOF observed with respect to PBN carbonyl hydrogenation.

Comparing the desorption constants of the intermediate products between two scales it is observed that the K_{PBL} is higher in 3000 mL while K_{CBN} is lower by an order of magnitude. Figure 4.34 shows the shift in desorption constants of PBL and CBN for both scales. Based on the kinetic results, PBL desorption from surface of the catalyst is faster in 3000 mL scale as opposed to CBN desorption in 100 mL scale. This conclusion justifies the selectivity differences observed between two scales demonstrating that in this current system where the shift in product distribution is independent of transport limitations there is a possible scale or reactor design effect on the desorption of intermediates from surface of the catalyst at micro-scale.

The question that arise here is that what triggers this shift in desorption process between intermediate products when scaling-up from 100 mL scale to 3000 mL scale and which reactor design variable might be the cause of this effect?

Table 4.18: Parameter estimates and confidence intervals for active site Model 4.35b for all mechanisms A, B, and C.

Parameter	A	B	C
k_{ket}	0.014 ± 0.003	0.017 ± 0.006	0.014 ± 0.002
k_{arom}	0.003 ± 0.001	0.007 ± 0.003	0.004 ± 0.0008
$K_{c,PBL}$	0.213 ± 0.158	0.050 ± 0.015	0.070 ± 0.009
$K_{c,CBN}$	0.026 ± 0.006	0.025 ± 0.009	0.034 ± 0.008
RSS	2.40×10^{-4}	3.12×10^{-4}	1.44×10^{-4}
MEA	7.32 %	8.12 %	4.98 %
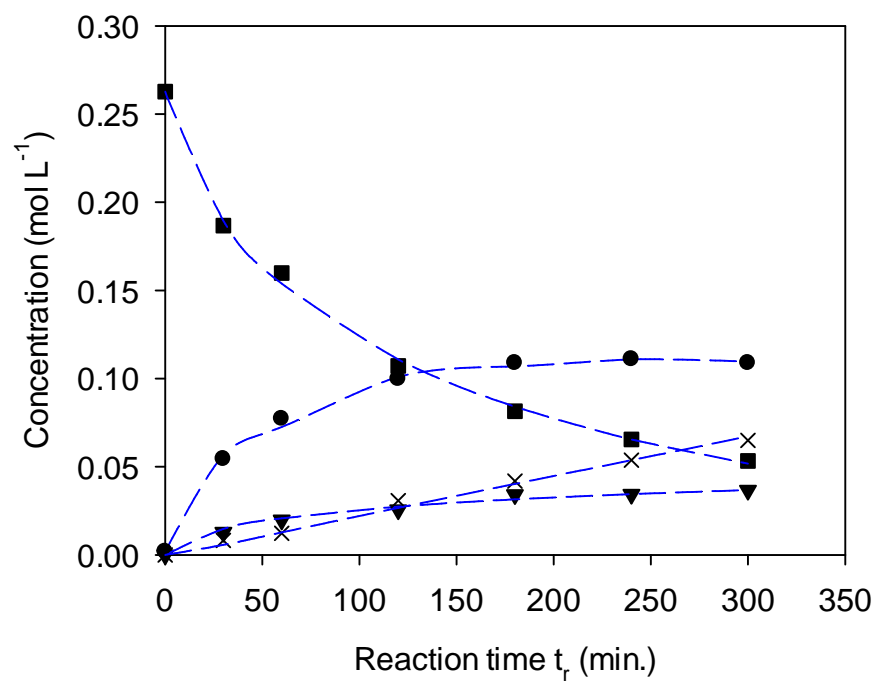
Figure 4.33: Concentration-time profile during PBN hydrogenation in 3000 mL reactor at base reaction conditions plotted against modelled results from Model 4.35b and mechanism C: PBN (□), PBL (○), CBN (▽), CBL (×). [343 K, P_T = 5 bar, C_{PBNi} = 0.270 mol L^{-1}, m_{CAT}/m_{PBN} = 0.05, $\bar{\varepsilon}_T$ = 3.5 W kg^{-1} / base conditions]
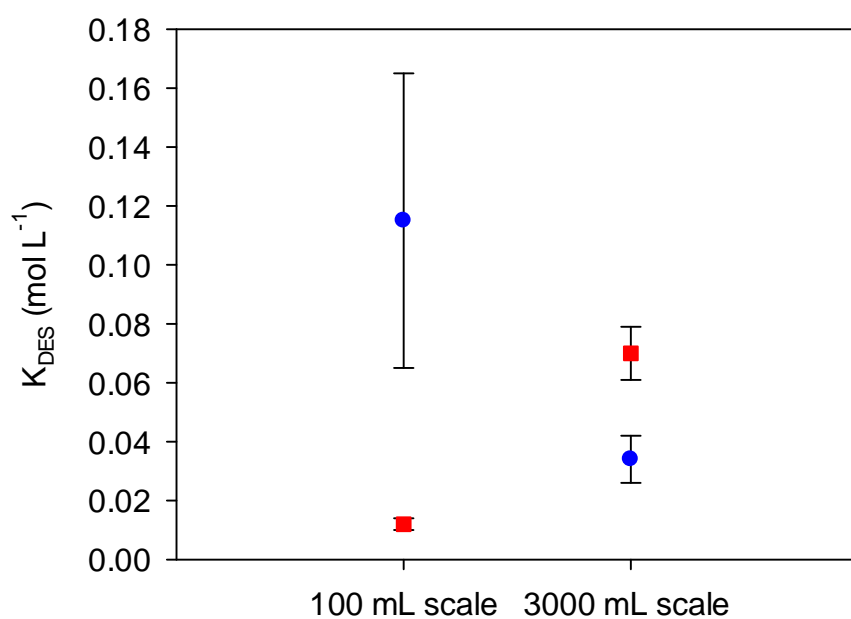
Figure 4.34: The estimated desorption constants from the best candidate active site model at 100 mL and 3000 mL scales for PBL (□) and CBN (○).

4.6 Conclusions

The following conclusions were drawn from the kinetic analysis of PBN hydrogenation at both 100 mL and 3000 mL scale.

- The proposed approach of model optimization was successful in finding a single kinetic model which was successfully fitted to the data at both scales suggesting the scalability of the proposed model.

- The kinetic parameters found in modelling of 100 mL scale data were not able to describe the selectivity in 3000 mL scale and there is shift in rate constants and desorption constants of intermediates with scale.

- A combination of the proposed kinetic modelling approach along with DFT and in-situ ATR-IR analysis can be a very powerful tool in investigating the selective active sites on catalysts leading to a more detailed catalyst design process and also further investigations on scale-up and mass transfer effects.

- Doping experiments with intermediate products PBL and CBN needs to be carried out as future work for both scales to investigate the adsorption/desorption dynamics of products when scaling-up.

Based on the kinetic investigation across both scales there seems to be a possible scale or reactor design variable effect on desorption of intermediates at micro-scale for this reaction system when scaling up. Potential causes are speculated and discussed below to layout the future work that needs be carried out in order to fully explain the outcomes of this chapter:

- The reactor design differences between the two equipment

1. The 100 mL reactor is a semi-batch gas inducing reactor (GIR), consequently the point of hydrogen induction being on impeller region where the heating coil is mounted resulting in the limiting reagent being introduced at region of high turbulence / high temperature possibly resulting in domination of ring hydrogenation over carbonyl.

2. The 3000 mL reactor is a semi-batch surface aeration reactor (SAR) with hydrogen introducing from head-space heated by an oil jacket around the reactor wall.

Looking back at the selectivity versus conversion profiles (§4.3.1 and §4.3.2), in 100 mL scale at the start of the reaction there is always some CBN formation observed as opposed to 3000 mL where there is no CBN at the start of the reaction. Based on the reactors design differences stated above there might be some form of micro-mixing effect causing this shift in product desorption.

- Reactor startup effect

    1. Another difference between two scales was the start-up process after the catalyst reduction. 3000 mL reactor usually took 40-45 mins to bring to temperature during which some PBL was always formed at t=0 (first sample taken). On the other hand, 100 mL reactor took much less time to bring to desired temperature and at the start-up always some CBN was present in the system along with PBL. Since these two intermediate compete with PBN for carbonyl and ring adsorption sites and CBN hydrogenation to CBL is always slow regardless of the scale its adsorption on carbonyl site is always an inhibiting factor for PBN carbonyl hydrogenation.

- Catalyst reduction process

    1. The reduction process for both scales consisted of 1 hr stirring of the catalyst in hexane under 1 bar of H_2. The preliminary reactions in 2-propanol carried out in 3000 mL scale showed no effect of ex-situ versus in-situ catalyst reduction on rate and selectivity as was stated in Chapter 3. Furthermore, an additional experiment done without reducing the catalyst still showed higher selectivity towards PBL in 3000 mL scale at conversions < 50% before CBL formation took over the selectivity rank among all products. QUB has previously reported no effect of catalyst reduction on rate and selectivity during the course of CASTech project. This observation also ruled out the possible catalyst size reduction due to breaking under higher turbulence at 3000 mL scale before reactor start-up.

Chapter 5: Kinetic analysis of 4-phenyl-2-butanone hydrogenation: roles of solvent, support and scale-up

5.1 Introduction

Liquid-phase reactions over heterogeneous catalysts often require the use of a solvent as reaction medium. Solvent selection has been known to have a critical impact on catalytic activity and selectivity for over 150 years (Abraham et al., 1988). In these catalytic processes, multiple components are present in reaction medium, namely reactant species adsorbing competitively, intermediates, and product species. The effect of solvent on rate and selectivity of liquid phase hydrogenation reactions has been reported before (Akpa et al., 2012), (Martin et al., 2013), (Mounzer et al., 2010), (Mukherjee and Vannice, 2006a). The role of solvent has been studied at some length and a number of attempts have been made to explain their role using mathematical methods based upon the physical and chemical interactions between the components and the catalyst. These methods include multiple linear regression analysis, factor analysis and principal component analysis. These methods have rendered some insight into solvent effects in chemical processes (Akpa et al., 2012). Most of these works tend to correlate the rate and selectivity to solvent physical and chemical properties such as dielectric constant of solvent, molar volume or bulkiness, H_2 solubility, etc. Recent works however suggest that the role of solvent in catalytic hydrogenation reactions is more significant in terms of adsorption/desorption strength of substrates on the catalyst surface, product desorption, and hydrogen bond capability of solvents (Mounzer et al., 2010) (Akpa et al., 2012), (Mitchell et al., 2013), (Ren et al., 2014). The kinetic approaches which have been used so far to elucidate solvent effects are extensively reviewed in Chapter 2.

In this Chapter, a novel approach is suggested based on previous kinetic investigations presented in Chapter 4 to correlate the selectivity of hydrogenation of PBN to the fitted adsorption constants of intermediate products CBN and PBL and site availability (rate constants). This approach results in a direct comparison of effect of solvent on product desorption from surface of the catalyst, and solvent/catalyst interactions.

In Chapter 4, experimental data were presented for 4-phenyl-2-butanone (PBN) hydrogenation using hexane as solvent and P25 4% Pt/TiO_2 as catalyst. A rigorous kinetic approach incorporating sensitivity and statistical analysis was employed to find a mechanistically sound and robust kinetic model. A 2-site model was found to be most appropriate, describing aromatic hydrogenation over a platinum site and ketone hydrogenation over a metal adjacent TiO_2 oxygen vacancy site.

Following the work in the previous chapter, another set of experiments were examined in 100 mL and 3000 mL scales over Pt/TiO_2 and Pt/SiO_2 using various solvents. The physical characteristics of catalysts can be found in Chapter 3.

This chapter will present and discuss the incorporation of the best derived kinetic model from previous chapter into the reactions performed under isothermal conditions over a range of solvents. For reactions done using Pt/TiO_2 catalyst, five solvents from each class are compared with the reactions done in 3000 mL scale for differences in rate and selectivity with scale. A larger range of solvents involving alkanes, aromatics, primary alcohols, secondary alcohols, halogenates and ethers are investigated at the 100 mL scale and are presented in this chapter. For Pt/SiO_2 catalyst a range of alcohols, alkanes, and aromatics in 100 mL scale are investigated and compared with a smaller range at the 3000 mL scale. All the solvents used are of >99% purity (Chapter 3).

5.2 Analysis of rate and selectivity in varying solvents

5.2.1 Experiments carried out using the 4% Pt/TiO$_2$ catalyst

Experiments using the 4% Pt/TiO$_2$ catalyst were carried out at both scales using a range of solvents in 100 mL scale and five solvents in 3000 mL scale as shown in Table 5.1, along with corresponding operating conditions.

Table 5.1: Summary of experiments carried out at both scales using different classes of solvents (4% Pt/TiO$_2$).

Solvents (Series C)		Operational conditions	
100 mL scale	**3000 mL scale**	**100 mL scale**	**3000 mL scale**
Decane	2-propanol	T = 343 K	T = 343 K
Hexane	1-propanol	P$_T$ = 5 bar	P$_T$ = 5 bar
Dichloroethane	Diethyl ether	C$_{PBNi}$ = 0.270 mol L^{-1}	C$_{PBNi}$ = 0.270 mol L^{-1}
Cyclohexane	t-butyl toluene	m$_{CAT}$/m$_{PBN}$ = 0.05	m$_{CAT}$/m$_{PBN}$ = 0.05
t-butyl toluene	hexane	$\bar{\varepsilon}_T$ = 10 W kg^{-1}	$\bar{\varepsilon}_T$ = 3.5 W kg^{-1}
Toluene			
p-xylene			
Trifluoroethanol			
Ethanol			
1-propanol			
1-butanol			
1-pentanol			
1-octanol			
2-propanol			
2-butanol			
2-pentanol			
2-octanol			

5.2.1.1 Rate and selectivity results in 100 mL scale

Alcohols

The highest selectivity towards CBN in 100 mL scale among all alcohols (Figure 5.1a) is observed using trifluoroethanol (TFE) as solvent. This solvent also resulted in the highest conversion after 2 hr. (~85%) demonstrating similar behaviour to alkanes. The highest rates among alcohols are followed by secondary alcohols 2-butanol, 2-pentanol, and 2-propanol. All other primary and secondary alcohols are more selective towards PBL. An increase in selectivity of PBL is observed as the chain length of alcohols is increased. The lowest rates were observed for the highest chain length alcohols 1-octanol and 2-octanol.

Alkanes

A range of alkanes with different chain lengths were tested including linear alkanes n-hexane and n-decane, cyclic alkane cyclohexane, and halogenated alkane 1,2-dichloroethane. CBN is the main product of all alkane solvents with slight selectivity variations among different types with 75% in hexane and increasing to ~80% in decane. 1,2-dichloroethane results in the lowest rate compared with non-halogenated alkanes and highest selectivity towards fully hydrogenated product CBL. The rate and selectivity in hexane was fully explained in Chapter 4, and other alkanes further in the kinetic section of this chapter.

Aromatics

The rate and selectivity in aromatic solvents varies significantly. While t-butyl toluene shows the highest rate and selectivity towards CBN, reactions in toluene and p-xylene are significantly slower and more selective towards PBL.
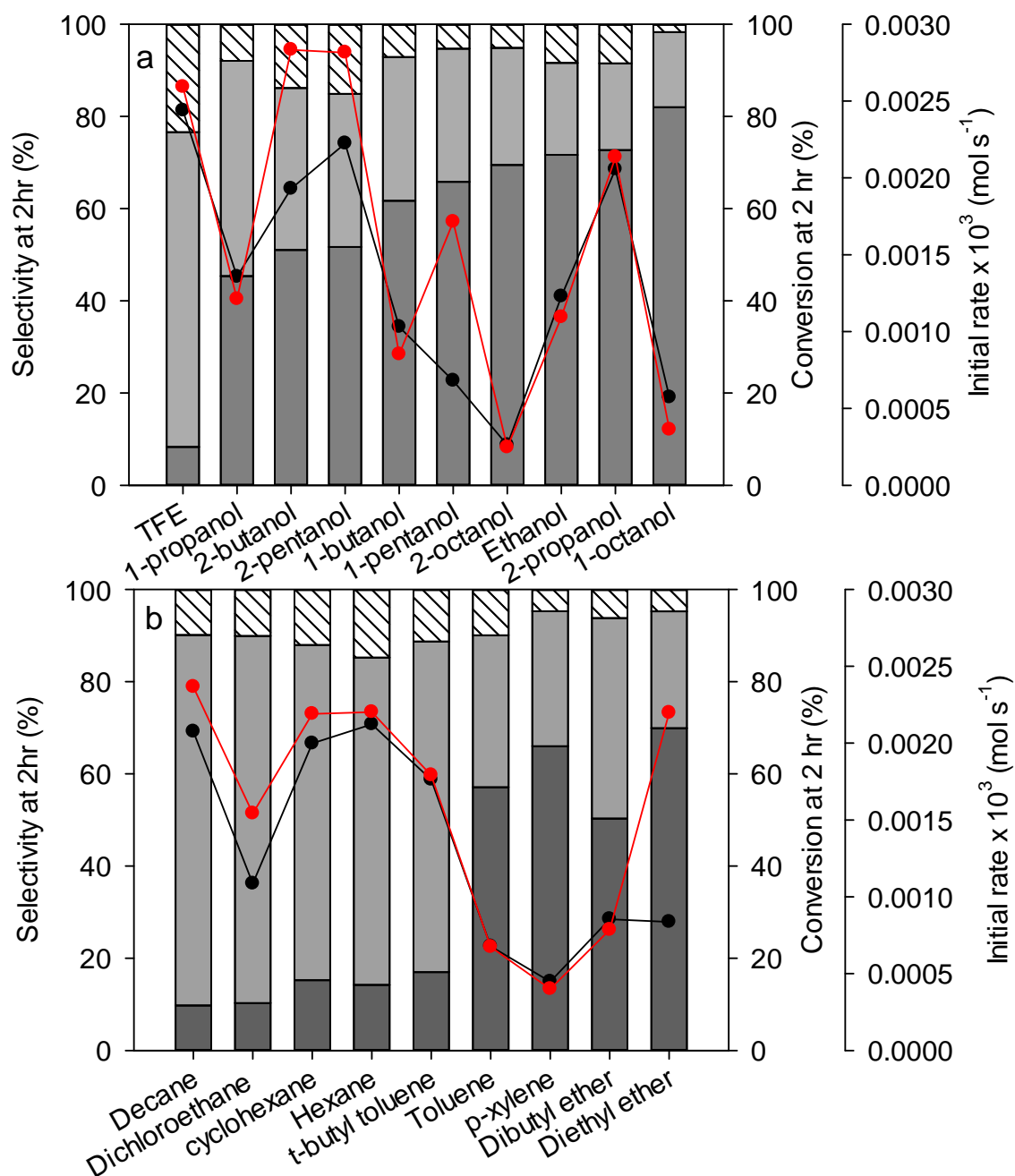
Figure 5.1: Selectivity of PBN hydrogenation products PBL (■), CBN (▨), and CBL (▨) after 2 hr. in 100 mL scale, conversion after 2 hr. (**black** dot-line), and initial rate of reaction (**red** dot-line) ordered from the highest selectivity towards CBN for all alcohols (a) and all other classes of solvents (b). [4% Pt/TiO$_2$, P$_T$ = 5 bar, C$_{PBNi}$ = 0.270 mol L^{-1}, m$_{CAT}$/m$_{PBN}$ = 0.05, $\bar{\varepsilon}_T$ = 10 W kg^{-1}]

Ethers

The reactions in diethyl ether and dibutyl ether were tested. Both these solvents contain linear alkyl chains. The reaction proceeded slowly in both of these solvents with higher selectivity towards PBL of ~50% and ~70% for diethyl ether and dibutyl ether, respectively.

Previous kinetic analysis in Chapter 4 demonstrated a 2-site model for 4% Pt/TiO_2 with a platinum site responsible for ring hydrogenation and an oxygen vacancy site at Pt and TiO2 interface responsible for ketone hydrogenation.

High activity in 2-propanol can be initially attributed to the hydrogen bond donation capability of this solvent. In-situ ATR-IR analysis has been used by QUB to investigate the strength of catalyst/reagent/solvent interface. It was found that saturating the surface of Pt/TiO2 with PBL and flushing it with 2-propanol removed all PBL, while with hexane it remained on catalyst surface (McManus et al., 2014a) (to be published). The higher selectivity towards PBL in alcohols can also be the result of alcohols seating on the oxygen vacancy sites, blocking the sites where C=O would sit and allow ring adsorption onto the Pt particle resulting in higher carbonyl hydrogenation to form PBL. This was confirmed by QUB using DRIFT (Diffuse Reflectance Infrared Fourier-Transform) of the catalyst/alcohol surface showing the formation of alkoxy species limiting the access of reagent to catalyst by altering the hydrophobicity of surface (McManus et al., 2014a). The rates of reaction in primary alcohols (1-propanol) in comparison to secondary alcohols (2-propanol) are significantly different for Pt/TiO_2 (Figure 5.1a). Both of these alcohols can adsorb into active sites through their hydroxyl groups; however the less bulky primary alcohols result in a more dense packing on the catalyst surface compared with secondary alcohol, thus reducing the rate and conversion.

In case of alkanes, the high selectivity towards CBN thought to be from strong adsorption of ring on active sites which was previously proved in kinetic analysis in Chapter 4.

In aromatic solvents, the bulkiness of t-butyl toluene prevents it from adsorbing on catalyst and thus the high rate and selectivity towards CBN compared with toluene and p-xylene which offer a competition for aromatic ring adsorption sites. The reaction in diethyl ether which has a linear alkyl chain showed a high initial rate but the reaction progresses slower compared with other solvent with only ~30% conversion after 2 hr. It is possible that diethyl ether also adsorbs on Pt blocking the ring hydrogenation; however the possible mobility in the linear alkyl chains allow some ring hydrogenation (McManus et al., 2014a).

5.2.1.2 Comparison of rate and selectivity results between 100 mL and 3000 mL scales

The reaction results in different solvents from 100 mL scale to 3000 mL scale are plotted in Figure 5.2. It was observed that in all the solvents tested except t-butyl toluene, reaction was more selective towards PBL. As was observed in previous chapter with hexane the initial rates are an order of magnitude higher in the larger 3000 mL scale. The lowest rate and conversion at the 3000 mL scale was observed in 1-propanol. The highest initial rates were observed in hexane and 2-propanol, however the reaction in 2-propanol progressed slower in 3000 mL scale compared with the 100 mL scale with only ~30% conversion being reached after 2 hr. as opposed to ~60% in 100 mL scale. The highest selectivity towards CBN at 3000 mL scale was observed in t-butyl toluene and then 2-propanol. The selectivity towards CBN was the least when using 1-propanol as solvent. From the observations above it can be concluded that one of the most important criteria ruling the selectivity of CBN in different solvents is the degree of interaction of ring on catalyst surface which is altered by using solvents that hinder ring adsorption by competing for active sites.
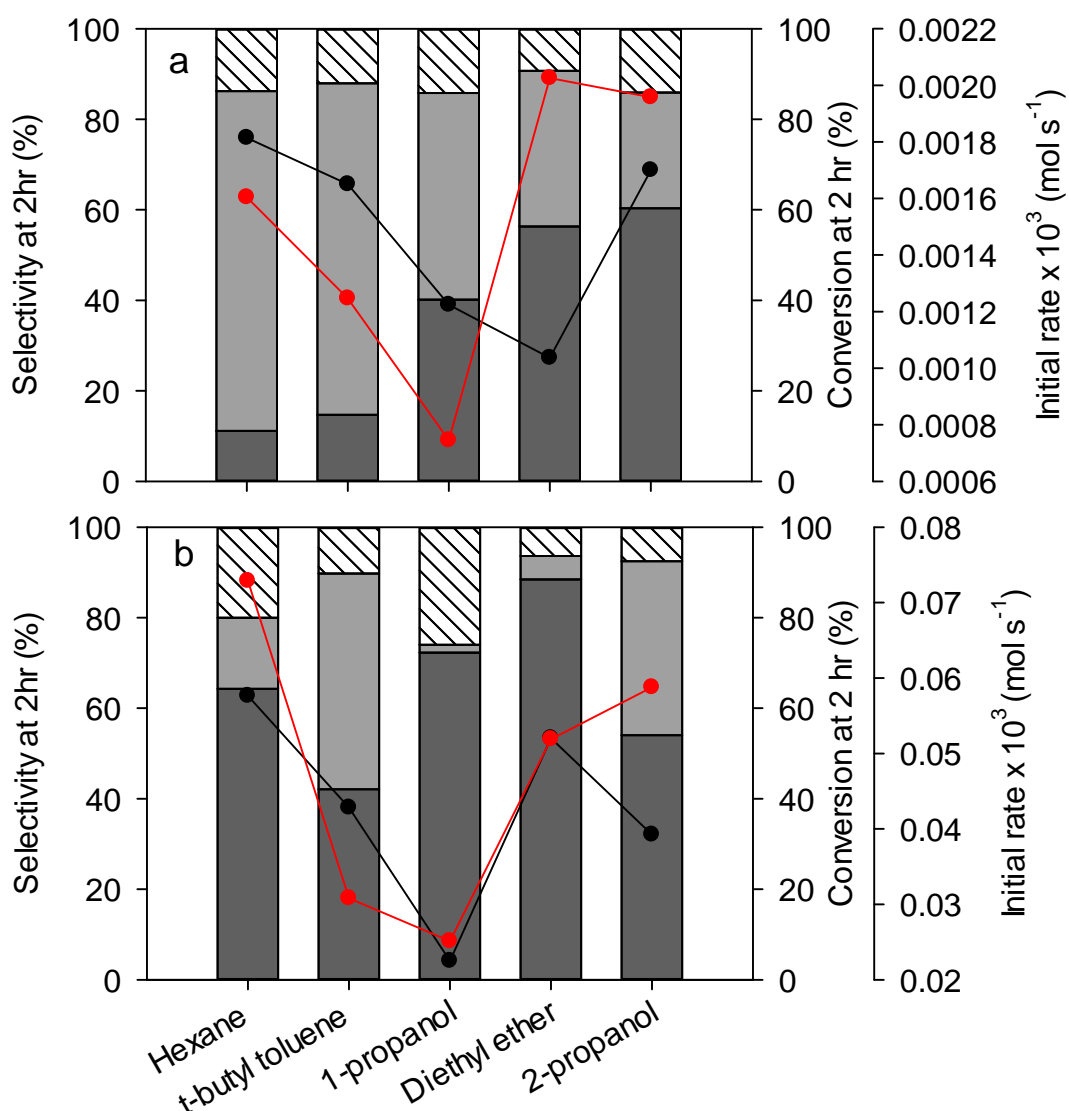
Figure 5.2: Selectivity comparison of PBN hydrogenation products PBL (■), CBN (■), and CBL (▨) after 2 hr. in both scales arranged from the highest selectivity towards CBN in 100 mL scale; conversion after 2 hr. (**black** dot-line), and initial rate of reaction (**red** dot-line) for 100 mL scale (a) and 3000 mL scale (b) data in varying solvents. [4% Pt/TiO$_2$, P$_T$ = 5 bar, C$_{PBNi}$ = 0.270 mol L^{-1}, m$_{CAT}$/m$_{PBN}$ = 0.05, 100 mL scale: $\bar{\varepsilon}_T$ = 10 W kg^{-1}, 3000 mL scale: $\bar{\varepsilon}_T$ = 10 W kg^{-1}]

223

This would consequently result in alteration of the catalyst surface properties and facilitating or hindering the product desorption. These three categories regarding solvent effects in catalytic processes have gained tremendous attention over the past few years. Methods like TG (Thermogravimetric) analysis, FFC NMR (Fast field cycling – nuclear magnetic resonance) relaxation, DRIFT, DFT molecular simulation, and *in-situ* ATR-IR have been used by various researchers in order to gain more understanding of reagent/solvent/catalyst interaction. As it was previously reported in Chapter 2 most of the kinetic analysis carried out in the field of solvent selection deals with incorporation of different solvatochromic properties into rate models. Little to no work has been done to investigate the adsorption/desorption of reagents and products from catalyst surface. By using the kinetic approach proposed in the previous chapter, this study will demonstrate the application of robust kinetic models in predicting the sorption constant and their correlation with reaction selectivity towards CBN in the current case study.

5.2.2 Experiments carried out using 5% Pt/SiO$_2$ catalyst

A standard Johnson Matthey$^{©}$ Pt/SiO$_2$ catalyst was used to compare the selectivity towards PBL and CBN using different classes of solvent with the results from Pt/TiO$_2$ catalyst. The silica support demonstrates different trends of selectivity from that of titania. Silica is less susceptible to varying classes of solvents in terms of selectivity towards PBL and CBN.

A summary of the experiments carried out using Pt/SiO$_2$ is presented in Table 5.2. The experimental conditions at both scales are similar to those of Pt/TiO$_2$ presented in Table 5.1.

Table 5.2: Summary of experiments carried out at both scales using different classes of solvents.

Solvents (Series C)		Operational conditions	
100 mL scale	3000 mL scale	100 mL scale	3000 mL scale
Decane	2-propanol	$T = 343$ K	$T = 343$ K
Hexane	Cyclohexanol	$P_T = 5$ bar	$P_T = 5$ bar
Dichloroethane		$C_{PBNi} = 0.270$ mol L^{-1}	$C_{PBNi} = 0.270$ mol L^{-1}
Cyclohexane	Ethanol	$m_{CAT}/m_{PBN} = 0.05$	$m_{CAT}/m_{PBN} = 0.05$
t-butyl toluene	1-propanol	$\bar{\varepsilon}_T = 10$ W kg^{-1}	$\bar{\varepsilon}_T = 3.5$ W kg^{-1}
Toluene	2-m-2-propanol		
p-xylene			
Trifluoroethanol	2-pentanol		
Ethanol	Hexane		
1-propanol	Heptane		
1-butanol			
1-pentanol	t-butyl toluene		
1-octanol	Diethyl ether		
2-propanol	Dioxane		
2-butanol			
2-pentanol			
2-octanol			

5.2.2.1 Rate and selectivity results in 100 mL scale

Looking into the various classes of solvents studied (Figure 5.3-4), a clear trend is observed between the rate and conversion with selectivity towards intermediate products when using alcohols and aromatics. As demonstrated in Figure 5.2, all the secondary alcohols show high initial rates accompanied by > 80 % selectivity towards CBN. Among primary alcohols, 1-propanol shows the highest initial rate followed by 1-pentanol, both solvents are highly selective towards CBN. Ethanol, 1-butanol, and methanol show the lowest initial rate among primary alcohols with less than 10% conversion after 2 hours. Amongst these solvents, methanol results in the highest selectivity towards PBL with > 80 % after 2 hr. Very little to no CBL is formed using any of these solvents.

Examining the alkanes (Figure 5.4a), hexane and cyclohexane demonstrate the highest initial rates and conversions after 2 hours with ~60% conversion. All alkanes are highly selective towards CBN with > 90% selectivity. Alkane solvents behave similarly towards both Pt/TiO_2 and Pt/SiO_2.

In case of aromatic solvents (Figure 5.4b), m-xylene shows the highest rate and conversion. All aromatic solvents except toluene result in CBN as the main product with more than 80% selectivity. Toluene is ~70% selective towards PBL after 2 hours of reaction.
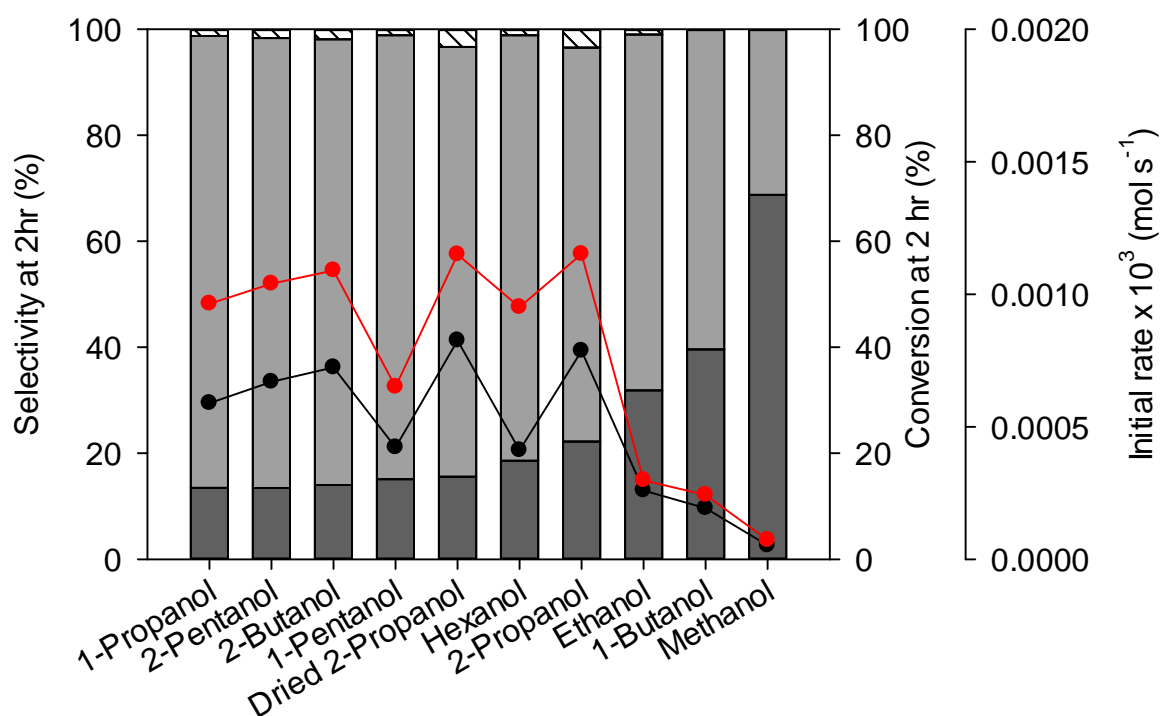
Figure 5.3: Selectivity of PBN hydrogenation products PBL (⬛), CBN (▮), and CBL (▨) after 2 hr. arranged from the highest selectivity towards CBN in 100 mL scale; conversion after 2 hr. (**black** dot-line), and initial rate of reaction (**red** dot-line) in primary and secondary alcohols. [5% Pt/SiO$_2$, P$_T$ = 5 bar, C$_{PBNi}$ = 0.270 mol L^{-1}, m$_{CAT}$/m$_{PBN}$ = 0.05, $\bar{\varepsilon}_T$ = 10 W kg^{-1}]

Little to no CBL is formed using any of these solvents as well. In all the solvents tested the lowest rates and conversions correspond to the lowest selectivity towards CBN and higher selectivity towards PBL.
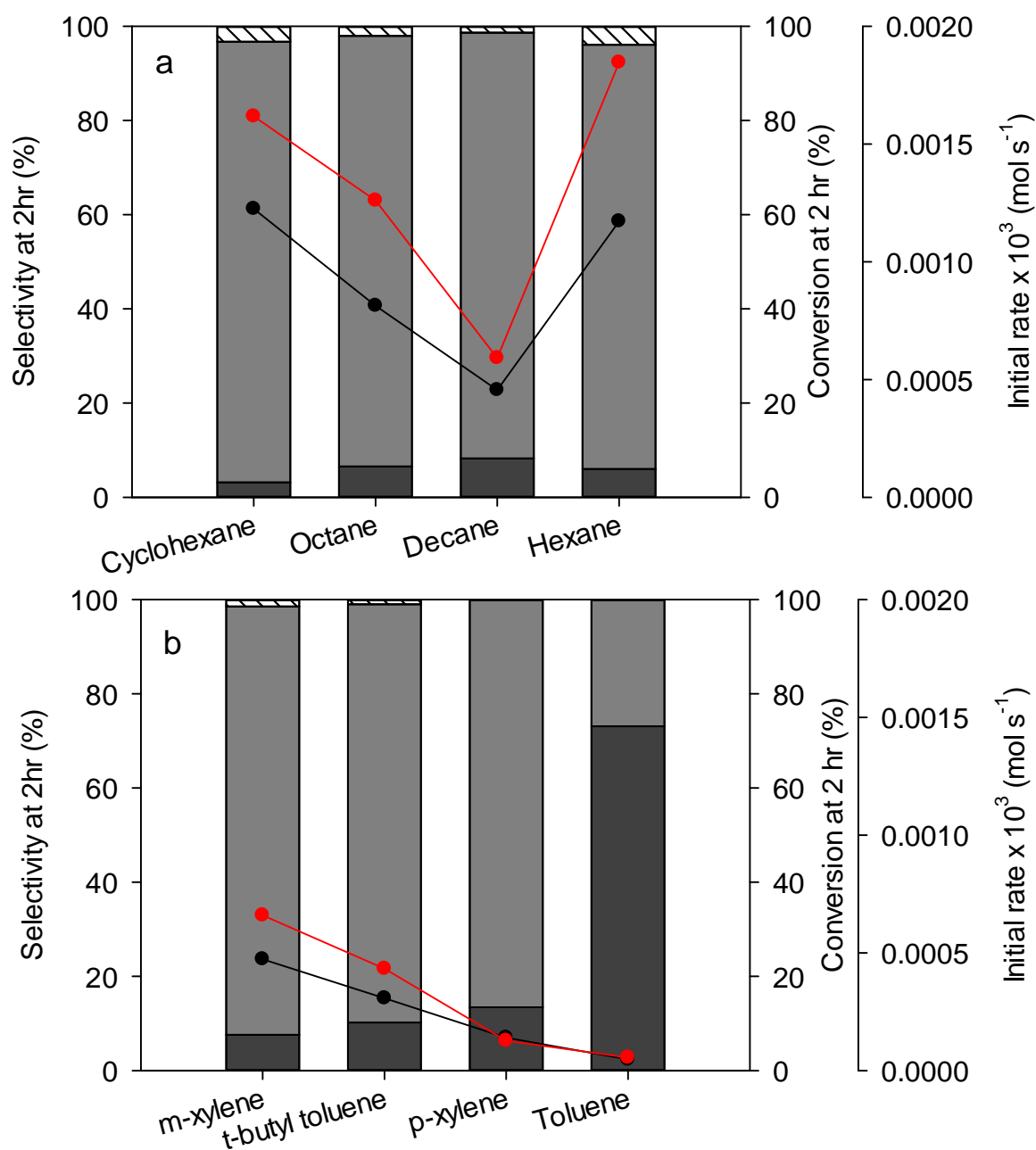
Figure 5.4: Selectivity of PBN hydrogenation products PBL (■), CBN (■), and CBL (▨) after 2 hr. arranged from the highest selectivity towards CBN in 100 mL scale; conversion after 2 hr. (**black** dot-line), and initial rate of reaction (**red** dot-line) in alkane (a) and aromatic solvents (b). [5% Pt/SiO_2, P_T = 5 bar, C_{PBNi} = 0.270 mol L^{-1}, m_{CAT}/m_{PBN} = 0.05, $\bar{\varepsilon}_T$ = 10 W kg^{-1}]

The only solvent that demonstrates interactions with active sites on Pt/SiO$_2$ is toluene which has been shown above to result in highest selectivity towards PBL when using the Pt/TiO$_2$ catalyst. Titania differs from silica in that the support contains oxygen vacancy sites at the interface with platinum nanoparticles which have been proven to increase the rate of C=O hydrogenation in the previous chapter. Consequently, titania offers different interactions with PBN and solvents that was not observed with silica. Compared with Pt/SiO2, most of the primary and secondary alcohols exhibit high rate/conversions and selectivity towards CBN thus indicating little to no solvent effect on product desorption (Figure 5.2). The low rate and conversions in methanol, ethanol, and 1-butanol then can be attributed to either catalyst/solvent interactions or the solvatochromic properties mainly the hydrogen solubility. The same conclusion can be made for alkanes specifically decane (Figure 5.3a). The only other solvent exhibiting high selectivity towards PBL ($\sim$ 60 %) for Pt/SiO$_2$ catalyst is toluene thus suggesting a possible adsorption of this solvent with active sites.

The above observations and speculations are further confirmed in kinetic analysis of experimental data in varying solvents for both Pt/TiO$_2$ and Pt/SiO$_2$ catalyst shown later in §5.3.

5.2.2.2 Rate and selectivity results in 3000 mL scale

The selectivity, conversion, and initial rates of reaction carried out in the 3000 mL reactor are presented in Figure 5.4. Reaction results for alcohols are plotted in Figure 5.4a and all other solvents in Figure 5.4b. All alcohols apart from 2-propanol are most selective towards PBL. In case of primary alcohols, both 1-propanol and ethanol showed very low initial rates and less than 10% conversion after 2 hours. Both solvents showed ~70% selectivity towards PBL after 2 hr. reaction time. No CBL formation was observed using these two solvents which is

in parallel with 100 mL scale data. In case of secondary alcohols, 2-pentanol and cyclohexanol both resulted in low initial rates and less than 20% conversion after 2 hr. 2-pentanol was the most selective solvent towards PBL with ~ 80% selectivity. 2-propanol showed the highest conversion among alcohols with 60% after 2 hr. and highest selectivity of ~50% towards CBN. Some CBL formation was observed using this solvent (20%). 2-m-2-propanol was the only tertiary solvent tested which resulted in the lowest rate and conversion among all solvents with the highest selectivity towards CBL compared with other alcohols. The same trend as observed at the 100 mL scale is found with alcohols at the 3000 mL scale with the highest rates and conversions coinciding with highest selectivity towards CBN. In case of alkanes both hexane and heptane show ~ 80% selectivity towards CBN similar to 100 mL scale data. Heptane resulted in the highest conversion of ~70% after 2 hr. followed by hexane. The highest selectivity towards CBN was observed using t-butyl toluene and diethyl ether with more than 90% after 2 hr. On the other hand, dioxane demonstrated the lowest rate and conversion with less than 1% after 2 hours. Comparing the two scales across classes of solvents, there are differences in rates and selectivity. While in 100 mL scale across majority of alcohols conversion of more than 30% was observed with CBN as major product in 3000 mL scale PBL is the main product of all the alcohols except 2-propanol.
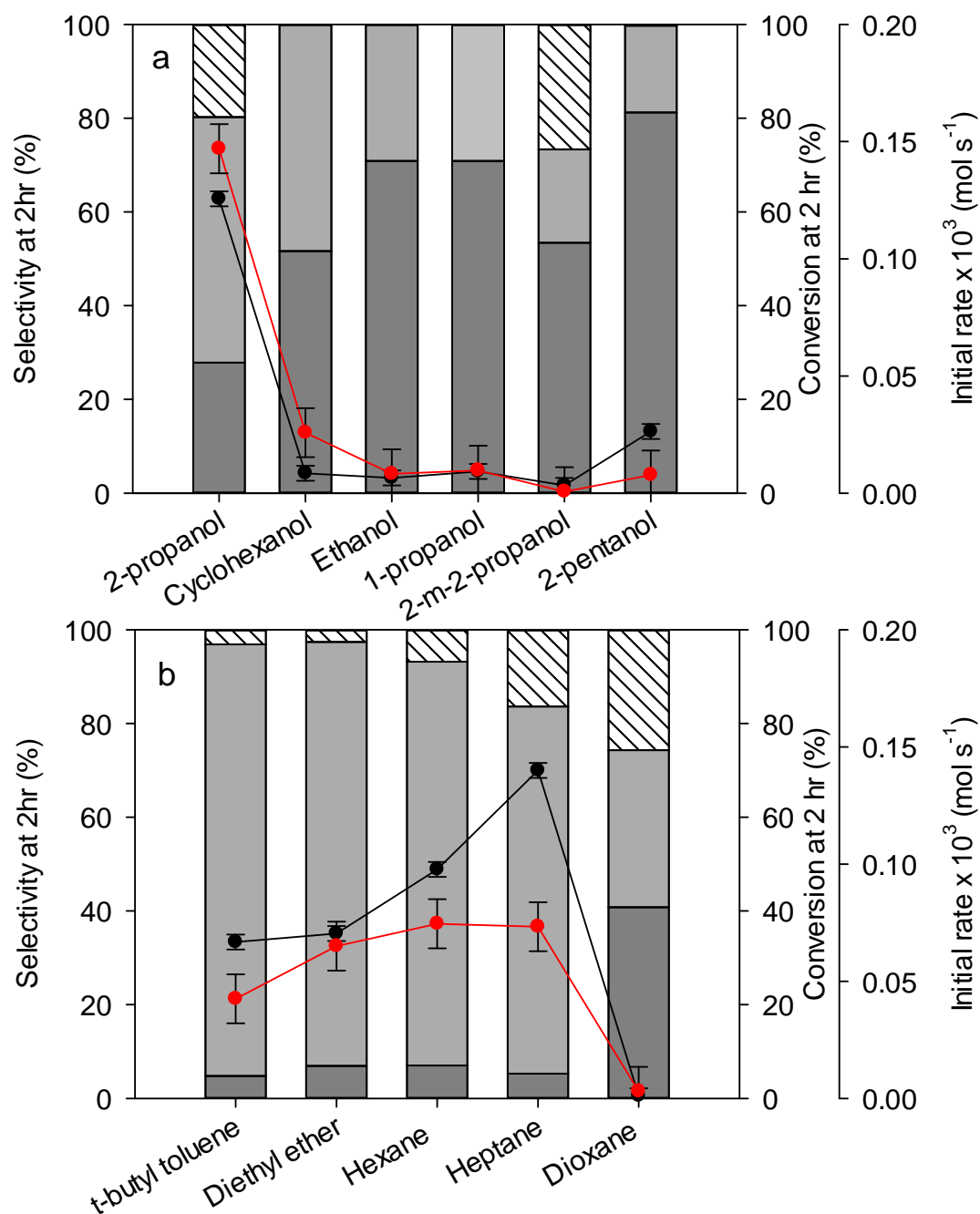
Figure 5.5: Selectivity of PBN hydrogenation products PBL (▓▓), CBN (▒▒), and CBL (▨▨) after 2 hr. arranged from the highest selectivity towards CBN in 3000 mL scale; conversion after 2 hr. (**black** dot-line), and initial rate of reaction (**red** dot-line) in alcohols (a), and all other solvents (aromatics, alkanes, ethers) (b). [5% Pt/SiO$_2$, P$_T$ = 5 bar, C$_{PBNi}$ = 0.270 mol L^{-1}, m$_{CAT}$/m$_{PBN}$ = 0.05, $\bar{\varepsilon}_T$ = 3.5 W kg^{-1}]

231

The results from alkanes and t-butyl toluene are more in line with 100 mL scale experiments in terms of high conversions and selectivity towards CBN. Furthermore, across alkanes, aromatics and ethers only the results from dioxane were in agreement with the previous trend observed between rate of reaction and selectivity towards CBN and PBL. Additionally, in 3000 mL scale experiments when using 1-propanol, ethanol, 2-propanol, hexane, heptane, and diethyl ether some traces of hydrogenolysis were observed (~ 1% selectivity wise). The hydrogenolysis of PBN resulted in two unwanted products butyl-cyclohexane and butylbenzene. In case of ethanol, 1-propanol, and 2-propanol small amounts of solvent oxidations to corresponding ketones and aldehydes was also observed. It should be noted that Pt/SiO_2 catalyst was not reduced at both scales prior to reaction as QUB results confirmed no impact on rate and selectivity with reduction. However, experiments done in hexane and 2-propanol with reduced Pt/SiO2 showed no traces of hydrogenolysis and solvent oxidation.

5.3 Kinetic modelling of PBN hydrogenation in a range of solvents at 100 mL scale

5.3.1 Modelling the experiments in P25 4% Pt/TiO_2 catalyst

The kinetic model elucidated in Chapter 4 was applied to the experimental data for a range of solvents (series C) in Table 5.1. For all solvent types, the individual data were fitted to the two-site model (Model No. 4.35b) with competition between hydrogen and the organics. The Quiney and Shrumuman method was then applied the same as described in Chapter 4 to reduce the number of parameters as needed (Quiney and Schuurman, 2007). The single-site model was also considered during modelling procedure however this model was found to degrade the residuals during the statistical analysis. This generalised model rendered a relatively satisfactory correlation when applied to the range of solvents. After the modelling procedure was finalized for all solvents, the kinetic parameters (K_{CBN}, K_{PBL}, k_{ket}, k_{arom}) were

232

accessed across the entire range of solvents. Figure 5.6 represents the log-linear plot of adsorption constants K_{CBN}, and K_{PBL} against CBN selectivity after 2 hours.

A clear trend is observed for the majority of solvents with acceptable 95 % confidence intervals for K_{CBN} for the individual classes of solvents in majority of cases. The general trend can be described as the adsorption constant decreases the higher selectivity towards CBN is observed. In case of K_{PBL} the adsorption constant progress with CBN selectivity is more subtle and can be described as relatively unchanged within a certain boundary.

These results suggest that desorption of CBN across all the solvents is the key factor governing the selectivity of this reaction system when using different solvents. This behaviour can be justified by the weaker solvation of the CBN in hydrophilic solvents compared with alkanes which are more likely to interact with cyclohexyl group on CBN resulting in favourable desorption of this product from catalyst surface. Looking at the individual classes of solvents more closely, in case of alkanes low adsorption constants lead to high selectivity towards CBN. In primary and secondary alcohols, the adsorption constant is higher and desorption of CBN product from catalyst surface is more difficult. In case of aromatic solvents the evolution of K_{CBN} with selectivity is relatively weaker across toluene, p-xylene and t-butyl toluene. The high CBN selectivity observed in t-butyl toluene (~70%) can be justified by the interaction of aromatic solvents with active sites responsible for ring hydrogenation.

Figure 5.6: Fitted adsorption constants, K_{CBN} (a) and K_{PBL} (b), against selectivity after 2 hr. across the range of solvents tested for Pt/TiO$_2$ catalyst in 100 mL scale: Alkanes (□), Primary alcohols (○), Secondary alcohols (▽), aromatics (×), Ethers (◇). [P$_T$ = 5 bar, C$_{PBNi}$ = 0.270 mol L^{-1}, m$_{CAT}$/m$_{PBN}$ = 0.05, $\bar{\varepsilon}_T$ = 10 W kg^{-1}]

As stated before the sterically demanding t-butyl toluene does not adsorb on the catalyst surface resulting the reaction to proceed similarly as alkanes. In other aromatic solvents and primary alcohols however, the ring hydrogenation is hindered by solvent adsorption on active sites. In case of secondary alcohols namely 2-propanol, PBN can longer sit in the oxygen vacancy sites and react through C=O resulting in high rate and selectivity towards PBL. Consequently, there is a trade-off between the solvent interaction with catalyst surface and the ability of solvent to facilitate desorption of products from catalyst surface. This is further discussed along with solvent effects towards phenyl and carbonyl group hydrogenation rate constants.

Figure 5.7 plots the rate constants for ketone and ring hydrogenation routes for the solvents examined. The rate of phenyl group hydrogenation (k_{arom}) demonstrates a stronger dependency towards the choice of solvent compared with the ketone hydrogenation group (k_{ket}). From these results it is concluded that the selectivity towards CBN as a function of solvent is highly dependent on its effect on the rate of ring group hydrogenation. This behaviour is consistent with proposed dual site nature of the catalyst. The exceptions to this trend are secondary alcohols and these will be discussed further.

As ring hydrogenation route occurs on Pt sites of the catalyst surface, k_{arom} can be described as $k_{pt}(1-\theta_{solv})$ which relates the number of active sites available as a function of solvent adsorption strength. While solvents like toluene, p-xylene can occupy the ring active sites the solvent inhibition is less prominent for sites available for ketone hydrogenation thus explaining the relative flatness of the k_{ket} parameter across most solvents. As the nature of this site was explained as an interfacial spot between Pt and TiO$_2$ which hydrogenates C=O bond,

lack of this functional group in any of the solvents investigated can justify the k_{ket} behaviour with solvents.

The clear exception among all classes of solvents in Figure 5.7 is the secondary alcohols which demonstrate TOF (k_{arom}) at comparable levels to alkanes and t-butyltoluene and high TOF towards ketone (k_{ket}) hydrogenation. The CBN selectivity is low in secondary alcohols and roughly follows the chain length of compounds. These solvents are suggested to be more sterically hindered than primary alcohols resulting in a much lower density over catalyst layer. Comparing the dipolarity of example alcohol and alkane solvents (π_1^X), 1-propanol and 2-propanol have the values 0.52 and 0.48 respectively, whereas hexane has the value of -0.08 (Abraham et al., 1988).

The exceptional behaviour of these solvents across their rate and selectivity suggest that polarity would be an unlikely explanation towards this behaviour. One way to explain the higher k_{ket} parameter for secondary alcohols suggests that this parameter might be coupled in this case, meaning C=O hydrogenation occurs on both Pt and TiO_2 oxygen vacancy sites. The results in Section 5.2.2 clearly demonstrated the PBL formation when using Pt/SiO_2 catalyst which does not demonstrate the dual-site behaviour observed using the Pt/TiO_2 catalyst. The behaviour of the secondary alcohols (rate and selectivity) can also be justified by their hydrogen donor capabilities as suggested by previous works (Toukoniitty et al., 2003a), (Martin et al., 2013). These studies single-out the protic solvents as inert, H-donor solvents which facilitate the hydrogenation towards higher reaction rates.
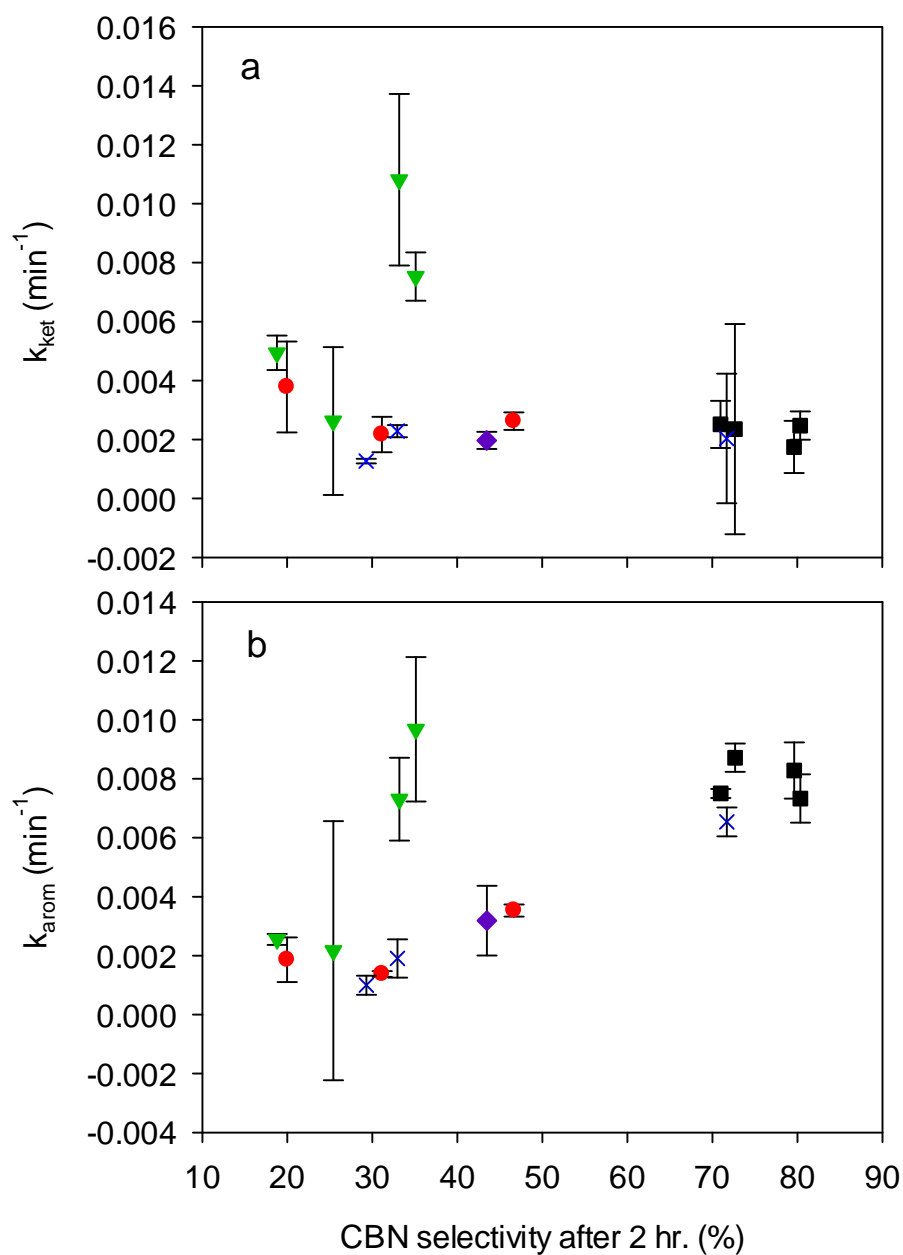
Figure 5.7: Fitted rate constants, K_{ket} (a) and K_{arom} (b), against selectivity after 2 hr. across the range of solvents tested for Pt/TiO$_2$ catalyst in 100 mL scale: Alkanes (□), Primary alcohols (○), Secondary alcohols (▽), aromatics (×), Ethers (◊). [P$_T$ = 5 bar, C$_{PBNi}$ = 0.270 mol L^{-1}, m$_{CAT}$/m$_{PBN}$ = 0.05, $\bar{\varepsilon}_T$ = 10 W kg^{-1}]

Normalised cross-correlation values ($norm(J_k)_m$), values between fitted k_{arom} and K_{CBN} did not reach a significant value (> ±0.95%). This value offers a statistical confirmation on key parameters used to describe the effect of solvents, which in this case are site availability for ring hydrogenation and ease of CBN desorption from Pt.

It should be noted that during the modelling procedure, PBL adsorption constant was not eliminated from the rate models. An improved CBN adsorption correlation was derived later by by Sam Wilkinson using further model refinement and the results are presented in a paper to be published (Wilkinson et al., 2014).

5.3.2 Modelling the experiments in 5% Pt/SiO2 catalyst

The experimental data obtained using the Pt/SiO2 catalyst across a range of solvents were modelled using both single-site and dual site models. As previously predicted, the two-site model failed to properly model the experimental data in majority of solvents. PBL adsorption constant for all solvents was found to be indeterminate and statistically insignificant and was thus eliminated during model refinement procedure.

Figure 5.8 represents the CBN adsorption constants across all solvents tested. A less prominent trend is observed for K_{CBN} term for Pt/SiO$_2$ catalyst, suggesting that the driving term for CBN selectivity is not product desorption, as the majority of solvents are more selective towards CBN as opposed to Pt/TiO$_2$ (where a range of selectivities was observed across different classes of solvents).
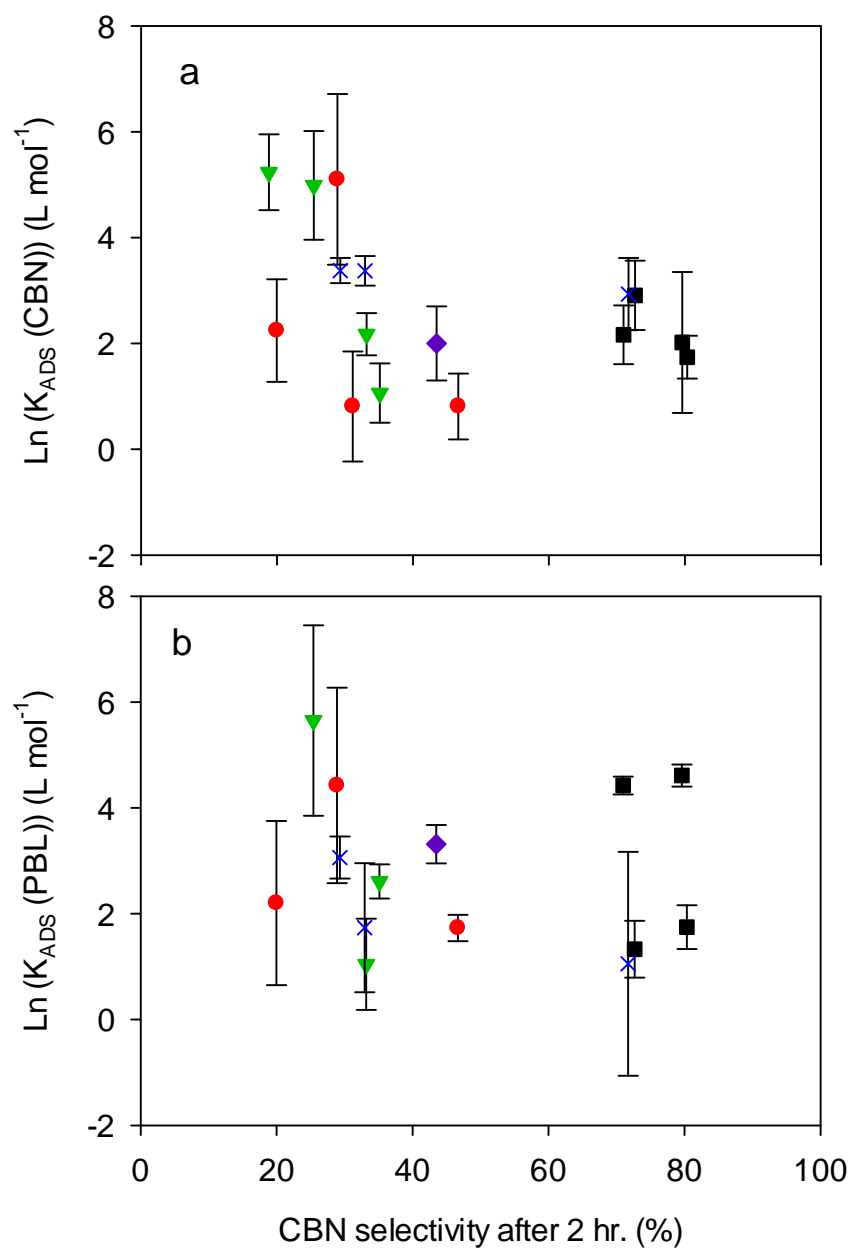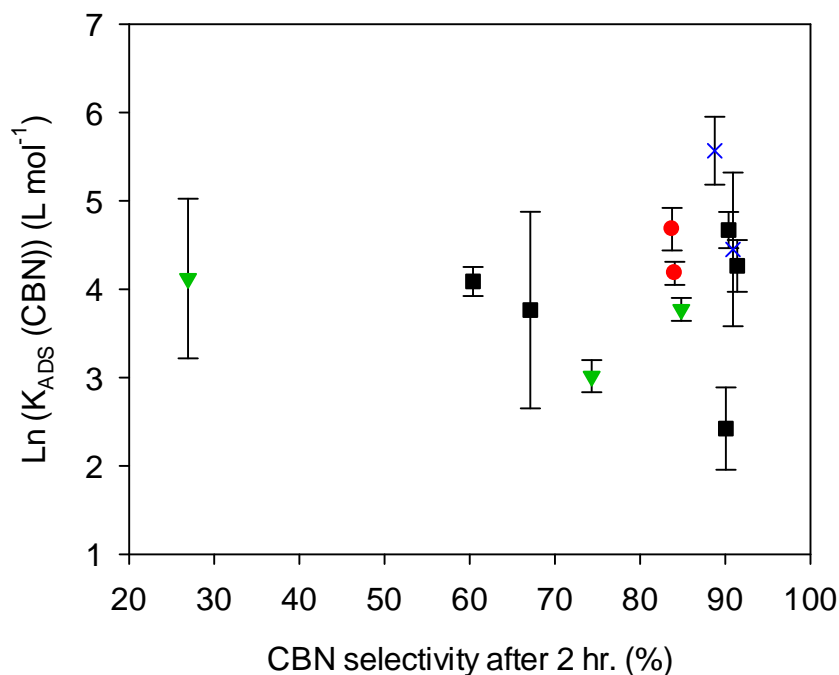
Figure 5.8: Fitted adsorption constants, K_{CBN}, against selectivity after 2 hr. across the range of solvents tested for Pt/SiO2 catalyst in 100 mL scale: Alkanes (□), Primary alcohols (○), Secondary alcohols (▽), aromatics (×). [P_T = 5 bar, C_{PBNi} = 0.270 mol L^{-1}, m_{CAT}/m_{PBN} = 0.05, $\bar{\varepsilon}_T$ = 10 W kg^{-1}]

Figure 5.9 plots the fitted rate constants k_{ket} and k_{arom} for all solvents tested using Pt/SiO$_2$ catalyst. As this plot suggests, both k_{ket} and k_{arom} rate constants are more prominently affected by the choice of solvent compared with Pt/TiO$_2$ where only k_{arom} indicated significant solvent sensitivity. This behaviour further confirms that a single site is available for both ketone and ring hydrogenation on Pt/SiO$_2$ and solvent interaction with Pt active sites impact TOF towards both functional groups on the same extent.
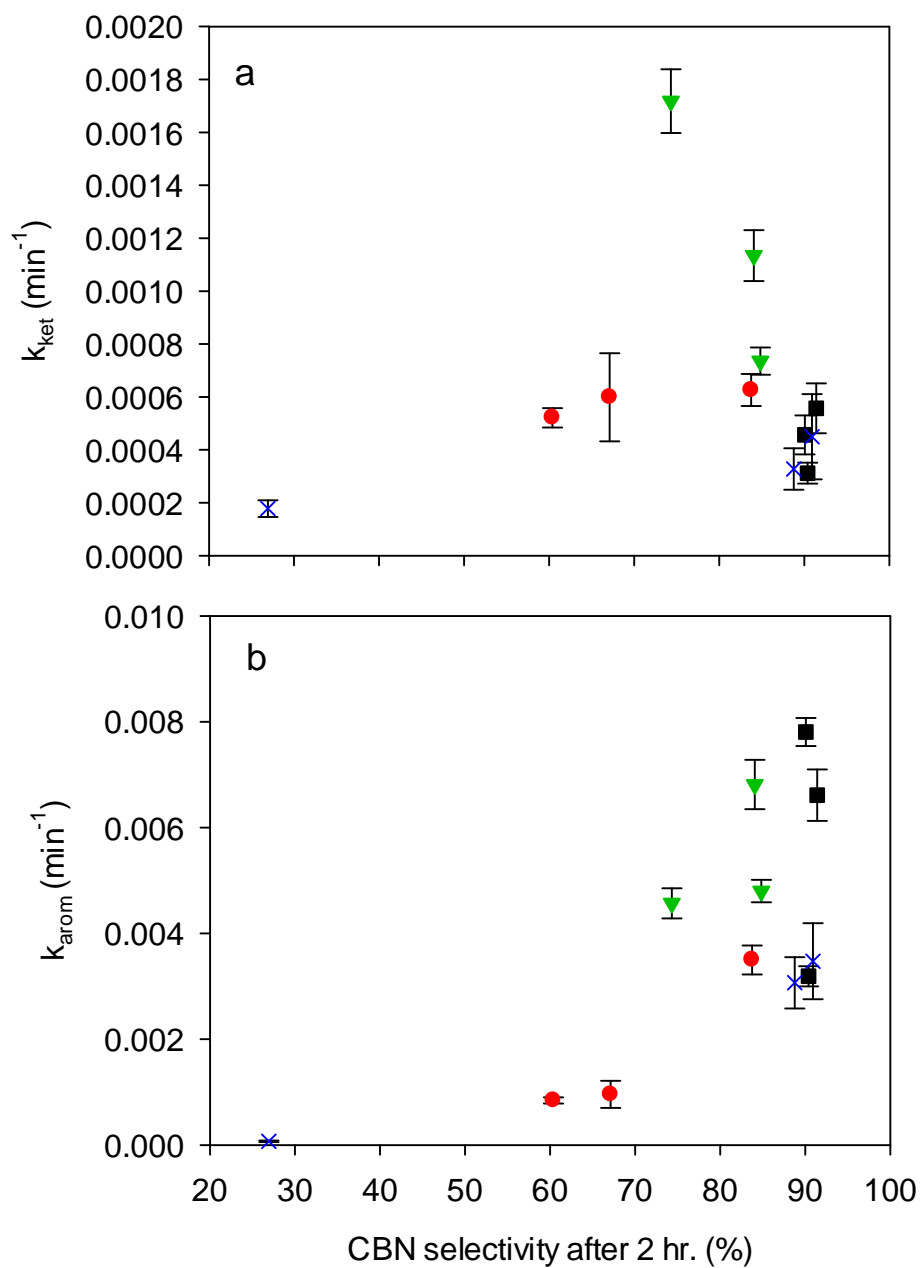
Figure 5.9: Fitted rate constants, k_{ket} (a) and k_{arom} (b), against selectivity after 2 hr. across the range of solvents tested for Pt/SiO2 catalyst in 100 mL scale: Alkanes (□), Primary alcohols (○), Secondary alcohols (▽), aromatics (×). [P_T = 5 bar, C_{PBNi} = 0.270 mol L^{-1}, m_{CAT}/m_{PBN} = 0.05, $\bar{\varepsilon}_T$ = 10 W kg^{-1}]

The majority of the solvents tested demonstrate a clear correlation with CBN selectivity. Higher selectivity towards CBN is observed when using secondary alcohols, alkanes and aromatics except toluene.

Looking into different classes of solvents for k_{ket} (Figure 5.8a), primary alcohols show a weak correlation for k_{ket} with increasing CBN selectivity whereas for k_{arom} a clear trend is observed. This suggests the interaction of primary alcohols with active sites is governing the TOF towards CBN. This is further justified with looking at k_{arom} values for primary alcohols. k_{arom} increases with increasing alcohol chain length from 1-butanol to 1-pentanol. As suggested before the bulkier solvents are more satirically hindered towards adsorption on catalyst surface. The solvent bulkiness would also result in lower hydrogen solubility. Selectivity towards PBL is independent of the type of primary alcohols used suggesting that unlike CBN, PBL selectivity is independent of solvent-catalyst interaction and other parameters like dipolarity, gas solubility, etc might be useful in order to further investigate k_{ket} across primary alcohols.

Aromatic solvents behave the same way as primary alcohols for k_{ket} values, which also demonstrate relatively no change with increasing CBN selectivity across toluene, m-xylene, and t-butyl toluene. k_{arom} and k_{ket} values are the smallest among all solvents for toluene. As both ring and ketone hydrogenation occurs on Pt sites in this catalyst, adsorption of toluene on Pt results in low values of k_{ket} and k_{arom}. On the other hand, t-butyl toluene and m-xylene exhibit k_{ket} and k_{arom} values in comparable levels with alkanes facilitating the ring hydrogenation via minimal interaction with catalyst surface. Similar to Pt/TiO$_2$ secondary alcohols show k_{ket} higher than all other solvents and k_{arom} at the same level as alkanes, t-butyl toluene and m-xylene. This behaviour further confirms the previous observations for Pt/TiO$_2$

catalyst where it was suggested that rate constants might be coupled between two active sites. In Pt/SiO$_2$ where the solvent interaction is with one type of site only, the increase in CBN selectivity and consequently k$_{arom}$ with increasing alcohol chain length from 2-propanol to 2-pentanol can be investigated against availability of sites and/or TOF (k$_{ket}$ and k$_{arom}$) when using different solvents as well as hydrogen donor capability or possible dissociative nature of alcohols, namely 2-propanol.

The experimental data at the 3000 mL scale were analysed as qualitative parallels between two scales in order to demonstrate the complications that could arise when scaling up and as a clear conclusion could not be reached on mass transfer limitations of each experimental point at 3000 mL scale (one isothermal experiment for each solvent), it is suggested that a more through design of experiments is required for experiments at bench scale in order to elucidate the solvent effects against lab-scale data.

5.4 Kinetic approach taken in context to previous work on solvent driven effects

In Chapter 4, it was strongly stated that in-order to build a robust kinetic model a combination of sound initial considerations and statistical approaches can be used to refine the kinetic models. Using this approach will ensure systematic building of kinetic models, reduce the need for complicated design of experiments and ensure solid mechanistic details on kinetics governing a reaction system. Furthermore, using such approach will overcome the difficulties most researchers face when either over-simplifying or over-complicating the kinetic models.

Most of the studies so far dealing with the kinetics of liquid phase hydrogenation in-order to elucidate the solvent effects deal with variety of approaches in order to include the solvent effects in rate models.

For the purpose of this chapter a few parallels are driven to compare the approaches taken so far. A more detailed discussion on elucidating solvent effects can be found in Chapter 2.

Among the kinetic works done so far on solvent behaviour a few important examples are works of (Singh and Vannice, 1999), (Toukoniitty et al., 2003a), (Mukherjee and Vannice, 2006a), (Mounzer et al., 2010), (Martin et al., 2013), and (Wan et al., 2014).

In the work carried out by (Singh and Vannice, 1999), liquid phase hydrogenation of benzene was studied on palladium supported on alumina catalyst. It was suggested that the fractional coverage of hydrogen on catalyst surface increases with hydrogen solubility through the partial pressure of hydrogen on gas phase. It was strongly recommended to utilize liquid-phase hydrogen concentration in rate models. Assuming no solvent adsorption on catalyst surface, an expression for surface coverage of hydrogen was derived based on site balance considering equilibrium between hydrogen in gas phase with hydrogen in liquid phase. Standard enthalpy of adsorption and entropy of adsorption of hydrogen derived from gas phase in literature is then can be used to determine the hydrogen adsorption constant before kinetic analysis.

Other forms of hydrogen inclusion to rate models were suggested by (Toukoniitty et al., 2003a). In this work hydrogenation of 1-phenyl-1,2-propanedione using platinum supported on alumina using a range of solvents was studied. Solvent/catalyst interaction was concluded to be significant for tetrahydrofuran and 1-pentanol where very low reaction rates were reported for both. The high hydrogenation rate in 2-propanol was attributed to the hydrogen donating properties. Among primary alcohols tested 1-pentanol resulted in exceptionally low rate compared with others. In order to explain the kinetics, the Kirkwood treatment was used to correlate the rate constants to solvent dielectric constant and dipole moment (Laidler,

1987). No discussion was made around the effect of solvents on product desorption. The fitted hydrogenation rates did not correlate with the experimentally recorded hydrogen solubility and no correlation with dielectric constant and dipole moment was observed. The same behaviour was observed in the current work where the high rates towards 2-propanol, and hexane and low reaction rate in 1-peopanol could not be explained using polarity. Thus the Kirkwood treatment based on transition state theory was used to correlate enantioselectivity with dielectric constant. The developed model was successful in describing the selectivity as function of dielectric constant.

As more research surfaces that suggests the catalyst/solvent interaction as one of the key factors driving the solvent effects some works have been done in order to contribute the solvent adsorption effect into the rate models. An example of such works is the research carried out by (Mukherjee and Vannice, 2006a). This work deals with hydrogenation of citral using Pt/SiO$_2$ catalyst in a range of solvents. An attempt was made to include a solvent adsorption constant into rate expressions. However, the solvent concentration was calculated using the linear relationship between the reactant and solvent. Doing this creates a mathematically high value over $K_{solv}C_{solv}$ in denominator thus creating a bias towards the K_{solv} value. A lumped adsorption value was suggested, constrained over a narrow range in order to fit the rest of the parameters. This resulted in satisfactory fits however narrowing the adsorption constants overt a range was not statistically justified. Other works which has previously taken a similar route are done by (Kishida and Teranishi, 1968), (Lemcoff, 1977).

The importance of product desorption term observed in the current study is also in line with the work of (Mounzer et al., 2010), where the desorption of the main product was observed to be highly dependent on the choice of solvent. Consequently, a product desorption term was

incorporated into the developed rate expression which was the most successful in describing the rate and selectivity.

Another recent work has been carried out by (Martin et al., 2013) around hydrogenation of ethyl benzoylformate using Pt/Al_2O_3 catalyst over a range of solvents. In general, protic solvents (2-propanol, 1-propanol, 1-octanol and ethanol) resulted in the higher initial rates compared to aprotic polar solvents. The high activity in protic solvents was attributed to their hydrogen donor capabilities. This work further confirmed the inability of hydrogen solubility and solvent dielectric constant in predicting rates and other solvent interactions was suggested to play a more significant role in the hydrogenation of this reaction system. For the kinetic analysis in this work the same approach as (Toukoniitty et al., 2003a) was utilised as described above. However, the modelling procedure was done by eliminating the solvents which exhibited hydrogen donor capabilities or strong interactions with catalyst in order to drive a good fit for other solvents investigated.

A parallel can be drawn with the works above and the exception solvents demonstrated in the current work which were not able to fall into the trends observed. This concludes that in order to progress further in modelling the kinetics of hydrogenation reactions in different solvents the way forward is a radical change in the way the researchers view and categorize the solvents. The traditional way of aprotic, protic, and non-polar etc will not be able to generate a robust way to group and approach the solvent effects. A way forward might be to start re-categorising the solvents in an algorithmic way based on their different interactions during catalytic processes. Some solvents might fall into more than one category. An example of a starting point based on the current work would be,

1. Solvents which exhibit hydrogen donor capabilities, are more sterically hindered towards catalyst surface or might have dissociative adsorption behaviour: 2-propanol, 2-butanol, etc

2. Solvents which do not have hydrogen donor capabilities and are inert towards surface: ethyl acetate

3. Solvents which exhibit hydrogen donor capabilities and adsorb more densely on the surface of the catalyst: 1-propanol

4. Solvents which exhibit high adsorption onto catalyst surface: THF

5. Solvents which exhibit adsorption to catalyst surface at certain temperatures: toluene

6. Solvents which are inert towards surface and facilitate product desorption depending on their hydrophobicity: hexane, t-butyl toluene

7. Solvents which show a correlation with solvent properties and gas solubility and might fall into any of the above categories as well.

The solvents falling into each category might vary depending on the reactant used, operational conditions and catalyst. This re-iterates the complexity of these systems considering all interactions but until a systematic way in categorising the solvents is established the research being done in this field will carry on over circles of observed behaviour and kinetically ruled out "exceptional" solvents.

5.5 Conclusions

To understand better the solvent effects in hydrogenation reactions, various approaches has been undertaken to drive the intrinsic kinetics of reactions in various solvents. Reaction kinetics with respect to solvent effects are governed by different interactions between

catalyst/solvent, reactant/solvent and gas/solvent. Data for PBN hydrogenation using Pt/TiO_2 and Pt/SiO_2 catalysts were provided by QUB to develop a robust kinetic analysis methodology in order to elucidate the solvent effects. The best kinetic model derived from the modelling procedure in Chapter 4 was fitted to PBN hydrogenation data in varying ranges of solvents for Pt/TiO_2 and Pt/SiO_2 catalysts. The role of solvent in determining catalytic activity and selectivity towards different functional groups is varied among literature data but a parallel can be drawn based on the exceptional solvents which do not correlate well using a single approach towards all classes of solvents. The modelling procedure taken here revealed that for Pt/TiO_2 catalyst the adsorption constant K_{CBN} is directly linked to product selectivity as well as the site availability for ring hydrogenation (k_{arom}). On the other hand, for Pt/SiO_2 catalyst the CBN desorption was found to be more or less independent of solvents used and product selectivity is governed by site availability and possible hydrogen/solvent effects.

The results of kinetic approach taken here demonstrated that kinetic model refinement based on systematic parameter elimination can be used to derive robust kinetic models that can be applied over a range of different solvents. Once the significant solvent interactions affecting a given catalytic system are established, further efforts can be taken towards quantification of solvent effects on kinetic parameters towards more fundamental understanding.

Chapter 6: Conclusions and future work

6.1 Conclusions

The catalytic hydrogenation of 4-phenyl-2-butanone (PBN) was investigated using Pt/TiO_2 as catalyst and hexane as solvent. Reactions were performed under different operational conditions at two scales of reactors, 100 mL (QUB) and 3000 mL (Birmingham). The selectivity profiles towards all products, intermediate (cyclohexyl butanone (CBN) and phenyl butanol (PBL)), and final (cyclohexyl butanol (CBL)) are independent of energy input, pressure, temperature, and catalyst loading. However, variations on selectivity values of PBL and CBN were observed when increasing temperature and catalyst loading. It was observed that selectivity towards CBN increased with increasing temperature and catalyst loading due higher activation barrier of phenyl ring and higher active site availability, respectively. Hydrogenation of PBN in 100 mL scale demonstrated > 70% selectivity towards CBN which starts to slightly decline at ~ 70% conversion towards the final products CBL. Selectivity towards PBL never goes higher than 40% at all conversions.

On the other hand, in 3000 mL scale, PBL is the main product of reaction with more than 50% selectivity at all conversions (at lower catalyst loadings including base condition). Increasing the catalyst amount showed that this product is generated with high selectivity (> 80%) at the start of the reaction and its selectivity continuously declines with conversion as the reaction goes near completion. 100% selectivity towards CBL was observed at a higher catalyst loading ($m_{CAT}/m_{PBN} = 0.07$), where in 100 mL scale the reaction was still 70% selective towards CBN and far from completion. The results from selectivity profiles with changing hydrodynamic parameters, catalyst activity with increasing catalyst input, and mass

transfer analysis based on Carberry number (Ca) for all temperatures and concentrations investigated demonstrated that the selectivity at both scales is independent of external/internal mass transfer limitations for H_2 and PBN. It was also observed that although reactions in 3000 mL scales were carried out in energy input an order of magnitude lower than 100 mL scale the rate of reactions was always an order of magnitude higher in 3000 mL and selectivity profile did not change even at energy input as high as 20 W kg^{-1}. Consequently, this shift in selectivity could not be due to mass transfer limitations.

In order to investigate this change in reaction mechanism and rate and selectivity profiles, a rigorous kinetic modelling approach was used. Two sets of data in 100 mL scale were used for kinetic modelling: temperature-varied and concentration-varied data. The first set was used to investigate different LHHW models based on rate determining steps and acquire the activation energy. The second set was used to fit kinetic models based on competitive adsorption of H_2, single- or two-site availability for hydrogenation of ketone and ring functional groups, and desorption of intermediate products from catalyst. It was found that the model incorporating competitive H_2 adsorption, two types of active sites, and product desorption terms for PBL and CBN was the best model describing the kinetics of this reaction. The success of two-site model was in agreement with previous literature data stating the availability of an oxygen vacancy site on TiO_x support responsible for ketone hydrogenation.

The kinetic procedure involved assessment of the relative significance of kinetic parameters on model response by using sensitivity analysis based on norms of Jacobian Matrix. The insignificant parameters were determined and systematically eliminated from rate models. The eliminations were justified by means of F-test, residuals, parity plots, and condition

numbers. The choice of model was based on Athena Visual Studio Model Discrimination protocol which involves the use of various statistical parameters to identify the best model. The robustness of the final model was tested against varying initial values of kinetic parameters within acceptable ranges. The fitted values of kinetic parameters were within acceptable physiochemical and probability ranges and were able to explain the mechanism of PBN hydrogenation.

The fitting of the chosen model to experimental data in 3000 mL scale was done by taking into account the slight variation of H_2 concentration calculated from mass transfer data. It was concluded that although the kinetic model can predict the rate in some extent the selectivity of products could not be estimated at all. Consequently, the parameter estimation was carried out from the beginning on 3000 mL scale data. It was observed that the mechanism in which the parameters were eliminated in 100 mL scale which involved equating the ketone and hydrogenation routes by means of pre-exponential factors and activation energies did not apply to 3000 mL scale. Furthermore, higher activation energies were observed in 3000 mL scale compared with 100 mL scale experiments. This raises the need for a more through mass transfer analysis to be carried out for both scales.

Although the derived kinetic parameters were significantly different between both scales the best model identified at 100 mL scale was also the only model which successfully described the kinetics in 3000 mL scale. The most significant shift in kinetic parameters were observed in desorption of PBL and CBN from catalyst surface. While, in 100 mL scale higher CBN desorption constant was determined to account for high selectivity of this product, in 3000 mL scale the desorption of PBL was faster from catalyst surface resulting in a shift in dominant reaction route from ring to ketone hydrogenation when scaling-up. Based on these

findings it was concluded that a systematic kinetic approach can greatly assist in investigations of chemistry sensitive reactions upon scale-up even if this increase in scale is of order of 10^1 in volume. However, the nature of this shift could not be determined within the timeframe of the current work.

The kinetic model derived in Chapter 4, was then applied to experiments in 100 mL scale using Pt/TiO_2 and Pt/SiO_2 catalysts and a range of solvents (protic, aprotic polar, apolar, ethers, halogens). Use of the Pt/TiO_2 catalyst resulted in significant changes in rate and selectivity of PBN hydrogenation in range of the solvents studied. Kinetic modelling made it possible to determine the ability of the solvents to remove CBN from catalyst surface and catalyst site availability for ring hydrogenation as the governing solvent interactions. On the other hand, reactions done using Pt/SiO_2 were less susceptible to solvent effect. This was justified by difference between the two oxide supports. In Pt/SiO_2 there is only one type of site available for hydrogenation and it is the metal surface of Pt. This postulation was verified by success of the single-site model in describing the kinetics over this catalyst.

The high selectivity towards CBN was observed in most of the solvents for this catalyst apart from toluene and methanol. The rate and selectivity in alcohols for this catalyst showed distinct trends with increasing carbon chain length confirming that other factors such as H_2 or substrate solubility might be significant. The kinetic modelling confirmed the selectivity of CBN over this catalyst to be governed by catalyst site availability.

The effect of scale-up in different solvents was demonstrated as qualitative demonstration. Over both of these catalysts, scale-up resulted in significant rate and selectivity variations. Still the rate of reaction was an order of magnitude higher in 3000 mL scale in reactions with high rates and conversions. For the Pt/TiO_2 catalyst, five solvents were investigated (2-

propanol, 1-propanol, hexane, t-butyl toluene, and diethyl ether). PBL was the main product of all these solvents except t-butyl toluene. For the Pt/SiO$_2$ catalyst, a wider range of solvents were investigated. Selectivity in all alcohols and dioxane was higher towards PBL apart from 2-propanol. In alkanes and ethers however, CBN was the main product. It was concluded that for investigations of scale-up effects in different solvents more kinetic data were needed, specifically a series of mass transfer experiments in order to carry out comprehensive kinetic analysis.

6.2 Recommendations for future work

In terms of future work recommendations, there are several aspects that need to be investigated to further analyze the mechanism in which solvents and scale-up affect the catalytic reaction performance.

Based on the findings of Chapter 4, it is concluded that by means of systematic kinetic modelling even for limited experimental/kinetic data it is possible to gain understanding on the ways the scale-up affects the chemistry of problematic multiphase reaction systems. A comprehensive design of experiments is needed however to approach this problem systematically. As it is shown in the current work, if the chemistry of a reaction system is problematic, it will show in scale-up in order of magnitude of 10^1, which would still be considered as lab-scale. The design of experiments should include a range of experiments in varying operational conditions over three or more reactors with linear scale-up volumes. For reactions where mass transfer is not an issue, the most prominent scale-up criterion needs to be applied which to current knowledge is constant turbulent mixing behavior ($\bar{\varepsilon}_T$). A combination of kinetic analysis (as demonstrated in this work), doping experiments, detailed mass transfer analysis and computational simulations need to be done to investigate the nature

of how the scale-up affects rate and selectivity towards different functional groups in catalytic hydrogenations.

Based on finding of Chapter 5, the nature of solvent effects on rate and selectivity is highly dependent upon the reaction system and catalyst used. The conventional classification of solvents is not the most effective way to elucidate solvent effects. As demonstrated in this work, different case studies can be beneficial in order to document the nature of solvent effects in similar reaction systems and gather comprehensive data bases. The kinetic parameters in modelling the solvent effects might be the key to go forward with this area of research. As discussed in Chapter 2 and demonstrated in finding of Chapter 5, the solvent/substrate interactions and solvent/catalyst interactions directly influence the rate and adsorption constants. Consequently, it is safe to draw the following hypothesis,

- Kinetic rate constants (TOF) are governed by the following interactions
    1. Adsorption strength of substrate
    2. Fractional coverage of substrate with respect to solvent
    3. Solvent ability to polarize functional groups towards lowering activation barrier
    4. Associative/dissociative nature of solvent adsorption
    5. Fractional coverage of H_2 on catalyst with respect to solvent
- Kinetic adsorption constants are governed by the following interaction(s)
    6. Solvent ability in product desorption from catalyst surface.

Not all the interactions above are applicable to all reaction systems. The inconsistent results of common approaches like Kamlet Taft parameters are due to their ability to quantify interactions **1** and **6** only. Further investigations are required to correlate the other interactions

with rate and adsorption constants. By means of systematic kinetic analysis it will be possible to identify the relevant functions and quantify them using novel characterization techniques such as NMR, THZ-TDS, DFT, and ATR-IR.

References:

ABID, M., EHRET, G. & TOUROUDE, R. 2001. Pt/CeO2 catalysts: correlation between nanostructural properties and catalytic behaviour in selective hydrogenation of crotonaldehyde. *Applied Catalysis A: General,* 217**,** 219-229.

ABID, M. & TOUROUDE, R. 2000. Pt/CeO2 catalysts in selective hydrogenation of crotonaldehyde: high performance of chlorine-free catalysts. *Catalysis Letters,* 69**,** 139-144.

ABRAHAM, M. H., GRELLIER, P. L., ABBOUD, J.-L. M., DOHERTY, R. M. & TAFT, R. W. 1988. Solvent effects in organic chemistry — recent developments. *Canadian Journal of Chemistry,* 66**,** 2673-2686.

AKPA, B. S., D'AGOSTINO, C., GLADDEN, L. F., HINDLE, K., MANYAR, H., MCGREGOR, J., LI, R., NEUROCK, M., SINHA, N., STITT, E. H., WEBER, D., ZEITLER, J. A. & ROONEY, D. W. 2012. Solvent effects in the hydrogenation of 2-butanone. *Journal of Catalysis,* 289**,** 30-41.

AMMARI, F., LAMOTTE, J. & TOUROUDE, R. 2004. An emergent catalytic material: Pt/ZnO catalyst for selective hydrogenation of crotonaldehyde. *Journal of Catalysis,* 221**,** 32-42.

ARAMENDíA, M. A., BORAU, V., JIMÉNEZ, C., MARINAS, J. M., PORRAS, A. & URBANO, F. J. 1997. Selective Liquid-Phase Hydrogenation of Citral over Supported Palladium. *Journal of Catalysis,* 172**,** 46-54.

AUGUSTINE, R. L. 1985. *Catalysis of Organic Reactions*, Taylor & Francis.

BAWANE, S. P. & SAWANT, S. B. 2004. Liquid-Phase Catalytic Hydrogenation of p-Chlorobenzophenone to p-Chlorobenzhydrol over a 5 % Pd/C Catalyst. *Chemical Engineering & Technology,* 27**,** 914-920.

BAWANE, S. P. & SAWANT, S. B. 2005. Hydrogenation of p-nitrophenol to metol using Raney nickel catalyst: Reaction kinetics. *Applied Catalysis A: General,* 293**,** 162-170.

BELOHLAV, Z. & ZAMOSTNY, P. 2000. A rate—controlling step in langmuir—hinshelwood kinetic models. *The Canadian Journal of Chemical Engineering,* 78**,** 513-521.

BENNETT, J. A., FISHWICK, R. P., SPENCE, R., WOOD, J., WINTERBOTTOM, J. M., JACKSON, S. D. & STITT, E. H. 2009. Hydrogenation of 2-pentyne over Pd/Al2O3 catalysts: Effect of operating variables and solvent selection. *Applied Catalysis A: General,* 364**,** 57-64.

BERG, J. M., TYMOCZKO, J. L. & STRYER, L. 2002. *The Michaelis-Menten Model Accounts for the Kinetic Properties of Many Enzymes* [Online]. Available: http://www.ncbi.nlm.nih.gov/books/NBK22430/ [Accessed].

BERGAULT, I., FOUILLOUX, P., JOLY-VUILLEMIN, C. & DELMAS, H. 1998. Kinetics and Intraparticle Diffusion Modelling of a Complex Multistep Reaction: Hydrogenation of Acetophenone over a Rhodium Catalyst. *Journal of Catalysis,* 175**,** 328-337.

BERGER, R. J., STITT, E. H., MARIN, G., KAPTEIJN, F. & MOULIJN, J. 2001. Eurokin. Chemical Reaction Kinetics in Practice. *CATTECH,* 5**,** 36-60.

BERTERO, N. M., APESTEGUÍA, C. R. & MARCHI, A. J. 2008. Catalytic and kinetic study of the liquid-phase hydrogenation of acetophenone over Cu/SiO2 catalyst. *Applied Catalysis A: General,* 349**,** 100-109.

BERTERO, N. M., TRASARTI, A. F., APESTEGUÍA, C. R. & MARCHI, A. J. 2011. Solvent effect in the liquid-phase hydrogenation of acetophenone over Ni/SiO2: A comprehensive study of the phenomenon. *Applied Catalysis A: General,* 394**,** 228-238.

BOUDART, M. & SAJKOWSKI, D. J. 1991. Catalytic hydrogenation of cyclohexene: liquid-phase reaction on rhodium. *Faraday Discussions,* 92**,** 57-67.

BOX, G. E. P. & DRAPER, N. R. 1965. The Bayesian estimation of common parameters from several responses. *Biometrika,* 52**,** 355-365.

CARACOTSIOS, M. 2013. *Athena visual studio programming guide* [Online]. Available: http://www.athenavisual.com/Instructions/Athena%20Visual%20Studio%20Technical%20Guide.pdf [Accessed].

CARACOTSIOS, M. & STEWART, W. E. 1985. Sensitivity analysis of initial value problems with mixed odes and algebraic equations. *Computers & Chemical Engineering,* 9**,** 359-365.

ČERVENÝ, L., BĚLOHLAV, Z. & HAMED, M. H. 1996. Catalytic hydrogenation of aromatic aldehydes and ketones over ruthenium catalysts. *Research on Chemical Intermediates,* 22**,** 15-22.

CHANG, M.-Y., EIRAS, J. G. & MORSI, B. I. 1991. Mass transfer characteristics of gases in n-hexane at elevated pressures and temperatures in agitated reactors. *Chemical Engineering and Processing: Process Intensification,* 29**,** 49-60.

CHANG, M.-Y. & MORSI, B. I. 1991. Mass transfer characteristics of gases in n-decane at elevated pressures and temperatures in agitated reactors. *The Chemical Engineering Journal,* 47**,** 33-45.

CHANG, N.-S., ALDRETT, S., HOLTZAPPLE, M. T. & DAVISON, R. R. 2000. Kinetic studies of ketone hydrogenation over Raney nickel catalyst. *Chemical Engineering Science,* 55**,** 5721-5732.

CHAPMAN, C. M., NIENOW, A. W., COOKE, M. & MIDDLETON, J. C. 1983. *Particle-gas-liquid mixing in stirred vessels. I: Particle-liquid mixing.*

CHEN, C.-S., CHEN, H.-W. & CHENG, W.-H. 2003. Study of selective hydrogenation of acetophenone on Pt/SiO2. *Applied Catalysis A: General,* 248**,** 117-128.

CHEN, M., MAEDA, N., BAIKER, A. & HUANG, J. 2012. Molecular Insight into Pt-Catalyzed Chemoselective Hydrogenation of an Aromatic Ketone by In Situ Modulation–Excitation IR Spectroscopy. *ACS Catalysis,* 2**,** 2007-2013.

CHIUSOLI, G. P. & MAITLIS, P. M. 2006. Metal-Catalysis in Industrial Organic Processes. Royal Society of Chemistry.

CONSONNI, M., JOKIC, D., YU MURZIN, D. & TOUROUDE, R. 1999. High Performances of Pt/ZnO Catalysts in Selective Hydrogenation of Crotonaldehyde. *Journal of Catalysis,* 188**,** 165-175.

CONSTABLE, D. J. C., JIMENEZ-GONZALEZ, C. & HENDERSON, R. K. 2006. Perspective on Solvent Use in the Pharmaceutical Industry. *Organic Process Research & Development,* 11**,** 133-137.

CRESPO-QUESADA, M., YARULIN, A., JIN, M., XIA, Y. & KIWI-MINSKER, L. 2011. Structure Sensitivity of Alkynol Hydrogenation on Shape- and Size-Controlled Palladium Nanocrystals: Which Sites Are Most Active and Selective? *Journal of the American Chemical Society,* 133**,** 12787-12794.

CREZEE, E., HOFFER, B. W., BERGER, R. J., MAKKEE, M., KAPTEIJN, F. & MOULIJN, J. A. 2003. Three-phase hydrogenation of d-glucose over a carbon supported ruthenium catalyst—mass transfer and kinetics. *Applied Catalysis A: General,* 251**,** 1-17.

DANDEKAR, A. & VANNICE, M. A. 1999. Crotonaldehyde Hydrogenation on Pt/TiO2and Ni/TiO2SMSI Catalysts. *Journal of Catalysis,* 183**,** 344-354.

DELANNAY, F. 1984. *Characterization of heterogeneous catalysts*, M. Dekker.

DIETRICH, E., MATHIEU, C., DELMAS, H. & JENCK, J. 1992. Raney-nickel catalyzed hydrogenations: Gas-liquid mass transfer in gas-induced stirred slurry reactors. *Chemical Engineering Science,* 47**,** 3597-3604.

DIVAKAR, D., MANIKANDAN, D., KALIDOSS, G. & SIVAKUMAR, T. 2008. Hydrogenation of Benzaldehyde over Palladium Intercalated Bentonite Catalysts: Kinetic Studies. *Catalysis Letters,* 125**,** 277-282.

DUMESIC, J. A. & TREVINO, A. A. 1989. Kinetic simulation of ammonia synthesis catalysis. *Journal of Catalysis,* 116**,** 119-129.

ELGUE, S., PRAT, L., CABASSUD, M. & CÉZERAC, J. 2006. Optimisation of solvent replacement procedures according to economic and environmental criteria. *Chemical Engineering Journal,* 117**,** 169-177.

ELGUE, S., PRAT, L., COGNET, P., CABASSUD, M., LE LANN, J. M. & CÉZERAC, J. 2004. Influence of solvent choice on the optimisation of a reaction–separation operation: application to a Beckmann rearrangement reaction. *Separation and Purification Technology,* 34**,** 273-281.

ENGLISCH, M., JENTYS, A. & LERCHER, J. A. 1997a. Structure Sensitivity of the Hydrogenation of Crotonaldehyde over Pt/SiO2and Pt/TiO2. *Journal of Catalysis,* 166**,** 25-35.

ENGLISCH, M., RANADE, V. S. & LERCHER, J. A. 1997b. Liquid phase hydrogenation of crotonaldehyde over Pt/SiO2 catalysts. *Applied Catalysis A: General,* 163**,** 111-122.

FAJT, V., KURC, L. & ČERVENÝ, L. 2008. The effect of solvents on the rate of catalytic hydrogenation of 6-ethyl-1,2,3,4-tetrahydroanthracene-9,10-dione. *International Journal of Chemical Kinetics,* 40**,** 240-252.

FOGLER, H. S. 2001. *Elements of Chemical Reaction Engineering*.

GAMEZ, A., KÖHLER, J. & BRADLEY, J. 1998. Solvent effects in the kinetics of the enantioselective hydrogenation of ethyl pyruvate. *Catalysis Letters,* 55**,** 73-77.

GANI, R. 2004. Chemical product design: challenges and opportunities. *Computers & Chemical Engineering,* 28**,** 2441-2457.

GANI, R., JIMÉNEZ-GONZÁLEZ, C. & CONSTABLE, D. J. C. 2005. Method for selection of solvents for promotion of organic reactions. *Computers & Chemical Engineering,* 29**,** 1661-1676.

GAO, F., ALLIAN, A. D., ZHANG, H., CHENG, S. & GARLAND, M. 2006. Chemical and kinetic study of acetophenone hydrogenation over Pt/Al2O3: Application of BTEM and other multivariate techniques to quantitative on-line FTIR measurements. *Journal of Catalysis,* 241**,** 189-199.

HÁJEK, J., KUMAR, N., MÄKI-ARVELA, P., SALMI, T., MURZIN, D. Y., PASEKA, I., HEIKKILÄ, T., LAINE, E., LAUKKANEN, P. & VÄYRYNEN, J. 2003. Ruthenium-modified MCM-41 mesoporous molecular sieve and Y zeolite catalysts for selective hydrogenation of cinnamaldehyde. *Applied Catalysis A: General,* 251**,** 385-396.

HÁJEK, J., WÄRNÅ, J. & MURZIN, D. Y. 2004. Liquid-Phase Hydrogenation of Cinnamaldehyde over a Ru−Sn Sol−Gel Catalyst. 2. Kinetic Modeling. *Industrial & Engineering Chemistry Research,* 43**,** 2039-2048.

HOANG-VAN, C. & ZEGAOUI, O. 1997. Studies of high surface area Pt/MoO3 and Pt/WO3 catalysts for selective hydrogenation reactions. II. Reactions of acrolein and allyl alcohol. *Applied Catalysis A: General,* 164**,** 91-103.

HOFFER, B. W., SCHOENMAKERS, P. H. J., MOOIJMAN, P. R. M., HAMMINGA, G. M., BERGER, R. J., VAN LANGEVELD, A. D. & MOULIJN, J. A. 2004. Mass transfer and

kinetics of the three-phase hydrogenation of a dinitrile over a Raney-type nickel catalyst. *Chemical Engineering Science,* 59**,** 259-269.

HOUGEN, O. A. 1962. *Chemical Process Principles: Part 3. Kinetics and Catalysis.*

HOUSON, I. 2011. *Process Understanding: For Scale-Up and Manufacture of Active Ingredients*, Wiley.

HSU, S.-H., STAMATIS, S. D., CARUTHERS, J. M., DELGASS, W. N., VENKATASUBRAMANIAN, V., BLAU, G. E., LASINSKI, M. & ORCUN, S. 2009. Bayesian Framework for Building Kinetic Models of Catalytic Systems. *Industrial & Engineering Chemistry Research,* 48**,** 4768-4790.

HUIDOBRO, A., SEPÚLVEDA-ESCRIBANO, A. & RODRíGUEZ-REINOSO, F. 2002. Vapor-Phase Hydrogenation of Crotonaldehyde on Titania-Supported Pt and PtSn SMSI Catalysts. *Journal of Catalysis,* 212**,** 94-103.

IDE, M. S., HAO, B., NEUROCK, M. & DAVIS, R. J. 2012. Mechanistic Insights on the Hydrogenation of α,β-Unsaturated Ketones and Aldehydes to Unsaturated Alcohols over Metal Catalysts. *ACS Catalysis,* 2**,** 671-683.

JENNINGS, J. R. 1985. Catalysis of organic reactions edited by J. R. Kosak, Marcel Dekker, Inc., New York, 1984. pp. xiii+482, price SFr212, $90.00. ISBN 0-8247-7153-2. *British Polymer Journal,* 17**,** 322-322.

KAMLET, M. J., ABBOUD, J. L. M., ABRAHAM, M. H. & TAFT, R. W. 1983. Linear solvation energy relationships. 23. A comprehensive collection of the solvatochromic parameters, .pi.*, .alpha., and .beta., and some methods for simplifying the generalized solvatochromic equation. *The Journal of Organic Chemistry,* 48**,** 2877-2887.

KHODADI-MOGHADDAM, M. & SADEGHZADEH DARABI, F. 2011. Effect of solvents polarity parameters on heterogeneous catalytic hydrogenation of cyclohexene in molecular solvents. *Journal of Physical and Theoritical Chemistry of Islamic Azad University of Iran,* 8**,** 39-45.

KIJEŃSKI, J., WINIAREK, P., PARYJCZAK, T., LEWICKI, A. & MIKOŁAJSKA, A. 2002. Platinum deposited on monolayer supports in selective hydrogenation of furfural to furfuryl alcohol. *Applied Catalysis A: General,* 233**,** 171-182.

KING, C. J., HSUEH, L. & MAO, K.-W. 1965. Liquid Phase Diffusion of Non-electrolytes at High Dilution. *Journal of Chemical & Engineering Data,* 10**,** 348-350.

KISHIDA, S. & TERANISHI, S. 1968. Kinetics of liquid-phase hydrogenation of acetone over Raney nickel catalyst. *Journal of Catalysis,* 12**,** 90-96.

KIWI-MINSKER, L. & CRESPO-QUESADA, M. 2011. Integrated approach for the intensification of heterogeneous catalytic processes. *Chimia,* 65**,** 699-703.

KLUSON, P. & CERVENY, L. 1995. Selective hydrogenation over ruthenium catalysts. *Applied Catalysis A: General,* 128**,** 13-31.

KOLÁŘ, P., SHEN, J.-W., TSUBOI, A. & ISHIKAWA, T. 2002. Solvent selection for pharmaceuticals. *Fluid Phase Equilibria,* 194–197**,** 771-782.

KONTOGEORGIS, G. M. & GANI, R. 2004. *Computer Aided Property Estimation for Process and Product Design: Computers Aided Chemical Engineering*, Elsevier Science.

KOPPEL, I. A. & PALM, V. A. 1972. The Influence of the Solvent on Organic Reactivity. *In:* CHAPMAN, N. B. & SHORTER, J. (eds.) *Advances in Linear Free Energy Relationships.* Springer US.

KOPYSCINSKI, J., CHOI, J. & HILL, J. M. 2012. Comprehensive kinetic study for pyridine hydrodenitrogenation on (Ni)WP/SiO2 catalysts. *Applied Catalysis A: General,* 445–446**,** 50-60.

KOPYSCINSKI, J., HABIBI, R., MIMS, C. A. & HILL, J. M. 2013. K2CO3-Catalyzed CO2 Gasification of Ash-Free Coal: Kinetic Study. *Energy & Fuels,* 27**,** 4875-4883.

KUN, I., SZÖLLÖSI, G. & BARTÓK, M. 2001. Crotonaldehyde hydrogenation over clay-supported platinum catalysts. *Journal of Molecular Catalysis A: Chemical,* 169**,** 235-246.

LAFAYE, G., EKOU, T., MICHEAUD-ESPECEL, C., MONTASSIER, C. & MARECOT, P. 2004. Citral hydrogenation over alumina supported Rh-Ge catalysts: Effects of the reduction temperature. *Applied Catalysis A: General,* 257**,** 107-117.

LAIDLER, K. J. 1987. *Chemical Kinetics*, Harper & Row.

LEMCOFF, N. O. 1977. Liquid phase catalytic hydrogenation of acetone. *Journal of Catalysis,* 46**,** 356-364.

LEMOINE, R., FILLION, B., BEHKISH, A., SMITH, A. E. & MORSI, B. I. 2003. Prediction of the gas–liquid volumetric mass transfer coefficients in surface-aeration and gas-inducing reactors using neural networks. *Chemical Engineering and Processing: Process Intensification,* 42**,** 621-643.

LEMOINE, R. & MORSI, B. I. 2005. An algorithm for predicting the hydrodynamic and mass transfer parameters in agitated reactors. *Chemical Engineering Journal,* 114**,** 9-31.

LEVENSPIEL, O. 1999. *Chemical Reaction Engineering,* USA, John Wiley & Sons.

LEVENSPIEL, O. 2006. *CHEMICAL REACTION ENGINEERING, 3RD ED*, Wiley India Pvt. Limited.

LIBERKOVÁ, K. & TOUROUDE, R. 2002. Performance of Pt/SnO2 catalyst in the gas phase hydrogenation of crotonaldehyde. *Journal of Molecular Catalysis A: Chemical,* 180**,** 221-230.

LIBERKOVA, K., TOUROUDE, R. & MURZIN, D. Y. 2002. Analysis of deactivation and selectivity pattern in catalytic hydrogenation of a molecule with different functional groups: crotonaldehyde hydrogenation on Pt/SnO2. *Chemical Engineering Science,* 57**,** 2519-2529.

LIU, H., LU, G., GUO, Y., WANG, Y. & GUO, Y. 2009. Synthesis of mesoporous Pt/Al2O3 catalysts with high catalytic performance for hydrogenation of acetophenone. *Catalysis Communications,* 10**,** 1324-1329.

LIU, Q., CONG, C. & ZHANG, H. 2007. Investigation on infrared spectra of androsterone in single solvents. *Spectrochimica Acta Part A: Molecular and Biomolecular Spectroscopy,* 68**,** 1269-1273.

LIU, Q., XU, X. & SANG, W. 2003. Solvent effects on infrared spectra of 2-acetylthiophene in organic solvents. *Spectrochimica Acta Part A: Molecular and Biomolecular Spectroscopy,* 59**,** 471-475.

LO, H. S. & PAULAITIS, M. E. 1981. Estimation of solvent effects on chemical reaction rates using UNIFAC group contribution. *AIChE Journal,* 27**,** 842-844.

MAIER, W. F. 1989. Reaction Mechanisms in Heterogeneous Catalysis; C□H Activation as a Case Study. *Angewandte Chemie International Edition in English,* 28**,** 135-145.

MÄKI-ARVELA, P., HÁJEK, J., SALMI, T. & MURZIN, D. Y. 2005. Chemoselective hydrogenation of carbonyl compounds over heterogeneous catalysts. *Applied Catalysis A: General,* 292**,** 1-49.

MÄKI-ARVELA, P., TIAINEN, L.-P., NEYESTANAKI, A. K., SJÖHOLM, R., RANTAKYLÄ, T.-K., LAINE, E., SALMI, T. & MURZIN, D. Y. 2002. Liquid phase hydrogenation of citral: suppression of side reactions. *Applied Catalysis A: General,* 237**,** 181-200.

MAKITRA, R. G., PIRIG, Y. N., ZELIZNYJ, A. M., DEAGUAR, M. A. D., MIKOLAJEV, V. L. & ROMANOV, V. A. 1977. INFLUENCE OF SOLVENT PROPERTIES ON DISTRIBUTION COEFFICIENTS .1. DISTRIBUTION OF CROTONIC ACID BETWEEN WATER AND ORGANIC-SOLVENTS. *Organic Reactivity,* 14**,** 421-428.

MALATHI, R. & VISWANATH, R. P. 2001. Citral hydrogenation on supported platinum catalysts. *Applied Catalysis A: General,* 208**,** 323-327.

MALYALA, R. V., RODE, C. V., ARAI, M., HEGDE, S. G. & CHAUDHARI, R. V. 2000. Activity, selectivity and stability of Ni and bimetallic Ni–Pt supported on zeolite Y catalysts for hydrogenation of acetophenone and its substituted derivatives. *Applied Catalysis A: General,* 193**,** 71-86.

MANYAR, H. G., MORGAN, R., MORGAN, K., YANG, B., HU, P., SZLACHETKO, J., SA, J. & HARDACRE, C. 2013a. High energy resolution fluorescence detection XANES - an in situ method to study the interaction of adsorbed molecules with metal catalysts in the liquid phase. *Catalysis Science & Technology,* 3**,** 1497-1500.

MANYAR, H. G., YANG, B., DALY, H., MOOR, H., MCMONAGLE, S., TAO, Y., YADAV, G. D., GOGUET, A., HU, P. & HARDACRE, C. 2013b. Selective Hydrogenation of α,β-Unsaturated Aldehydes and Ketones using Novel Manganese Oxide and Platinum Supported on Manganese Oxide Octahedral Molecular Sieves as Catalysts. *ChemCatChem,* 5**,** 506-512.

MARCHI, A. J., PARIS, J. F., BERTERO, N. M. & APESTEGUÍA, C. R. 2007. Kinetic Modeling of the Liquid-Phase Hydrogenation of Cinnamaldehyde on Copper-Based Catalysts. *Industrial & Engineering Chemistry Research,* 46**,** 7657-7666.

MARQUARDT, D. W. 1963. An algorithm for least-squares estimation of nonlinear parameters. *SIAM Journal on Applied Mathematics,* 11**,** 431-441.

MARTIN, G., MÄKI-ARVELA, P., MURZIN, D. & SALMI, T. 2013. Solvent Effects in the Enantioselective Hydrogenation of Ethyl Benzoylformate. *Catalysis Letters,* 143**,** 1051-1060.

MASEL, R. I. 1996. *Principles of Adsorption and Reaction on Solid Surfaces*, Wiley.

MASSON, J., CIVIDINO, P. & COURT, J. 1997. Selective hydrogenation of acetophenone on chromium promoted Raney nickel catalysts. III. The influence of the nature of the solvent. *Applied Catalysis A: General,* 161**,** 191-197.

MATHEW, S. P., RAJASEKHARAM, M. V. & CHAUDHARI, R. V. 1999. Hydrogenation of p-isobutyl acetophenone using a Ru/Al2O3 catalyst: reaction kinetics and modelling of a semi-batch slurry reactor. *Catalysis Today,* 49**,** 49-56.

MCMANUS, I., DALY, H., THOMPSON, J. M., MANYAR, H., HARDACRE, C., WILKINSON, S. K., SEDAIE BONAB, N., TEN DAM, J., SIMMONS, M. J. H., STITT, E. H., AGOSTINO, C. D., MCGREGOR, J. & GLADDEN, L. F. 2014a. Solvent effects in the liquid-phase hydrogenation of 4-phenyl-2-butanone over Pt / TiO2 : Part I. *Journal of Catalysis*.

MCMANUS, I., DALY, H., THOMPSON, J. M., MANYAR, H., HARDACRE, C., WILKINSON, S. K., SEDAIE BONAB, N., TEN DAM, J., SIMMONS, M. J. H., STITT, E. H., AGOSTINO, C. D., MCGREGOR, J. & GLADDEN, L. F. 2014b. TBD. *Journal of Catalysis*.

MEILLE, V., PESTRE, N., FONGARLAND, P. & DE BELLEFON, C. 2004. Gas/Liquid Mass Transfer in Small Laboratory Batch Reactors: Comparison of Methods. *Industrial & Engineering Chemistry Research,* 43**,** 924-927.

MIKKOLA, J.-P., SALMI, T. & SJÖHOLM, R. 2001. Effects of solvent polarity on the hydrogenation of xylose. *Journal of Chemical Technology & Biotechnology,* 76**,** 90-100.

MITCHELL, J., BROCHE, L. M., CHANDRASEKERA, T. C., LURIE, D. J. & GLADDEN, L. F. 2013. Exploring Surface Interactions in Catalysts Using Low-Field Nuclear Magnetic Resonance. *The Journal of Physical Chemistry C,* 117**,** 17699-17706.

MIZAN, T. I. 1992. *Characterization of mass transfer of gases in olefinic polymerization solvents and slurries in agitated reactors.* MS. Dissertation, University of Pittsburgh.

MOHR, C. & CLAUS, P. 2001. Hydrogenation properties of supported nanosized gold particles. *Science Progress,* 84**,** 311-334.

MOUNZER, H. 2009. *Heterogeneous oxidation of alcohols.* Ph.D., University of Birmingham.

MOUNZER, H. N., WOOD, J. & STITT, E. H. 2010. Heterogeneous oxidation of 2-octanol on 5 wt%Pt–1 wt%Bi/Carbon catalyst. *Chemical Engineering Science,* 65**,** 179-185.

MUKHERJEE, S. & VANNICE, M. A. 2006a. Solvent effects in liquid-phase reactions II. Kinetic modeling for citral hydrogenation. *Journal of Catalysis,* 243**,** 131-148.

MUKHERJEE, S. & VANNICE, M. A. 2006b. Solvent effects in liquid-phase reactions: I. Activity and selectivity during citral hydrogenation on Pt/SiO2 and evaluation of mass transfer effects. *Journal of Catalysis,* 243**,** 108-130.

NEHLSEN, J., MUKHERJEE, M. & PORCELLI, R. V. 2007. Apply an integrated approach to catalytic process design. *Chemical Engineering Progress,* 103**,** 31-38.

NERI, G., BONACCORSI, L. & GALVAGNO, S. 1997. Kinetic Analysis of Cinnamaldehyde Hydrogenation over Alumina-Supported Ruthenium Catalysts. *Industrial & Engineering Chemistry Research,* 36**,** 3554-3562.

NIENOW, A. W. 1997. On impeller circulation and mixing effectiveness in the turbulent flow regime. *Chemical Engineering Science,* 52**,** 2557-2565.

NORMAN R. DRAPER, H. S. 1998. *Applied Regression Analysis, 3rd Edition,* New York, Wiley.

OLDSHUE, J. Y. 1983. *Fluid mixing technology*, Chemical Engineering.

PATIL, N. G., ROY, D., CHAUDHARI, A. S. & CHAUDHARI, R. V. 2006. Kinetics of Reductive Alkylation of p-Phenylenediamine with Methyl Ethyl Ketone Using 3% Pt/Al2O3 Catalyst in a Slurry Reactor. *Industrial & Engineering Chemistry Research,* 46**,** 3243-3254.

PATTERSON, G. 2005. Modeling and Scale-Up of Mixing- and Temperature-Sensitive Chemical Reactions. *Industrial & Engineering Chemistry Research,* 44**,** 5325-5341.

PATWARDHAN, A. W. & JOSHI, J. B. 1998. Design of stirred vessels with gas entrained from free liquid surface. *The Canadian Journal of Chemical Engineering,* 76**,** 339-364.

PAUL, E. L., ATIEMO-OBENG, V. & KRESTA, S. M. 2004. *Handbook of Industrial Mixing: Science and Practice*, Wiley.

PRITCHARD, D. J. & BACON, D. W. 1975. Statistical assessment of chemical kinetic models. *Chemical Engineering Science,* 30**,** 567-574.

QUINEY, A. S. & SCHUURMAN, Y. 2007. Kinetic modelling of CO conversion over a Cu/ceria catalyst. *Chemical Engineering Science,* 62**,** 5026-5032.

RAJASHEKHARAM, M. V., BERGAULT, I., FOUILLOUX, P., SCHWEICH, D., DELMAS, H. & CHAUDHARI, R. V. 1999. Hydrogenation of acetophenone using a 10% Ni supported on zeolite Y catalyst: kinetics and reaction mechanism. *Catalysis Today,* 48**,** 83-92.

RAUTANEN, P. A., AITTAMAA, J. R. & KRAUSE, A. O. I. 2000. Solvent Effect in Liquid-Phase Hydrogenation of Toluene. *Industrial & Engineering Chemistry Research,* 39**,** 4032-4039.

REBROV, E. V., KLINGER, E. A., BERENGUER-MURCIA, A., SULMAN, E. M. & SCHOUTEN, J. C. 2009. Selective Hydrogenation of 2-Methyl-3-butyne-2-ol in a Wall-Coated Capillary Microreactor with a Pd25Zn75/TiO2 Catalyst. *Organic Process Research & Development,* 13**,** 991-998.

RECCHIA, S., DOSSI, C., POLI, N., FUSI, A., SORDELLI, L. & PSARO, R. 1999. Outstanding Performances of Magnesia-Supported Platinum–Tin Catalysts for Citral Selective Hydrogenation. *Journal of Catalysis,* 184**,** 1-4.

REDDY, B., RAO, K. & REDDY, G. 2009. Controlled Hydrogenation of Acetophenone Over Pt/CeO2–MO x (M = Si, Ti, Al, and Zr) Catalysts. *Catalysis Letters,* 131**,** 328-336.

REN, B., ZHAO, M., DONG, L. & LI, G. 2014. Catalytic hydrogenation of 2,4-dinitroethylbenzene to 2,4-diaminoethylbenzene over Ni/HY catalysts: The solvent effect. *Catalysis Communications,* 50**,** 92-96.

RODE, C. V., VAIDYA, M. J., JAGANATHAN, R. & CHAUDHARI, R. V. 2001. Hydrogenation of nitrobenzene to p-aminophenol in a four-phase reactor: reaction kinetics and mass transfer effects. *Chemical Engineering Science,* 56**,** 1299-1304.

ROJAS, H., FIERRO, J. L. G. & REYES, P. 2007. THE SOLVENT EFFECT IN THE HYDROGENATION OF CITRAL OVER Ir AND Ir-Fe/TiO2 CATALYSTS. *Journal of the Chilean Chemical Society,* 52**,** 1155-1159.

RUSZKOWSKI, S. Year. A rational method for measuring blending performance, and comparison of different impeller types. *In*, 1994. HEMSPHERE PUBLISHING CORPORATION, 283-283.

RYLANDER, P. N., GREENFIELD, H., AUGUSTINE, R. L. & DEKKER, M. 1988. *Catalysis of organic reactions,* New York, Organic Reactions Catalysis Society.

RYNDIN, Y. A., SANTINI, C. C., PRAT, D. & BASSET, J. M. 2000. Chemo-, Regio-, and Diastereoselective Hydrogenation of Oxopromegestone into Trimegestone over Supported Platinoids: Effects of the Transition Metal, Support Nature, Tin Additives, and Modifiers. *Journal of Catalysis,* 190**,** 364-373.

SÁ, J. & SZLACHETKO, J. 2014. Heterogeneous Catalysis Experiments at XFELs. Are we Close to Producing a Catalysis Movie? *Catalysis Letters,* 144**,** 197-203.

SALMI, T., MÄKI-ARVELA, P., WÄRNÅ, J., ERÄNEN, K., DENECHEAU, A., ALHO, K. & MURZIN, D. Y. 2007. Modelling of Consecutive Reactions with a Semibatch Liquid Phase: Enhanced Kinetic Information by a New Experimental Concept. *Industrial & Engineering Chemistry Research,* 46**,** 3912-3921.

SANO, Y., YAMAGUCHI, N. & ADACHI, T. 1974. MASS TRANSFER COEFFICIENTS FOR SUSPENDED PARTICLES IN AGITATED VESSELS AND BUBBLE COLUMNS. *Journal of Chemical Engineering of Japan,* 7**,** 255-261.

SANTORI, G. F., MOGLIONI, A. G., VETERE, V., IGLESIAS, G. Y. M., CASELLA, M. L. & FERRETTI, O. A. 2004. Hydrogenation of aromatic ketones with Pt- and Sn-modified Pt catalysts. *Applied Catalysis A: General,* 269**,** 215-223.

SCHOTTE, W. 1992. Prediction of the molar volume at the normal boiling point. *The Chemical Engineering Journal,* 48**,** 167-172.

SCHWAAB, M., LEMOS, L. P. & PINTO, J. C. 2008. Optimum reference temperature for reparameterization of the Arrhenius equation. Part 2: Problems involving multiple reparameterizations. *Chemical Engineering Science,* 63**,** 2895-2906.

SCHWARZ, J. A., CONTESCU, C. & CONTESCU, A. 1995. Methods for Preparation of Catalytic Materials. *Chemical Reviews,* 95**,** 477-510.

SERNA, P., CONCEPCIÓN, P. & CORMA, A. 2009. Design of highly active and chemoselective bimetallic gold–platinum hydrogenation catalysts through kinetic and isotopic studies. *Journal of Catalysis,* 265**,** 19-25.

SHI, J., NIE, R., CHEN, P. & HOU, Z. 2013. Selective hydrogenation of cinnamaldehyde over reduced graphene oxide supported Pt catalyst. *Catalysis Communications,* 41**,** 101-105.

SHIRAI, M., TANAKA, T. & ARAI, M. 2001. Selective hydrogenation of α-, β-unsaturated aldehyde to unsaturated alcohol with supported platinum catalysts at high pressures of hydrogen. *Journal of Molecular Catalysis A: Chemical,* 168**,** 99-103.

SILVESTRE-ALBERO, J., RODRíGUEZ-REINOSO, F. & SEPÚLVEDA-ESCRIBANO, A. 2002. Improved Metal-Support Interaction in Pt/CeO2/SiO2 Catalysts after Zinc Addition. *Journal of Catalysis,* 210**,** 127-136.

SILVESTRE-ALBERO, J., SEPULVEDA-ESCRIBANO, A., RODRIGUEZ-REINOSO, F. & ANDERSON, J. A. 2003. Infrared study of CO and 2-butenal co-adsorption on Zn modified Pt/CeO2-SiO2 catalysts. *Physical Chemistry Chemical Physics,* 5**,** 208-216.

SINGH, U. K. & ALBERT VANNICE, M. 2000a. The influence of metal-support interactions during liquid-phase hydrogenation of an α, β-unsaturated aldehyde over Pt. *In:* AVELINO CORMA, F. V. M. S. M. & JOSÉ LUIS, G. F. (eds.) *Studies in Surface Science and Catalysis.* Elsevier.

SINGH, U. K. & ALBERT VANNICE, M. 2000b. Liquid-Phase Hydrogenation of Citral over Pt/SiO2 Catalysts: I. Temperature Effects on Activity and Selectivity. *Journal of Catalysis,* 191**,** 165-180.

SINGH, U. K., SYSAK, M. N. & VANNICE, M. A. 2000. Liquid-Phase Hydrogenation of Citral over Pt/SiO2 Catalysts: II. Hydrogenation of Reaction Intermediate Compounds. *Journal of Catalysis,* 191**,** 181-191.

SINGH, U. K. & VANNICE, M. A. 1999. Kinetic and thermodynamic analysis of liquid-phase benzene hydrogenation. *AIChE Journal,* 45**,** 1059-1071.

SINGH, U. K. & VANNICE, M. A. 2000. Influence of metal–support interactions on the kinetics of liquid-phase citral hydrogenation. *Journal of Molecular Catalysis A: Chemical,* 163**,** 233-250.

SINGH, U. K. & VANNICE, M. A. 2001a. Kinetics of liquid-phase hydrogenation reactions over supported metal catalysts — a review. *Applied Catalysis A: General,* 213**,** 1-24.

SINGH, U. K. & VANNICE, M. A. 2001b. Liquid-Phase Citral Hydrogenation over SiO2-Supported Group VIII Metals. *Journal of Catalysis,* 199**,** 73-84.

SITTHISA, S., SOOKNOI, T., MA, Y., BALBUENA, P. B. & RESASCO, D. E. 2011. Kinetics and mechanism of hydrogenation of furfural on Cu/SiO2 catalysts. *Journal of Catalysis,* 277**,** 1-13.

SMEDS, S., MURZIN, D. & SALMI, T. 1995. Kinetics of ethylbenzene hydrogenation on Ni/Al2O3. *Applied Catalysis A: General,* 125**,** 271-291.

SMITH, M. B. 2010. Chapter 4 - Reduction. *In:* SMITH, M. B. (ed.) *Organic Synthesis (Third Edition).* Oxford: Academic Press.

SONG, H., ZHANG, H., YANG, H. & LIU, Q. 2009. FTIR spectral studies of methyltestorone in single and binary solvent systems. *Spectrochimica Acta Part A: Molecular and Biomolecular Spectroscopy,* 72**,** 709-714.

STITT, E. H. 2002. Alternative multiphase reactors for fine chemicals: A world beyond stirred tanks? *Chemical Engineering Journal,* 90**,** 47-60.

STITT, E. H. & SIMMONS, M. J. H. 2011. Scale-Up of Chemical Reactions. *Process Understanding.* Wiley-VCH Verlag GmbH & Co. KGaA.

TAKAGI, H., ISODA, T., KUSAKABE, K. & MOROOKA, S. 1999. Effects of Solvents on the Hydrogenation of Mono-Aromatic Compounds Using Noble-Metal Catalysts. *Energy & Fuels,* 13**,** 1191-1196.

TATTERSON, G. B. 1991. *Fluid mixing and gas dispersion in agitated tanks*, McGraw-Hill.

THAKAR, N., BERGER, R. J., KAPTEIJN, F. & MOULIJN, J. A. 2007a. Modelling kinetics and deactivation for the selective hydrogenation of an aromatic ketone over Pd/SiO2. *Chemical Engineering Science,* 62**,** 5322-5329.

THAKAR, N., SCHILDHAUER, T. J., BUIJS, W., KAPTEIJN, F. & MOULIJN, J. A. 2007b. Evaluation of deactivation mechanisms of Pd-catalyzed hydrogenation of 4-isobutylacetophenone. *Journal of Catalysis,* 248**,** 249-257.

TOEBES, M. L., ALEXANDER NIJHUIS, T., HÁJEK, J., BITTER, J. H., JOS VAN DILLEN, A., MURZIN, D. Y. & DE JONG, K. P. 2005. Support effects in hydrogenation of cinnamaldehyde over carbon nanofiber-supported platinum catalysts: Kinetic modeling. *Chemical Engineering Science,* 60**,** 5682-5695.

TOPPINEN, S., SALMI, T., RANTAKYLÄ, T. K. & AITTAMAA, J. 1997. Liquid-Phase Hydrogenation Kinetics of Aromatic Hydrocarbon Mixtures. *Industrial & Engineering Chemistry Research,* 36**,** 2101-2109.

TORRES, G. C., LEDESMA, S. D., JABLONSKI, E. L., DE MIGUEL, S. R. & SCELZA, O. A. 1999. Hydrogenation of carvone on Pt–Sn/Al2O3 catalysts. *Catalysis Today,* 48**,** 65-72.

TOUKONIITTY, E., MÄKI-ARVELA, P., KUUSISTO, J., NIEMINEN, V., PÄIVÄRINTA, J., HOTOKKA, M., SALMI, T. & MURZIN, D. Y. 2003a. Solvent effects in enantioselective hydrogenation of 1-phenyl-1,2-propanedione. *Journal of Molecular Catalysis A: Chemical,* 192**,** 135-151.

TOUKONIITTY, E., ŠEVČíKOVÁ, B., MÄKI-ARVELA, P., WÄRNÅ, J., SALMI, T. & MURZIN, D. Y. 2003b. Kinetics and modeling of 1-phenyl-1,2-propanedione hydrogenation. *Journal of Catalysis,* 213**,** 7-16.

TUNDO, P., ZINOVYEV, S. & PEROSA, A. 2000. Multiphase Catalytic Hydrogenation of p-Chloroacetophenone and Acetophenone. A Kinetic Study of the Reaction Selectivity toward the Reduction of Different Functional Groups. *Journal of Catalysis,* 196**,** 330-338.

USMAN, M., CRESSWELL, D. & GARFORTH, A. 2011. Detailed Reaction Kinetics for the Dehydrogenation of Methylcyclohexane over Pt Catalyst. *Industrial & Engineering Chemistry Research,* 51**,** 158-170.

VAIDYA, P. D. & MAHAJANI, V. V. 2003. Kinetics of Liquid-Phase Hydrogenation of Furfuraldehyde to Furfuryl Alcohol over a Pt/C Catalyst. *Industrial & Engineering Chemistry Research,* 42**,** 3881-3885.

VANNICE, M. A. 2005a. *Kinetics of Catalytic Reactions,* New York, Kluwer-Springer.

VANNICE, M. A. 2005b. Modeling Reactions on Uniform (Ideal) Surfaces. *Kinetics of Catalytic Reactions.* Springer US.

VANNICE, M. A. & POONDI, D. 1997. The Effect of Metal-Support Interactions on the Hydrogenation of Benzaldehyde and Benzyl Alcohol. *Journal of Catalysis,* 169**,** 166-175.

VERGUNST, T., KAPTEIJN, F. & MOULIJN, J. A. 2001. Kinetics of cinnamaldehyde hydrogenation–concentration dependent selectivity. *Catalysis Today,* 66**,** 381-387.

VIRTANEN, P., SALMI, T. & MIKKOLA, J.-P. 2009. Kinetics of Cinnamaldehyde Hydrogenation by Supported Ionic Liquid Catalysts (SILCA). *Industrial & Engineering Chemistry Research,* 48**,** 10335-10342.

VON ARX, M., MALLAT, T. & BAIKER, A. 1999. Unprecedented selectivity behaviour in the hydrogenation of an α,β-unsaturated ketone: hydrogenation of ketoisophorone over alumina-supported Pt and Pd. *Journal of Molecular Catalysis A: Chemical,* 148**,** 275-283.

W. E. STEWART, M. C. 2008. *Computer-Aided Modeling of Reactive Systems,* New Jersey, Wiley & Sons.

W.E. STEWART, M. C. *Athena Visual Studio* [Online]. Available: www.athenavisual.com [Accessed 01.01.10 2010].

WAN, H., VITTER, A., CHAUDHARI, R. V. & SUBRAMANIAM, B. 2014. Kinetic investigations of unusual solvent effects during Ru/C catalyzed hydrogenation of model oxygenates. *Journal of Catalysis,* 309**,** 174-184.

WEBER, D., MITCHELL, J., MCGREGOR, J. & GLADDEN, L. F. 2009. Comparing Strengths of Surface Interactions for Reactants and Solvents in Porous Catalysts Using Two-Dimensional NMR Relaxation Correlations. *The Journal of Physical Chemistry C,* 113**,** 6610-6615.

WICAKSONO, D. S., MHAMDI, A. & MARQUARDT, W. 2014. Computer-aided screening of solvents for optimal reaction rates. *Chemical Engineering Science,* 115**,** 167-176.

WILKE, C. R. & CHANG, P. 1955. Correlation of diffusion coefficients in dilute solutions. *AIChE Journal,* 1**,** 264-270.

WILKINSON, S. K., I., M., DALY, H., THOMPSON, J. M., MANYAR, H., HARDACRE, C., SEDAIE BONAB, N., TEN DAM, J., SIMMONS, M. J. H., STITT, E. H., AGOSTINO, C. D., MCGREGOR, J. & GLADDEN, L. F. 2014. *Solvent effects in liquid-phase*

hydrogenation of 4-phenyl-2-butanone over Pt/TiO₂; Part 2: A kinetic analysis methodology to elucidate the roles of metal, support and solvent. Eng.D, University of Birmingham.

WILKINSON, S. K., SIMMONS, M. J. H., STITT, E. H., BAUCHEREL, X. & WATSON, M. J. 2013. A novel approach to understanding and modelling performance evolution of catalysts during their initial operation under reaction conditions – Case study of vanadium phosphorus oxides for n-butane selective oxidation. *Journal of Catalysis,* 299**,** 249-260.

WOOD, J., BODENES, L., BENNETT, J., DEPLANCHE, K. & MACASKIE, L. E. 2009. Hydrogenation of 2-Butyne-1,4-diol Using Novel Bio-Palladium Catalysts. *Industrial & Engineering Chemistry Research,* 49**,** 980-988.

YADAV, G. D. & MEWADA, R. K. 2012. Selective hydrogenation of acetophenone to 1-phenyl ethanol over nanofibrous Ag-OMS-2 catalysts. *Catalysis Today,* 198**,** 330-337.

YAWS, C. 1999. *Chemical Properties Handbook: Physical, Thermodynamics, Environmental Transport, Safety & Health Related Properties for Organic &*, McGraw-Hill Education.

ZHANG, L., WINTERBOTTOM, J. M., BOYES, A. P. & RAYMAHASAY, S. 1998. Studies on the hydrogenation of cinnamaldehyde over Pd/C catalysts. *Journal of Chemical Technology & Biotechnology,* 72**,** 264-272.

ZWIETERING, T. N. 1958. Suspending of solid particles in liquid by agitators. *Chemical Engineering Science,* 8**,** 244-253.

Appendices

Appendix A:
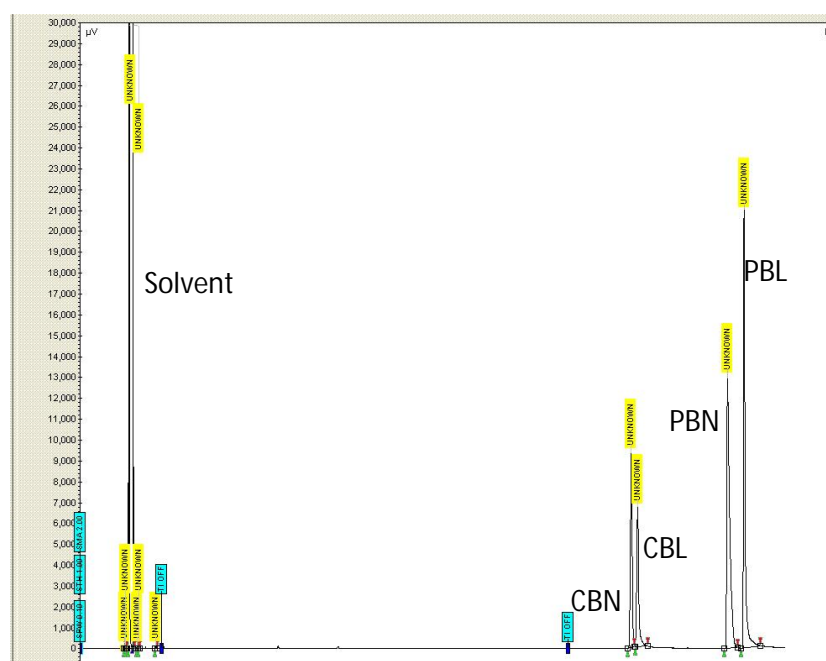
Figure A.1: An example of the Chromatogram for GC analysis of experimental data in 3000 mL scale.

Table A.1: Experimental conditions of reactions in 100 mL reactor for 4% Pt/TiO$_2$ catalyst

Run	Initial Conc. (mol)	Catalyst mass (g)	Pressure (bar)	Energy input (W kg^{-1})	Temperature (K)	Solvent
Varying catalyst mass m$_{cat}$ (g)						
1	0.270	0.02	5	10	343	Hexane
2	0.270	0.04	5	10	343	Hexane
3	0.270	0.06	5	10	343	Hexane
4	0.270	0.08	5	10	343	Hexane
5	0.270	0.10	5	10	343	Hexane
6	0.270	0.14	5	10	343	Hexane
Varying pressure P$_T$ (bar)						
7	0.270	0.10	2	10	343	Hexane
5	0.270	0.10	5	10	343	Hexane
8	0.270	0.10	8	10	343	Hexane
9	0.270	0.10	10	10	343	Hexane
10	0.270	0.10	12	10	343	Hexane
Varying energy input $\bar{\varepsilon}_T$ (W kg^{-1})						
11	0.270	0.10	5	0.1	343	Hexane
5	0.270	0.10	5	0.5	343	Hexane
12	0.270	0.10	5	2.0	343	Hexane
13	0.270	0.10	5	5.0	343	Hexane
14	0.270	0.10	5	10	343	Hexane
Varying Temperature T$_r$ (°C)						
15	0.270	0.10	5	10	303	Hexane
16	0.270	0.10	5	10	313	Hexane
17	0.270	0.10	5	10	323	Hexane
18	0.270	0.10	5	10	333	Hexane
5	0.270	0.10	5	10	343	Hexane
19	0.270	0.10	5	10	353	Hexane
Varying initial PBN concentration C$_i$ (mol l^{-1})						
20	0.135	0.10	5	10	343	Hexane
21	0.202	0.10	5	10	343	Hexane
5	0.270	0.10	5	10	343	Hexane
22	0.337	0.10	5	10	343	Hexane
23	0.405	0.10	5	10	343	Hexane

Table A.1: Continued.

Run	Initial Conc. (mol)	Catalyst mass (g)	Pressure (bar)	Energy input (W kg^{-1})	Temperature (°C)	Solvent
			Varying Solvents			
5	0.270	0.10	5	3.5	343	Decane
24	0.270	0.10	5	3.5	343	Hexane
25	0.270	0.10	5	3.5	343	Dichloroethane
26	0.270	0.10	5	3.5	343	Cyclohexane
27	0.270	0.10	5	3.5	343	t-butyl toluene
28	0.270	0.10	5	3.5	343	Toluene
29	0.270	0.10	5	3.5	343	p-xylene
30	0.270	0.10	5	3.5	343	Trifluoroethanol
31	0.270	0.10	5	3.5	343	Ethanol
32	0.270	0.10	5	3.5	343	1-propanol
33	0.270	0.10	5	3.5	343	1-butanol
34	0.270	0.10	5	3.5	343	1-pentanol
35	0.270	0.10	5	3.5	343	1-octanol
36	0.270	0.10	5	3.5	343	2-propanol
37	0.270	0.10	5	3.5	343	2-butanol
38	0.270	0.10	5	3.5	343	2-pentanol
39	0.270	0.10	5	3.5	343	2-octanol

Table A.2: Experimental conditions of reactions in 100 mL reactor for 5% Pt/SiO$_2$ catalyst

| Run	Initial Conc. (mol)	Catalyst mass (g)	Pressure (bar)	Energy input (W kg^{-1})	Temperature (°C)	Solvent
				Varying Solvents		
1	0.270	0.10	5	10	70	Hexane
2	0.270	0.10	5	10	70	Cyclohexane
3	0.270	0.10	5	10	70	Octane
4	0.270	0.10	5	10	70	Decane
5	0.270	0.10	5	10	70	Methanol
6	0.270	0.10	5	10	70	Ethanol
7	0.270	0.10	5	10	70	1-propanol
8	0.270	0.10	5	10	70	2-propanol
9	0.270	0.10	5	10	70	1-butanol
10	0.270	0.10	5	10	70	2-butanol
11	0.270	0.10	5	10	70	1-pentanol
12	0.270	0.10	5	10	70	2-pentanol
13	0.270	0.10	5	10	70	Hexanol
14	0.270	0.10	5	10	70	Toluene
15	0.270	0.10	5	10	70	t-butyl toluene
16	0.270	0.10	5	10	70	p-xylene
17	0.270	0.10	5	10	70	m-xylene
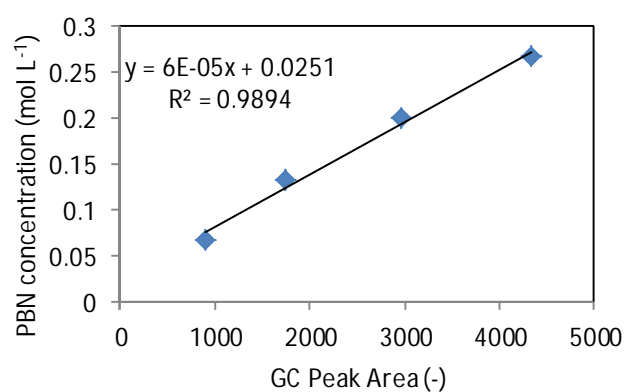
Figure A.2: PBN calibration curve for Column#1.
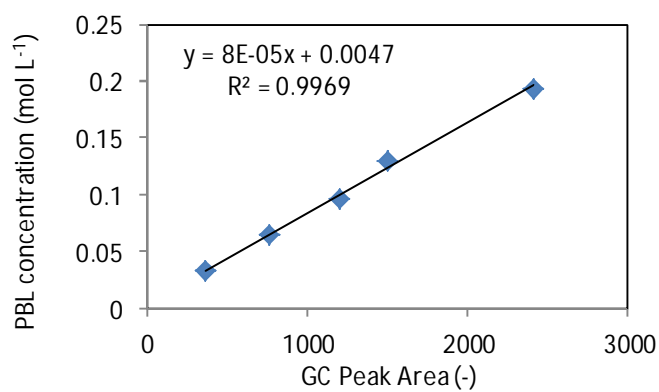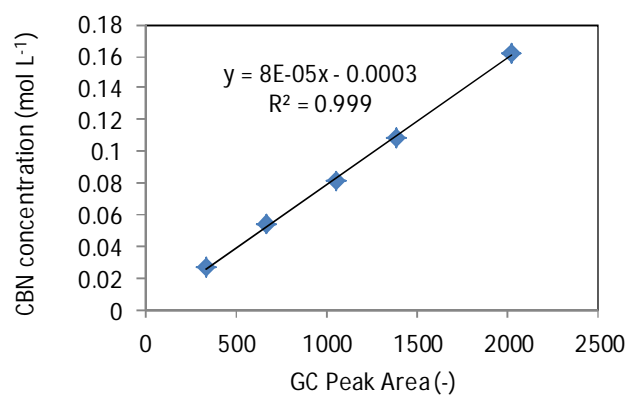

Figure A.3: PBL calibration curve for Column#1.
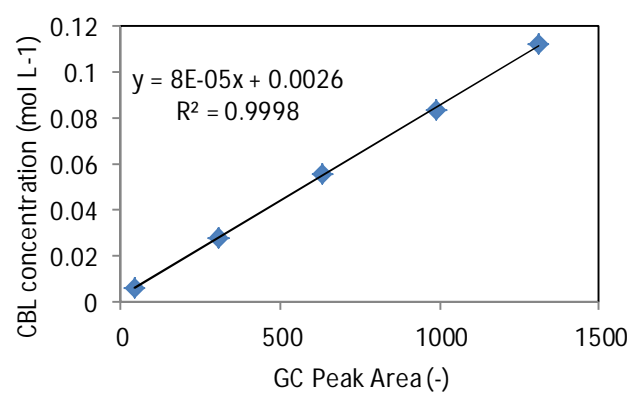

Figure A.4: CBN calibration curve for Column#1.

$$y = 8E\text{-}05x + 0.0026$$
$$R^2 = 0.9998$$

Figure A.5: CBL calibration curve for Column#1

Appendix B:

Mass transfer analysis for Chapter 4

The mass transfer calculations for experiments with varying temperature and concentrtion at both scales involved the following procedure (example results for 3000 mL scale reported):

1. The reactor operational conditions and catalyst properties are listed as shown in Table B.1.

2. The solvent density, viscousity and surface tension were gathered for all corresponding temperatures from online academic database (www.knovel.com).

3. Hydrogen concentration in hexane was calculated from Henry's law,

$$P = K_H C^*$$
(B.1)

Where P ia the partial pressure of the solvent, K_H is Henry's constant and C^* is the equilibrium concentration of H_2 in bulk liquid. The values of K_H for hexane were taken from (Chang et al., 1991).

4. The following dimensionless numbers were calculated for gas-liquid mass transfer coefficients,

$$Re = \frac{d_i^2 \rho_L N}{\mu_L}$$
(B.2)

$$fr = \frac{d_i N^2}{g}$$
(B.3)

$$Sh = \frac{K_L a d_i}{D}$$
(B.4)

$$We = \frac{d_i^3 \rho_L N^2}{\sigma_L}$$
(B.5)

The values of H_2 diffusivity in hexane were determined using Wilke-Chang correlation,

$$D = \frac{1.173 \times 10^{-16} (\emptyset M)^{1/2} T}{\mu_L V_m^{0.6}}$$ (B.6)

5. Subsequently, the gas-liquid mass transfer coefficients were calculated by the following correlations as discussed in §2.5.2,

$$Sh = 3 \times 10^{-4} Re^{1.45} Sc^{0.5} We^{0.5} \quad \text{(100 mL scale GIR reactor)}$$

$$Sh = 51.7 \times 10^9 Re^{-1.12} Fr^{2.20} (1 - W_s)^{4.31} \quad \text{(3000 mL scale SAR reactor)}$$

6. The Values of $K_L a$ derived from correlations above is used to calculate gas-liquid Carberry numbers,

$$\boldsymbol{Ca_{G-L}} = \frac{r_v^{obs}}{K_L a C^*}$$ (B.7)

The external gas-liquid effectiveness factor was then calculated as,

$$\eta_{G-L} = 1 - Ca_{G-L}$$ (B.8)

7. Solid-liquid mass transfer coefficients (K_{LS}) were determined using the following correlation,

$$Sh = 2 + 0.4 \, Re_P^{3/4} Sc^{1/3}$$ (B.9)

The following dimensionless numbers were determined for the above correlation,

$$Re_P = \left(\frac{N_P d_i^5 N_I^3 d_P^4 \rho_L^3}{\mu_L^3 V_L} \right)^{1/3}$$ (B.10)

$$Sc = \frac{\mu_L}{\rho_L D}$$ (B.11)

8. Assuming that gas-liquid interface at the bubble surface is saturated with H_2 (C^*), the concentration in liquid phase (C_b) following the mass transfer limitation would be equal to,

$$C_b = C^* - \frac{R_A}{K_L a} \qquad (B.12)$$

9. The values of K_{LS} from Equation B.9 were then used to calculate solid-liquid Carberry numbers and effectivess factors,

$$a_P = \frac{6}{d_P \rho_P} \qquad (B.13)$$

$$Ca_{L-S} = \frac{r_v^{obs}}{K_{LS} a_P C_b} \qquad (B.14)$$

$$\eta_{L-S} = 1 - Ca_{L-S} \qquad (B.15)$$

10. The internal diffusion limitations were determined using Wanger-Weisz-Wheeler modulus (Mw),

$$M_w = L^2 \frac{(-r_v^{obs}/C_b)}{D_{eff}} \qquad (B.16)$$

The effective diffusivities (D_{eff}) were determined by,

$$D_{eff} = D \frac{\varepsilon_P}{\tau_P} \qquad (B.17)$$

And characteristic length for spherical catalyst (*L*) was determined by,

Spheres: $L = \frac{d_m}{3}$ \qquad (B.18)

11. The internal mass transfer limitation for PBN was also determined using the same criteria as above by using the following correlation to calculate diffusivity of PBN in hexane,

$$D_{ij}^0 = 4.4 \times 10^{-15} \frac{T}{\eta_2} \left(\frac{v_2}{v_1}\right)^{1/6} \left(\frac{L_2^{vap}}{L_1^{vap}}\right)^{1/2} \qquad (B.19)$$

Please refer to §4.4.2 for refernces on correlations above.

The resulting calculations are listed in Table B.2 for 3000 mL scale experiments as an example for the procedure.

Table B.1: Parameters used in mass transfer calculations for PBN hydrogenation using 4% Pt/TiO$_2$ in hexane in 3000 mL reactor.

Parameters	Unit	Value
Impeller diameter, d_i	m	0.075
Tank diameter, T	m	0.15
Power number, N_p	-	5
Particle density, ρ_P		
Particle mean diameter (mean), d_m	m	12.17E-06
Particle sauter mean diameter, d_{32}	m	3.55E-06
Impeller speed, N	s^{-1}	9.167
Solvent association factor (Wikle-Chang) – Hexane	-	1
Hexane molecular weight	g mol^{-1}	86.18
Molar volume of PBN at its boiling point	m3 kmol^{-1}	
Catalyst particle density, ρ_P	kg m^{-3}	3565.2
Catalyst porosity, ε_P	%	80.05
Catalyst tortuosity, τ_P		2.935
Characteristic length, L, for spheres	m	4.056E-06
BET surface area	m^2 g^{-1}	46.06
Measured Characteristic length, L	nm	6.720E-05
Total Pore Area	m^2 g^{-1}	96.682
Tortuosity factor		1.166
Liquid height in reactor H=T	m	0.15
Volume of hexane in reacor	m^3	2.550E-03
External solid-liquid interfacial area, a_p	m^2 kg^{-1}	138.319
Hexane molar volume at T$_b$	m^3 kmol^{-1}	0.14
Hexane enthalpy of vaporisation	J kmol^{-1}	2.91E+07
PBN molar volume at T$_b$	m^3 kmol^{-1}	0.1843
PBN enthalpy of vaporisation	J kmol^{-1}	4.70E+07
Height of liquid above impeller	m	0.093
Catalyst wt% in reactor, W_s	%	0.003

Table B.2: Mass transfer results scale for PBN hydrogenation in 3000 mL scale reactor with hexane as solvent and 4% Pt/TiO$_2$ catalyst.

Run	T_r K	C_i mol m^{-3}	r_v^{obs} mol m^{-3} s^{-1}	ρ_L kg m^{-3}	μ_L pa s
1	313	241.130	0.0036	642.5	0.000250
2	323	271.832	0.01176	633.0	0.000229
3	333	269.636	0.02001	623.3	0.000211
4	343	191.435	0.03001	613.4	0.000194
5	343	279.716	0.02581	613.4	0.000194
6	343	482.175	0.01473	613.4	0.000194
7	353	277.010	0.03454	603.1	0.000179

σ_L kg s^{-2}	D m^2 s^{-1}	D_{eff}	We	Re	Fr
0.0163	1.15E-08	3.14E-09	1397.308	132515.625	0.642
0.0153	1.3E-08	3.53E-09	1466.625	142528.657	0.642
0.0142	1.45E-08	3.95E-09	1556.021	152317.091	0.642
0.0132	1.62E-08	4.43E-09	1647.314	163033.183	0.642
0.0132	1.62E-08	4.43E-09	1647.314	163033.183	0.642
0.0132	1.62E-08	4.43E-09	1647.314	163033.183	0.642
0.0122	1.81E-08	4.94E-09	1752.412	173728.177	0.642

Eu	C^* mol m^{-3}	Sh_{G-L}	$K_L a$ s^{-1}	Ca_{G-L}	η_{G-L}
0.016	16.465	35331.408	0.072	0.002	0.998
0.017	16.712	32557.479	0.075	0.005	0.995
0.017	16.972	30217.596	0.078	0.009	0.991
0.017	17.246	27984.308	0.081	0.012	0.988
0.017	17.246	27996.398	0.081	0.010	0.990
0.017	17.246	28007.762	0.081	0.006	0.994
0.018	17.540	26067.725	0.084	0.013	0.987

Re_P	Sc	Sh_{S-L}	K_{LS} m^3 m^{-2} s^{-1}	$K_{LS}a_p$ s^{-1}	C_b mol m^{-3}
1.255	33.828	3.369	0.003	0.813	27.162
1.561	27.918	3.356	0.004	0.912	26.448
1.905	23.348	3.343	0.004	1.017	26.168
2.409	19.471	3.341	0.004	1.173	26.043
2.336	19.471	3.330	0.004	1.135	26.791
2.268	19.471	3.321	0.004	1.098	28.767
2.827	16.382	3.317	0.005	1.261	27.167

Table B.2: Continued.

Mw	D_{12} (PBN) $m^2\ s^{-1}$	D_{12} eff (PBN) $m^2\ s^{-1}$	Sc (PBN)	Sh (PBN)	K_{LS} (PBN) $m^3 m^{-2} s^{-1}$
0.000191	4.14E-09	1.13E-09	93.975	3.925	0.0013
0.000568	4.66E-09	1.27E-09	77.556	3.907	0.0015
0.000873	5.22E-09	1.42E-09	64.859	3.888	0.0017
0.001175	5.85E-09	1.59E-09	54.090	3.885	0.0019
0.000982	5.85E-09	1.59E-09	54.090	3.870	0.0019
0.000522	5.85E-09	1.59E-09	54.090	3.856	0.0019
0.001162	6.52E-09	1.78E-09	45.508	3.852	0.0021

Ca_{L-S} (PBN)	η_{L-S} (PBN)	M_w (PBN)
4.38E-05	1.0000	0.00006
0.000113	0.9999	0.00015
0.000174	0.9998	0.00024
0.000319	0.9997	0.00044
0.000194	0.9998	0.00026
6.65E-05	0.9999	0.00009
0.000237	0.9998	0.00032

Appendix C:

Athena code used for parameter estimation of temperature-varied data:

Global RxnTime,Temp,Tref,Alph, KSOL As Real

Global Rg,wt,CH21, CH22 As Real

Global kB(Nrx),EB(Nrx),kRATE(Nrx) As Real

Global KADS(Nrx),KH As Real

Global ED(Nrx),CD(Nrx) As Real

Global E1,E2,E3,E4 As Real

Parameter Nrx=4 As Integer   ! Number of Chemical Reactions

Tref=100+273.15   ! Base Temperature, deg K

Rg=8.314   ! Universal Gas Constant, J/mol K

@Initial Conditions

 U(1:4)=Xu(4:7)

@Model Equations

Dim CBNZ,CPNY,CCBN,CCBL As Real

CBNZ=U(1)   !PBN

CPNY=U(2)   !PBL

CCBN=U(3)   !CBN

CCBL=U(4)   !CBL

Alph=1.0-(Tref/Temp)   !Arrhenius

kRATE(1)=kB(1)*exp(EB(1)*Alph)

kRATE(2)=kB(2)*exp(EB(2)*Alph)

kRATE(3)=kB(2)*exp(EB(2)*Alph)

kRATE(4)=kB(1)*exp(EB(1)*Alph)

!MODEL#A1 no KADS on top

 F(1)=(-
(kRATE(1)*CBNZ+kRATE(2)*CBNZ)/(1+KADS(1)*CBNZ+KADS(2)*CPNY+KADS(3)*
CCBN+KADS(4)*CCBL))

 F(2)=((kRATE(1)*CBNZ-
kRATE(3)*CPNY)/(1+KADS(1)*CBNZ+KADS(2)*CPNY+KADS(3)*CCBN+KADS(4)*C
CBL))

 F(3)=((kRATE(2)*CBNZ-
kRATE(4)*CCBN)/(1+KADS(1)*CBNZ+KADS(2)*CPNY+KADS(3)*CCBN+KADS(4)*C
CBL))

F(4)=((kRATE(3)*CPNY+kRATE(4)*CCBN)/(1+KADS(1)*CBNZ+KADS(2)*CPNY+KA
DS(3)*CCBN+KADS(4)*CCBL))

@Response Model

 Y(1:4)=U(1:4)

@Connect Variables

 RxnTime=Xu(3)   ! Reaction Sampling Time

 Temp=Xu(2)+273.15   ! Experimental Temperature, deg K

 kB(1:4)=Par(1:4)

 EB(1:4)=Par(5:8)

 KADS(1:4)=Par(9:12)

@Solver Options

Headers=RunID;Temp;RxnTime;CBNZ0;CPNY0;CCBN0;CCBL0;CBNZ;CPNY;CCBN;CC
BL;wt(1);wt(2);wt(3);wt(4);Replicate

Appendix D:

Residuals for PBN, PBL, CBN, and CBL for Model No. 4.35b with respect to increasing PBN
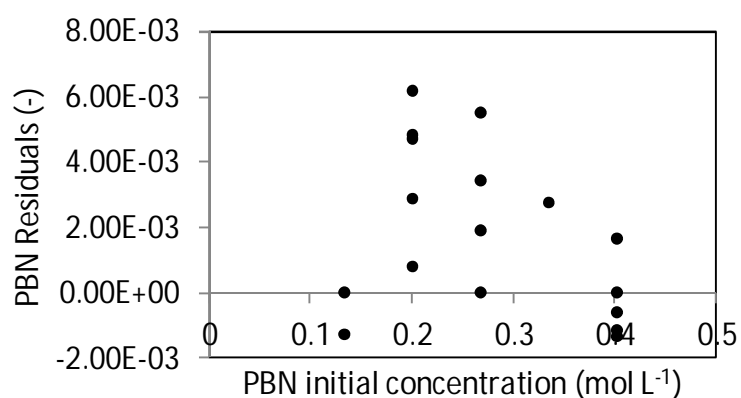
initial concentration. .

Figure C1: Model residuals of PBN for kinetic modelling of concentration varied-data: Model
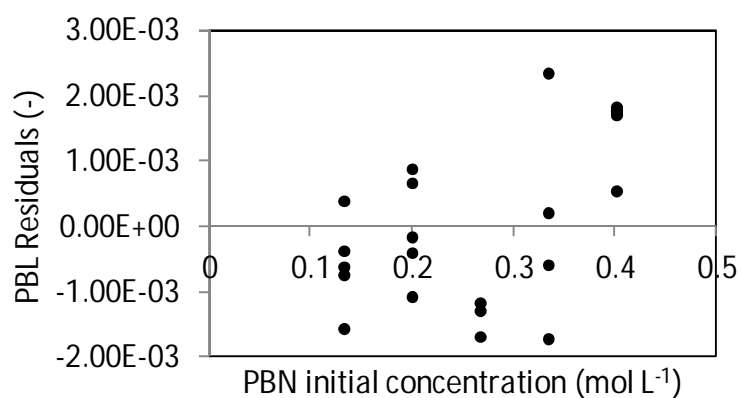
No. 4.35b

Figure C2: Model residuals of PBL for kinetic modelling of concentration varied-data: Model
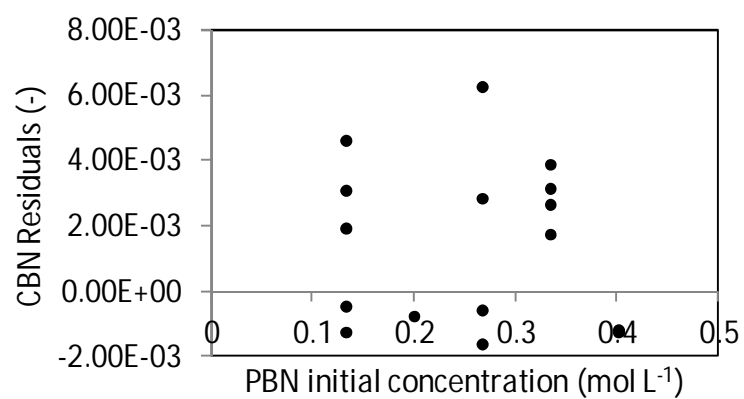
No. 4.35b

Figure C3: Model residuals of CBN for kinetic modelling of concentration varied-data: Model
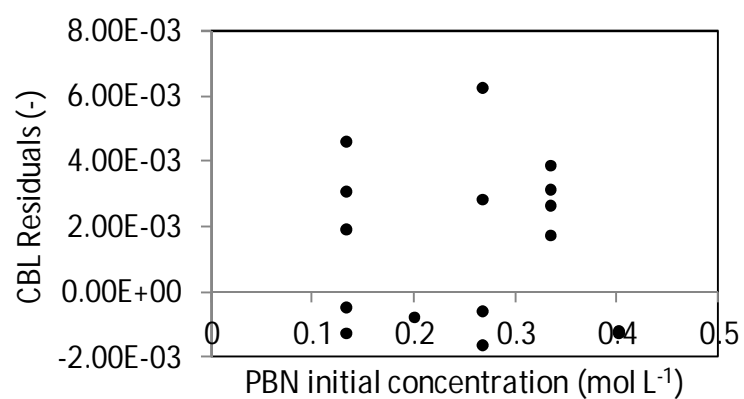
No. 4.35b

Figure C4: Model residuals of PBN for kinetic modelling of concentration varied-data: Model

No. 4.35b